UNIVERSITY OF SOUTHAMPTON

THE USE OF THE ELECTROCHEMICAL QUARTZ CRYSTAL MICROBALANCE FOR THE ANALYSIS OF POLY(ANILINE) COMPOSITE FILMS

Luciana Sampaio Pitta

Doctor of Philosophy

Department of Chemistry

June 2002

UNIVERSITY OF SOUTHAMPTON

ABSTRACT

FACULTY OF SCIENCE

CHEMISTRY

Doctor of Philosophy

THE USE OF THE ELECTROCHEMICAL QUARTZ CRYSTAL MICROBALANCE FOR THE ANALYSIS OF POLY(ANILINE) COMPOSITE FILMS

by Luciana Sampaio Pitta

The Electrochemical Quartz Crystal Microbalance has been largely used for the analysis of conducting polymers. Many groups quantify the mass increase or decrease on the surface of the quartz crystal directly from the changes in the resonant frequency of the crystal by applying the Sauerbrey equation. However this correlation can be used only if the material coated on the crystal is a thin, smooth and rigid layer. We treat the quartz crystal and the coating as a single resonator which can be represented as an equivalent electrical circuit (Butterworth-Van Dyke). The variation in the coating mass is compared to the changes in the inductance and the viscoelasticity is related to the resistance of the electrical circuit. Only in the case when the resistance is maintained close to zero throughout an experiment can the Sauerbrey equation be applied. The components of the equivalent electrical circuit are obtained by using the transfer function method, which is faster than an impedance measurement. The non-validity of the Sauerbrey equation is demonstrated for the hydration of a hydrophilic polymer film. The polymer swells considerably in water creating a very soft hydrated film. The use of mathematical simulations was then necessary in order to calculate of the rate of hydration, i.e. changes in the thickness of the film.

We have applied the transfer function method on the Electrochemical Quartz Crystal Microbalance to study the electrodeposition and the redox switching of conducting polymers. The poly(aniline) films were electropolymerised in the presence of poly(vinylsulfonate) or poly(styrenesulfonate) counterions. The polymer films presented different morphology depending on the poly(anion) used during polymerisation. The polymer film which obeyed the Sauerbrey approximation was used in studies of ionic movement during voltammetric cycles in different inorganic acids. From experiments coupling the Electrochemical Quartz Crystal Microbalance with the Scanning Electrochemical Microscopy, protons were found to be responsible for maintaining charge neutrality on the poly(aniline)/poly(anion) composite film during redox switching. Water also moves into and out of the polymer film in the opposite direction to the motion of the protons.

Para minha sobrinha linda
Thais

Table of Contents

Acknowledgements

Phil Bartlett for the supervision and perseverance. Also thanks for the financial help.

Jo Nesbitt for the studentship.

Maria Helena Troise Frank who stimulated me to come to Southampton.

Bernhard for being my guru during the beginning of this project.

Evelyne, Chee Seng and Stuart for being so helpful and friendly.

People for the Institute of Sound and Vibration for building the QCM. People from the Mechanical Workshop for providing the electrochemical cells. People from the technical glassblower for the microelectrodes.

Alastair Clark for the SEM images.

Prof Calvo and his group at the University of Buenos Aires for the hospitality.

Roberto Etchenique for his clarification about the basis of the QCM.

Prof Schuhmann and his group for being understanding when the writing of my thesis took a bit longer than expected.

My flatmates and all my friends from Montefiore. My housemates for the friendship and making me feel well going home after a day in the lab. And never complaining about my endless phone calls.

All my Brazilian colleagues for making me feel a bit closer to home. Especially for Silvia and Cesar for giving me home on my last weeks in England.

Nicolas and Evelyne for read proofing my thesis. And Arne for discussing about the introduction with me innumerable times.

My family who I miss a lot and always supports me. I wish I were closer to you.

Arne for everything he means to me and for all the moments we shared.

Nomenclature

ϑ	number of moles exchanged
δ	decay length of the acoustic wave (170 nm, for water, at f_0 =10 MHz)
α	internal friction, loss tangent
ξ	length of permeability of a porous material
γ	shearing strain
σ	shearing stress / applied pressure
η	viscosity
θ	angle between a disk of quartz and a mother quartz crystal
ϕ	angle for a polar co-ordinate system placed at the centre of the quartz
Θ	volumetric flow rate in a defined direction / angle between axes of a mother quartz crystal
Ψ	thickness of a porous material
ω	angular frequency of the quartz crystal
ω_0	angular resonant frequency of a 10 MHz quartz crystal (62831853 rad s^{-1})
ε_0	permittivity of free space
ξ^2	permeability of a porous material
τ_K	retardation time
τ_M	relaxation time
ρ_q	density of the quartz (2.650 g cm^{-3})
η_q	effective viscosity of the quartz crystal (7.6 x 10^{-3} Pa s)
a	direction of vector of pressure applied on a disk of quartz
a	area of microelectrode
A_e	electrochemical quartz crystal area (2.2 x 10^{-5} m^2)
A_m	mass sensitive area of the quartz crystal (2 x 10^{-5} m^2)
b	direction of vector of strain suffered by a disk of quartz
B	susceptance
c	compliance
c	concentration of the species analysed
c_{66} or μ_q	elastic constant of the quartz (2.947 x 10^{10} N m^{-2})

C_f	integral sensitivity constant of the quartz crystal
C_m	capacitance located in the QCM circuit (5.5×10^{-11} F)
C_o	parallel capacitance of the BVD equivalent electrical circuit
C_q	capacitance of the motional branch of the BVD equivalent electrical circuit (3.36×10^{-14} F)
D	diffusion coefficient
d_i	thickness of a non-piezoelectric material
D_o	dielectric constant of the quartz
e_{26}	piezoelectric stress constant for quartz (9.652×10^{-2} C m^{-2}).
e_a	energy loss from the spring to the viscous environment
F	Faraday constant (96480 C mol^{-1})
f	frequency of the quartz
f_o	resonant frequency of the quartz
G	conductance
$\boldsymbol{G}(\omega)$	frequency dependent complex shear modulus
G'	storage modulus or elasticity
G''	loss modulus or viscosity
h	distance between the microelectrode and the substrate
i	current
i	$\sqrt{-1}$ / indication of a non-piezoelectric material
i_{ss}	steady state current
$\boldsymbol{k}$	constant of the wave propagation
k_o	coefficient of electromechanical coupling of the quartz (0.089)
L_q	inductance of the motional branch of the BVD equivalent electrical circuit
l_q	thickness of the quartz crystal (for AT-cut 10 MHz: 1.68×10^{-4} m)
MW	relative molecular mass
m	mass
n	harmonic
n	number of electrons transferred
N/A_m	number of moles deposited per mass sensitive area
Δp	pressure difference
Q	quality factor of the quartz (≈78500)

r	distance for a polar co-ordinate system placed at the centre of the quartz
R	real part of the impedance
R_g	insulator/disk radius ratio of a microelectrode
R_q	resistance of the motional branch of the BVD equivalent electrical circuit
S	stiffness
S_f	differential sensitivity constant
t	time
U	average velocity of flow of an incompressible, viscous fluid
v	transverse speed of acoustic wave in the AT-cut quartz (3.34×10^4 m s^{-1})
V	amplitude of the shear oscillation on the surface of the quartz crystal
V_i	alternating voltage input
V_o	alternating voltage output
V_R	amplitude of the shear oscillation
X, Y, Z	crystallographic axis of a mother quartz crystal
X', Y', Z'	crystallographic axis of a disk of quartz
X_L	imaginary part of the impedance
$\boldsymbol{Y}$	admittance
$\boldsymbol{Z}_c$	measuring impedance
$\boldsymbol{Z}_e$	electrical impedance of a bare quartz crystal
$\boldsymbol{Z}_{e,i}$	electrical impedance of a non-piezoelectric material
$\boldsymbol{Z}_{e,m}$	electrical impedance of a bare quartz crystal loaded with a non-piezoelectric material
$\boldsymbol{Z}_m$	mechanical impedance of a bare quartz crystal
$\boldsymbol{Z}_{m,i}$	mechanical impedance of a non-piezoelectric material

List of Abbreviation

AT	special cut of a slice of quartz
BVD	Butterworth-Van Dyke equivalent circuit
(E)QCM	(Electrochemical) Quartz Crystal Microbalance
SECM	Scanning Electrochemical Microscopy
SEM	Scanning Electron Microscopy

1. Introduction

The Nobel Prize in Chemistry in 2000 was awarded to A. J. Heeger, A. G. MacDiarmid and H. Shirakawa for the discovery and development of conducting polymers. Conducting polymers combine the electrical and optical properties of metals or semiconductors and the attractive processing advantages of plastics.[1] Materials with high electrical conductivity and excellent mechanical properties can be produced from conducting polymers. Conducting polymers have recently received a lot of attention because of the many possible applications, such as artificial muscles,[2,3] bioelectrochemical fuel cells[4-6], (bio)sensors[7,8], rechargeable batteries[9] and electrochromic displays[9].

The understanding of electron and ion transport in conducting polymers is crucial for the success and improvement of their employment. Conducting polymeric materials are electrochemically active films and, when deposited on electrode surfaces, they form modified electrodes. The electron transfer between the electrode and the electroactive material and the consequent movement of ions and solvent between electroactive material and the electrolyte solution are illustrated in Figure 1.1. The transport of ions is necessary for the maintenance of the electroneutrality of the conducting polymer. The thickness, density, elasticity and viscosity of the electroactive material are modified by the insertion and ejection of ions and solvent into and out of the polymer film.[10-12]

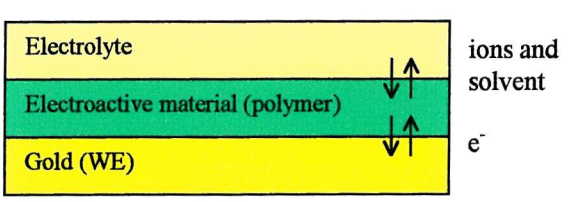

Figure 1.1: Scheme of the electronic and ionic movement in a polymer film during an electrochemical reaction. The electrons move between the working electrode (WE) and the electroactive material and ions move between the electroactive material and the electrolyte to maintain the electroneutrality of the material.

Even with substantial interest in conducting polymers, there is still much to be clarified about these special materials. Non-electrochemical techniques for the *in situ* characterisation of the modified electrode/electrolyte interface can provide important information about the processes of electrochemical film growth and conversion. Many analytical techniques combined with electrochemical methods have been used to investigate ion transport in conducting polymers, including probe beam deflection[13], ellipsometry[14], ESR[15] and spectroelectrochemical techniques.[16] However the most common method used is the Electrochemical Quartz Crystal Microbalance.[17] The aim of this thesis is to understand the potential and the limitations of the Electrochemical Quartz Crystal Microbalance for the analysis of conducting polymers.

The most common application of ellipsometry is the analysis of very thin films. The ellipsometry is a nondestructive optical technique that uses polarised light to investigate the dielectric properties of a sample. Through the analysis of the state of polarisation of the light that is reflected from the sample, ellipsometry can provide information about layers that are thinner than the wavelength of the light itself. The technique can probe a range of properties including the layer thickness, morphology, or chemical composition. The Probe Beam Deflection technique is based on the illumination of a surface by a specific light. The refractive-index gradient caused by the electrochemical processes can be measured by the deflection of the probe beam. This analytic technique has been widely used in electrochemistry for studying mass transfers between electroactive films and the electrolyte. Its main advantage is the *in situ* monitoring of mass fluxes and the ability to discriminate between ionic fluxes during potential cyclings.

1.1. The Electronic Conductivity of Polymers

Electronic conducting polymers, in contrast with insulating polymers, have extended conjugation.[1] In the structure of conjugated polymers there are alternating single and double bonds. Conducting polymers can be switched from insulating to conducting (doping) by removing or adding π electrons on the polymeric chains.[1] As a result a

positive charge ('hole') or negative charge (electron) is created on the polymeric chain. The polymer chain have dicrete positions of acceptors and donors of eletrons and the mechanism of electron self-exchange reaction, or electron hopping, create charge mobility along the backbone of the polymer as shown in Figure 1.2. [18]

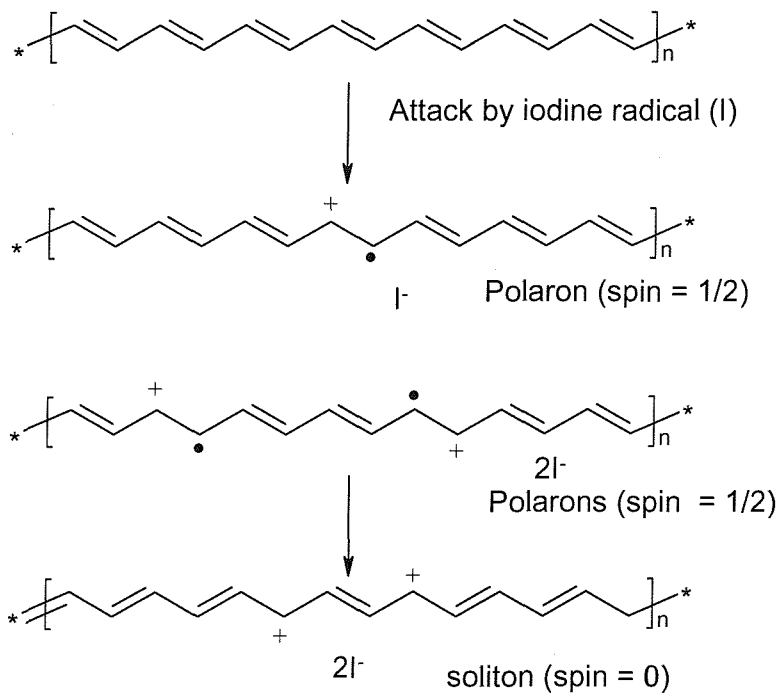

Figure 1.2: Chemical structure of poly(acetylene), the simplest conjugated polymer.

Conjugated polymers are predisposed to undergo doping by redox reaction, known as electrochemical doping, or reaction with chemical oxidants such as oxygen or halogens or even by an acid-base reaction, i.e., chemical doping.[1] The concept of doping in conducting polymers means the conversion of the neutral insulating polymer into a cationic or anionic conducting polymer. The electronic conducting polymers are also ionically conducting. The overall charge balance is recovered by the incorporation of counterions (dopants), which are supplied by the supporting electrolyte in the case of electrochemical doping.[1]

1.1.1. Choice of polymers

There is a large number of conducting polymers that could have been selected for the experimental work of this thesis. Poly(aniline) was chosen because the monomer is inexpensive and the polymer is very stable.[1] Also because there are current projects in the research group investigating the catalysis of the NADH oxidation using electrodes modified with poly(aniline)-poly(vinylsulfonate) and poly(aniline)-poly(styrenesulfonate) films.[19,20] There is a broad interest in this particular process[21] because, since there are several dehydrogenase enzymes which use NADH as a coenzyme, many specific devices can be developed.[19,22] Furthermore, the electrochemical deposition and redox switching of poly(aniline) films and composites are very reproducible. The insertion of large anions in the poly(aniline) films is necessary for the maintenance of the film conductivity at neutral pH, which is fundamental for bioelectronic devices.[8,19]

In addition, a non-conducting viscoelastic polymer film supplied by Biocompatibles Ltd was also studied. The polymer is hydrophilic and expands considerably in contact with water.[23] The density of the polymer film and the amount of water uptaken during hydration are known by the manufacturers. This is convenient for the verification of the Quartz Crystal Microbalance as an appropriate instrument for the analysis of viscoelastic polymers.

1.2. Principle of the Electrochemical Quartz Crystal Microbalance

The Electrochemical Quartz Crystal Microbalance is broadly used for the analysis of conducting polymers[24,25], electrodeposition[26,27], corrosion[28,29] and in biosensors[8,30]. However the way in which the measurements are performed and the way in which the results are interpreted differ from group to group. We present here the general principles of the Quartz Crystal Microbalance, and its electrochemical version, the Electrochemical Quartz Crystal Microbalance, and the method of interpretation used in this project.

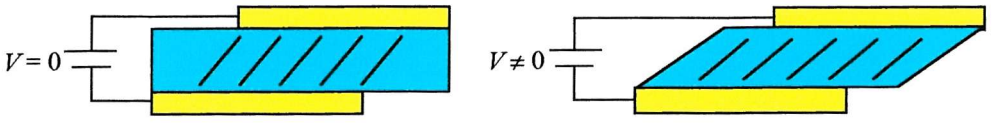

Figure 1.3: Schematic representation of the inverse piezoelectric effect on anisotropic materials covered by electrodes. When the initial voltage across the material is zero the material is in the relaxed state. The material suffers a proportional deformation when a voltage is applied.

1.2.1. Piezoelectricity

In 1880 the brothers Pierre and Jacques Curie [31] were the first to notice the piezoelectric effect. They observed that some materials were charged when compressed in specific directions and that the charge was proportional to the compression. The initial electrically neutral state of these materials was recovered when the compression was removed. In the following year they verified the converse piezoelectric effect, which means that with the application of voltage across some materials, a proportional deformation was obtained, see Figure 1.3.

The piezoelectric effect exists only in anisotropic materials. Anisotropic materials are characterised by the absence of a centre of symmetry in the internal structure. The physical (mechanical or electrical) properties of anisotropic materials depend on the direction of the crystallographic axis.[32] The parallel lines shown inside the crystals in Figure 1.3 represents the crystallographic axis of the slice of quartz. In the case of anisotropic materials the crystallography is represented by long, thin features aligned in one predominant direction. The cut of the material determines the physical characteristics of the slice of quartz because its properties differ if the surface is along the thin features or across them.

Anisotropic materials have to be covered on both sides by electrodes parallel to each other to show piezoelectricity. Because the mechanical energy is transformed to electrical energy, when a sinusoidal pressure is exerted on the electrodes, an alternating current is created. On the other hand, if an alternating voltage is applied across the

electrodes, a reversible proportional deformation is observed in the crystal. The piezoelectricity is noticed only on the area where the electrodes overlap each other.

Quartz, chemical composition SiO_2, is a piezoelectric material.[32] Quartz is easily available in nature, is chemically stable at reasonable temperatures and has a very small internal loss of energy during oscillation.

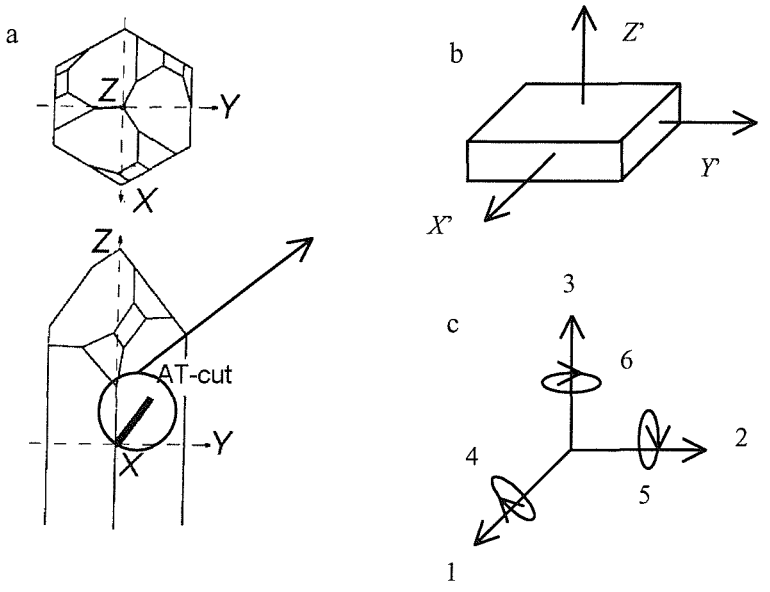

Figure 1.4: a) Crystallographic axes of a mother quartz crystal. b) The axes of an AT-cut quartz crystal. c) The subscripts for the directions of force and shear strain occurring at the quartz crystal ($X'\equiv1$, $Y'\equiv2$ and $Z'\equiv3$).

The cut of the quartz crystal is specially chosen to provide the best properties for the particular application. AT-cut quartz crystal is the most suitable cut for measurements of variation in mass in the range of micrograms.[33] The frequency temperature coefficient of an AT-cut quartz is approximately zero[32], which means that the resonant frequency of the quartz is not affected by small changes in temperature when it is near room temperature. When a quartz crystal is used as a resonator, the crystal is cut as a thin disk with crystallographic directions tilted with respect to the reference axis. Figure 1.4 shows an AT-cut disk from a mother quartz crystal. It was specified that the length, width and thickness of the disk of quartz are the axes X', Y', and Z'.[34] The crystallographic axis of the mother quartz crystal are X, Y and Z. The most important

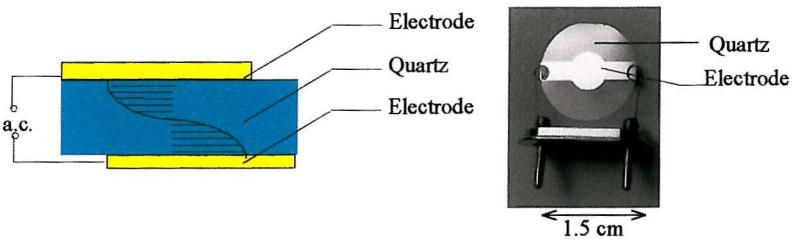

Figure 1.5: a) Sketch of the quartz crystal in a transversal view. b) Picture of an AT-cut quartz crystal of 10 MHz resonant frequency.

specifications of the AT-cut of the crystal are the angles: θ, between Z' and Y, (35°15' clockwise), and Θ, between Z and X, (54°15' anticlockwise).[32]

When there is a pressure on the $X'Y'$ plane of the quartz crystal, a transverse deformation occurs. With the application of an alternating voltage (stress), the quartz vibrates with proportional amplitude parallel to the surface of the quartz as shown in Figure 1.5a. This occurrence is known as the thickness shear mode. The linear Hooke's law expression for small strain is:[32]

$$\sigma_a = c_{ab}\, \gamma_b \tag{1.1}$$

where σ_a is the applied pressure, c_{ab} is the elastic constant and γ_b is the shear strain.

The directions of the vectors σ_a and γ_b are represented by the subscripts a and b, respectively. In the case of an AT-cut quartz crystal, the elastic constant c_{66} relates the stress, σ, applied on plane 6 to a strain, γ, with shear on plane 6, see Figure 1.4c.

The disks of quartz used for measurements of frequency in the range of MHz possess thickness much smaller than the length and the width, and the latter two are of the same order of magnitude as can be seen in a picture of the type of quartz crystal used in this project shown in Figure 1.5. This cut allows us to consider the shear displacement occurring exclusively in one direction, which is across the thickness of the quartz.[32]

The shear deformation on the quartz crystal is elastic. The quality factor, Q, of the quartz makes it ideal for frequency control. The quality factor Q quantifies the ratio of the energy stored in the quartz to the energy dissipated per cycle. Quartz has a high quality factor ($Q \approx 78500$), which means that the quartz vibrates with minimum loss.[32]

$$Q = 2\pi \frac{\text{energy stored per cycle}}{\text{energy lost per cycle}} = \left(\frac{\omega_o L_q}{R_q} \right) \tag{1.2}$$

where ω_o is the angular resonant frequency of the quartz, L_q and R_q are respectively the inductance and resistance parts of the Butterworth Van Dyke (BVD) electrical equivalent circuit of the quartz.

1.2.2. Electroacoustic waves

As a consequence of the vibration on the quartz crystal, an acoustic wave propagates from the quartz crystal outwards with a resonant frequency, f_o, given by:

$$f_o = \frac{v}{2l_q} = \frac{1}{2l_q}\sqrt{\frac{\mu_q}{\rho_q}} \tag{1.3}$$

where v is the transverse speed of the acoustic wave (sound) in the AT-cut quartz and l_q is the thickness of the crystal, μ_q ($=c_{66}$) is the elastic constant of the quartz and ρ_q is the density of the quartz. The vibrating parts in mechanical systems are formed from solids. In acoustic systems, the vibration occurs in gas or liquid phases.

As can be seen in equation (1.3), the thickness of the quartz crystal determines the frequency at which resonance occurs. Other parameters such as temperature, pressure, viscosity and density of the solution in contact with the quartz crystal must be maintained constant for the validity of the relation between frequency and thickness of the quartz. The metallic electrodes at both surfaces of the quartz crystal are very thin and rigid. The metallic layers (100 nm) are one thousand times thinner than the quartz crystal (165 μm). The disk of quartz and the gold electrodes vibrate together as one single material. The thickness of the attached electrodes is therefore included in the total thickness, which determines the resonant frequency of the quartz crystal. One of the electrode layers is in contact with the material to be analysed by the Quartz Crystal Microbalance. From now on, when we say that a material is in contact with the quartz crystal, we will take this to mean that it is actually in contact with one of the electrodes.

1.2.3. Electrochemical Quartz Crystal Microbalance

The quartz is covered on both sides by electrodes in order to make use of the piezoelectricity. The use of the upper layer of the metal electrode as a working electrode in a three-electrode set up has been used for studies of electrochemical processes.[10] Apart from being the working electrode, the gold layer is always used in the application of high frequency voltages across the quartz crystal. The gold electrode is the common ground for both the ac circuit (QCM) and the dc circuit (electrochemical instrument). The design of the instrumentation needs to be carried out with care in order to avoid any possible interference between the two signals. The placement of a capacitor (1 to 5 nF) between the potentiostat and the QCM filters the dc signals, impeding its transmission to the high frequency ac signals, as shown in Figure 1.6.[35] The electrochemical equipment and the QCM are coupled to perform synchronised measurements and the equipment is then called an Electrochemical Quartz Crystal Microbalance.

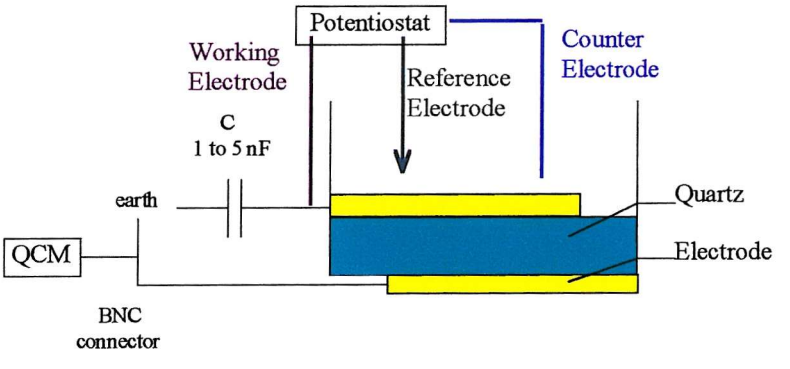

Figure 1.6: Circuitry of the coupled dc (potentiostat) and ac (QCM) signals.

The EQCM is commonly used for studying the redox systems of conducting polymers. The EQCM has been broadly used by electrochemists to investigate physical changes, i.e. thickness, density, viscosity and elasticity, of coatings on the working electrode during electrochemical reactions.[12,36,37] The estimation of mass and viscoelastic changes on the surface of the working electrode facilitates the comprehension of complex electrochemical reactions.[28,38]

1.2.4. Loading by a non-piezoelectric material

When a thin layer of a non-piezoelectric material is rigidly attached to the quartz crystal, the quartz and the non-piezoelectric material vibrate in synchrony. The layer of the material can be considered an extension of the quartz crystal, as sketched in Figure 1.7.

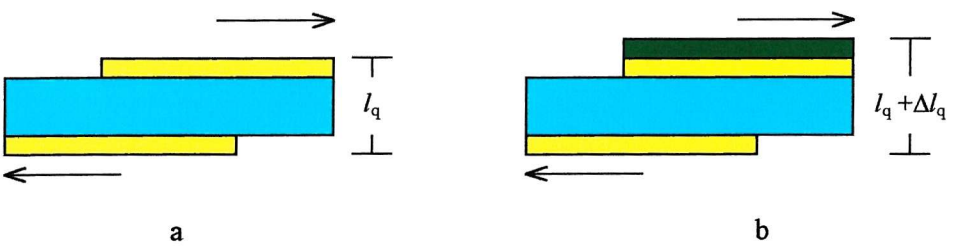

Figure 1.7: a) quartz crystal (blue) covered by electrodes (yellow) with thickness l_q, b) quartz crystal covered with electrodes and a non-piezoelectric material (green) with thickness $l_q + \Delta l_q$.

The film deposited on the quartz crystal must have uniform thickness, because the mass sensitivity of the quartz crystal has a Gaussian distribution with the highest sensitivity at the centre and decreasing close to the edge.[39] This difference in sensitivity can be attributed to the difference in shear velocity and amplitude of the crystal oscillations. The shear velocity is the maximum at the centre of the crystal and it is reduced to close to zero at the electrode edges. The equation that correlates the integral sensitivity constant, C_f, with the angle, ϕ, and distance, r, for a polar co-ordinate system placed at the centre of the quartz crystal is:[10]

$$C_f = \int_0^{2\pi} \int_0^r S_f(r,\phi) r \, dr \, d\phi \qquad \textbf{(1.4)}$$

where $S = df / dm$, is the differential sensitivity constant and represents the differential frequency shift, df, for a corresponding mass change, dm.

A thin layer of a rigid non-piezoelectric material coated on the quartz crystal forms a film. The film and the quartz crystal are assumed to be acoustically identical, which means the transverse speed of the acoustic wave and density are equal for the two materials.[10] The film of the material attached on the crystal must be firmly bound and must not slide against the metallic surface during the shear motion of the disk.[10] The quartz and the film attached to it vibrate together as a composite resonator, with

the same displacement and shear stress throughout the interface.[10] The change in the film thickness can then be treated in terms of a change in the thickness of the quartz crystal itself. It is then possible to calculate the increase in the thickness of the composite resonator, Δl_q, from the change in the resonant frequency of the quartz, Δf_o, and the initial thickness, l_q, and resonant frequency, f_o.

$$\frac{\Delta f_o}{f_o} = -\frac{\Delta l_q}{l_q} \tag{1.5}$$

The combination of equations (1.3) and (1.5) gives the well known Sauerbrey equation:[40]

$$\Delta f_o = -\frac{2 f_o^2 \Delta m}{A_m \sqrt{\mu_q \rho_q}} \tag{1.6}$$

where Δf_o is the change in resonant frequency, f_o is the resonant frequency of the bare quartz crystal, Δm is the change in mass of the crystal, and A_m is the mass sensitive area of the quartz crystal.

For an ideal perfectly rigid material, the relationship between the mass and frequency is limitless. On the other hand there is a maximum thickness of a layer of a non-ideal material where the relationship between the frequency and mass is no longer valid.[41] The upper layer of the film does not move in synchrony with the lower surface of the film and the Sauerbrey equation cannot be applied.

Originally the Quartz Crystal Microbalance was mainly used for detection of small changes in mass on the surface of the quartz crystal in vacuum.[42] With continued increase in interest in this technique, it was found that the use of liquids would not dampen completely the oscillation of the quartz crystal.[43] Although when the quartz crystal is in contact with a liquid, the resonant frequency is damped considerably. The oscillation of the quartz crystal causes a laminar flow on the liquid in contact with the quartz. The decrease in frequency is proportional to the square of the product of the density of the liquid, ρ_l, and the viscosity of the liquid, η_l. Kanazawa correlated the change in the resonant frequency of the quartz crystal to the properties of the liquid in contact with it, giving the relationship[44]

$$\Delta f = -f_o^{3/2} \sqrt{\frac{\Delta(\rho_l \eta_l)}{\pi \mu_q \rho_q}} \tag{1.7}$$

Equation (1.7) is valid only for Newtonian liquids. The energy applied to a Newtonian liquid during agitation is completely dissipated. None of the energy is recovered elastically. The height of liquid above the crystal does not influence the resonant frequency of the quartz crystal because the fraction of liquid that vibrates with the crystal is orders of magnitude smaller than the height of the liquid.[45] Variation in temperature modifies the viscosity and density of most liquids, so the temperature should be kept constant during such experiments.[46]

In Figure 1.8a there is no damping of the acoustic wave because the material attached to the quartz crystal is a thin layer of an elastic solid and the decay of oscillation is negligible. In this case, the resonant frequency decreases (the period increases) with the increase in thickness of the composite resonator. In Figure 1.8b, the penetration of the acoustic wave is damped when the quartz is in contact with a viscous material.

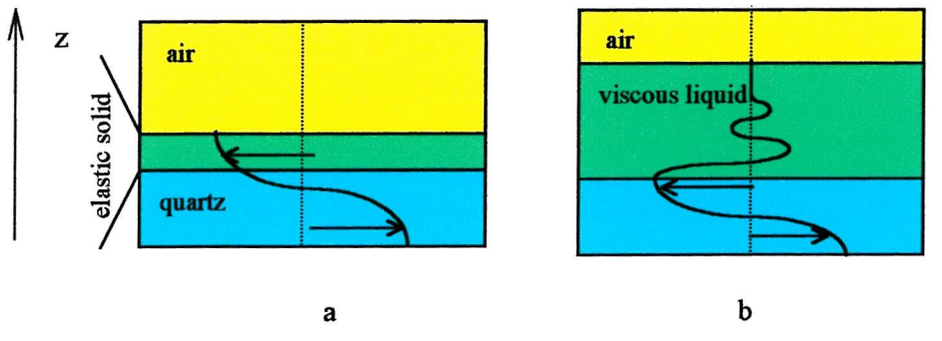

Figure 1.8: Acoustic wave from the quartz crystal (blue) in contact a non-piezoelectric material (green) in air (yellow). a) for a load of an elastic material, there is a decrease in frequency and no damping on the acoustic wave, b) for a viscous liquid, there is a slight decrease in frequency and the acoustic wave is damped.

The quartz emits acoustic waves that are damped when a viscous material is in contact with the quartz. The amplitude of the shear oscillation, V_x, decays as a damped exponential function according to the equation:[47]

$$V_x(z,t) = Ve^{-kz}e^{i\omega t} \qquad \textbf{(1.8)}$$

where V is the amplitude of the shear wave at the surface of the quartz crystal, k is the constant of wave propagation, z is the normal direction for the quartz crystal, ω the angular frequency and t is the time. The inverse of the constant of wave propagation, k, is the decay length of the acoustic wave, δ, which for a Newtonian liquid is:[47]

$$\delta = \sqrt{\frac{2\eta_i}{\rho_i \omega}} \tag{1.9}$$

where ω is the angular frequency of the quartz crystal and η_i and ρ_i are the viscosity and the density of the non-piezoelectric material, a Newtonian liquid in this case. There the subscript i is used to denote the non-piezoelectric material.

Part of the viscous material in contact with the quartz crystal moves with the same velocity and amplitude as the vibrating surface causing a decrease in the resonant frequency. The decay length of the acoustic wave in solution can also be defined in terms of the depth of penetration of the acoustic wave. The effect of the liquid in contact with the crystal is like attaching a layer of a material whose thickness varies with the viscosity, density and frequency of oscillation.[45]

We have shown that it is possible to interpret physical changes on the surface of the quartz from changes in the resonant frequency by using either the Sauerbrey or the Kanazawa equations. For the application of the Sauerbrey equation, the material has to be thin and acoustically rigid. For the use of the Kanazawa equation, the liquid has to be Newtonian and semi-infinite in extent. New methods need to be developed for the fast verification of the nature of the material analysed and the evaluation of non-ideal cases.

The mechanical properties of the non-piezoelectric material influence the electrical properties of the quartz crystal. Information about the mechanical properties of the non-piezoelectric film can be obtained from the measurement of the electrical parameters of the equivalent circuit of the oscillating quartz crystal.

1.2.5. Relation of Mechanical and Electrical Impedance

Due to the piezoelectricity of the quartz crystal, the mechanical load of a layer of a non-piezoelectric material deposited on one face of the quartz crystal is recognised as an electrical impedance. For a quartz crystal with one side in contact with a non-piezoelectric material the electrical impedance, Z_e, of the quartz crystal can be described as a function of the mechanical impedance, Z_m[39]

$$\boldsymbol{Z}_e = \frac{2\,\omega_o\,L_q}{\pi\sqrt{\mu_q\,\rho_q}}\boldsymbol{Z}_m = R + \mathrm{i}X_L \tag{1.10}$$

where,

$$L_q = \frac{l_q^3\,\rho_q}{8\,A_m\,e_{26}^2} \tag{1.11}$$

ω_o is the angular resonant frequency of the quartz, L_q is the inductance of the bare quartz crystal (typical value for a bare AT-cut 10 MHz quartz crystal is 75 mH)[10], μ_q and ρ_q are elasticity and density of the quartz crystal, R and X_L are the real and imaginary parts of the electrical impedance, l_q is the quartz crystal thickness, A_m is the mass sensitive area of the quartz crystal, e_{26} is the piezoelectric constant of the quartz.

The complete equation for the mechanical impedance of two layers deposited onto the quartz crystal proposed by Martin and Granstaff is:[42]

$$\boldsymbol{Z}_{m,i} = \frac{\boldsymbol{Z}_2\tanh(\boldsymbol{k}_2 d_2) + \boldsymbol{Z}_1\tanh(\boldsymbol{k}_1 d_1)}{\left(\boldsymbol{Z}_2/\boldsymbol{Z}_1\right)\tanh(\boldsymbol{k}_1 d_1)\tanh(\boldsymbol{k}_2 d_2) + 1} \tag{1.12}$$

where the subscript 1 is for the material directly in contact with the crystal and the subscript 2 is for the material in contact with material 1, $\boldsymbol{Z}_1$ and $\boldsymbol{Z}_2$ are the characteristic impedances of the two layers[42]

$$\boldsymbol{Z}_1 = \sqrt{\rho_1\boldsymbol{G}_1} \text{ and } \boldsymbol{Z}_2 = \sqrt{\rho_2\boldsymbol{G}_2} \tag{1.13}$$

where the $\boldsymbol{G}_i$ is the complex shear modulus of the material.

$$\boldsymbol{G}_i = G'_i + \mathrm{i}\,G''_i \tag{1.14}$$

G'_i is the storage modulus and G''_i is the loss modulus and they are related respectively to the elasticity and viscosity of the material. $\boldsymbol{k}_i$ is the acoustic wave propagation constant for a viscoelastic material, i.[42]

$$\boldsymbol{k}_i = \mathrm{i}\omega_o\sqrt{\frac{\rho_i}{\boldsymbol{G}_i}} = \frac{\omega_o}{v_i} \tag{1.15}$$

where v_i is the transverse speed of the acoustic wave. We explain in Appendix 8.2 the meaning of the complex quantity represented in bold.

The interaction between any two layers is represented by the term:[11,42]

$$\left(Z_2/Z_1\right)\tanh(k_1 d_1)\tanh(k_2 d_2) \qquad \textbf{(1.16)}$$

because it contains the ratio of the layer impedances multiplied by the two terms representing the phase shift and attenuation in each of the layers. If one of the three components of this term is small, i.e.

a) if the film is thin, $d_1 \rightarrow 0$

b) if the film is rigid, $k_1 \rightarrow 0$ (or $G \rightarrow \infty$)

c) if layer 1 is relatively hard compared to layer 2 $|Z_2| << |Z_1|$, or $G''_2 << G''_1$.

If any one of the three options above is satisfied, the term $\left(Z_2/Z_1\right)\tanh(k_1 d_1)\tanh(k_2 d_2) << 1$ and the approximation of additivity[28,38] is valid simplifying equation (1.12) to give:

$$Z_{m,i} = \sqrt{(\rho_1 G_1)}\tanh(k_1 d_1) + \sqrt{(\rho_2 G_2)}\tanh(k_2 d_2) \qquad \textbf{(1.17)}$$

The assumptions a and b ensure synchronised movement between the non-piezoelectric materials and the oscillating surface of the crystal. On the other hand the approximation of additivity is not valid if the layer of material 1 is very thick, viscoelastic or porous. The upper layer of the film can oscillate in-phase or out-of-phase with the lower surface. The transition between these two modes occurs with the change of sign of tan (k_i d_i), causing an increase in the quartz resonant frequency and a damping in the resonance peak.[42]

If the decay length in material 2 is less than its thickness, its upper surface will be 'invisible' to the quartz crystal. Consequently, material 2 appears to be infinity thick and no mass information can be obtained.

The mechanical impedance of a single layer deposited onto the quartz crystal has the form:[42]

$$Z_{m,i} = \sqrt{\rho_i G_i}\,\tanh\left(k_i\, d_i\right) \qquad \textbf{(1.18)}$$

From equations (1.15) and (1.18) we obtain:

$$Z_{m,i}(\omega) = \sqrt{\rho_i G_i}\tanh\left(i\omega_o\, d_i \sqrt{\frac{\rho_i}{G_i}}\right) \qquad \textbf{(1.19)}$$

where ρ_i and d_i are the density and thickness of the non-piezoelectric material attached on the quartz crystal. The error in considering the angular frequency equal to the

resonant angular frequency, $\omega = \omega_o$, is smaller than 0.25 %, because the range of angular frequency is very small compared to the value of the resonant frequency, $\Delta\omega < 0.001\omega_o$.[11]

Assuming additivity, the electrical impedance equivalent of a non-piezoelectric material, $Z_{e,i}$, in contact with a quartz crystal can be calculated from the difference between the electrical impedance of the quartz loaded with a non-piezoelectric material, $Z_{e,m}$, and the electrical impedance of the bare crystal, Z_e,

$$Z_{e,i} = Z_{e,m} - Z_e \tag{1.20}$$

The evaluation of the electrical impedance generates the parameters: mass, density, elasticity and viscosity of a non-piezoelectric material. By combining equations (1.10) and (1.19)

$$Z_{e,i}(\omega) = R + iX_L = \left(\frac{2\omega_o L_q}{\pi\sqrt{\mu_q \rho_q}}\right)\sqrt{\rho_i (G'_i + iG''_i)}\tanh\left[i\omega_o d_i \sqrt{\frac{\rho_i}{G'_i + iG''_i}}\right] \tag{1.21}$$

1.2.6. Electrical Equivalent Circuit of the Quartz Crystal

The comparison between the mechanical and electrical impedance of the quartz crystal oscillator is very useful because the equations applied for electric circuits, such as Ohm's and Kirchoff's laws, can be used to describe the mechanical system. Butterworth and Van Dyke [48] proposed an electrical equivalent circuit for an oscillating system under an electrical field; the BVD equivalent circuit is shown in Figure 1.9.

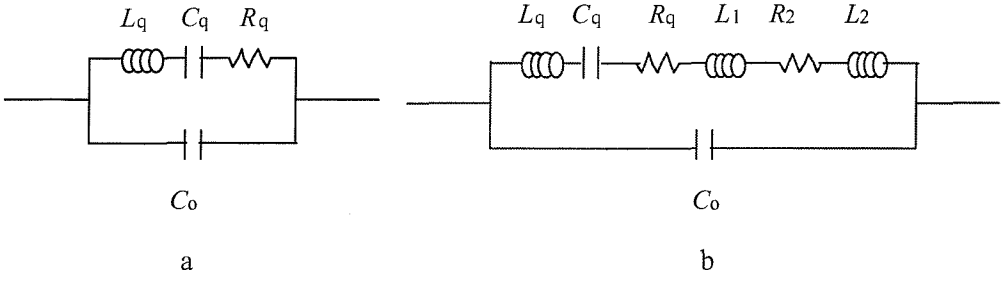

Figure 1.9: Butterworth-Van Dyke (BVD) electrical equivalent circuit for a) a bare resonant quartz crystal close to its resonant frequency and b) quartz crystal loaded with a solid 1 and a liquid 2.

The relation between the electrical and the mechanical parameters of an oscillating system[49] is described in Table 1.1, where σ and δ are sinusoidally dependent on time.

Table 1.1: Relation between the parameters of the electrical and mechanical circuits of an oscillating system. The mechanical system can be a spring where R corresponds to the energy loss from the spring to the viscous environment e_a, L represents the mass m, and C is related to the elastic constant of the spring k.[10]

Electrical circuit	$\boldsymbol{Z}_e$ /N m s C^{-2}	V /N m C^{-1}	q /C	i /C s^{-1}	R /N m s C^{-2}	L /N m s^2 C^{-2}	C /C^2 N^{-1} m^{-1}
Mechanical circuit	$\boldsymbol{Z}_m$ /kg s^{-1}	σ /kg m s^{-2}	δ /m	$d\delta / dt$ /m s^{-1}	e_a /kg s^{-1}	m /kg	k^{-1} /(kg s^{-2})$^{-1}$

Resonance occurs in a wide variety of mechanical systems and takes place with a periodic stimulus with frequency close to the natural resonant frequency of the system. When an object is excited it tends to oscillate at its natural frequencies. An oscillatory mechanical system stores potential and kinetic energy. In Figure 1.10 a *RLC* circuit represents the oscillatory mechanism of the quartz crystal.[10] The *RLC* circuit has input voltage V_i at variable angular frequency ω as driving force. When the switch S is open, the capacitor C is charged. By closing the switch S, the capacitor C is discharged with a flow of current through the inductor L, where a magnetic field is built up. When the capacitor is completely discharged, the flow of current to the direction of the inductor stops and the electromagnetic field in L decreases creating a flow of current in the opposite direction to the initial one. The current flows until the electromagnetic field is empty and the capacitor is fully charged, but now with an opposite polarity. The resonant frequency occurs when maximum current, i, or minimum impedance, $\boldsymbol{Z}$, is achieved. The current oscillates continuously if the resistor R is negligible. However, if the value of R is substantial, the oscillations are slowly damped over time.

By comparing the electrical and mechanical systems the capacitor is related to the potential energy while the inductor is related to the kinetic energy of the system.

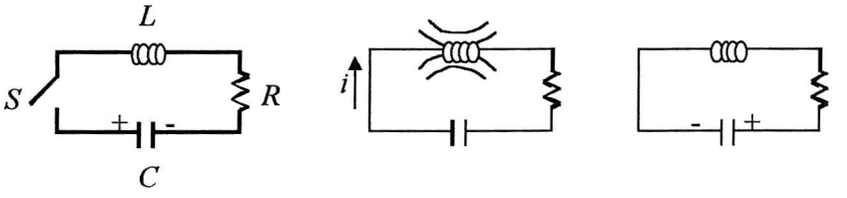

Figure 1.10: *RLC* circuit in parallel represents an oscillatory system.

The relation between the physical properties of a piezoelectric material and an electrical equivalent circuit is valid only when the piezoelectric material is driven at frequencies close to its resonant frequency. At these frequencies, the electrical parameters can be considered to be independent on the frequency.[32] The resonance is very sharp, i.e. the range of frequency close to the resonant frequency is very narrow.

In addition to the *RLC* circuit, the electrical equivalent of the quartz crystal has a capacitance in parallel, C_o (Figure 1.9). This parameter corresponds to the capacitance created by the insulating quartz crystal covered with conducting gold electrodes on both sides and the connections between the quartz crystal and the instrumentation.[10] The load on the quartz crystal is sensed only by the motional branch of the BVD circuit, the *RLC* circuit, where R_q represents the mechanical loss from the vibrating quartz to a viscous medium, L_q represents the mass of the quartz crystal and C_q represents the elastic properties of the quartz.

For the BVD circuit loaded with a non-piezoelectric material, the parameter L_1 corresponds to the mass of a material 1, assumed to be a thin elastic solid deposited on the quartz crystal. The parameters L_2 and R_2 correspond to the density and viscosity of a material 2, assumed to be a Newtonian liquid placed in contact with material 1 as shown in Figure 1.11.

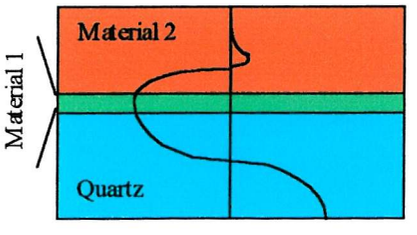

Figure 1.11: Acoustic wave propagated from the quartz crystal (blue) in contact with two non-piezoelectric sequential layers: material 1 (green) and material 2 (orange).

The mathematical equations that convert the components of the BVD equivalent circuit to the physical properties of the resonant quartz and the materials attached on it are present in Appendix 8.1.[32,43]

The parameters L and C_q define the resonant frequency of the quartz crystal.

$$f_o = \sqrt{\frac{1}{2\pi L C_q}} \tag{1.22}$$

The capacitance, C_q, is a physical property of the quartz crystal and it is not influenced by the load on the surface of the quartz crystal. The load on the surface of the quartz crystal is represented by changes in L and consequently f_o, where L is the sum of L_q, L_1 and L_2. The change in frequency can be written as:[43]

$$\frac{\Delta f_o}{f_o} = -\frac{\Delta L}{2L} = -\frac{1}{2}\left(\frac{L_1 + L_2}{L_q + L_1 + L_2}\right) \tag{1.23}$$

If we consider the mass contributions of the solid and liquid to be very small compared to the mass of the quartz crystal (so $L_1 + L_2 << L_q$), the variation in resonant frequency applying the values of L shown in Appendix 8.1 results in[43]

$$\Delta f_o = -\frac{2f_o^2}{\sqrt{\mu_q \rho_q}}\left(\rho_1 + \sqrt{\frac{\rho_2 \eta_2}{4\pi f_o}}\right) \tag{1.24}$$

The equation above shows the changes in frequency caused by an elastic solid (first term) and a viscous liquid (second term). It demonstrates that it is not possible to differentiate between the influence of a solid and a liquid load on the surface of the quartz crystal based on the measurement of the frequency alone.[10]

The theory described up to this point is applicable for any method applied to obtain QCM measurements. In the next section we show how the (Electrochemical) Quartz Crystal Microbalance developed.

1.2.7. The History of the Electrochemical Quartz Crystal Microbalance

Sauerbrey was the first to demonstrate the principle of the Quartz Crystal Microbalance in 1959.[40] He showed that the deposition of a thin uniform layer of a non-piezoelectric

material on the surface of a plate of quartz crystal would change the resonant frequency of the quartz crystal. The shift in the resonant frequency was proportional to the thickness of the material deposited. The relationship between the frequency and the additional mass was linear only for changes in frequency smaller than 2% of the resonant frequency of the bare quartz. With an increase in thickness, the accuracy of the measurements decreased considerably.[50]

In 1962, Behrndt and Love[51] used the Quartz Crystal Microbalance to monitor the mass deposition of thin metallic films in vacuum. Followed by King [52], who created in 1964 the first selective gas sensor by depositing materials used in gas chromatography on the surface of the quartz crystal.

Miller and Bolef [53] presented a model for the propagation of acoustic waves through a film deposited on the quartz crystal in 1968. In 1979 Mecea and Bacur [54] proposed a method that correlated the energy transferred from the vibration of the quartz crystal to the film deposited on it. The energy stored in the material was related to the elastic properties of the film, and the energy lost was related to the viscous properties of the film.

The use of the Quartz Crystal Microbalance in liquid medium started with the discovery that the liquid would not stop the oscillation of the quartz.[44,45] In 1990, Kanazawa [55] proposed a model based on admittance for the analysis of density and viscosity of Newtonian liquids.

With the possibility of making measurements in a liquid environment and using the upper electrode as a working electrode, a new tool was created for the investigation of electrochemical reactions.

The correlation between frequency and mass/thickness is valid only if the material in contact with the quartz crystal is thin and rigid. Nevertheless some research groups still measure only the changes in resonant frequency of the quartz crystal and apply the Sauerbrey equation to calculate the changes in mass on the surface of the crystal.[56-58] However the Sauerbrey equation can only be used for rigid and smooth thin layers when the films vibrate together with the quartz crystal.[10] In the case of viscous films, the density and viscosity of the material modify the resonant frequency.[44] Also for rough surfaces, liquid trapped in the cavities will cause erroneously bigger changes in the resonant frequency.[59] For thick layers, the sensitivity of the QCM decreases until the layer no longer vibrates together with the crystal.[10] These cases are discussed later in this thesis.

In 1991, Martin and Granstaff [43] used impedance measurements described by Kanazawa to calculate the parameters of the electrical equivalent circuit proposed by Butterworth-Van-Dyke [48] for the oscillating quartz crystal. The changes in mass and viscosity can then be calculated from the determination of the parameters of the electrical equivalent circuit.[10] The methods used to calculate the parameters of the electrical equivalent circuit are the impedance analysis, the oscillation method and the transfer function method.

- Impedance analysis is the most commonly used method due to the ready availability of commercial instruments such as impedance analysers and network analysers.[27,30,60,61] Nevertheless, these instruments have some disadvantages concerning the price and speed of the measurements. An impedance spectrum around the crystal's resonant frequency recorded by an average commercial instrument takes several seconds which is usually too slow to use for the study of fast electrochemical phenomena.[62] There are network analysers with faster rate acquisition data, but it comes with a further increase in price.
- The oscillation method was proposed by Soares.[63] The method distinguishes between the resonant frequency and the equivalent resistance of the quartz.[64] The method is much cheaper to implement than Impedance Analysis, but not faster.
- The transfer function method was developed by Granstaff and Martin[42] and improved by Calvo and Etchenique.[35,39] This technique was developed after the introduction of a voltage divider circuit for rapid measurement of the modulus of the transfer function.[65] At the moment, this approach is only used by the Calvo group[35,39] at the University of Buenos Aires and the Bartlett group at the University of Southampton.[66]

Quartz Crystal Microbalances are also commercially available. The different types of commercial equipment vary a lot and it is necessary to specify very carefully the experimental needs before buying the right equipment. O'Sullivan has reported a table with commercially available instruments.[67]

In 1992, Buttry and Ward[10] published a very extended review about the measurement of interfacial processes on the surface of the quartz crystal with the Electrochemical Quartz Crystal Microbalance. The basic principles of the quartz resonator and the main limitations and applications of the Electrochemical Quartz Crystal Microbalance were discussed in detail.

In recent publications, Hillman[41,68] uses extensively the Electrochemical Quartz Crystal Microbalance to analyse the redox system of conducting polymers. The influence of the viscoeleasticity of polymers on the response of the EQCM is one of the most discussed points in his work.

The main topics in modern research using EQCM are corrosion[28,29], current efficiency during electrochemical deposition[26,27], mass transport during redox reactions[56,69-74], biosensor applications.[8,30]

Although the EQCM may detect changes in the mass of modified electrodes, charged and non-charged species cannot be distinguished. In order to overcome this problem, other analytical techniques are associated with the EQCM in recent work. Simultaneous ellipsometry and EQCM[75] combine information about optical properties of the film and its thickness and the overall mass changes. Simultaneous UV-Vis absorption spectroscopy[76] and EQCM was used in studies of polymers used as electrochromic displays. EQCM measurements were combined with Raman spectroscopy[77] to identify the charge compensation process and the extent to which certain species participate in the redox process. EQCM was coupled with electrochemical ICP-atomic emission spectrometry[37] to detect metal ions released by the film. Ion transport during redox switching of conducting polymers was investigated combining EQCM and in situ Fourier transform infra red (FTIR) reflection spectroscopy.[78] An association of differential electrochemical mass spectrometry (DEMS) and EQCM performed simultaneous measurements of volatile products and deposited (or dissolved) species.[79] EQCM and atomic force microscopy (AFM) were used in the characterisation of redox-active dendrimers on electrodes.[80] A combined EQCM and probe beam deflection was used in studies of solvent and ion transfer of conducting polymers during redox switching.[36,81] In situ EQCM and STM were applied in studies of corrosion.[82] QCM, Electrochemical Impedance Spectroscopy (EIS), AFM and ellipsometry were used to study deposition of phospholipid films.[83]

In this project, we introduced for the first time EQCM, analysed by the transfer function method, combined with Scanning Electrochemical Microscopy (SECM) to allow the identification of ion movement between conducting polymers and electrolytes during redox reactions. The design used in this project was proposed by Gollas et. al.[62] The instrument was tested by plating and stripping a copper film on the quartz crystal. The QCM detects the mass of the film of Cu^0 while the SECM tip positioned close to the substrate detects the changes in the concentration of Cu^{+1} amperometrically. The

SECM consists of a microelectrode positioned very close to the modified electrode with a defined potential that oxidises or reduces certain species.[84] The movement of the species of interest is quantified by the oxidation or reduction current, which is proportional to its concentration.

1.2.8. Transfer Function Analysis

The measurement of the Quartz Crystal Microbalance used in this thesis is the transfer function analysis that was firstly proposed by Calvo and Etchenique.[39] The main advantage over the use of an impedance analyser is in the speed of acquisition of the transfer function measurements. Another important bonus is the low cost of the QCM operated by the transfer function method. An alternating voltage, V_i, is applied over a range of frequencies across the thickness of the quartz crystal. The quartz crystal oscillates around its resonant frequency. The oscillation of the quartz generates an alternating voltage output, V_o, which is measured.

The input voltage is applied to a known capacitor C_m that has impedance Z_c. The circuit of the QCM shown in Figure 1.12 was proposed by Muramatsu[85] and refined by Calvo.[39]

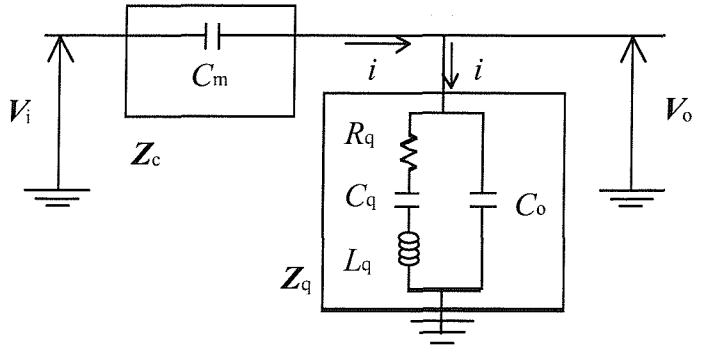

Figure 1.12: Circuit of the QCM used during transfer function measurements. V_i and V_o are respectively the voltages input and output, Z_c is the measuring impedance, Z_q is the impedance of the quartz crystal, which represented by the BVD electrical equivalent circuit.

According to Thévenin's theorem,[49] equation (1.25), the current that flows through the capacitive impedance, $\boldsymbol{Z}_c$, is equal to the voltage input divided by the sum of the impedances.

$$i = \frac{V_i}{Z_c + Z_q} \tag{1.25}$$

In order to increase the speed of the measurements, the ratio of the output voltage to the input voltage was measured. This ratio is a function of the frequency and it is called the transfer function

$$\frac{V_i}{V_o} = \frac{Z_c}{Z_q} + 1 \tag{1.26}$$

where

$$Z_q = \frac{\frac{L_q}{C_o} - \frac{1}{\omega^2 C_q C_o} - \frac{i R_q}{\omega C_o}}{R_q + i\omega L_q - i\left(\frac{1}{\omega C_q} + \frac{1}{\omega C_o}\right)} \tag{1.27}$$

and, assuming the measuring impedance is a pure capacitor,

$$Z_c = -i\frac{1}{\omega C_m} \tag{1.28}$$

It is possible to calculate the electrical parameters of the BVD equivalent circuit from the modulus of the transfer function by combining equations (1.26), (1.27) and (1.28),

$$\left|\frac{V_o}{V_i}\right| = \left|\frac{Z_q}{Z_q + Z_c}\right| = \sqrt{\frac{\left(\omega L_q - \frac{1}{\omega C_q}\right)^2 + R_q^{\,2}}{\left(\omega L_q - \frac{1}{\omega C_q} + \frac{\omega L_q C_o}{C_m} - \frac{C_o}{\omega C_q C_m} - \frac{1}{\omega C_m}\right)^2 + \left(R_q + \frac{R_q C_o}{C_m}\right)^2}} \tag{1.29}$$

The modulus of the ratio of output to input voltages in equation (1.29) produces only real values which make the measurement of the phase of the alternating voltages not necessary since all the information necessary is available when using the transfer function method. (More information about complex numbers and the measurement of phase and amplitude can be found in Appendix 8.2.) This is a great advantage because the measurements can be realised considerably faster than the impedance

measurements. The speed of the measurements depends on the range of frequency scanned, the number of points taken per transfer function and the average used. Although for very fast measurements the sensitivity of the measurements decrease. We have measured one transfer function every 0.15 s, shown in Figure 6.4, with very good stability.

The parameters from the BVD electrical equivalent circuit are calculated from equation (1.29) using a Quick Basic program written by Etchenique.[35] The values of C_m and C_q are constant and known.[43] The experimental values C_o, R_q and L_q are then mathematically fitted. The parameter C_o does not vary significantly during the experiments because the load on the quartz crystal does not have any influence on this parameter. It is convenient to convert L to $X_L = \omega L$ to have the quantities R and X_L with the same units (Ω). R and X_L are the fitted components of the electroacoustic impedance of the QCM. The two experimental values obtained from the QCM experiments, R and X_L, generate four physical parameters of the non-piezoelectric material: G' (storage modulus, or elasticity), G'' (loss modulus, or viscosity), ρ_i (density) and d_i (thickness).

$$\boldsymbol{Z}_e(\omega) = R + iX_L = \left(\frac{2\omega_o L_q}{\pi\sqrt{\mu_q \rho_q}}\right)\sqrt{\rho_i (G'_i + iG''_i)}\tanh\left[i\omega_o d_i \sqrt{\frac{\rho_i}{G'_i + iG''_i}}\right] \qquad (1.21)$$

d_i can be substituted by the mass of the non-piezoelectric material m_i because

$$m_i = d_i A_m \rho_i \qquad \mathbf{(1.30)}$$

where and A_m is the mass sensitive area of the quartz crystal.

There are only two experimental initial values, R and X_L, so only two physical parameters of the non-piezoelectric material can be calculated.

Calvo[11] introduced the parametric impedance plane plots in order to accelerate the classification of the type of material analysed by QCM measurements. The parametric plots consist of plotting R as function of X_L using the same scale. Examples of parametric and transfer function plots for a perfectly elastic solid, a perfectly elastic liquid and a viscoelastic material are shown in the next figures.

Figure 1.13 shows the parametric and transfer function plots during the deposition of a perfectly elastic solid onto the quartz crystal. The deposition of a rigid mass causes an increase in the value of X_L while R remains constant. The transfer function indicates changes only in the resonant frequency of the quartz crystal. In this case, the elasticity, G'_i, and the viscosity, G''_i, are not modified and the density, ρ_i, and thickness, d_i, can be calculated from equation (3.4). This simplification will be explained further in Chapter 3.

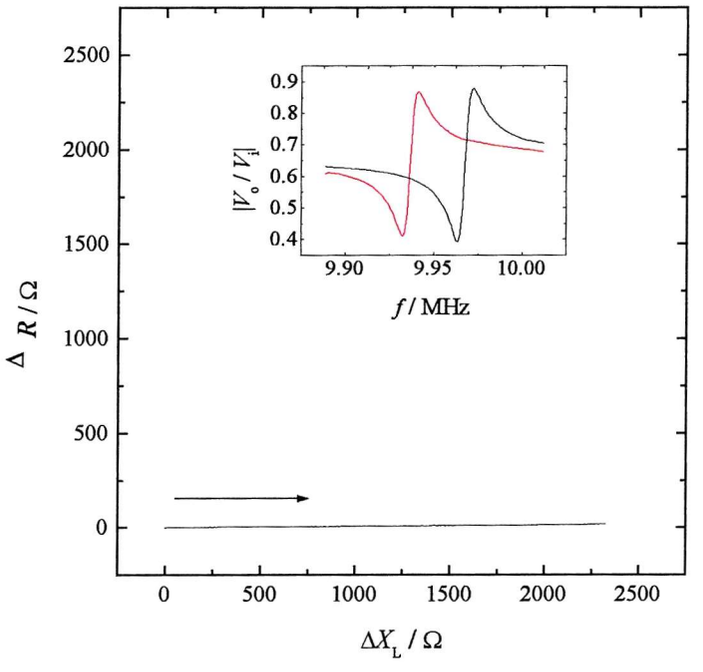

Figure 1.13: Parametric plot and inset transfer function of a thin elastic solid where R remains constant. The transfer functions are calculated from equation (1.29) using the fixed values of $C_m = 5.5 \times 10^{-11}$ F and $C_q = 3.36 \times 10^{-14}$ F. The resonance frequency of the transfer functions is shifted without broadening. The transfer function in black is for a blank crystal and the one in red is after the deposition of a perfectly elastic solid.

In Figure 1.14, the results obtained for perfectly viscous liquids of different viscosities and densities are shown causing an equal increase in X_L and R as shown by the line in the parametric plot. The resonance frequency gets broader and the frequency is shifted. The density, ρ_i, and viscosity of the Newtonian liquid, η_i, can be calculated from equation (3.9). This case is also explained in Chapter 3.

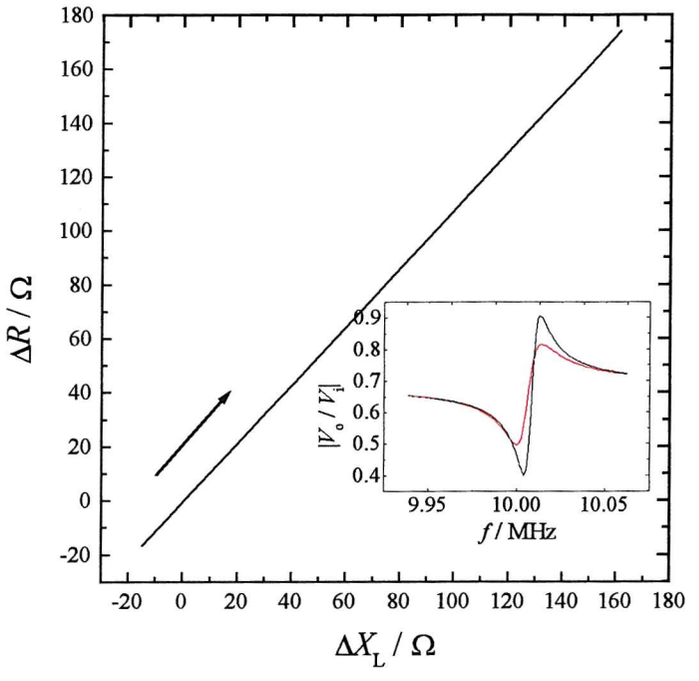

Figure 1.14: Parametric plot and inset transfer function of a perfectly viscous liquid where R and X_L have equal growth. The transfer functions are calculated from equation (1.29) using the fixed values of $C_m = 5.5 \times 10^{-11}$ F and $C_q = 3.36 \times 10^{-14}$ F. The resonance frequency gets broader and the frequency is shifted. The transfer functions are for two different concentrations of glucose solution. The one in black is more diluted than the one in red.

In Figure 1.15, both X_L and R grow but the gradient of the line in the parametric plot is neither 0 or 0.5. There are changes in the resonant frequency and broadening of the resonance. This case is obtained with the growth of a viscoelastic material when none of the four variables of equation (1.21) are maintained constant. Viscoelastic materials are discussed in Chapter 4.

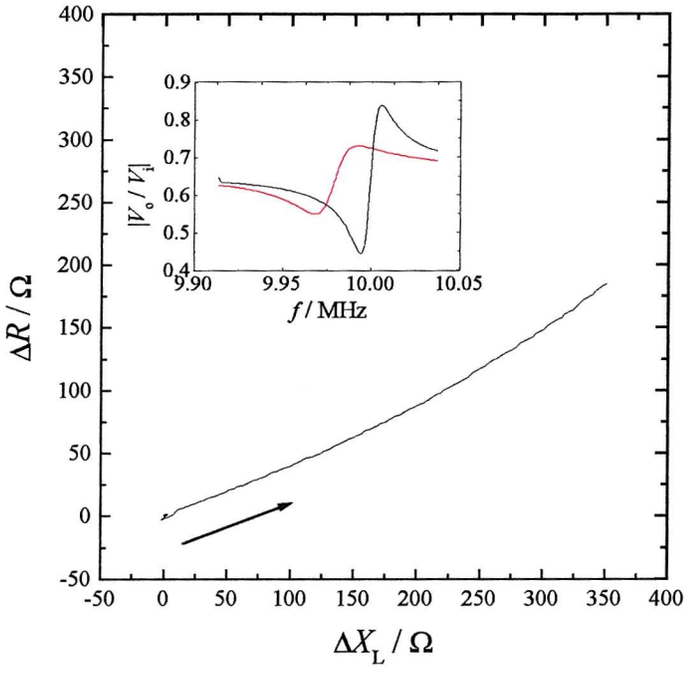

Figure 1.15: Parametric plot and inset transfer function of a viscoelastic material where R and X_L grow without any predefined relation. The transfer functions are calculated from equation (1.29) using the fixed values of C_m = 5.5 x 10^{-11} F and C_q = 3.36 x 10^{-14} F. The resonant frequency on the transfer functions is shifted and broadening. The transfer function in black is for a bare quartz crystal and the one in red after the deposition of a viscoelastic material.

1.3. Overview of this thesis

In this chapter the importance of conducting polymers has been illustrated. In order to improve the performance of possible devices, the redox mechanism of the conducting polymers should be better understood. The principle of the Electrochemical Quartz Crystal Microbalance was described. We commented on the piezoelectric effect of the quartz crystal, the possibility of analysing the mechanical parameters of the oscillating quartz crystal and its load as an electrical equivalent circuit, and the transfer function method applied to the interpretation of the EQCM measurements. In this thesis, we investigate whether the Electrochemical Quartz Crystal Microbalance combined with

the Scanning Electrochemical Microscopy offers a suitable way of analysing conducting polymers during the electrochemical deposition and redox reactions.

The chemicals and the equipment used in this project are described in Chapter 2. Also the QCM instrumentation is explained in more detail there.

As the conducting polymers possess complex redox mechanism, we start the studies of the Electrochemical Quartz Crystal Microbalance in Chapter 3 with simpler cases, such as the deposition of a thin layer of a silver metallic film and the effects of sucrose solutions at different concentrations. These materials represent respectively perfectly elastic solids and perfectly viscous liquids, which simplifies the interpretation of the EQCM data.

In Chapter 4 a highly hydrophilic polymer is analysed. This is not a straightforward case because equation (1.29) cannot be simplified and from two experimental values, four variables are generated. Therefore, the use of mathematical fitting is necessary for the calculation of the mass and viscoelastic changes at the polymer. In this chapter, we conclude that viscoelastic polymers should be avoided if one is exclusively interested in the calculation of changes in mass.

Finally, in Chapter 5, the Electrochemical Quartz Crystal Microbalance is used to monitor changes in mass and viscoelasticity of conducting polymer films during electrodeposition. The poly(aniline) films are polymerised on the presence of poly(vinylsulfonate) and poly(styrenesulfonate) counterions. The polymer film that behaves as an elastic solid was chosen for further analysis during redox cycles in strong acids described in Chapter 6. The Scanning Electrochemical Microscopy is coupled with the Electrochemical Quartz Crystal Microbalance to obtain more information about the electrochemical process.

In the final Chapter **Fehler! Verweisquelle konnte nicht gefunden werden.** the final conclusions are summarised.

2. Experimental Methods

2.1. Chemicals

All solutions were prepared using deionised water (Whatman 'STILLplus' system coupled to a Whatman RO 50) of 18 MΩ cm resistivity.

Silver nitrate (general purpose reagent, BDH), potassium nitrate (AR grade, Fisons) and sucrose (AR grade, M&B), poly(vinylsulfonic acid, sodium salt) (tech., 25 wt. % solution in water, Aldrich), poly(sodium 4-styrenesulfonate) (average M_W *ca.* 70,000, Aldrich), Amberlyst® 15 ion-exchange resin (Aldrich), perchloric acid (70%, ARISTAR grade, BDH), hydrochloric acid (ARISTAR grade, BDH), sodium chloride (ARISTAR grade, BDH) and sodium perchlorate (AnalaR grade, BDH) were used as purchased.

The viscoelastic polymers provided by Biocompatibles Ltd (Farnham Business Park, Weydon Lane, Farnham, GU9 8QL, UK) were used as received.

Aniline (99.5%, BDH) was distilled under vacuum prior to use and stored in the fridge at 4 °C under argon.

2.2. Electrochemical Cell

The cell body is made of Teflon® with the quartz crystal placed at the bottom of the cell. There is a Luggin capillary that places the reference electrode located inside the wall of the cell at a constant close distance to the working electrode.

A three-electrode cell was used (see Figure 2.1). The working electrode was the upper gold layer of the quartz crystal, the counter electrode was a platinum wire and the reference electrode was a saturated calomel for all the experiments except for the deposition of silver, where a Ag/0.01 M $AgNO_3$ reference electrode was used.

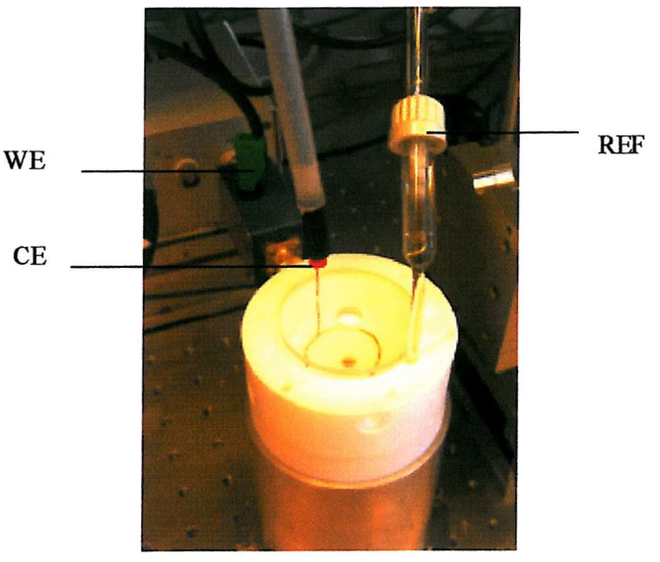

Figure 2.1: Electrochemical cell formed by the SCE reference electrode (REF), platinum counter electrode (CE) and the gold layer on the quartz crystal at the bottom of the cell as working electrode (WE).

The cell was thermostatted at 25.0 ± 0.5 °C with a water bath during the experiments of the hydration of the viscoelastic polymers. The other experiments were carried out at room temperature (15 to 25 °C).

The solutions were regularly purged with argon and kept under an argon blanket during the experiments of the conducting polymers.

Unpolished, gold-coated AT-cut 10 MHz quartz crystals (International Crystal Manufacturing Company Inc., Oklahoma City, USA) 14 mm diameter, 165 μm thick (Figure 1.5) were sealed between two O-rings and formed the bottom of the cell made of Teflon. The crystals are used as received. The layer of gold is 100 nm thick. The mass sensitive area of the quartz crystal, A_m, is the area where the gold electrodes on both surfaces of the quartz crystal overlap each other (A_m = 0.20 cm^2). This circular area vibrates with an applied alternating voltage. The electroactive area, A_e, is the area of gold exposed to the electrolyte, which is delimited by the O-ring (A_e = 0.22 cm^2). The O-ring must not touch the mass sensitive area of the quartz crystal, as it would affect the resonant frequency of the crystal. The gold electrode on the crystal is the common ground both for the ac circuit (QCM) and the dc circuit (potentiostat). The quartz crystals are used without any pre-treatment.

A 10 μm diameter platinum electrode was used in the Scanning Electrochemical Microscopy experiments. The microelectrode was modelled in a cone shape, initially using wet/dry paper (CC-400, Silicon Carbide) and then lapping film sheets (3M). The

tip was polished with alumina (0.3 μm, Buehler). The microelectrode was rinsed with deionised water very carefully before the experiments to remove any particles of alumina remaining in contact with the platinum.

2.3. Instrumental techniques

2.3.1. QCM

The QCM experiments were realised using the transfer function method described by Calvo[39] with instrumentation built to our specification in the workshop of the Institute of Sound and Vibration of the University of Southampton. A simple diagram of the QCM is shown in Figure 2.2. An alternating voltage, V_i, with constant amplitude is applied over a range of frequencies controlled by a voltage-controlled oscillator. The range of frequency is 0.1 MHz for a voltage scan from –5 V to +5 V (the maximum range permitted by the DAQ card). The voltage output, V_o, is generated from the oscillation of the quartz crystal.

The voltage output is in the same range of frequency as the voltage input. The input and output voltages both run through diodes being filtered, amplified and measured by an analogic/digital converter.[35] The Schmitt Trigger was used to synchronise measurements between the QCM and the potentiostat for the EQCM measurements. The frequency range of the QCM is defined by the voltage ramp [66] generated by a DAQ Board PC-MIO-16XE-10 from National Instruments (Austin, TX, USA) in a Personal Computer with an AMD K6 233 MHz processor running under Windows 95. The same board acquires the input and output voltages from the rectifier. Counters on two DAQ boards PC-MIO-16XE-10 were necessary for frequency baseline measurements. The minimum and maximum frequencies are measured at the beginning of each measurement and the maximum frequency is measured frequently during the experiments to correct any drift in frequency that occurs in the voltage controlled oscillator. The variation in the maximum frequency during EQCM measurements due to drift of the oscillation is of the order of 10 Hz (1 part in 10^6).

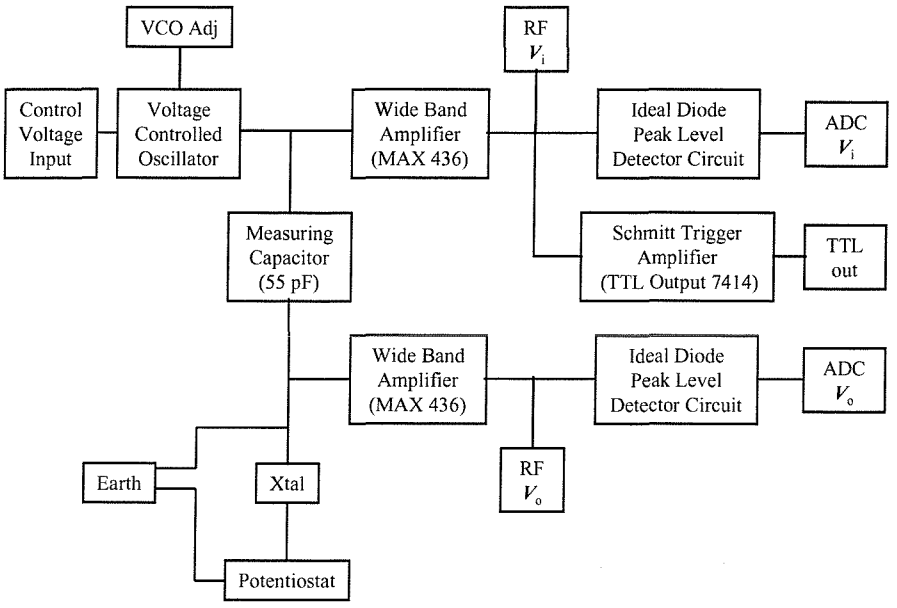

Figure 2.2: EQCM diagram Block

The data obtained by the QCM measurements is plotted in the form of a transfer function, see Chapter 1 Figure 1.13, Figure 1.14 and Figure 1.15. Once the experiment is finished, the analytical expression of the transfer function modulus, equation (1.29), is fitted to calculate the electrical parameters of the BVD equivalent circuit of the quartz crystal and the non-piezoelectric layer deposited on it.[39] The real and the imaginary components of the quartz crystal's electroacoustic impedance, R and X_L, are obtained from the non-linear least squares fitting program for equation (1.29) written in Quick Basic 4.5 by Etchenique[35] and it can be seen in Appendix 8.3.

2.3.2. Electrochemistry

The potential of the substrate (gold electrode) and the microelectrode were controlled by a homebuilt bipotentiostat with grounded working electrode. The bipotentiostat is fully computer controlled via a DAQ board PC-MIO-16XE-10 (National Instruments). The computer board generates the potential waveforms and acquires the data (current) from the substrate and the microelectrode. The computer programs were written in the G language with LabVIEW 5.1 (National Instruments).

2.3.3. Temperature Control

There is temperature control in the experiments described in Chapter 4. Water at 25 °C comes from a water bath to a glass coil placed inside the electrochemical cell. A thermistor (Radio Spares) positioned at the centre of the coil registered changes in the temperature inside the cell smaller than 1 °C during the 1.5 h of experiment. The water level in the cell was maintained high enough to keep the thermostat coil totally immersed to ensure good temperature control.

2.3.4. Scanning Electrochemical Microscopy

The positioner for the Scanning Electrochemical Microscopy microelectrode was controlled by a Model 6000 ULN Series Ultra Low Noise Inchworm Controller (Burleigh Instruments, Fishers, NY). The mechanical resolution of the driven stage for the *z* axis is 4 nm. The Inchworm controller was also commanded by LabVIEW.

2.3.5. Scanning Electron Microscopy

The SEM pictures were taken on the Environmental Scanning Electron Microscope XL30, Phillips, at the Department of Chemistry of the University of Southampton.

2.4. Software - LabVIEW

The EQCM is controlled by LabVIEW® software. LabVIEW is a program development application,[86] much like C or BASIC. It uses a graphical programming language G to create programs in block diagram form. LabVIEW programs are called virtual instrument (VI), because their appearance and operation imitate the instruments used in the laboratory. A VI consists of an interactive user interface, a dataflow diagram that serves as the source code, and icon connections that allow the VI to be called from higher level VIs. This program structure provides significant versatility for the EQCM experiments. The software control the equipments via the cards of National Instrument (PC-MIO-16XE-10).

Details of the program used to control and acquire the QCM data is given in the Appendix 8.7. The program can register one transfer function in 0.25 s for 100 frequencies around the resonant frequency of the quartz crystal, 10 MHz, detecting most of the changes occurred during fast electrochemical reactions.

3. QCM Analysis of Elastic Solids and Viscous Liquids

The parametric plots for the growth of a thin layer of an elastic material and for Newtonian liquids at different concentrations were shown in Chapter 1. In these two cases, equation (1.21) is considerably simplified and the relevant mechanical changes of these materials can be easily calculated.

$$Z_e(\omega) = R + iX_L = \left(\frac{2\omega_0 L_q}{\pi \sqrt{\mu_q \rho_q}} \right) \sqrt{\rho_i (G'_i + iG''_i)} \tanh \left[i\omega_0 d_i \sqrt{\frac{\rho_i}{G'_i + iG''_i}} \right] \qquad (1.21)$$

In the QCM measurements the mechanical changes of the load of the quartz crystal are determined from the experimental results, R and X_L. But there are four parameters, the density, ρ_i, elasticity, G'_i, viscosity, G''_i, and thickness, d_i, to be extracted from the two values obtained experimentally. In general there are not singular values, but several that fit four unknown parameters from two values in an equation. In the analysis of a thin layer of a rigid material, for which $d \to 0$ and $G'' \to 0$, and of a Newtonian liquid, for which $G' \to 0$ and $d \to \infty$, two parameters are fixed and the other two are easily obtained from the values of R and X_L. We discuss now in detail how these simplifications occur.

3.1. Thin layer of perfectly elastic solid

The oscillation of the quartz crystal works as a transverse force applied in the load on the surface of the crystal. Solids and liquids differ in behaviour when an external stress is applied on them. When a transverse force is applied to a perfectly elastic solid, there is a proportional deformation in the material as shown in Figure 3.1. For an applied shear stress, σ, a proportional shear strain, γ, is obtained.

$$\sigma = S\gamma \qquad (3.1)$$

where the proportionality constant, S, is the stiffness of the material and its inverse is the compliance, c. The shear stress, σ, is defined as the applied transverse force per unit area. The shear strain, γ, is defined as the displacement per unit distance.[87]

Figure 3.1: Transverse force applied on an elastic solid of length x causing a deformation Δx between the surface before and after the applied force.

For a perfectly elastic solid the energy gained from the applied force is stored during the deformation and reused on the recovery of the initial shape of the material. A perfectly elastic solid can be mechanically represented as a massless spring.

Equation (1.21) is simplified in the case when a thin layer of a perfectly elastic film is deposited on the quartz crystal. A layer loaded on the quartz crystal is considered acoustically thin when the penetration depth of the shear wave, δ, (equation (1.9)) is much bigger than the thickness of the layer. For acoustically thin films, the thickness is considered to be close to zero, $d_i \rightarrow 0$, or $d_i \langle\langle \delta$. Substituting δ for a viscoelastic material[42]:

$$d_i \langle\langle \frac{1}{\omega_o}\sqrt{\frac{G_i}{\rho_i}} \tag{3.2}$$

As consequence the term $\left(i\omega_o d_i\sqrt{\frac{\rho_i}{G'_i+iG''_i}}\right)$ of equation (1.21) is very small, i.e. $\left(i\omega_o d_i\sqrt{\frac{\rho_i}{G'_i+iG''_i}}\right) \langle\langle (1+i)$ and $\tanh\left[i\omega_o d_i\sqrt{\frac{\rho_i}{G'_i+iG''_i}}\right] \approx \left[i\omega_o d_i\sqrt{\frac{\rho_i}{G'_i+iG''_i}}\right]$. By applying these approximations in equation (1.21), we obtain

$$Z_e(\omega) = \left(\frac{2\omega_o L_q}{\pi\sqrt{\mu_q \rho_q}}\right) i\omega_o \rho_i d_i \tag{3.3}$$

Note that equation (3.3) does not have a real part. For thin layers of elastic materials the real part, ΔR, equals zero. From the value of the imaginary part, ΔX_L, the mass of the film, m_i, deposited on the quartz crystal can be calculated, since $\rho_i d_i = m_i / A_m$.

$$\Delta X_{\mathrm{L,Sauer}} = \left(\frac{2\,\omega_{\mathrm{o}}\,L_{\mathrm{q}}}{\pi \sqrt{\mu_{\mathrm{q}}\,\rho_{\mathrm{q}}}} \right) \omega_{\mathrm{o}}\,\frac{\Delta m_{\mathrm{i}}}{A_{\mathrm{m}}} \tag{3.4}$$

ΔX_{L} is named $\Delta X_{\mathrm{L,Sauer}}$ because equation (3.4) is the Sauerbrey equation (1.6)

$$\Delta f_o = -\frac{2 f_o^2\,\Delta m}{A_{\mathrm{m}}\sqrt{\mu_q \rho_q}} \tag{1.6}$$

with the following substitutions:

$X_{\mathrm{L}}=2\,\pi f_{\mathrm{o}} L$ and since what is obtained from the QCM measurements is the changes in L and not in f, $\Delta X_{\mathrm{L}}=2\,\pi f_{\mathrm{o}}\,\Delta L$. From equation (1.23), $\Delta L = -\frac{\Delta f_{\mathrm{o}}\,2\,L_q}{f_{\mathrm{o}}}$. By combining the last two equations, we get $\Delta X_{\mathrm{L}}= -\Delta f_{\mathrm{o}}\,4\,\pi\,L_{\mathrm{q}}$, which is the constant that relates the Sauerbrey equation (1.6) to equation (3.4), remembering that $\omega_{\mathrm{o}}=2\,\pi f_{\mathrm{o}}$. From the comparison of these two different forms of Sauerbrey equations we can conclude that the changes in the inductance measured by the QCM, ΔX_{L}, are the same as the changes in the resonant frequency of the quartz crystal, Δf_{o}, multiplied by a constant, $4\,\pi\,L_{\mathrm{q}}$.

The viscosity of perfectly elastic materials is considered to be close to zero, so the elasticity is much bigger than the viscosity, $G'>>G''$, so that the variable $\boldsymbol{G}_{\mathrm{i}}$ has only a real part, $\boldsymbol{G}=G'$. Note that the simplified equation (3.3) from where the Sauerbrey equation, (3.4), is derived was obtained with the single assumption that the material analysed is acoustically thin. It can be observed from equation (3.2) that for the maintenance of the validity of the Sauerbrey equation, the thickness of the material for which this analysis is valid depends on its elasticity and density. A material with high elasticity and low density will obey the Sauerbrey equation to a greater thickness than materials without these properties.

3.2. Perfectly viscous liquid

When a force is applied to a perfectly viscous liquid (or Newtonian liquid), the stress causes a proportional movement in the adjacent liquid. The energy gained from the applied force is completely lost in the form of heat that is dissipated with the flow of

the liquid.[87] For a small stress on the material, Newton's law is obeyed and a proportional rate of strain is sensed,

$$\sigma = \eta \frac{d\gamma}{dt} \tag{3.5}$$

The proportionally constant is called the coefficient of viscosity, η.

A liquid must fulfil some requirements to be considered Newtonian, or perfectly viscous; specifically the shear viscosity should not vary with the shear rate, the viscosity should be constant and independent of the duration of stirring and the stress should cease immediately after the stimulation is stopped. The viscosity of Newtonian liquids decreases with an increase in temperature following the Arrhenius equation,[88]

$$\eta = A\mathrm{e}^{-B/T} \tag{3.6}$$

where T is the absolute temperature and A and B are constants for the liquid.

The viscosity of most materials (non-Newtonian materials) is very dependent on the shear rate, duration of shearing, temperature and pressure. In addition, the process of stirring can produce enough heat to change the viscosity of the liquid. A viscous liquid can be mechanically represented as a dashpot.

The thickness of liquid in contact with the quartz crystal is much bigger than the penetration depth of the shear wave of the oscillating quartz, so the liquid can be considered infinitely thick, $d \rightarrow \infty$, or $d_\mathrm{i} \rangle\rangle \frac{1}{\omega_o}\sqrt{\frac{\boldsymbol{G}_\mathrm{i}}{\rho_\mathrm{i}}}$. The thickness of liquid that actually vibrates with the quartz corresponds to half of the penetration depth of the shear wave.[32] By applying this approximation in equation (1.21), the term $\left|\mathrm{i}\omega_o d_\mathrm{i}\sqrt{\frac{\rho_\mathrm{i}}{G'_\mathrm{i}+\mathrm{i}G''_\mathrm{i}}}\right| \rangle\rangle (1+\mathrm{i})$ and so $\tanh\left[\mathrm{i}\omega_o d_\mathrm{i}\sqrt{\frac{\rho_\mathrm{i}}{G'_\mathrm{i}+\mathrm{i}G''_\mathrm{i}}}\right] \approx 1$. Equation (3.7) is then obtained.

$$\mathbf{Z}_e(\omega) = \frac{2\omega_\mathrm{o} L_\mathrm{q}}{\pi\sqrt{\mu_\mathrm{q}\rho_\mathrm{q}}}\sqrt{\rho_\mathrm{i}\left(G'_\mathrm{i}+G''_\mathrm{i}\right)} \tag{3.7}$$

The elasticity of perfectly viscous liquids is considered to be zero, $G' \rightarrow 0$, because all the energy is lost in the flow of the liquid, so $G' << G''$ and $\boldsymbol{G} = G''$. The viscosity of Newtonian liquids is not influenced by the shear rate. The shear rate of a liquid close to the surface of the quartz crystal is determined by the angular frequency of the crystal,

ω. The viscosity of Newtonian liquids is represented as $\eta = G''/\omega$, and equation (3.7) can be further simplified to equation (3.8)

$$\mathbf{Z}_e(\omega) = \frac{2\omega_o L_q}{\pi\sqrt{\mu_q \rho_q}}\sqrt{\left(\frac{\omega_o}{2}\rho_i \eta_i\right)}(1+i) \qquad \textbf{(3.8)}$$

where the real and imaginary parts of the impedance have the same value.

The Kanazawa equation, (1.7), is one limiting case of equation (1.21) and it can be rewritten to correlate the product of the density, ρ_i, and viscosity, η_i, of the liquid in contact with the quartz crystal to the experimental values of R and X_L.

$$\Delta X_{L,Kan} = \Delta R_{Kan} = \frac{2\omega_o L_q}{\pi\sqrt{\mu_q \rho_q}}\sqrt{\left(\frac{\omega_o}{2}\Delta(\rho_i \eta_i)\right)} \qquad \textbf{(3.9)}$$

The density of the liquid contributes to the mass on the surface of the resonator, sensed by X_L. The viscosity provides an additional damping on the oscillation which is recognised by R.

3.3. Results

The limiting cases described above are demonstrated in the following experiments where the application of the proper equations to obtain the different relevant parameters is described. The electrochemical deposition of silver was used to demonstrate a thin layer of perfectly elastic solid and sucrose solutions at different concentrations were used as an example of a perfectly viscous liquid. The deposition of silver is understood to occur with 100 % faradaic efficiency and is therefore very suitable to test the experimental response of the EQCM.[39] The solutions of sucrose at different concentrations have their physical characteristics tabled in the literature, which is convenient to compare to the QCM measurements and check the response of the instrumentation and software. The error limits of the EQCM instrumentation can also be estimated from these experiments. The reproducibility of the experiments was also verified.

3.3.1. Thin layer of perfectly elastic solid

The QCM measurement of a potentiostatically deposited thin layer of silver film was used as an example of a perfectly elastic material.[39,46] The cell was filled with a solution of 0.01 M of $AgNO_3$ in 0.1 M KNO_3. The cell was purged with argon for 3 min. The electrode potential is held at 0.1 V *vs.* $Ag/AgNO_3$ for 5 s, stepped to –0.1 V and maintained for 280 s.

The parametric plot representing the growth of the metallic silver film is shown in Figure 3.2. This is the standard parametric plot for a perfectly elastic thin film, where ΔR is close to zero and the mass can be calculated directly from ΔX_L. The small variation in R ($\approx$ 10 Ω) is negligible.

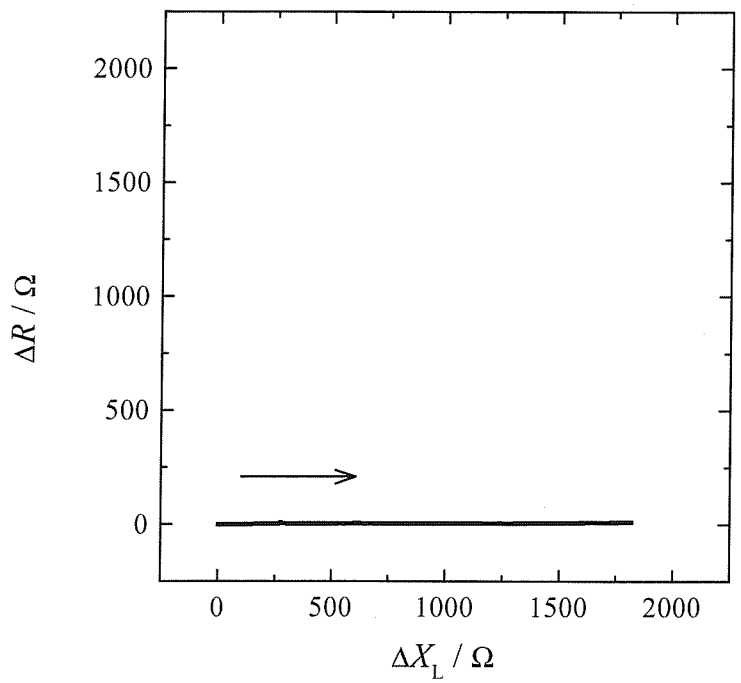

Figure 3.2: Parametric plot for the potentiostatically deposition of silver. For solution of 0.01 M of $AgNO_3$ in 0.1 M KNO_3 with potential held at 0.1 V *vs.* $Ag/AgNO_3$ for 5 s, stepped to –0.1 V and maintained for 280 s. Total charge of 67.27 mC cm^{-2} was passed during deposition.

The values of ΔR and ΔX_L were calculated by subtracting the values of R and X_L obtained during the electrochemical deposition from the values of the quartz crystal

covered with electrolyte solution before the beginning of the silver deposition. This subtraction can be done because additivity is obeyed in the case of thin rigid layers.[28,38]

In this case, where ΔR is close to zero, the mass of the film deposited on the quartz crystal can be calculated by using equation (3.4). The experimental value of ΔX_L for the deposition of silver metal was 1820 Ω, which gives a calculated mass for the deposited film of 75.9 μg cm^{-2}. The good response of the EQCM measurements and the software used can be verified by comparing the values of the masses obtained from the Sauerbrey equation (QCM measurements) and from the Faraday law (electrochemically).

The mass of silver calculated from the charge passed during the electrodeposition of the film, by assuming that the deposition occurred with 100 % efficiency, and applying Faraday's law

$$\frac{Q}{A_e} = \frac{n F N}{A_m} \qquad \textbf{(3.10)}$$

where Q/A_e is the charge consumed during deposition divided by the electroactive area[a], N/A_m is number of moles of silver deposited per mass sensitive area (MW_{Ag} = 107.868 g mol^{-1}), n is number of electrons involved in the reduction (1), and F is the Faraday constant (96484 C mol^{-1}).

The value calculated for the mass of silver deposited with a charge of 67.27 mC cm^{-2} was 75.2 μg cm^{-2}. There is 0.9 % discrepancy (standard deviation=0.089 μg cm^{-2} [b]) between the masses obtained from QCM measurements and from the potentiostatic deposition. The small difference might have occurred because the deposition does not happen with 100 % efficiency or the value of A_e can be slightly different form the estimated or even the error in the instrumentation can be considered to be close to 1 %.

---

[a] The difference of the electroactive area A_e and mass sensitive area A_m of the quartz crystal has to be considered because the electroactive sensitive area is delimited by the O-ring that seals the crystal and it is about 10% bigger than the mass sensitive area of the quartz, which consists of the area of the two circular electrodes that overlap each other.

[b] The standard deviation is calculated from the equation $\sqrt{\frac{1}{n-1}\sum_{i=1}^{n}(x_i - \bar{x})^2}$, where n is the size of the sample and $\bar{x}$ is the mean.

3.3.2. Perfectly viscous liquid

Sucrose solutions at different concentrations were used to exemplify the QCM measurements for Newtonian liquids. The solutions were prepared by weight according to Table 3.1,[39] in which the value of the square root of the product of the density and the viscosity are given.

Table 3.1: Square root of the product of the viscosity and the density for sucrose solutions at different concentrations at room temperature.[89]

Sucrose concentration (%)	$(\rho_i \eta_i)^{1/2}$ / kg m^{-2} s$^{-1/2}$
0.00	0.975
11.10	1.168
16.50	1.300
21.55	1.481
25.21	1.628
26.80	1.700
31.90	1.979
36.40	2.303

The parametric plot in Figure 3.3 shows linear behaviour for the solutions at different concentrations of sucrose. It is a standard parametric plot for a Newtonian liquid, where ΔR is equal to ΔX_L, and the experimental values of the viscosity and density can be calculated from equation (3.9). All the values of R and X_L are normalised by subtracting them from the values obtained from the QCM measurement of the dry quartz crystal.

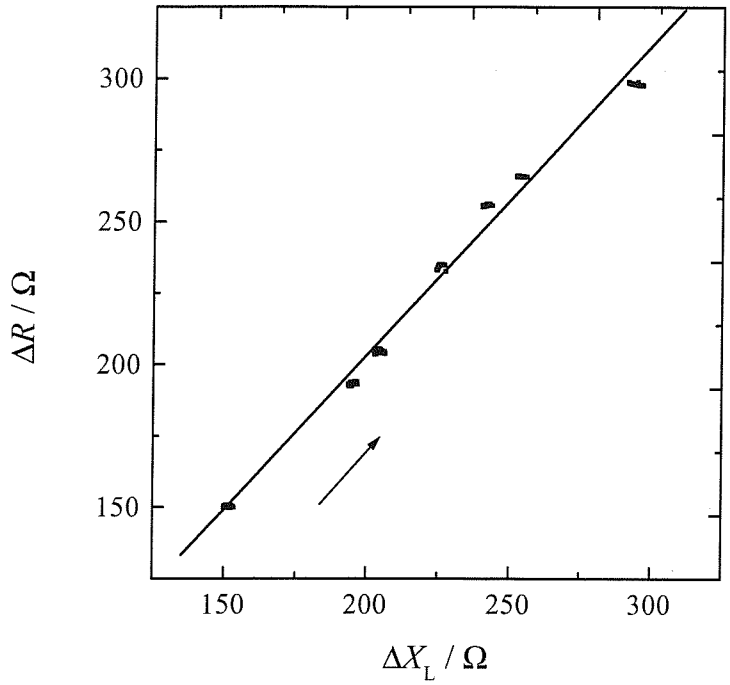

Figure 3.3: Parametric plot for solutions at different concentrations of sucrose at room temperature. The concentrations of the solutions are, from the left to right, 0 %, 11.10 %, 16.50 %, 21.55 %, 25.21 %, 26.80 % and 31.90 %. The measurement of each solution lasts 1 min with one point per second.

In Figure 3.4 the experimental and the theoretical values of the product of the density and viscosity for the solutions at different concentrations of sucrose are compared. The experimental values are obtained by applying the values of R and X_L in equation (3.9) and the theoretical values are obtained from Table 3.1. A very good agreement is obtained between the theoretical and the experimental values. The QCM experiments presented very good reproducibility on the measurements of sucrose solutions.

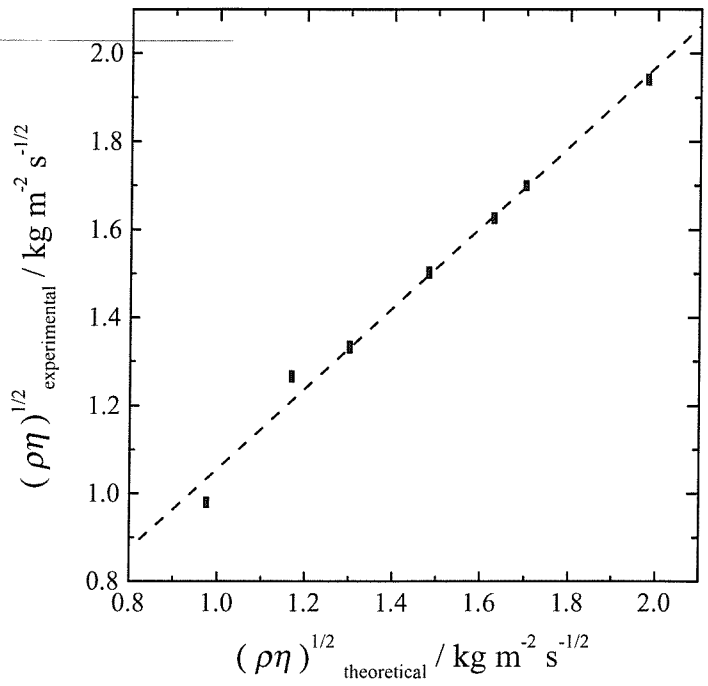

Figure 3.4: Experimental values of product of viscosity and density of sucrose solutions at different concentrations calculated by Kanazawa equation as a function of theoretical values given in Table 3.1. The concentrations of the solutions are, from the left to right, 0 %, 11.10 %, 16.50 %, 21.55 %, 25.21 %, 26.80 % and 31.90 %.

3.4. Conclusion

In this chapter we have demonstrated how to interpret the results of the EQCM experiments for the two limiting cases: mass of a thin layer of an elastic solid and the value of density and viscosity of a Newtonian liquid.

The first step is to look at the parametric plot. If the parametric plot consists of a horizontal line, the material analysed is a thin layer of an elastic solid, and the change in mass can be calculated using the following equation:

$$\Delta X_{\text{L,Sauer}} = \left(\frac{2\,\omega_o\, L_q}{\pi \sqrt{\mu_q\, \rho_q}} \right) \omega_o \frac{\Delta m_i}{A_m} \tag{3.4}$$

If the parametric plot consists of a 45° line, the material analysed is a Newtonian liquid and the change in the product of its density and viscosity can be extracted using

$$\Delta X_{\mathrm{L,Kan}} = \Delta R_{\mathrm{Kan}} = \frac{2\omega_{\mathrm{o}} L_{\mathrm{q}}}{\pi\sqrt{\mu_{\mathrm{q}}\rho_{\mathrm{q}}}}\sqrt{\left(\frac{\omega_{\mathrm{o}}}{2}\Delta(\rho_{\mathrm{i}}\eta_{\mathrm{i}})\right)} \tag{3.9}$$

The EQCM measurements showed very good response on the analyses of both the perfectly elastic solid and the Newtonian liquid. For a perfectly elastic solid, the mass of the material electrochemically deposited on the quartz crystal was calculated using the Sauerbrey equation and compared to the mass obtained from the charge passed during the electrochemical deposition, assuming 100 % efficiency of deposition. For Newtonian liquids the values of the product of viscosity and density were obtained by QCM measurements and compared to values tabled in the literature.

In the next chapter we explain the difficulties in analysing changes in mechanical parameters of viscoelastic films, when equation (1.21) cannot be simplified and there are four variables to be estimated, ρ, d, G' and G'', from two experimental values, R and X_{L}.

4. QCM Analysis of Viscoelastic Polymers

4.1. Viscoelastic Materials

In reality, most materials are neither perfectly elastic solids nor perfectly viscous liquids. Polymer films, behave somewhere in between elastic solids and viscous liquids due to their chain-like structure. They are examples of viscoelastic materials. If the material in Figure 3.1 is viscoelastic, the block does not regain its original shape once the force is removed. Part of the energy gained from the stress applied is used to restore its initial form, but part of the energy is lost in the form of heat.[68]

Figure 3.1: Shear stress, σ, applied to a solid of length x causing a deformation Δx between the surface before and after the applied force.

A popular way of investigating viscoelastic materials is to apply a small-amplitude oscillatory dynamic test, which involves the use of a harmonically varying shear strain.[88] The Quartz Crystal Microbalance is a dynamic method that can be used to analyse the linear viscoelastic behaviour of polymers.[90] Linear viscoelastic behaviour is obtained when the strain and rate of strain are infinitesimal. A constant sinusoidally time-varying force is applied to the polymer at different frequencies. For viscoelastic materials, the response will be an out of phase sinusoidal signal. For a small deformation, Δx, a shear stress, σ, produces a proportional shear strain, γ. The proportionality constant is called the shear modulus, $\boldsymbol{G}$.[91]

$$\sigma = G\gamma \tag{4.1}$$

The shear modulus is expressed as a function of the angular frequency, ω, in complex notation.[88] (Complex notation is explained in Appendix 8.2.)

$$G(\omega) = G'(\omega) + i\, G''(\omega) \qquad (4.2)$$

where $G(\omega)$ is the frequency dependent complex shear modulus, $G'(\omega)$ is the real part in phase with the stress, $G''(\omega)$ is the imaginary part, out of phase with the stress. G' is the shear storage modulus and it is related to the elasticity of the polymer. G'' is the shear loss modulus and measures the viscosity of the polymer. The ratio G''/G' is represented by the loss tangent α which is a dimensionless quantity which is used as a measure of the internal friction of the polymer.

The two mechanical models, analogies of viscoelastic materials shown in Figure 4.1, although oversimplified, help in the understanding of the behaviour of polymer films.[87] The models consist in combinations of springs and dashpots. Springs have stiffness (force/displacement) corresponding to the shear elasticity, G_i'. And dashpots represent frictional resistance (force/velocity) analogous to the viscosity, G_i''.[87] More complicated models can be created by adding several springs and dashpots in series and parallel.

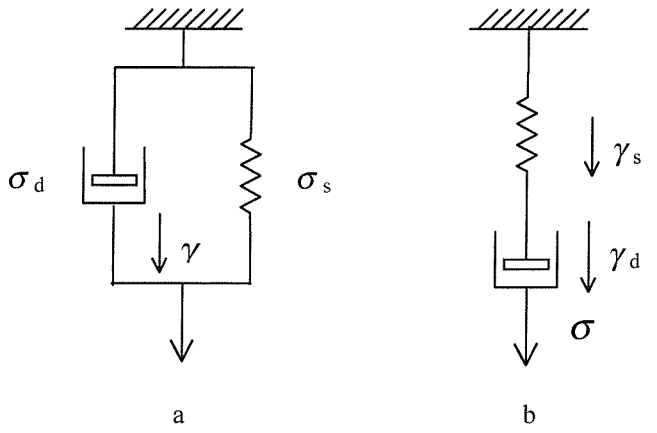

Figure 4.1: The simplest mechanical models analogous to a viscoelastic materials: a) the Voigt-Kelvin model; b) the Maxwell model. σ is the shear stress and γ is the shear strain. The subscripts d means dashpot and s stands for spring.

In the Voigt-Kelvin model the spring and the dashpot are in parallel. The stress, σ, is distributed between the two components and they experience the same strain rate, $\partial\gamma/\partial t$, at all times. The sum of the stress on the spring and on the dashpot is equal to the total stress on the system

$$\sigma_t = \sigma_s + \sigma_d \tag{4.3}$$

and the strain on the spring is equal to the strain on the dashpot.

$$\gamma_s = \gamma_d \tag{4.4}$$

where the subscript t means total, s spring and d dashpot.

For systems represented by the Voigt-Kelvin model equation (4.1) can be rewritten as[88]

$$\sigma = G'\gamma + \eta\left(\frac{\partial\gamma}{\partial t}\right) \tag{4.5}$$

where the viscosity, η, is frequency dependent, $\eta = G''/\omega$. The first term of the equation above indicates an elastic solid (3.1) and the second term corresponds to a viscous liquid (3.5).

If an initial stress is applied to a Voigt-Kelvin element, the system will eventually reach the proportional strain, γ, but the dashpot delays the process. The time of delay is called retardation time, τ_K. The Voigt-Kelvin model can be compared to a perfectly elastic solid, although the elastic solid reaches the equilibrium state 'instantaneously' while in the Voigt-Kelvin model the final strain is retarded as demonstrated in Figure 4.2a.

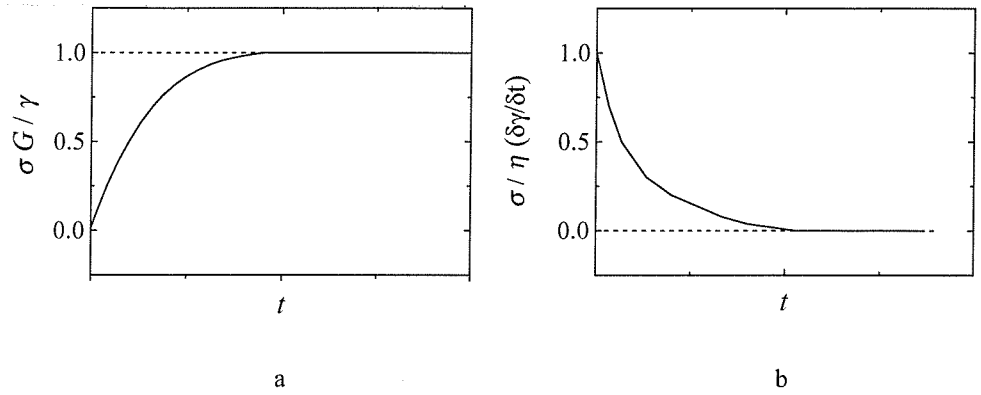

Figure 4.2: Viscoelastic models compared to ideal materials: a) the Voigt-Kelvin model: delay of the strain after a stress is applied before reaching the perfect elastic behaviour where $\sigma G / \gamma = 1$. b) the Maxwell model: after the strain stops there is a delay on the stress response. In a perfectly viscous liquid $\sigma / \eta\ (\partial\gamma / \partial t) = 0$ 'instantaneously'.

In the Maxwell model the spring (the elastic component) and the dashpot (the viscous component) are in series. The two components are under the same stress and respond with different strains that sum up to the total strain. The stress on the spring is the same as that applied to the dashpot

$$\sigma_s = \sigma_d \tag{4.6}$$

and the sum of the strains experienced by the spring and the dashpot results in the total strain

$$\gamma_t = \gamma_s + \gamma_d \tag{4.7}$$

For the Maxwell model the equation (4.1) can be represented as

$$(\partial\gamma / \partial t) = \frac{(\partial\sigma / \partial t)}{G'} + \frac{\sigma}{\eta} \tag{4.8}$$

If a continuous strain rate is suddenly removed from a Maxwell element, the initial stress will decrease exponentially from its equilibrium value to zero. The Maxwell model can be compared to a perfectly viscous liquid; although the viscous liquid reaches the equilibrium state 'instantaneously' while in the Maxwell model the

decay of the stress is delayed as shown in Figure 4.2b. The time of delay is called the relaxation time, τ_M.

The time dependent behaviour of the Voigt-Kelvin or Maxwell models can be easily associated with time dependent electrical circuits, where springs are represented by capacitors and dashpots by resistors.[87] In the Voigt-Kelvin model the electric parameters are in series and in the Maxwell model they are in parallel.

4.1.1. Influence of the frequency on the viscoelasticity of polymers

In the Voigt-Kelvin model, the storage modulus is not influenced by the frequency, $G'=\mu$, and the loss modulus is proportional to the frequency, $G''=\omega\ \eta$. On the other hand, for the Maxwell model, the storage modulus increases reaching a constant value of μ for frequencies bigger than τ^{-1}. The loss modulus reaches a peak at $\omega = \tau^{-1}$ and decreases again as shown in Figure 4.3, where:[68]

For the Voigt-Kelvin model

$G'(\omega) = \mu$

$G''(\omega) = \mu\,(\omega\tau) = \omega\eta$

$$\alpha = \frac{G''}{G'} = \omega\tau$$

For the Maxwell model

$G'(\omega) = \mu\,(\omega\tau)^2 / 1+(\omega\tau)^2$

$G''(\omega) = \mu\,(\omega\tau) / 1+(\omega\tau)^2$

$$\alpha = \frac{G''}{G'} = \frac{1}{\omega\tau}$$

where μ is the shear elasticity of the material.

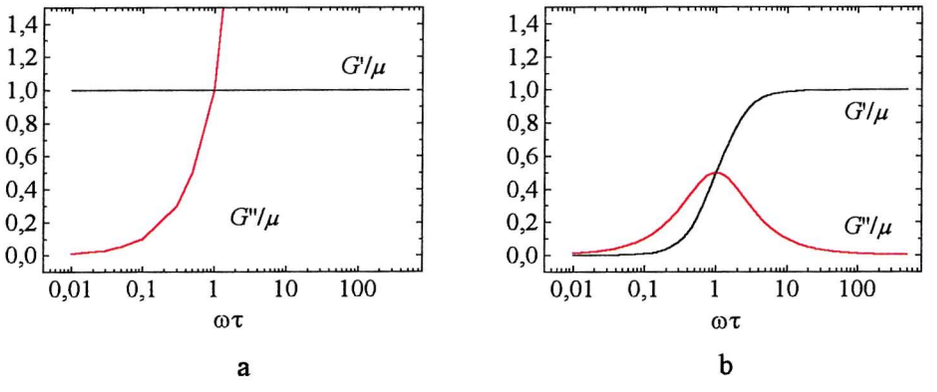

Figure 4.3: Frequency dependency of G' and G'' for a) Voigt-Kelvin model and b) Maxwell model.[87]

The viscoelasticity of polymer films is better described by the Maxwell model.[68,92] In the case of QCM measurements, the shear rate is determined by the frequency of the oscillation of the quartz (in our case 10 ± 0.05 MHz). When a relatively low frequency measurement is used ($\omega << 1/\tau$), the polymer is deformed slowly with the chains slipping past each other so that most polymers behave like viscous liquids ($G''>>G'$). If a relatively high frequency measurement is applied ($\omega >> 1/\tau$), the polymer chains have no time to reorient and all move together; the material behaves like an elastic solid ($G'>>G''$).[88] The transition at $\omega = 1/\tau$ is analogous to the zero-frequency glass transition.[92] The viscoelasticity of polymer films also varies widely depending on the temperature, pressure and the composition of the environment.

4.2. Polymer films containing phosphorylcholine (PC) groups

In this chapter, we analyse the viscoelastic and mass changes of polymers containing phosphorylcholine (PC) groups during hydration at constant temperature. Polymer films containing PC groups are used by Biocompatibles Ltd as haemocompatible coatings, for example on stents.[93] The PC coating mimics the biologically inert cell wall, and it is resistant to protein adsorption and cell interactions.[94] Phosphorylcholine is the head group of phosphatidylcholine, a major component of the extracellular side of membrane cells.[23] Cell walls are composed of various amphiphilic molecules. The phosphorylcholine molecules have one polar end and one apolar end as shown in Figure 4.4. In contact with water, the outer layer of the film is the hydrophilic part and the inner portion is hydrophobic. Molecules of water are strongly bound on the hydrophilic outer layer of the polymer. The PC coatings cover medical devices, that come in contact with blood and tissue, greatly reducing protein adsorption on the synthetic materials.[23] This is important because the adsorption of proteins on the surface of the material causes rejection from the body. The surface of the devices can be modified by coating a thin layer of hydrophilic polymer causing a decrease on the

adsorption of proteins from the blood. In addition to biocompatibility they also give a reduced coefficient of friction and enhance the manoeuverability of coated devices.

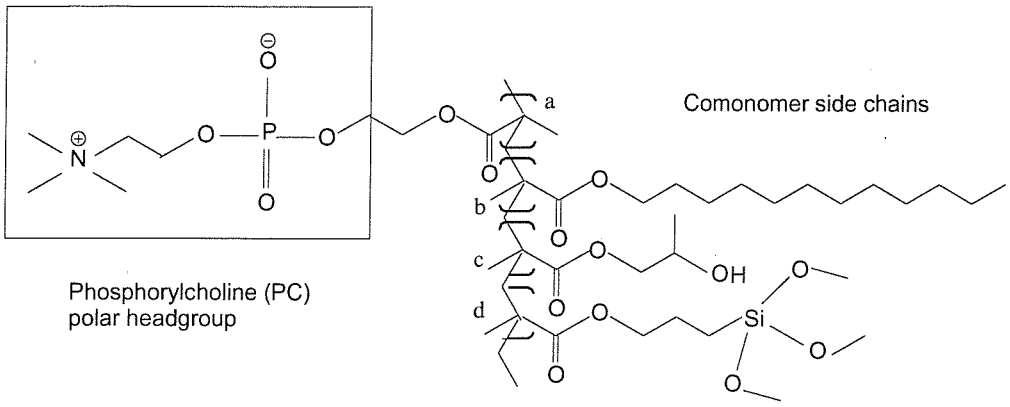

Figure 4.4: Chemical structure of the copolymer formed by: a) methacryloylphosphorylcholine (polar headgroup), b) laurylmethacrylate, c) 2-hydroxypropylmethacrylate, d) trimethoxysilylpropylmethacrylate, as cross-linker. The approximate mole fractions are 23 % for a, 47% for b, 25% for c and 5% for d.[95]

4.2.1. Modification on the rheology of polymers during hydration

Polymer films containing PC groups swell in contact with water. The balance between the tendency of the water molecules to percolate through the polymer structure and the propensity of the polymer structure to regain the previous form controls the amount of swelling. The swelling occurs by the diffusion of water molecules into the polymer structure. The rate of diffusion is determined by the facility of movement of the water molecules among the polymer chains.[96] The incorporation of water causes an expansion in the volume of the polymer. The deformability of the polymer depends on its elasticity.

The incorporation of solvent in polymer films causes a decrease in viscosity.[87] The solvent 'lubricates' the interaction between polymer chains by increasing the free volume and consequently decreasing the viscosity.

4.3. Experimental

The quartz crystal microbalance was used to measure changes in mass and viscoelasticity of hydrophilic polymer films of two different thicknesses during hydration at constant temperature and pressure. The quartz crystal microbalance is potentially a highly sensitive and yet inexpensive method for studying this process in real time.

The samples were prepared by Dr. Wang from Biocompatibles by casting a solution of the hydrophilic polymer containing PC groups shown in Figure 4.4 on a AT-cut, polished, gold coated 10 MHz quartz crystals. The solution was spread over the circular area of one of the gold electrodes of the quartz crystal, using a mixed solvent of ethanol and water. The circular area of the gold electrode is the mass sensitive area of the quartz crystal (see Figure 1.5). The polymer film covers only the mass sensitive area of the quartz crystal to avoid any inaccuracy in the QCM response due to interference between the polymer film and the "O"-ring used to clamp the quartz crystal in the cell.

The masses of polymer deposited on each crystal were approximately 10 μg and 15 μg, which corresponds to thicknesses of 0.50 μm and 0.75 μm respectively, since the density of the polymer is 1000 kg m^{-3} and the mass sensitive area of the quartz crystal is 2 x 10^{-5} m^2. The experiments were carried out for 1.5 h, starting by adding deionised water at 25 °C in the cell containing the polymer-coated quartz crystal. A glass coil connected to a thermostat bath was placed into the cell to maintain the temperature at 25 ± 0.5 °C throughout the experiments. A thermistor was positioned in the middle of the coil, above the quartz crystal, to record the temperature. The water level in the cell was maintained high enough to keep the thermostat coil totally immersed to ensure good temperature control. Care was taken to avoid air bubbles trapped on the surface of the polymer film, which would lead to misinterpretation of the results.

The viscoelastic properties of the polymer film, measured by R and X_L, are strongly dependent on the temperature. Preliminary measurements were performed to check the influence of the temperature on the QCM results. It was observed that during the first 1.5 h of the experiment, the changes in the physical properties of the film due to hydration are much larger than those due to variation in temperature. After 1.5 h the

changes in the polymer decreases considerably and small fluctuations in temperature influence the QCM measurements by masking the results. Therefore, the experiments are carried out for 1.5 h only.

4.4. Results and Discussion

Firstly we measure the electroacoustic impedance for the dry polymers containing PC groups of two different thicknesses. As it is shown in Figure 4.5 the values of ΔX_L and ΔR for sample a) dry are 346 Ω and 0 Ω respectively. For sample b) dry the corresponding values are 809 Ω and 35 Ω. The mass of the dry films can be obtained using the Sauerbrey equation because the values of ΔR are close to zero and the films can be considered as thin rigid layers. Sample a) has a mass of 2.89 μg and sample b) has a mass of 6.75 μg, which gives dry initial thicknesses of 0.14 μm and 0.34 μm respectively. These thicknesses are calculated from the values of the density of the dry polymer, 10^3 kg m^{-3}, and that the mass sensitive area of the quartz crystal, 2 x 10^{-5} m^2. The values of mass obtained by the QCM measurements are smaller than the expected values. The polymers were coated on quartz crystals at Biocompatibles Ltd and they were specified as being 0.50 and 0.75 μm thick. This difference could arise beacause of errors during the coating of the film due to experimental difficulties or as a result of the loss of part of the film during the transport and manipulation of the samples. In the following we adopt the values of the thicknesses obtained by the QCM measurements in order to be consistent in our analysis of the results.

There is a big change in the values of X_L and R for the two films between the dry polymer and the beginning of hydration. This change happens in 3.1 s, which is the time between each measurement. Immediately after water was poured on the dry polymer films, the values of X_L and R increase equally, which corresponds to the Kanazawa approximation for a Newtonian liquid (in this case water), and these changes in the parametric plot is shown by the arrows in Figure 4.5. There is also a rise in X_L proportional to the dry mass (dashed line in Figure 4.5). The increase in X_L is 96 Ω (or 0.80 μg) for sample a) and 279 Ω (or 2.32 μg) for sample b). The calculation of mass was made by applying the Sauerbrey equation since the parameter R, and consequently

the viscoelasticity of the films are assumed to remain constant during this instantaneous process. This increase in X_L might be accounted for by a fast process (faster than 3.1 s) such as water being rigidly trapped in the structure of the polymer film. This increase in mass is proportional to the dry thickness of polymer films and it corresponds to a 28 and 34 % increase in original mass.

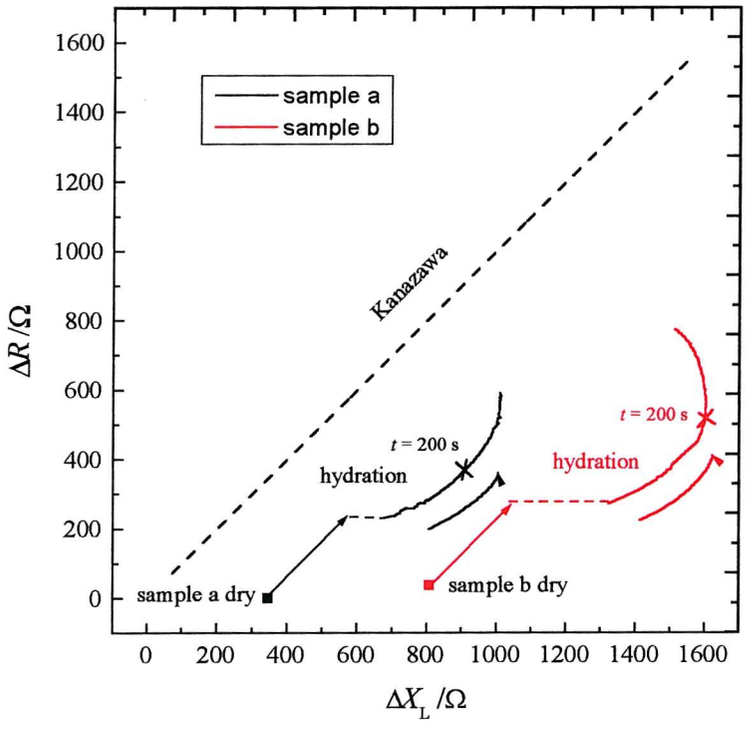

Figure 4.5: Parametric plots during hydration of viscoelastic polymer films containing PC groups at 25 °C for 1.5 h. Time follows the direction of the arrows. The experimental dry initial thicknesses of the samples are: sample a) 0.14 μm and sample b) 0.34 μm (calculated by applying Sauerbrey equation and assuming the density of the polymer is 10^3 kg m^{-3}). The measurements are done every 3.1 s.

The values of ΔX_L and ΔR during hydration account for the modification in the physical parameters of the polymer films. These values are obtained by subtracting the values of X_L and R during the experiments from the values previously measured for the respective bare quartz crystals. As we can see in Figure 4.5 the parametric plots during the hydration of the polymer films containing PC groups of two different thicknesses differ significantly from the two limiting cases presented in Chapter 3. Although viscoelastic materials have properties of both elastic solids and viscous liquids, the

analysis of the data cannot be made using either the Sauerbrey or the Kanazawa equations.

The hydration of the polymer films is qualitatively reproducible for films of same thicknesses although there is a small discrepancy in the quantitative results, which could be caused by irregularity on the polymer surface.

The approximation of additivity (Section 1.2.5) cannot be applied to evaluate the physical changes in the polymer films during hydration because during swelling the conditions of a thin and rigid film are not satisfied. The complete equation for the electroacoustic impedance of two layers deposited onto the quartz crystal is obtained by combining equations (1.12), (1.13) and (1.15):

$$Z_e(\omega) = R + iX_L = \left(\frac{2\omega_0 L_q}{\pi\sqrt{\mu_q \rho_q}}\right) \frac{\sqrt{\rho_1(G'_1 + iG''_1)}\tanh\left[i\omega_0 d_1\sqrt{\frac{\rho_1}{G'_1+iG''_1}}\right] + \sqrt{i\rho_2 G''_2}}{\frac{\sqrt{i\rho_2 G''_2}}{\sqrt{\rho_1(G'_1+iG''_1)}}\tanh\left[i\omega_0 d_1\sqrt{\frac{\rho_1}{G'_1+iG''_1}}\right]+1} \qquad \textbf{(4.9)}$$

where the subscript 1 stands for the viscoelastic polymer and the subscript 2 corresponds to the water.

The two experimental values generated from the QCM measurements during hydration, R and X_L, produce four variables for the polymer films: the density, ρ_1, the thickness, d_1, the elasticity, G'_1, and the viscosity, G''_1.[23] The parameters for water are known: $\rho_2 = 10^3$ kg m^{-3} and $G''_2 = 6.3 \times 10^4$ kg m^{-1} s^{-2}. Some assumptions about the polymer must be made for the estimation of the four unknown parameters. Two variables are kept constant while the variations in the other two are calculated. The choice of the variables to remain constant depends on the characteristics of the material analysed and the experimental conditions. In order to evaluate this complex mathematical equation a software program was developed by M. Otero and E. Calvo using Mathematica® software.[36]

4.4.1. Mathematical fitting

Two variables were held constant during the evaluation of the other two variables. In the case of the hydration of the polymer films containing PC groups, the density, ρ, was kept constant since both the dry polymer and water have densities of 10^3 kg m^{-3}.

Therefore the density of the polymer can be assumed to be constant throughout the hydration. The films are expected to swell in contact with water because the polymer is hydrophilic and absorbs water, increasing the thickness, d, of the film. Therefore d is expected to increase as the polymer films absorb water and swell. The changes in G' and G'' cannot be predicted a priori. Dr. J. H. Wang from Biocompatibles Ltd supplied information about the rheology of the polymer studied here. This polymer in ethanol at 63% (wt.) has similar physical properties as the swollen films on the quartz crystal. An oscillation technique employing an applied torque of 10-100 μN m was used to measure the elastic modulus, G', which results in a value of 300 Pa for the swollen polymer film. On a preliminary mathematical fitting using equation (4.9) ρ_1 was held at 10^3 kg m^{-3} and G'_1 at 300 Pa during the evaluation of the parameters d_1 and G''_1. The value obtained for G''_1 were at the range of MPa, i.e. G''_1 is 10^4 times bigger than G'_1 during the hydration of the polymer. As a result the precise value selected for G'_1 has no effect on the fitting of the polymer data since $G''_1 >> G'_1$. For this reason the parameter G'_1 can be eliminated in equation (4.9) generating a simpler equation:

$$Z_e(\omega) = R + iX_L = \left(\frac{2\omega_o L_q}{\pi\sqrt{\mu_q \rho_q}}\right) \frac{\sqrt{i\rho_1 G''_1}\tanh\left[i\omega_o d_1\sqrt{\frac{\rho_1}{iG''_1}}\right] + \sqrt{i\rho_2 G''_2}}{\sqrt{\frac{\rho_2 G''_2}{\rho_1 G''_1}}\tanh\left[i\omega_o d_1\sqrt{\frac{\rho_1}{iG''_1}}\right] + 1} \qquad \textbf{(4.10)}$$

Equation (4.10) was used for the fitting of the thickness, d_1, and viscosity, G''_1, of the viscoelastic polymers using Mathematica software (Appendix 8.4) with the following parameters: ω_o is the angular resonant frequency of the quartz (62831853 rad s^{-1}), L_q is the inductive reactance of the bare quartz crystal (typical value for a bare AT-cut 10 MHz quartz crystal is 7.5 mH)[10], μ_q and ρ_q are elasticity and density of the quartz crystal (2.947 x 10^{10} N m^{-2} and 2.650 x 10^3 kg m^{-3}), ρ_1 and ρ_2 are the density of the viscoelastic polymer and the water respectively (10^3 kg m^{-3}), G''_2 ($\eta_2\ \omega_o$) is the shear viscosity of the water (6.3 x 10^4 kg m^{-1} s^{-2}).

The electroacoustic parameters, ΔR and ΔX_L, and the data fitted using equation (4.10) during the hydration of 0.14 μm and 0.34 μm thick polymer films are shown in Figure 4.6 and Figure 4.7 respectively.

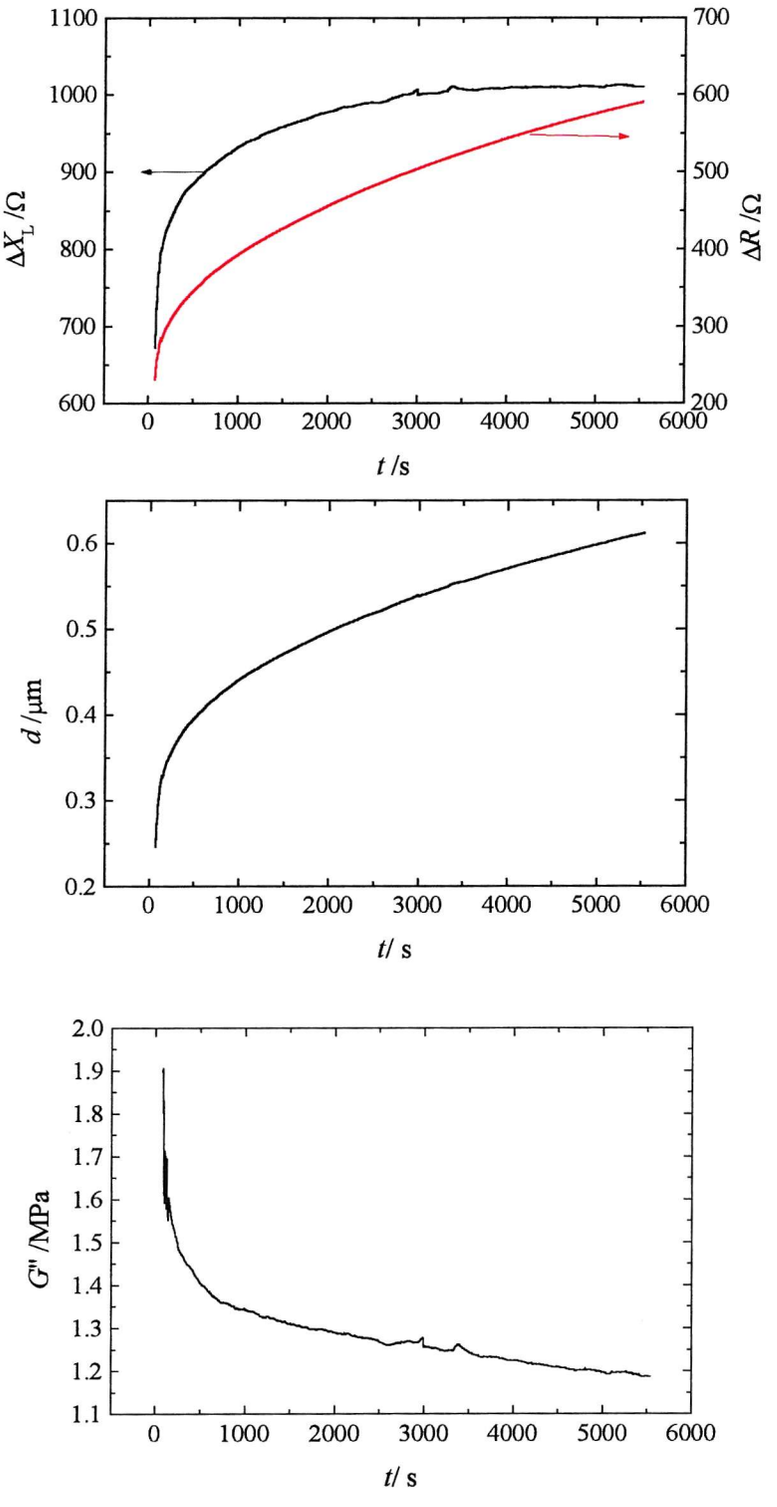

Figure 4.6: Experimental results of the real and imaginary parts of the electroacoustic impedance, ΔR and ΔX_L, and the fitted values of the thickness, d, and the shear modulus, G'', plotted against time of the 0.14 μm thick viscoelastic film during hydration at 25 °C. The value of $\rho_1 = 10^3$ kg m^{-3} is kept constant during the fitting using equation (4.10).

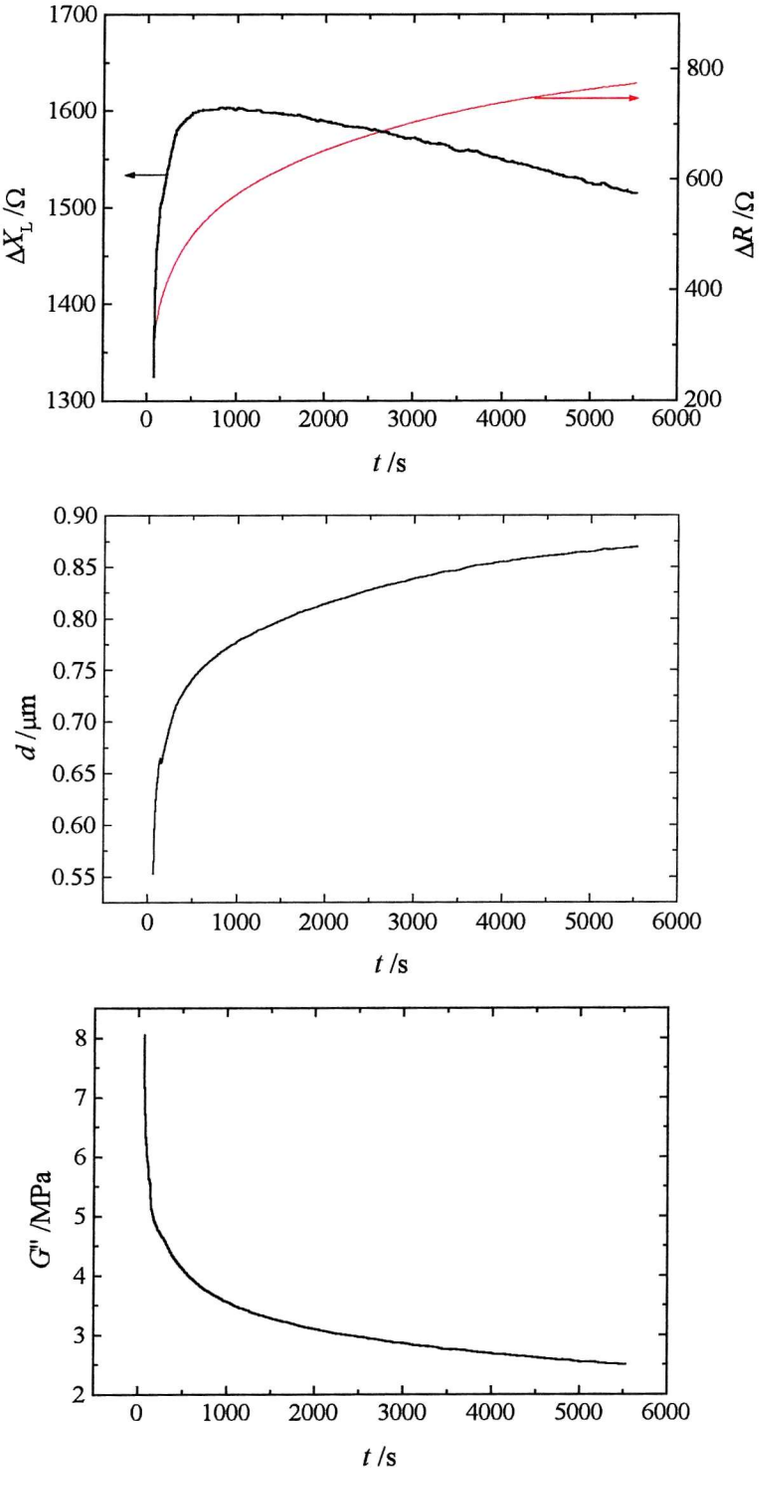

Figure 4.7: Experimental results of the real and imaginary parts of the electroacoustic impedance, ΔR and ΔX_L, and the fitted values of the thickness, d, and the shear modulus, G'', plotted against time of the 0.34 μm thick viscoelastic film during hydration at 25 °C. The value of $\rho_l = 10^3$ kg m^{-3} is kept constant during the fitting using equation (4.10).

Table 4.1 summarises the mathematically fitted results for the growth in thickness of the polymer films during hydration, which is assumed to occur uniformly throughout the polymer film. The changes in thickness and mass of the polymer film during hydration are proportional to each other, since $d = m/(\rho A_m)$ and ρ and A_m remain constant. In this case the changes in mass of the polymer, m, during hydration can be calculated from the changes in thickness, d. The increase in the polymeric mass is assumed to be exclusively due to water uptake.

Table 4.1: Initial thicknesses of the dry polymer films containing PC groups, changes in thickness during the hydration of the polymer films and the percentage of increase in the polymer thickness.

Polymer sample	d_{dry} initial / μm	Δd / μm	% d = % m
a	0.14	0.47	336
b	0.34	0.53	156

Table 4.2 compares the hydrated masses of the polymer films obtained with the use of the non-additive viscoelastic model, equation (4.9), to the masses obtained with the use of the Sauerbrey equation (3.4). For the viscoelastic model, the final masses are obtained by adding the percentage of increase in thickness, which is the same as increase in mass, to the initial masses. For the Sauerbrey model, the changes in mass are obtained by the application of the Sauerbrey equation on the variation of X_L during hydration of the films. Clearly the Sauerbrey equation should not be applied for the calculation of mass in this case because the value of R is not negligible, which is not equivalent of a rigid layer. After the application of valid assumptions the use of equation (4.9) allows us to evaluate changes in masses of thin films when the Sauerbrey equation is not applicable.

Table 4.2: Initial dry mass of the polymer films and the hydrated mass of the polymer films calculated using equation (4.9) and the Sauerbrey equation.

Polymer sample	m_{dry} initial / μg	m final / μg	
		Viscoelastic	Sauerbrey
a	2.89	12.60	5.70
b	6.75	17.28	8.24

The results imply that the thicker the polymer is, the smaller is the relative amount of water absorbed. For the thinner film, the thickness of the hydrated polymer is three times bigger than the dry polymer. For the thicker polymer the increase in thickness during hydration is only one and a half times the value of the dry film. Maybe one or both films are not fully hydrated after 1.5 h of experiments. The changes in the absolute thickness for both films are very similar (Δd = 0.45 and 0.53 μm for the thinnest and thickest film respectively). This suggests that the swelling is uniform throughout the film. The higher viscosity presented by the thickest film after 1.5 h of hydration (2.5 MPa for the thickest film and 1.2 MPa for the thinnest film) reinforce the idea that this film is relatively less hydrated than the thinnest film. With an uniform increase in volume of polymer, V_s, due to the incorporation of solvent, there is an exponentially decrease in the viscosity, η, according to the equation[68]

$$\eta = \eta_o \exp(-k V_s) \text{ or } G'' = G''_o \exp(-k A_m \Delta d) \qquad \textbf{(4.11)}$$

where G'' is the shear viscosity of the polymer in the presence of solvent and G''_o is the shear viscosity of the polymer in the absence of solvent, k is the plasticization constant and A_m is the area of the polymer.

4.4.2. Simulation of Viscoelastic Materials

In order to analyse the influence of the parameters of the viscoelastic films in the parametric plots, the QCM measurement for sample a) is compared to mathematically simulated materials using equation (4.9), with water as material 2. The parameters of the simulated materials are similar to the values obtained for the sample a) and the density is maintained at 10^3 kg m^{-3} and the elasticity is zero. There are three simulations: For sample b) the shear viscosity is maintained at 1.2 MPa and the thickness of the film increases from 0.25 μm to 1.8 μm. For sample c) the shear viscosity has a higher value of 1.5 MPa and the thickness increases from 0.25 μm to 1.8 μm, and the sample d) has the same shear viscosity as sample s2) but the thickness grows only 0.25 μm to 0.75 μm. The parametric plots of the simulated materials and the sample a) are plotted in Figure 4.8. They have the form of curves and at high

thicknesses the QCM sees the materials as infinetely thick Newtonian liquids. As the elasticity of these materials is negligible, when the thickness of the material is bigger than the decay length of the acoustic wave, the line of the parametric plot touches the Kanazawa approximation (green line) and the correspondent value of the density and the viscosity of the materials can be calculated. For the experimental data, the curvature of the parametric plot decreases during hydration, which is reasonable since the viscosity of the polymer film also decreases. At the end of the experiment, the film of sample a) is not thick enough to reach the Kanazawa approximation.

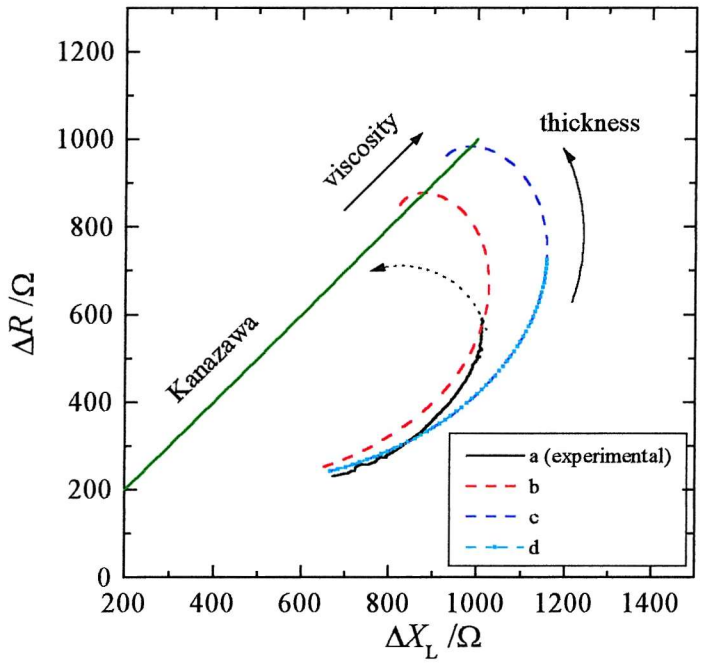

Figure 4.8: Parametric plots during hydration of sample a) and ΔR and ΔX_L values calculated for viscoelastic films from equation (4.9) with parameters $\rho_2 = 10^3$ kg m^{-3} and $G''_2 = 6.3 \times 10^4$ kg m^{-1} s^{-2}, b) $G'_1 = 0$, $\rho_1 = 10^3$ kg m^{-3}, $G''_1 = 1.2$ MPa and d_1 from 0.25 µm to 1.8 µm, c) $G'_1 = 0$, $\rho_1 = 10^3$ kg m^{-3}, $G''_1 = 1.5$ MPa and d_1 from 0.25 µm to 1.8 µm, d) $G'_1 = 0$, $\rho_1 = 10^3$ kg m^{-3}, $G''_1 = 1.5$ MPa and d_1 from 0.25 µm to 0.75 µm.

4.5. Conclusion

The analysis of the QCM measurements of viscoelastic materials is mathematically complex because from the two experimental results, R and X_L, four mechanical parameters of the viscoelastic material are generated: the density, ρ, the thickness, d, the elasticity, G', and the viscosity, G'', from the equation

$$\boldsymbol{Z}_{e,i}(\omega) = R + iX_L = \left(\frac{2\omega_o L_q}{\pi\sqrt{\mu_q \rho_q}}\right)\sqrt{\rho_i\left(G'_i + iG''_i\right)}\tanh\left[i\omega_o d_i\sqrt{\frac{\rho_i}{G'_i + iG''_i}}\right] \qquad \textbf{(1.21)}$$

Some assumptions must be made for the material to be analysed to make solution of the equation (1.21) possible, i.e. some of the parameters must have fixed values for the evaluation of the others. Although for most of the materials it is complicated because the parameters change with no obvious relationship between them. It would be convenient to use another technique to complement the QCM experiments and set up reasonable values in equation (1.21). In this chapter, we used mathematical fitting to establish the physical changes of a hydrophilic polymer during hydration at controlled temperature. The changes in thickness, d, and viscosity, G'', of the polymer film during hydration were calculated with the assumptions that the density, ρ, is kept at 10^3 kg m^{-3} and the elasticity, G', is negligible. The polymers analysed in this section may be regarded as 'soft liquids' because the viscosity, G'', is much bigger than the elasticity, G', of the hydrated films.

Figure 4.9 is a SEM image of the viscoelastic film after hydration showing that the film is smooth. We do not mention the thickness of the hydrated film because the vacuum necessary for the SEM image modifies the amount of water inside the film, altering the final hydrated thickness. EQCM analysis of porous polymer films is introduced in the next Chapter. For these films the shape of the parametric plots are very different.

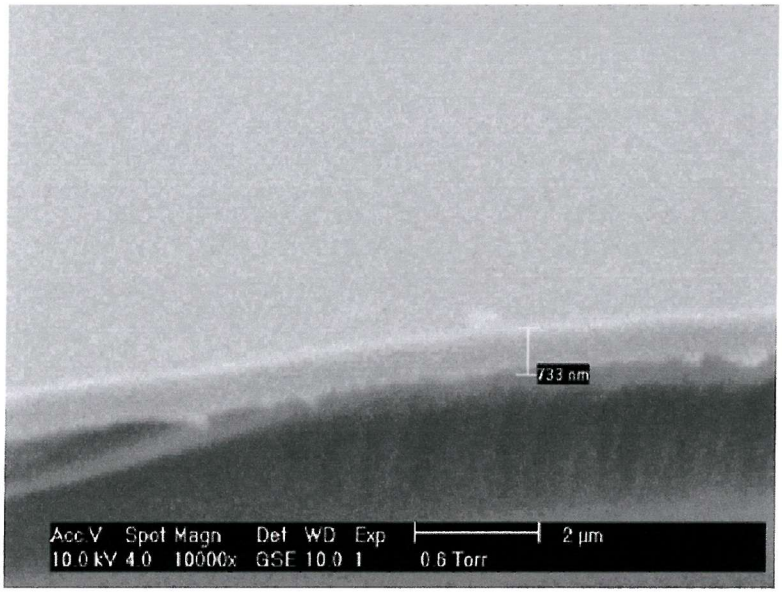

Figure 4.9: SEM image of the polymer film containing PC groups after hydration.

5. EQCM Analysis of the Electrochemical Deposition of Conducting Polymers

In the last chapter changes in viscoelasticity during hydration of non-conducting polymer films have been analysed. In this chapter, the EQCM is used to study the electrochemical deposition of conducting polymers. The study of the growth of thin layers of conducting polymers using EQCM measurements provide information about the physical and electrochemical properties of the material. Many people have studied deposition of conducting polymers using EQCM, but the methods used for interpretation of the results vary considerably.[97-100] Before the analysis of the EQCM measurements there is a brief introduction on conducting polymers

5.1. Conducting Polymers

Polymers were believed to be insulators until it was found that conjugated polymers were electronically conducting.[101] Electronically conducting polymers possess a conjugated π backbone. Since π electrons can be easily removed or added to these polymeric chains to form poly(ions), such π-conjugated polymers are predisposed to undergo doping by redox reactions, i.e. electrochemical doping.[1] The concept of doping in conducting polymers means the conversion of the neutral insulating polymer into a cationic or anionic conducting polymer. The electrical conductivity is a consequence of the existence of charge carriers and of the mobility of these charge carriers along the conjugated π-bonded backbone as shown in Figure 2.1. The movement of an electron from one repeat unit to the nuclei in the adjacent units leads to electron hopping along the polymer chain and to charge mobility.[1] This characteristic ability to switch on and off the conductivity of the polymer with very little degradation of the conducting material is very attractive for industrial use.[102]

Conducting polymers can be used to coat electrode surfaces modifying their original properties. Modified electrodes with conducting polymers are replacing conventional electrodes, due to the facility in altering the chemical, electrochemical and

physical properties of organic polymers, creating an unlimited number of electroactive materials, which exhibit many desired, pre-selected properties.[102]

The development of a range of sophisticated sensors and other devices has been possible with the use of polymer-coated electrodes. Some electrochemical processes of commercial importance rely on the use of polymeric materials for efficient operation. The polymer-modified electrode must be well characterised for the improvement in the performance of the resulting interface. Some information about the polymer films are of vital importance like the polymer structure, the film thickness and uniformity, the influence of the local environment on the properties of the conducting material and the mechanism of charge transport.[102]

5.1.1. Poly(aniline)

Poly(aniline) is a very attractive conducting polymer because it has a high conductivity, and it is easily synthesised chemically or electrochemically in aqueous or non-aqueous medium from the cheap industrial monomer aniline; furthermore it is insoluble and stable under ambient conditions.[1,103] Electropolymerization of aniline can be carried out potentiostatically, potentiodynamically or galvanostatically. Scanning electron microscopy investigations have shown that deposition by cycling the potential leads to a more homogeneous film.[104]

The characteristic of being easily switched between the insulating and conducting state by reducing and oxidising the film makes poly(aniline) very attractive for commercial device applications.

Poly(aniline) has been studied intensively because of the fundamental interest in understanding its redox reaction mechanism.[105,106] The electrode potential and, in contrast with other conducting polymers, the pH of the solution defines the redox state for poly(aniline). Figure 5.2 summarises the proposed redox and protonation balance for the three oxidation states of poly(aniline).[107] The redox reaction is accompanied by ion transport into or out of the polymer film to maintain electroneutrality. This ionic movement seems to be the kinetic step which determines the switching rate of poly(aniline).[98,108] In the fully reduced form (leucoemeraldine), the polymer is insulating in its unprotonated (L) and protonated (LH) forms. In the intermediate

oxidation state (emeraldine), the protonated (EH) form is conducting, but the unprotonated (E) form is insulating. Protonation is essential for the charge carrier motion and consequently for the conductivity of the emeraldine state of poly(aniline). In the fully oxidised state (pernigraniline), the polymer is insulating in both protonated and deprotonated states (PH and P). This form of poly(aniline) is unstable in acidic solution and it has been less well characterised than the other oxidation states.[109] The repeated cycling of the polymer into the fully oxidised state leads to the degradation of the polymer because imine units of the poly(aniline) are hydrolysed causing the rupture of the polymer chain producing quinone groups. This causes a decrease in size of the characteristic electrochemical peaks of the poly(aniline) due to the damage of the polymer film showing the degradation of the film and new peaks are developed due to the formation of quinoidal structures.

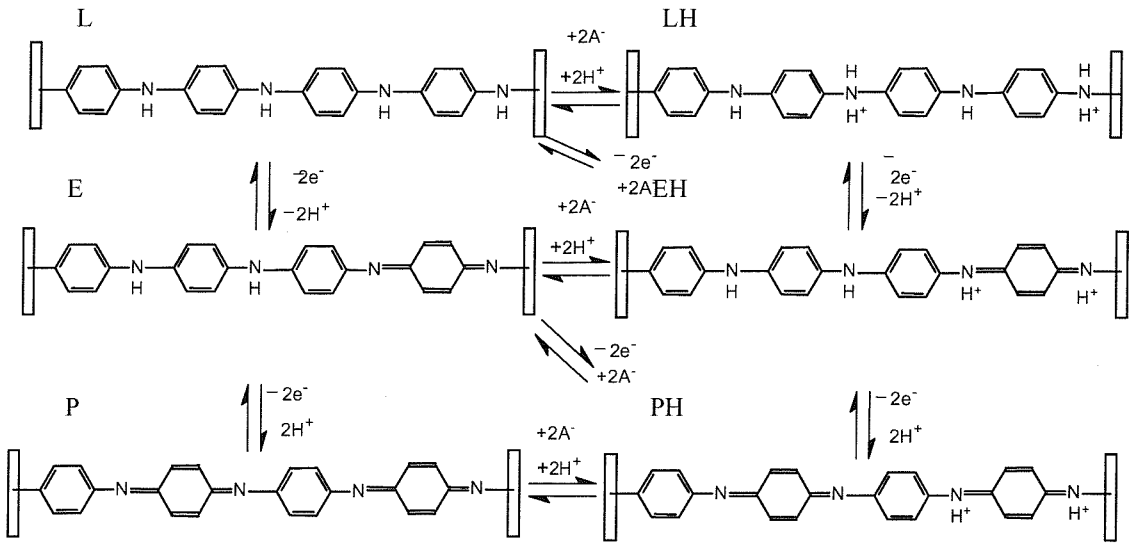

Figure 5.1: Scheme for the redox reactions of poly(aniline). The protonated form of the emeraldine (EH) is the only conducting state of poly(aniline).[110]

A major disadvantage of working with poly(aniline) is that the polymer film is conducting only in acidic conditions. The emeraldine state is deprotonated at pH higher than 5 and becomes insulating. This property of the poly(aniline) decreases the possibility of its use in biological devices where environments with mild pH are necessary. One way to maintain the poly(aniline) protonated at higher pHs is to manipulate the transport of the counterions during redox reactions.[110] This can be done by inserting large poly(anions) within the poly(aniline) film during the polymerisation.

In these 'modified' poly(aniline) films, the counterions are trapped inside the structure of the film, keeping the polymer conducting (protonated) in solutions with higher pH.[8,19]

5.1.2. Poly(aniline) composites with polymeric counterions

With the aim of keeping the emeraldine form of the poly(aniline) protonated in neutral pH, poly(anions) are added to the aniline solution prior to electropolymerisation.[17,19,20] In the present study, aniline was polymerised with poly(sodium 4-styrenesulfonate) (PSS), and poly(vinylsulfonic acid, sodium salt) (PVS), these structures are shown in Figure 5.2.

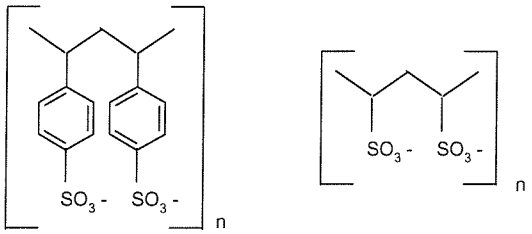

a b

Figure 5.2: Poly(anions) used for poly(aniline) modification. a) poly(4-styrenesulfonate), PSS, b) poly(vinylsulfonate), PVS.

The negatively charged sites provided by the poly(anions) keep the positively charged protons within the polymer structure during redox reactions[110] (see Figure 5.3). The poly(aniline) composites with poly(anionic) counterions will not be deprotonated as long as the ionic strength of the electrolyte is low (< 0.1 M) because the poly(anions) are entrapped in the polymer film during the electropolymerisation and they are too large to leave the polymer chain. The ions present in the electrolyte are forced to move within the film to maintain the electroneutrality.

Electrochemical analyses of conducting poly(aniline)-poly(vinylsulfonate) and poly(aniline)-poly(styrenesulfonate) composite films in solutions close to neutral pH can be found in the literature.[111,112]

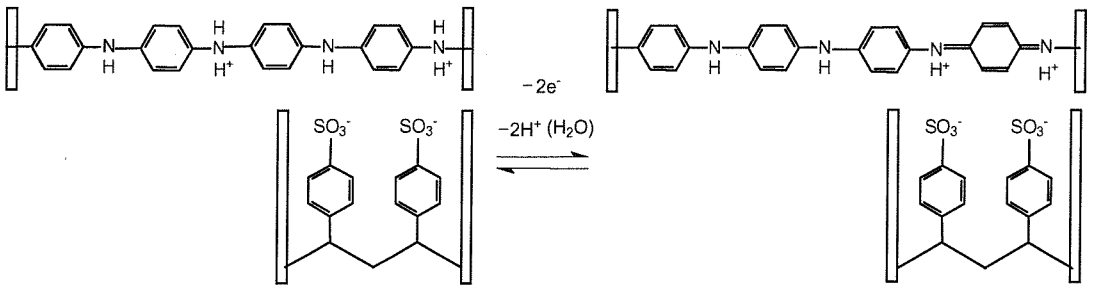

Figure 5.3: Poly(aniline)-poly(styrenesulfonate) in the reduced and oxidised forms. The sketch shows the movement of anions or protons consequent on the electron movement in order to maintain electroneutrality of the polymer.

Poly(aniline)-poly(vinylsulfonate) and poly(aniline)-poly(styrenesulfonate) modified electrodes are used in the catalysis of NADH oxidation.[19] There is a vast interest in this specific process[21] because many amperometric enzyme electrodes can be developed for a wide range of substrates since there are a large number of dehydrogenase enzymes which use NADH as the coenzyme. The Electrochemical Quartz Crystal Microbalance can be useful in the analysis of the mechanism of the catalysis of NADH oxidation by the redox mediators (poly(aniline) composites).

In the following section we present the results of electrochemical quartz crystal microbalance studies of the electrochemical deposition of poly(aniline) and poly(aniline) composite films. Later, one polymer is chosen for further analyses during redox reactions.

5.2. Deposition of poly(aniline) composite films

Three types of poly(aniline) films were studied: poly(aniline), poly(aniline)-poly(vinylsulfonate) and poly(aniline)-poly(styrenesulfonate). The depositions of the polymer films were carried out from the respective aqueous solutions: 0.44 M aniline and 2 M H_2SO_4; 0.44 M aniline and 22.4 wt. % poly(vinylsulfonate); 0.44 M aniline and 22.4 wt. % poly(styrenesulfonate).

The electrodeposition of conducting poly(aniline) films is possible only at extreme acidic conditions. At higher pHs the aniline monomer is oxidised but it forms an insulating film preventing further polymerisation. The addition of inorganic acids to the aniline solutions is not desirable in our experiments. As we are interested in the ion movement between the electrolyte solution and the polymer film during redox reactions, the film should be as pure as possible. The three polymers reported in this thesis have sulphate (SO_4^{2-}) or sulfonate (SO_3^-) anions incorporated in them. During cyclic voltammetry perchlorate (ClO_4^-) and chloride (Cl^-) are available from the electrolytes. A restricted number of different anions helps in the interpretation of the experiments designed to analyse the transport of anions between the polymer film and the electrolyte.

Commercially available solutions of poly(vinylsulfonate) and poly(styrenesulfonate) in water with sodium counter ions have neutral pH. In order to convert them to the corresponding acidic polymer solutions, we have used a strongly acidic insoluble resin, Amberlyst® 15. The resin exchanges H^+ cations for the Na^+ cations present in the neutral polymer solution. The polymeric solutions reach pH values lower than 0.2 after this treatment.

The reproducibility of the deposition of the films is pH dependent. Reproducible depositions have been achieved experimentally when electrolyte solutions have pH values lower than 0.2. Figure 5.4 shows a potentiodynamic deposition of poly(aniline)-poly(styrenesulphonate) at pH 0.4. The formation of an insulating film during the electropolymerisation of aniline is observed from the stabilisation of the current after nine cycles (i.e. the film no longer grows). The electropolymerisation of poly(aniline) films in weakly acidic solutions does not cause the decomposition of polymer chains,[113] so the inactivation of the polymer film is probably caused because the poly(aniline) film has a structure like the leucoemeraldine base.[113]

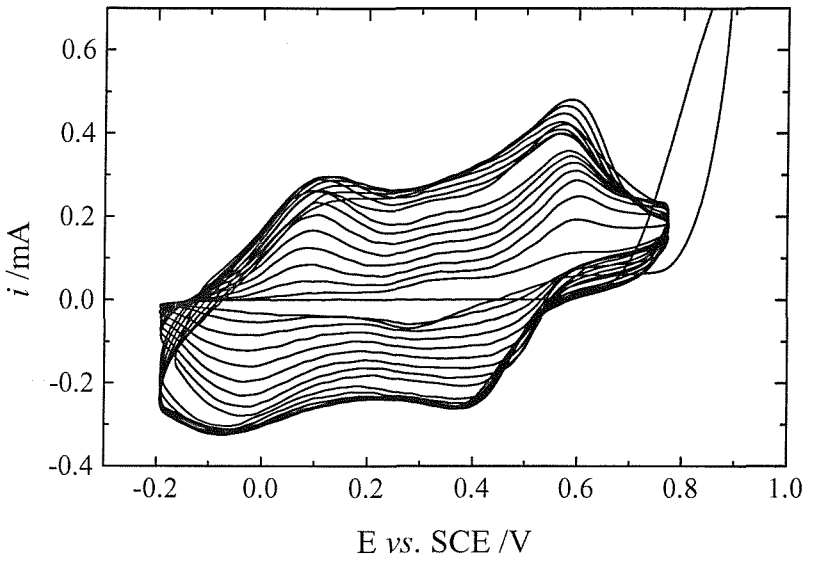

Figure 5.4: Cyclic voltammetry during potentiodynamic deposition of poly(aniline)-poly(styrenesulphonate) at 50 mV s^{-1}. The pH of the solution was 0.4.

The depositions of the polymer films were carried out potentiostatically and potentiodynamically. In the potentiostatic deposition, the potential was stepped from -0.20 V to 0.78 V *vs.* SCE with a first step at 0.90 V. The potentiodynamic deposition started by cycling the potential from –0.20 V to 0.90 V *vs.* SCE on the first scan and then continuing cycling between –0.20 V and 0.78 V, at 50 mV s^{-1}. The higher potential applied on the first step and on the first cycle is necessary for the nucleation of the aniline. Once the poly(aniline) film is formed, the oxidation of the monomer is catalysed by the polymer film itself.[114] The first step in the polymerisation is believed to be the oxidation of the aniline monomer to a radical cation.[115] The radical cation dimerizes forming neutral species with elimination of protons. The dimer (E = 0.6 V *vs.* SSCE) is more easily oxidisable than the monomer (E = 1.2 V *vs.* SSCE) and under the experimental conditions it is reoxidised to a cation. The polymer chain grows with the addition of new cations of the monomer to the already charged oligomer.

SEM images were taken for the poly(aniline), poly(aniline)-poly(vinylsulfonate) and poly(aniline)-poly(styrenesulfonate) films deposited potentiostatically and potentiodynamically to observe the morphology of the dry polymer films.

5.2.1. Potentiostatic deposition of poly(aniline) films

The parametric plots for the potentiostatic deposition of poly(aniline), poly(aniline)-poly(vinylsulfonate) and poly(aniline)-poly(styrenesulfonate) films are shown in Figure 5.5, Figure 5.6 and Figure 5.7, respectively. The films deposited under the same conditions are reproducible. The parametric plots of the deposition of the composite polymers differ a lot in shape. The poly(anions) inserted in the poly(aniline) structure seem to have a large influence on the viscoelasticity of the films. Using the theory presented in previous chapters, the increase in the value of ΔR shown in the plots of the poly(aniline) and the poly(aniline)-poly(vinylsulfonate) films is characteristic of viscoelastic materials. The oscillation of the quartz crystal is damped when it is covered with poly(aniline) and poly(aniline)-poly(vinylsulfonate) films. In contrast, the value of ΔR remains close to zero when a thin layer of poly(aniline)-poly(styrenesulfonate) film is deposited. The poly(aniline)-poly(styrenesulfonate) film vibrates together with the quartz crystal, and the oscillation of the quartz is not damped.

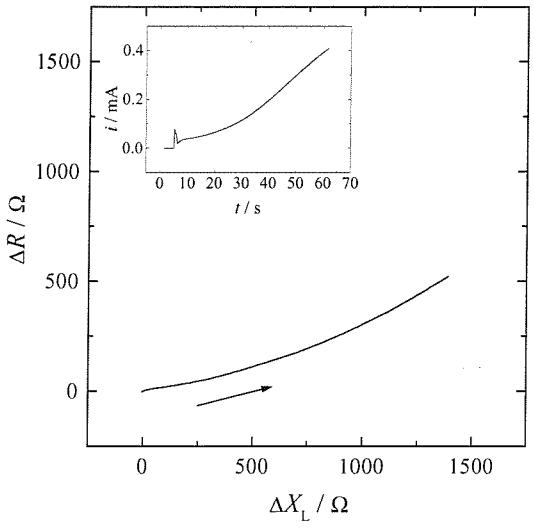

Figure 5.5: EQCM parametric plot recorded during the potentiostatic deposition of poly(aniline) in 2 M H_2SO_4 following a potential step from –0.2 V to 0.9 V for 1 s and then back to 0.78 V *vs.* SCE to grow the film for 60 s. 44.1 mC cm^{-2} of charge was passed in the growth. The inset shows the corresponding current transient. The initial spike at 5 s corresponds to step at 0.9 V.

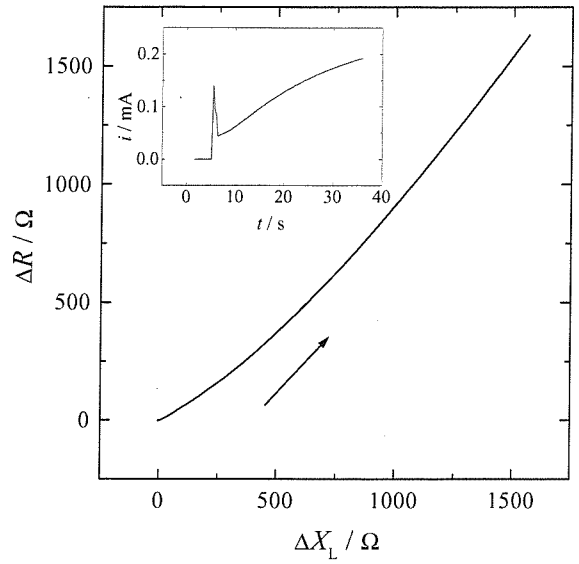

Figure 5.6: EQCM parametric plot recorded during the potentiostatic deposition of poly(aniline)-poly(vinylsulfonate) following a potential step from –0.2 V to 0.9 V for 1 s and then back to 0.78 V *vs.* SCE to grow the film for 36 s. 17.6 mC cm^{-2} of charge was passed in the growth. The inset shows the corresponding current transient. The initial spike at 5 s corresponds to step at 0.9 V.

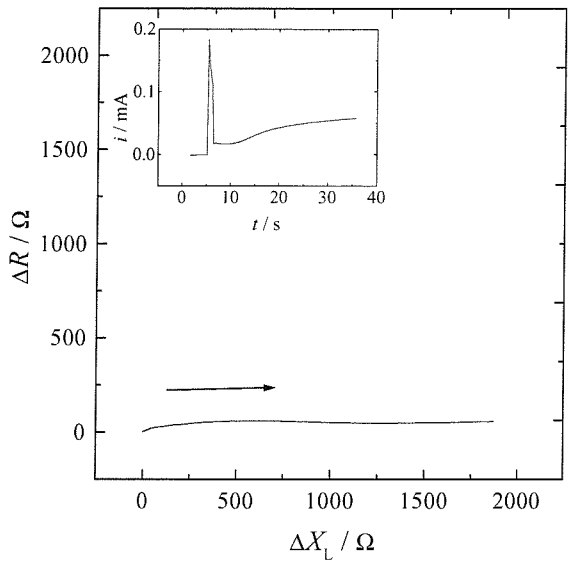

Figure 5.7: EQCM parametric plot recorded during the potentiostatic deposition of poly(aniline)-poly(styrenesulfonate) following a potential step from –0.2 V to 0.9 V for 1 s and then back to 0.78 V *vs.* SCE to grow the film for 36 s. 6.06 mC cm^{-2} of charge was passed in the growth. The inset shows the corresponding current transient. The initial spike at 5 s corresponds to step at 0.9 V.

Figure 5.8, Figure 5.9 and Figure 5.10 show the mass of polymer deposited as a function of charge. The mass is calculated by applying the Sauerbrey equation assuming that the polymer films are rigid layers. Although from the analysis of the parametric plots, it is known that the assumptions that the poly(aniline) and poly(aniline)-poly(vinylsulfonate) films are rigid is not valid. The graph mass *vs.* charge can also be used to check rigidity where a relatively straight line indicates a rigid film. The mass is proportional to X_L which is proportional to the frequency of the quartz crystal. The linearity for the polymer films is observed only at the beginning of the deposition, being replaced by a curvature which represents the loss of mass sensitivity due to damping of the shear wave through the film.[10] The mass of poly(aniline)-poly(styrenesulfonate) film was expected to be linearly deposited as a function of charge, indicating a rigid film. The density of the poly(aniline) film is reported to be 1250 kg m^{-3}.[116] If we adopt this value for the three polymer films we can estimate the thickness above which the polymer films are no longer rigid. Considering all the errors included by applying the Sauerbrey equation and the density value, it seems that the films need to be thinner than 0.1 μm to be treated as rigid films. We are not interested in finding the exact thickness of the polymer here, otherwise the mathematical fitting of equation (4.9) would have to be used.

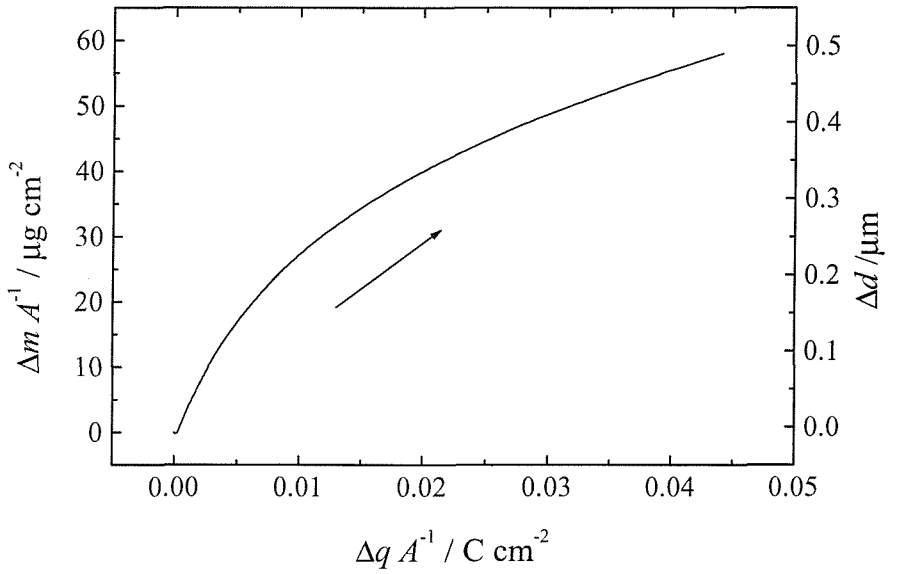

Figure 5.8: Plot of the calculated mass of poly(aniline) as a function of charge passed. The mass was calculated from the data of ΔX_L assuming that the film was rigid and that the Sauerbrey equation can be used. The thickness ($d = m / A \rho$) was calculated from the mass and area 0.2 x 10^{-5} m^2 and density of the polymer as 1250 kg m^{-3}.

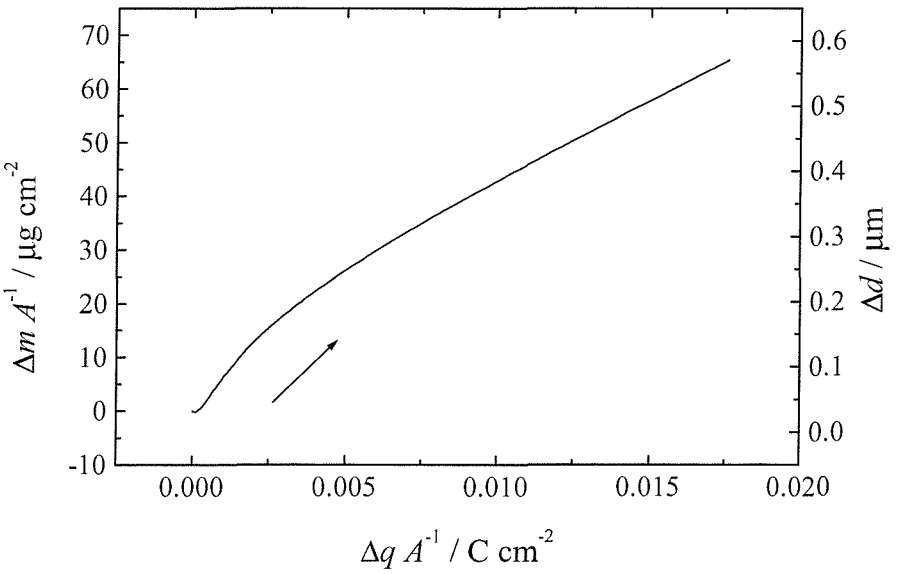

Figure 5.9: Plot of the calculated mass of poly(aniline)-poly(vinylsulfonate) as a function of charge passed. The mass was calculated from the data of ΔX_L assuming that the film was rigid and that the Sauerbrey equation can be used. The thickness ($d = m / A \rho$) was calculated from the mass and area 0.2 x 10^{-5} m^2 and density of the polymer as 1250 kg m^{-3}.

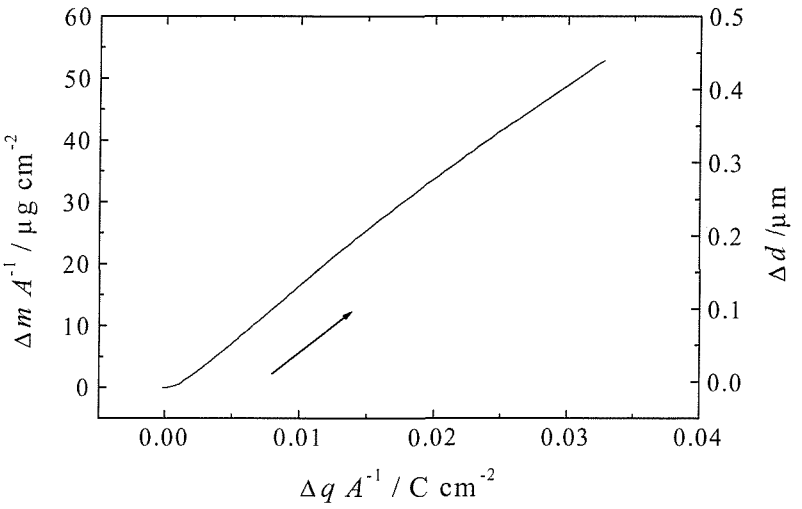

Figure 5.10: Plot of the calculated mass of poly(aniline)-poly(styrenesulfonate) as a function of charge passed. The mass was calculated from the data of ΔX_L assuming that the film was rigid and that the Sauerbrey equation can be used. The thickness ($d = m / A \rho$) was calculated from the mass and area 0.2 x 10^{-5} m^2 and density of the polymer as 1250 kg m^{-3}.

SEM images of the surface of the polymer films magnified 5000 times are shown in Figure 5.11, Figure 5.12 and Figure 5.13. The morphology of the films is characterised by the porosity of the interfacial layer. The images show that the poly(aniline) film has a fibrous structure, the poly(aniline)-poly(vinylsulfonate) film has a globular structure and the poly(aniline)-poly(styrenesulfonate) film has a more compact structure. The structure of the poly(aniline)-poly(vinylsulfonate) film was reported to possess higher conductivity for the same mass of poly(aniline)-poly(styrenesulfonate) deposited in the same conditions, because of its higher surface area.[110]

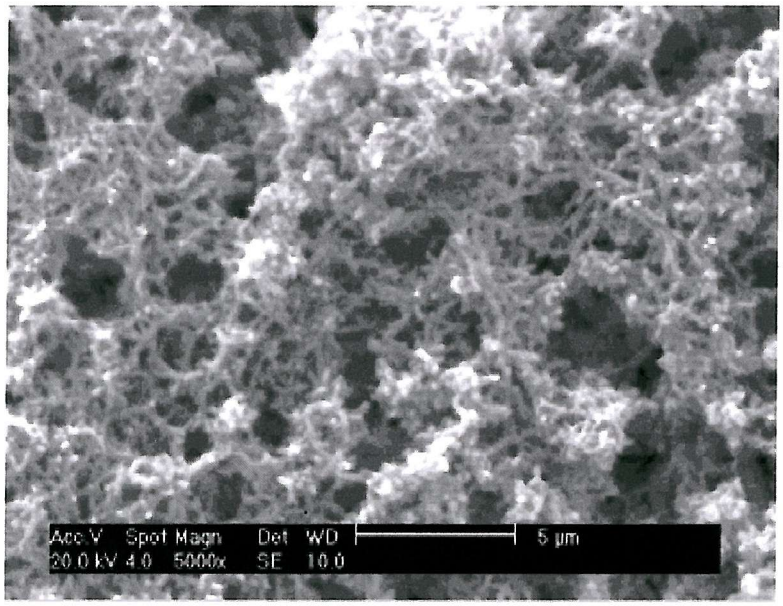

Figure 5.11: SEM image of the surface of the poly(aniline) film deposited potentiostatically.

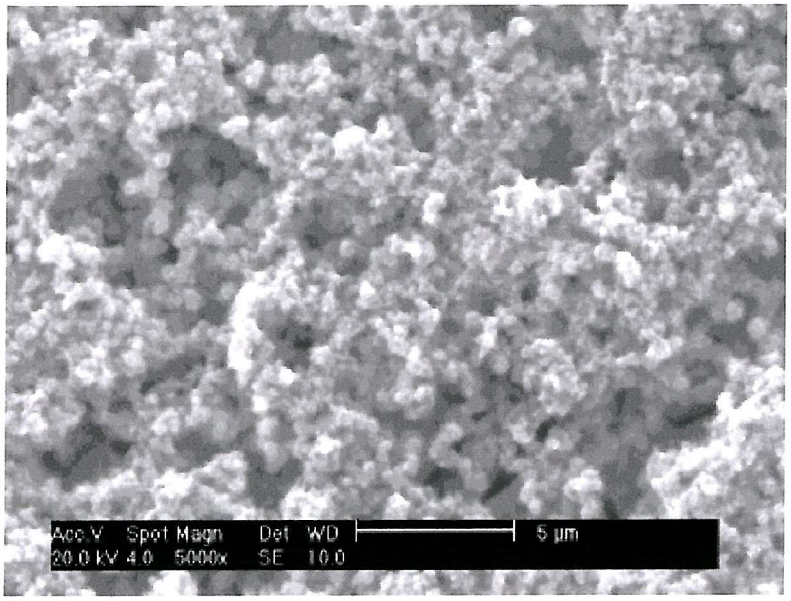

Figure 5.12: SEM image of the surface of the poly(aniline)-poly(vinylsulfonate) film deposited potentiostatically.

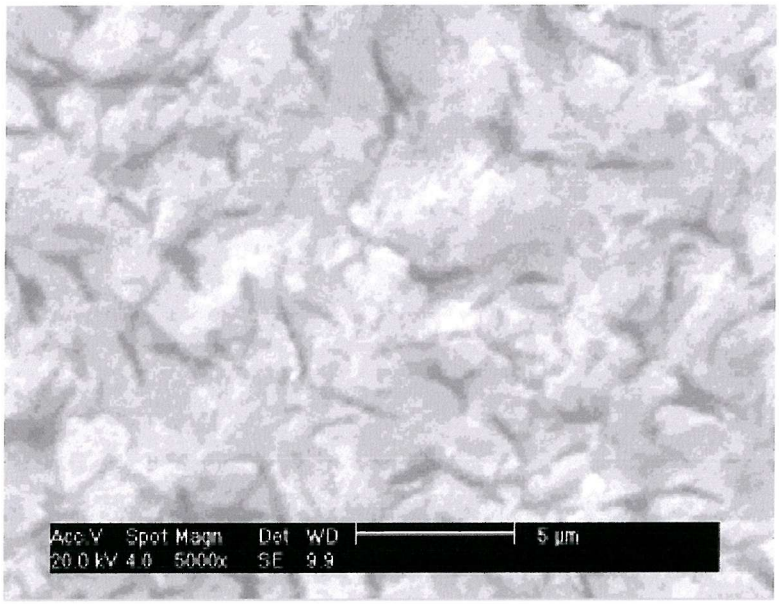

Figure 5.13: SEM image of the surface of the poly(aniline)-poly(styrenesulfonate) film deposited potentiostatically.

5.2.2. Potentiodynamic deposition of poly(aniline) films

The results shown here for the polymer films deposited potentiostatically are reproducible under the same conditions. The parametric plots of the potentiodynamic deposition of the poly(aniline) and poly(aniline) composite films are shown in Figure 5.14, Figure 5.15 and Figure 5.16. The parametric plots of the polymer films deposited potentiostatically or potentiodynamically have very similar shapes. This is indicative that the polymers do not present significant changes if deposited potentiostatically or potentiodynamically.

During the potentiodynamic deposition, the polymers are constantly being reduced and oxidised introducing the movement of ions and solvent between the film and the electrolyte solution during growth. The movement of ions and solvent between the film and the electrolyte solution can be very well observed on the parametric plot of the deposition of the poly(aniline) film. At each voltammetric cycle, there is a loop on the values of X_L and R.

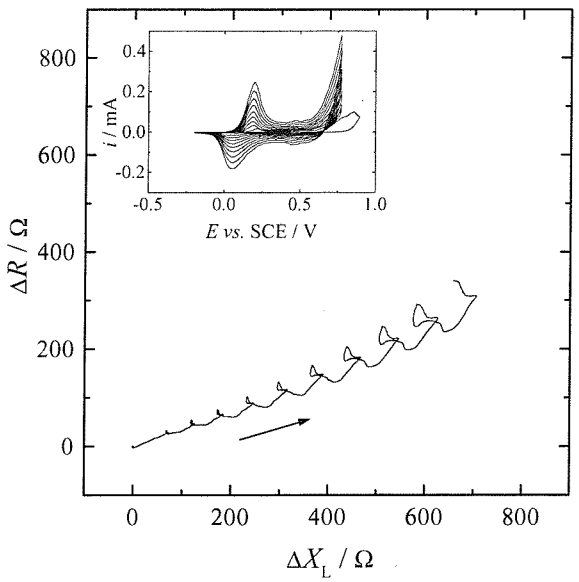

Figure 5.14: EQCM parametric plot recorded during the potentiodynamic deposition of poly(aniline) in 2 M H_2SO_4 following a potential sweep from –0.2 V to 0.78 V *vs.* SCE at 50 mV s^{-1}. The inset shows the corresponding voltammogram during the deposition.

For the poly(aniline)-poly(vinylsulfonate) and poly(aniline)-poly(styrenesulfonate) films, changes in X_L and R during the redox process (insertion and extraction of ions) are small compared thus which occur for poly(aniline) films. This is because in case of the composite films the large anions are already inside the structure of the polymer and the light protons might move to balance the charge during the redox reactions. The movement of protons is not easily detected by the QCM measurements because their molecular mass is very small.

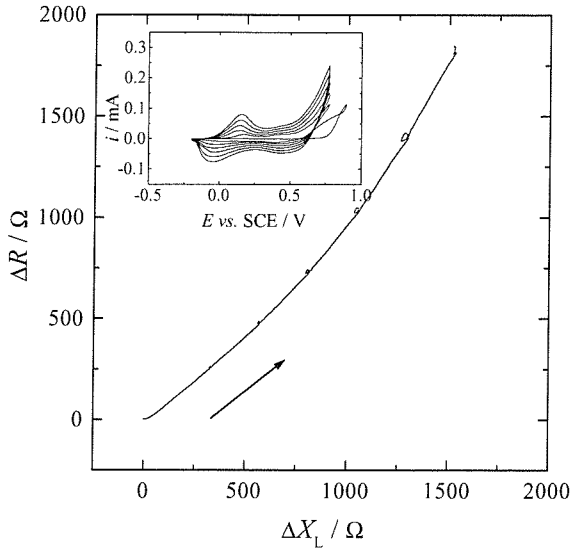

Figure 5.15: EQCM parametric plot recorded during the potentiodynamic deposition of poly(aniline)-poly(vinylsulfonate) following a potential sweep from –0.2 V to 0.78 V *vs.* SCE at 50 mV s^{-1}. The inset shows the corresponding voltammogram during the deposition.

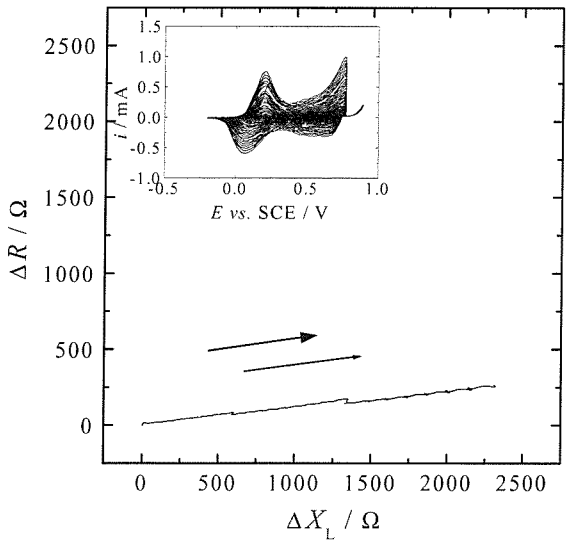

Figure 5.16: EQCM parametric plot recorded during the potentiodynamic deposition of poly(aniline)-poly(styrenesulfonate) following a potential sweep from –0.2 V to 0.78 V *vs.* SCE at 50 mV s^{-1}. The inset shows the corresponding voltammogram during the deposition.

Figure 5.17 show the increase of the imaginary part of the impedance of the poly(aniline) film, X_L, which is related to the mass of the polymer film during the potentiodynamic growth assuming a rigid film. At the beginning of the oxidation scan, the amine groups in the deposited polymer are converted to radical cations. This causes a temporary and reversible increase in mass of the polymer film supposed to be due to transport of anions into the film to neutralise the charge of the polymer. The polymer film is formed at more positive potential (> 0.5 V *vs.* SCE) where the process is irreversible and generates permanent gain of mass.

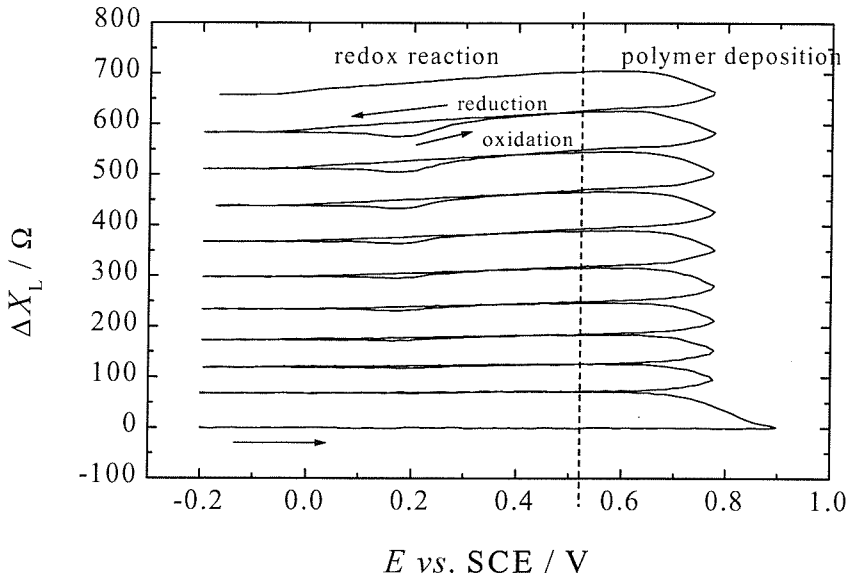

Figure 5.17: Plot of ΔX_L during the potentiodynamically deposition of poly(aniline) as a function of potential. The value of ΔX_L can be related to mass in case of a rigid film. Note the increase in X_L occurs at two different potentials. The dotted line marks out the potential where the deposition of the polymer occurs and the changes in ΔX_L are irreversible.

Figure 5.18 shows the changes in X_L during the potentiodynamic deposition of poly(aniline)-poly(styrenesulfonate), which is considerably smaller during redox reactions.

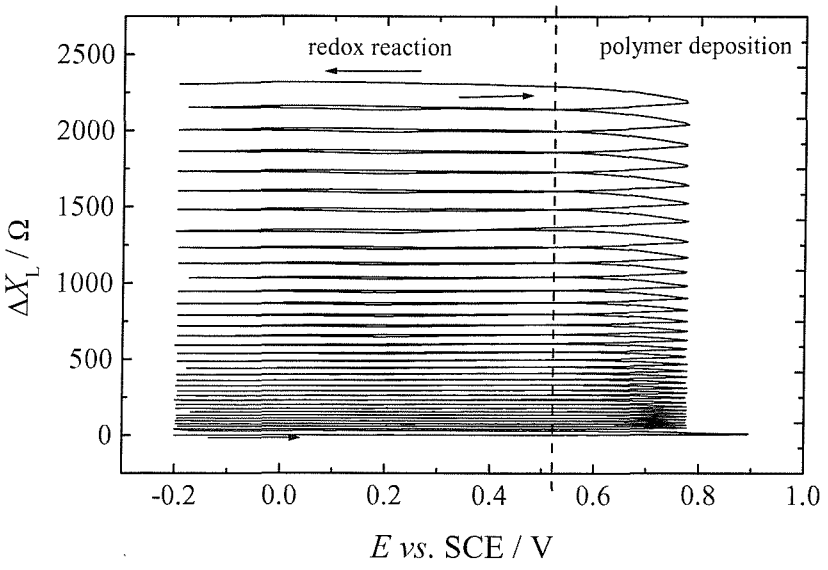

Figure 5.18: Plot of ΔX_L during the potentiodynamically deposition of poly(aniline)-poly(styrenesulfonate) as a function of potential. The value of ΔX_L can be related to mass in case of a rigid film.

Figure 5.19 shows the relationship between mass and charge during the electropolymerisation of poly(aniline) film. The mass gain is calculated from the values of ΔX_L by applying the Sauerbrey equation. The reversible movement of ions in the polymer films during redox reactions also can be observed in these plots with reversible decrease in mass during the reduction of the film. The plot of mass vs. charge during poly(aniline) growth is not linear as expected for non rigid films. The plot of mass vs. charge for the potentiodynamically growth of poly(aniline)-poly(vinylsulfonate) is very similar to the one for poly(aniline) film and it is not shown here.

The relation between mass and charge of the reduced and oxidised film can be measured on the plot of poly(aniline)-poly(styrenesulfonate) shown in Figure 5.20. It can be noticed that the poly(aniline)-poly(styrenesulfonate) film is rigid in both the reduced and oxidised states because the linearity between mass and charge is observed for the reduced film (minimum charge) and the oxidised film (maximum charge).

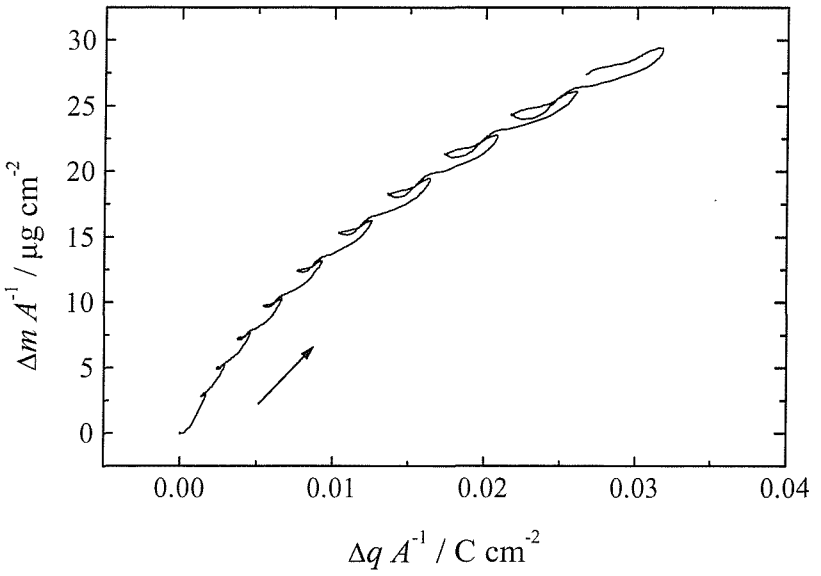

Figure 5.19: Plot of the calculated mass of poly(aniline) as a function of charge passed. The mass is calculated from the data for ΔX_L assuming the film is rigid and Sauerbrey equation can be applied.

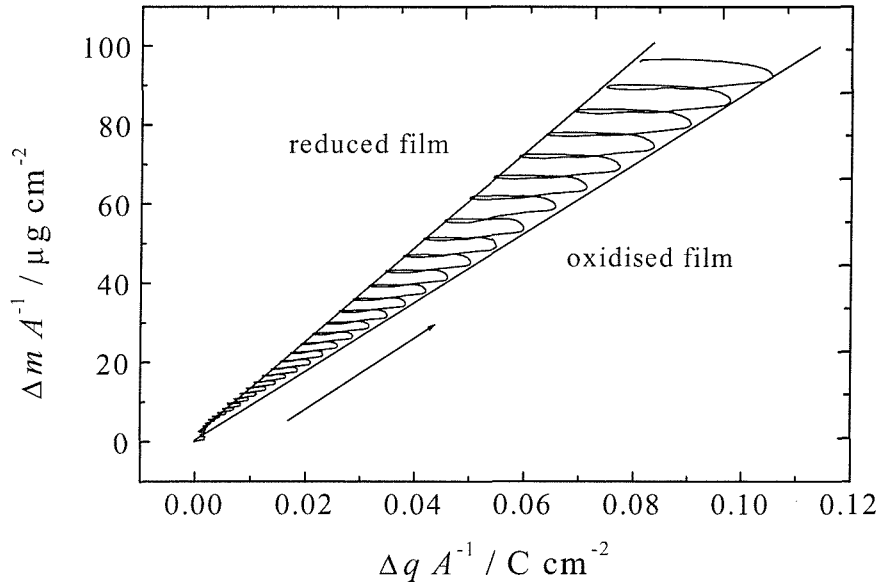

Figure 5.20: Plot of the calculated mass of poly(aniline)-poly(styrenesulfonate) as a function of charge passed. The mass is calculated from the data for ΔX_L assuming the film is rigid and Sauerbrey equation can be applied.

Figure 5.21, Figure 5.22 and Figure 5.23 show SEM images of the surface of the films magnified 5000 times. The morphology of poly(aniline) films depends on the nature of anions used during the electropolymerisation.[103] But the morphology does not seem to be influenced if the polymer is deposited potentiostatically or potentiodynamically since the images shown below are like the ones shown in the section for the potentiostatical deposition of the same polymers.

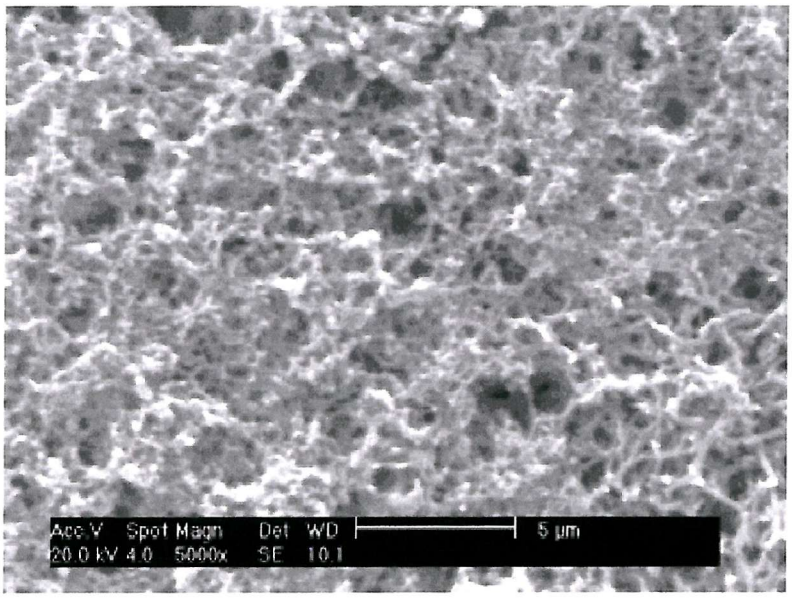

Figure 5.21: SEM image of the surface of the poly(aniline) film deposited potentiodynamically.

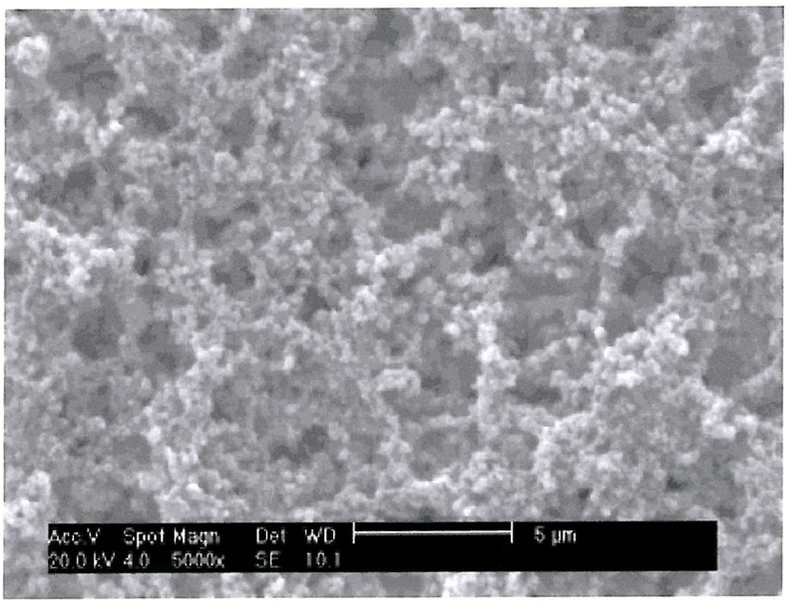

Figure 5.22: SEM image of the surface of the poly(aniline)-poly(vinylsulfonate) film deposited potentiodynamically.

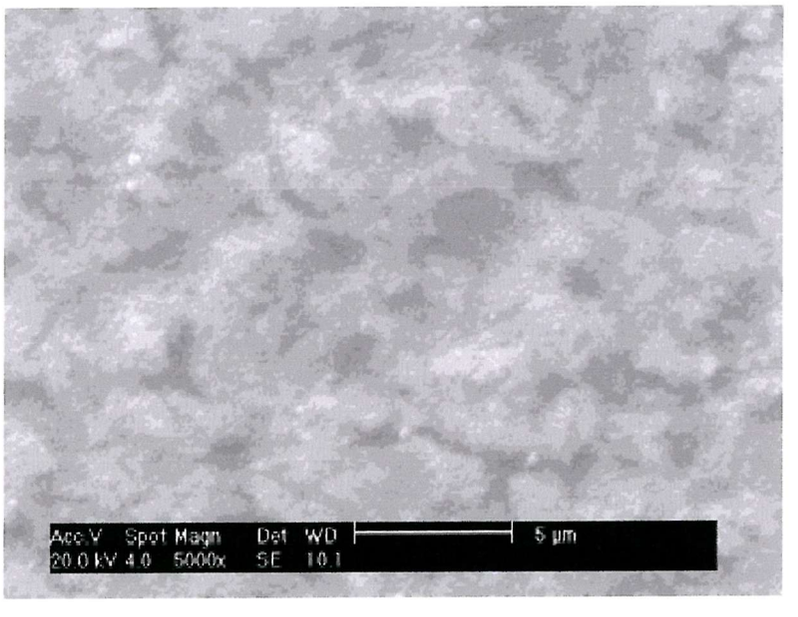

Figure 5.23: SEM image of the surface of the poly(aniline)-poly(styrenesulfonate) film deposited potentiodynamically.

5.2.3. Discussion

The polymers are constantly in the partially oxidised state during the potentiostatic deposition. When the polymer is deposited potentiodynamically, the film is reduced and oxidised during electropolymerisation generating movement of ions and solvent in and out of the polymer film. Although the polymer films have different redox states when deposited potentiodynamically or potentiostatically, each polymer film shows the same morphology when grown in either way. The similarity among the films is observed in the curvature of the parametric plots and in the SEM images.

The parametric plots differ considerably among the different polymers studied. Up to now in this thesis the damping on the acoustic wave, represented by the increase of the real part of the impedance, R, was related to the viscoelasticity of the film. Although the parametric plot obtained during the deposition of poly(aniline)-poly(vinylsulfonate) film differs from a mathematical simulation of viscoelastic films shown in Figure 5.24.

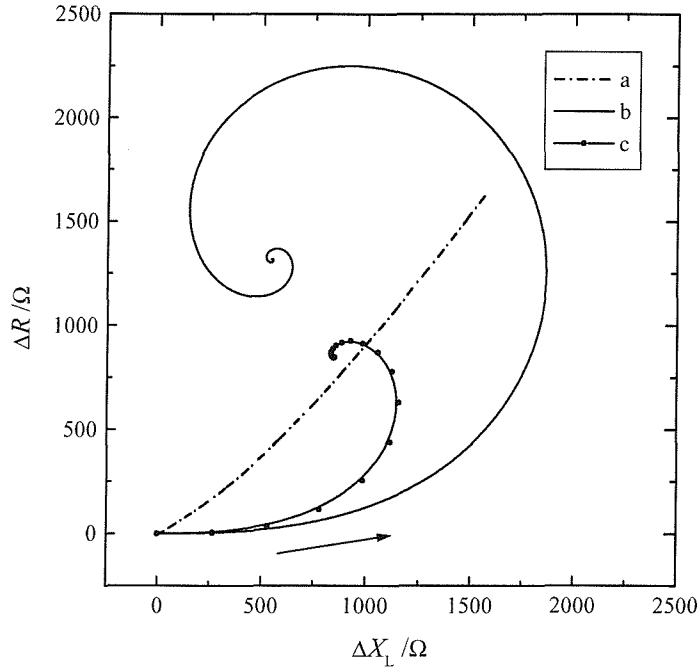

Figure 5.24: a) EQCM parametric plot recorded during the potentiodynamic deposition of poly(aniline)-poly(vinylsulfonate) following a potential sweep from –0.2 V to 0.78 V *vs.* SCE at 50 mV s^{-1}. b) simulation of the growth of viscoelastic layer in contact with water d from 0 to 5 μm, ρ = 1250 kg m^{-3} and $G' = G'' = 1$ MPa. c) simulation of the growth of viscoelastic layer in contact with water d from 0 to 5 μm, ρ = 1250 kg m^{-3} and $G' = 0$ and $G'' = 1$ MPa.

The simulation for the growth of a viscoelastic layer in contact with water is done by applying equation (4.9)

$$Z_e(\omega) = R + iX_L = \left(\frac{2\omega_o L_q}{\pi\sqrt{\mu_q \rho_q}}\right) \frac{\sqrt{\rho_1(G'_1 + iG''_1)}\tanh\left[i\omega_o d_1\sqrt{\frac{\rho_1}{G'_1+iG''_1}}\right] + \sqrt{i\rho_2 G''_2}}{\frac{\sqrt{i\rho_2 G''_2}}{\sqrt{\rho_1(G'_1+iG''_1)}}\tanh\left[i\omega_o d_1\sqrt{\frac{\rho_1}{G'_1+iG''_1}}\right]+1} \qquad \textbf{(4.9)}$$

with the values of ρ_1 = 1250 kg m^{-3}, d_1 increasing from 0 to 5 μm and $G'_1 = G''_1$ = 1 MPa and G'_1=0 and G''_1 = 1 MPa. The values for parameter 2 are the ones for water: ρ_2 = 1000 kg m^{-3} and G''_2 = 0.001 Pa. The parametric plots for these two viscoelastic films are compared to the experimental parametric plot of the potentiostatic growth of poly(aniline)-poly(vinylsulfonate). The plot of the polymer film does not have the shape expected for viscoelastic films. For the viscoelastic films modelled by equation (4.9), the parametric plots start as rigid materials for very thin films where the Sauerbrey equation could be applied. By increasing the thickness of the films the parametric plots take the form of a curve and ΔR has large values. On the parametric plot for the potentiodynamical deposition of poly(aniline)-poly(vinylsulfonate) the values of ΔR are very similar to the values of ΔX_L since the beginning of the deposition, and the plots do not take the shape of curve with the increase in thickness.

By analysing the parametric plots and the SEM images of the polymers electrochemically deposited in this chapter, there seems to be a relationship between the values of R and the morphology of the film.[117] By comparing the SEM images with the parametric plots it can be noticed that the larger the porosity of dry film, the higher the values of R.

In the next section we present the model proposed by Urbakh[59] which describes the decrease of the acoustic wave of the quartz crystal on a porous surface. As a way of motivating the reader through the mathematical equations that describe the Urbakh model, parametric plots for simulation of equations (5.21) and (5.22) that are defined later according to Urbakh model for growth of rigid porous layers in contact with water are shown in Figure 5.25. The parameters used in these simulations are the acoustic decay length, δ, which is 0.17 μm in water, the thickness of the porous polymer, ψ, goes from 0 to 0.25 μm and each curve represents a polymer with length of

permeability, ξ, from 0.2 to 0.7 μm. The parametric plot does not take in consideration the rigid mass of the polymer. The increase in ΔX_L is due to water rigidly trapped in the porous structure of the film. The curves obtained from the simulation are similar to the experimental results for the electrodeposition of poly(aniline) composite films since the higher the permeability, ξ^2, the bigger the angle between the parametric plot and the axis ΔX_L.

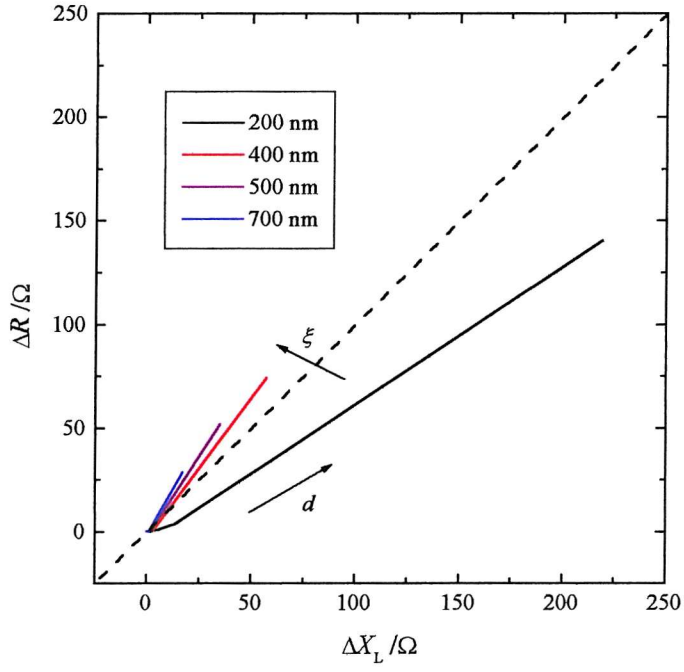

Figure 5.25: EQCM parametric plots simulated from equations (5.21) and (5.22) for the growth of rigid porous layers in contact with water. δ = 170 nm, d from 0 to 250 nm and ξ from 200 to 700 nm. The parametric plot does not take in consideration the rigid mass of the polymer film. The increase in ΔX_L is accounted for by liquid rigidly trapped in the porous structure.

5.2.3.1. Acoustic analysis of porous films

The poly(aniline) films deposited with different counterions have different morphologies in the dry state, as can be seen in the SEM pictures shown previously. The poly(aniline) film has long entangled fibres, the poly(aniline)-poly(vinylsulfonate) present a granular structure and the poly(aniline)-poly(styrenesulfonate) is a dense film. Thus this model appears to be able to describe the general shape of the plots.

Porous conducting films attract interest among scientists because their high surface areas produce more current for the same volume when compared to dense films. One characteristic of porous materials is the flow of liquid through the pores. The pores are voids created by aggregates of solid elements in the form of grains or fibres. The porosity is defined as the ratio of the volume of pores to the total volume of the material.[49] The extent to which a fluid saturates the pores of a material is called permeability.[118] The permeability length scale, ξ, is associated to the porosity as can be seen in the Appendix 8.5.

It has been experimentally demonstrated that QCM experiments can detect the existence of porosity in a coating on the quartz crystal by a shift in the resonant frequency and damping of the resonance.[117,119] The shift is caused by the mass of liquid rigidly trapped in the pores of the material. The shear waves created by the oscillation of the quartz crystal are damped due to the non-laminar flow of the liquid through the porous layer.

The acoustic analysis of porous material has not been completely understood yet. Daikhin and Urbakh[59] have proposed a model to analyse the liquid motion produced by the oscillation of porous solid surfaces. The method is based on Brinkman equation, which is used to treat the liquid flow through porous media (see Appendix 8.5). This model considers only the coupling between the liquid and the porous structure and assumes that the porous polymer coated on the quartz crystal is rigid and that the mass can be calculated by the Sauerbrey equation. This means that there is no damping of the resonance caused by viscoelastic changes of the polymer itself. Daikhin and Urbakh[59] describe the acoustic response of porous materials by the shift of the resonant frequency of the quartz crystal, $\Delta\omega$, and the damping of the resonance, represented by the width at half-height of the real part of the admittance, 2Γ (see Figure 5.26). The shift of the resonant frequency is calculated by subtracting the resonant frequency during the loading of the porous material, ω_c, from the resonant frequency of the bare crystal, ω_0. The Brinkman equation has already been used on the characterisation of the porosity of poly(aniline)-poly(styrenesulfonate) film by EQCM measurements.[97,120]

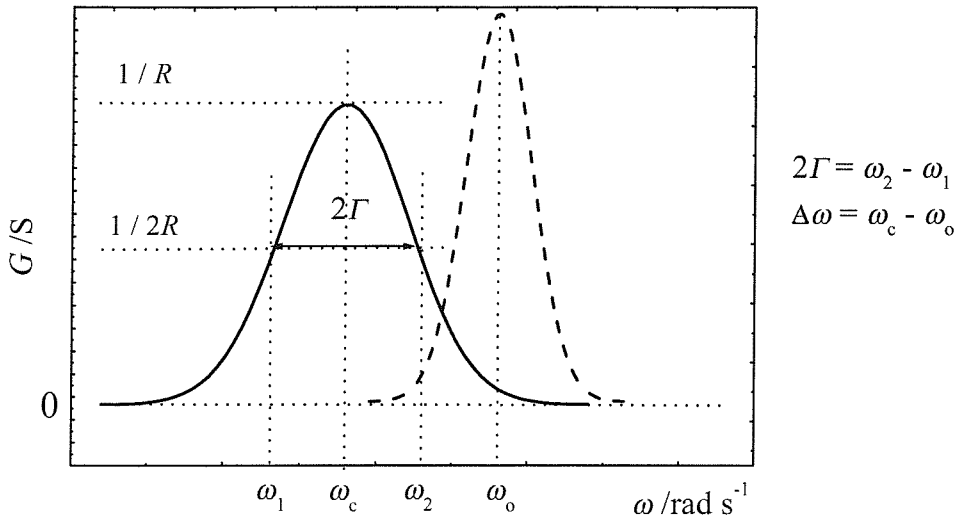

Figure 5.26: Graph of real part of the admittance, G, versus angular frequency, ω, showing the width at half maximum 2Γ and the angular resonant frequency ω_c of a coated quartz crystal (—). ω_o is the resonant frequency of the bare quartz crystal in air (---).

The equations proposed for the QCM experiments for porous structures are:[59]

$$\Delta\omega = -\frac{\omega_o^2 \rho}{\pi\sqrt{\mu_q \rho_q}} \mathrm{Re}[\mathcal{J}] \tag{5.1}$$

$$\Gamma = -\frac{\omega_o^2 \rho}{\pi\sqrt{\mu_q \rho_q}} \mathrm{Im}[\mathcal{J}] \tag{5.2}$$

where $\Delta\omega$ is the shift of the resonant frequency, Γ is half of the width at half-height of the admittance, ω_o is the resonant frequency of the bare crystal in air, ρ is the density of the liquid, μ_q and ρ_q are constants for quartz and

$$\mathcal{J} = \frac{1}{q_o} + \frac{\Psi}{\xi^2 q_1^2} - \frac{1}{W}\frac{1}{\xi^2 q_1^2}\left[\frac{2q_o}{q_1}\left(\cosh(q_1\Psi) - 1\right) + \sinh(q_1\Psi)\right] \tag{5.3}$$

where:

$$q_0 = \sqrt{\frac{i\omega_o \rho}{\eta}} = \frac{\sqrt{2i}}{\delta} \tag{5.4}$$

$$q_1^2 = q_o^2 + \xi^{-2} \tag{5.5}$$

$$W = q_1 \cosh(q_1 \Psi) + q_o \sinh(q_1 \Psi) \tag{5.6}$$

where δ is the decay length of the acoustic wave in a Newtonian liquid in contact with the porous film, ξ^2 is the permeability of the film and Ψ is the thickness of the porous film.

The first term in equations (5.1) and (5.2) represents the QCM response for a bare quartz crystal interface and the complex term represents the interaction of the liquid with the porous material.

The first term in equation (5.3) shows the purely viscous coupling of the liquid. In the second term, the ratio Ψ/ξ corresponds to the amount of liquid that moves together with the porous film during the oscillation of the quartz crystal. The third term is important when the value of the length of permeability, ξ, is of the same order of magnitude as the thickness of the porous film, Ψ. The rigid mass of the porous material is not included in equation (5.3), but it can be inserted as an additional term in equation (5.1).

In order to apply the Urbakh model in our EQCM data for poly(aniline) films, the values of $\Delta\omega$ and Γ have to be transformed to the values extracted from the QCM measurements, which are X_L and R.

Firstly we represent $\Delta\omega$ according to equation (1.22):

$$\Delta\omega = \omega_c - \omega_o = \frac{1}{\sqrt{LC_q}} - \frac{1}{\sqrt{L_q C_q}} = \frac{1}{\sqrt{L_q C_q}}\left(\sqrt{\frac{L_q C_q}{LC_q}} - 1\right) = \omega_o\left(\sqrt{\frac{L_q}{L}} - 1\right),$$

$$\sqrt{\frac{L_q}{L}} = \frac{\Delta\omega}{\omega_o} + 1 \qquad \text{and}$$

$$L = \frac{L_q}{\left(\frac{\Delta\omega}{\omega_o} + 1\right)^2} \tag{5.7}$$

where L represents the inductance of the loaded quartz and L_q is the inductance of the bare crystal. Assuming that the shift in resonant frequency (of the order of kHz) is much smaller than the resonant frequency (of the order of MHz), $\Delta\omega \langle\langle \omega_o$:

$$L_q \approx L\left(1+\frac{2\Delta\omega}{\omega_o}\right) \tag{5.8}$$

$$L_q \approx L+2L\frac{\Delta\omega}{\omega_o} \tag{5.9}$$

For $\Delta L = L - L_q$:

$$\Delta L \approx -2L\frac{\Delta\omega}{\omega_o} \tag{5.10}$$

Considering that $\Delta X_L = \omega_o \Delta L$:

$$\Delta X_L = \omega_o \Delta L = -2L\Delta\omega \tag{5.11}$$

And finally:

$$\boxed{\Delta\omega = -\frac{\Delta X_L}{2L}} \tag{5.12}$$

Now, we consider the representation of Γ in terms of the parameters of the BVD equivalent electrical circuit. Referring to Figure 5.26, where the peak of the admittance plot is equal to the inverse of R, $G_{\max} = \frac{1}{R}$. The value of the admittance at half-height is the inverse of two times the value of R.

$$\frac{G_{\max}}{2} = \frac{1}{2R} \tag{5.13}$$

where the real part of the admittance

$$G(\omega) = \frac{R}{R^2 + \left(\omega L - \frac{1}{\omega C}\right)^2} \tag{5.14}$$

By combining equations (5.13) and (5.14), at half maximum:

$$2R^2 = R^2 + \left(\omega L - \frac{1}{\omega C}\right)^2 \tag{5.15}$$

$$\pm R = \left(\omega L - \frac{1}{\omega C} \right) \tag{5.16}$$

We can consider that $C = C_q$ because the capacitance of the quartz is constant and it is not influenced by any load on the surface. Then, applying $LC_q = \frac{1}{\omega_c^2}$ in equation (5.16):

$$\pm R = L\left(\omega - \frac{\omega_c{}^2}{\omega} \right) \tag{5.17}$$

$$L\omega^2 \pm R\omega - L\omega_c^2 = 0 \tag{5.18}$$

Calculating the value of ω in the quadratic equation above:

$$\omega_1 = \frac{-R \pm \sqrt{R^2 + 4L^2\omega_c^2}}{2L}, \quad \omega_2 = \frac{R \pm \sqrt{R^2 + 4L^2\omega_c^2}}{2L} \tag{5.19}$$

Only the positive roots in equation (5.19) are considered because the frequencies ω_1 and ω_2 have positive values. By applying them in the definition $2\Gamma = \omega_2 - \omega_1$:

$$2\Gamma = \frac{R}{L} \quad \text{or} \quad \boxed{\Gamma = \frac{R}{2L}} \tag{5.20}$$

Thus there are simple relationships between $\Delta\omega$ and Γ and R and X_L. Therefore equations (5.1) and (5.2) can then be rewritten as:

$$X_L = \frac{2\omega_o^2 L\rho}{\pi\sqrt{\mu_q \rho_q}} \mathrm{Re}[\mathcal{J}] \tag{5.21}$$

$$R = \frac{2\omega_o^2 L\rho}{\pi\sqrt{\mu_q \rho_q}} \mathrm{Im}[\mathcal{J}] \tag{5.22}$$

As we have already said this model does not include the rigid mass of the polymer on the quartz crystal. We can include this in equation (5.21) by adding the Sauerbrey contribution of the mass loading for the rigid porous solid in the term ΔX_L.

$$X_L = \frac{2\omega_o^2 L}{\pi\sqrt{\mu_q \rho_q}}(\Psi\rho_f + \rho\,\mathrm{Re}[\mathrm{J}]) \tag{5.23}$$

where ρ_f and Ψ are the density and the thickness of the dry porous film, respectively.

Note that the term ΔR is not affected by the addition of a rigid layer on the quartz crystal.

Fortunately, the term J in equations (5.21) and (5.22) can be simplified depending on the relative sizes of three important lengths: the permeability length scale, ξ, the thickness of the polymer layer, Ψ, and the decay length of the acoustic wave, δ.

Considering that the porous film is thin and the acoustic decay length is the longest length ($\delta >> \Psi$ and $\delta >> \xi$), equation (5.5) becomes:

$$q_1^2 = \frac{-2}{\delta^2} + \frac{1}{\xi^2} \quad \text{and} \quad q_1 \approx \frac{1}{\xi} \tag{5.24}$$

and equation (5.3) is simplified to:

$$\mathrm{J} = \frac{\delta}{\sqrt{2\mathrm{i}}} + \Psi - \frac{1}{W}\left[\frac{2\xi\sqrt{2\mathrm{i}}}{\delta}\left(\cosh\left(\frac{\Psi}{\xi}\right) - 1\right) + \sinh\left(\frac{\Psi}{\xi}\right)\right] \tag{5.25}$$

The interaction between the liquid and the porous material depends on the ratio of Ψ to ξ. For very porous films, $\xi >> \Psi$, the liquid can move freely inside the voids. The liquid vibrates as if there were no film attached to the quartz crystal and equation (5.3) is simplified to.

$$\mathrm{J} = \frac{\delta}{\sqrt{2\mathrm{i}}} \tag{5.26}$$

The only parameters that influence the QCM response in this case are the density and the viscosity of the liquid, since the decay length of the acoustic wave depends on these parameters $\left(\delta = \sqrt{2\eta/\omega_o\rho}\right)$. For a material with relatively low porosity, $\Psi >> \xi$, the liquid trapped in the porous surface moves with the velocity of the quartz surface. Equation (5.3) is simplified to

$$\mathrm{J} = \frac{\delta}{\sqrt{2\mathrm{i}}} + \Psi \tag{5.27}$$

Finally if the film is very porous and the permeability length is the longest length, $\xi >> \Psi$ and $\xi >> \delta$, equation (5.5) becomes:

$$q_1 = q_o = \frac{\sqrt{2i}}{\delta} \tag{5.28}$$

And equation (5.3) can be represented as:

$$\mathrm{J} = \frac{\delta}{\sqrt{2i}} + \left(\frac{\delta}{\xi}\right)^2 \frac{\Psi}{2i} - \frac{\delta^2}{\xi^2 2i} \frac{1}{W}\left[2\left(\cosh\left(\frac{\Psi\sqrt{2i}}{\delta}\right) - 1\right) + \sinh\left(\frac{\Psi\sqrt{2i}}{\delta}\right)\right] \tag{5.29}$$

For thin porous films, $\delta >> \Psi$, the simplifications result in the same case as equation (5.26) where the amplitude of the acoustic wave generated by the oscillation of the quartz crystal is smaller than the pores of the film.

$$\mathrm{J} = \frac{\delta}{\sqrt{2i}} \tag{5.30}$$

For very thick films, $\Psi >> \delta$, the term J is influenced by the three parameters δ, Ψ and ξ. The third term of equation (5.29) is cancelled resulting in:

$$\mathrm{J} = \frac{\delta}{\sqrt{2i}} + \left(\frac{\delta}{\xi}\right)^2 \frac{\Psi}{2i} \tag{5.31}$$

The simplifications obtained by the correlation between ξ, δ and Ψ can be summarised in three cases. (Note that the Sauerbrey contribution for the rigid mass is not considered on the term ΔX_L.)

Case I ($\delta >> \Psi$ and $\xi >> \Psi$): Corresponds to a very porous and thin material for which we obtain

$$X_L = \frac{2\omega_o^2 L}{\pi\sqrt{\mu_q \rho_q}}\left(\sqrt{\frac{\eta\rho}{2\omega_o}}\right), \quad R = \frac{2\omega_o^2 L}{\pi\sqrt{\mu_q \rho_q}}\sqrt{\frac{\eta\rho}{2\omega_o}} \tag{5.32}$$

In case I, ΔR and ΔX_L have the same values, which corresponds to the Bruckenstein and Kanazawa equation. The viscosity and density of the liquid determine the values of ΔX_L and ΔR. When the size of the pores are much bigger than the decay length of the

acoustic wave, the wave decays as no rigid material is in contact with the crystal. The response of the QCM is the same as that for a bare crystal in contact with a liquid.

Case II ($\Psi >> \xi$ and $\delta >> \xi$): Represents a film with low porosity. Part of the liquid is trapped in the porous structure of the material and vibrates as if it were part of the material itself. The effect caused by mass loading is much bigger than the viscous energy dissipation. In this case we find:

$$X_L = \frac{2\omega_o^2 L}{\pi\sqrt{\mu_q \rho_q}}\left(\sqrt{\frac{\eta\rho}{2\omega_o}} + \Psi\rho\right), \quad R = \frac{2\omega_o^2 L}{\pi\sqrt{\mu_q \rho_q}}\left(\sqrt{\frac{\eta\rho}{2\omega_o}} - \Psi\rho\right) \tag{5.33}$$

The parameter R cannot be smaller than the value obtained for a bare quartz crystal, so ΔR is assumed to be constant and close to zero. This corresponds to the Sauerbrey approximation.

Case III ($\Psi > \delta$ and $\xi >> \delta$): This is the case for very thick and porous films. The energy dissipation depends on the permeability and thickness of the film and on the viscosity and density of the liquid. The liquid vibrates freely inside the open porous structure but the QCM does not sense the total liquid trapped when the height of liquid is larger than the decay length of the acoustic wave. In this case we have:

$$X_L = \frac{2\omega_o^2 L}{\pi\sqrt{\mu_q \rho_q}}\left(\sqrt{\frac{\eta\rho}{2\omega_o}}\right), \quad R = \frac{2\omega_o^2 L}{\pi\sqrt{\mu_q \rho_q}}\left(\sqrt{\frac{\eta\rho}{2\omega_o}} + \frac{\eta\Psi}{\omega_o \xi^2}\right) \tag{5.34}$$

The relationship between these three cases is shown in the case diagram in Figure 5.27. The boundaries are defined by the relative sizes of the important lengths in equation (5.3): the permeability length scale, ξ, the thickness of the polymer layer, Ψ, and the decay length of the acoustic wave in the bulk, δ. On the boundaries between the cases the term $\mathcal{J}$ cannot be simplified and it has to be calculated by using equation (5.3).

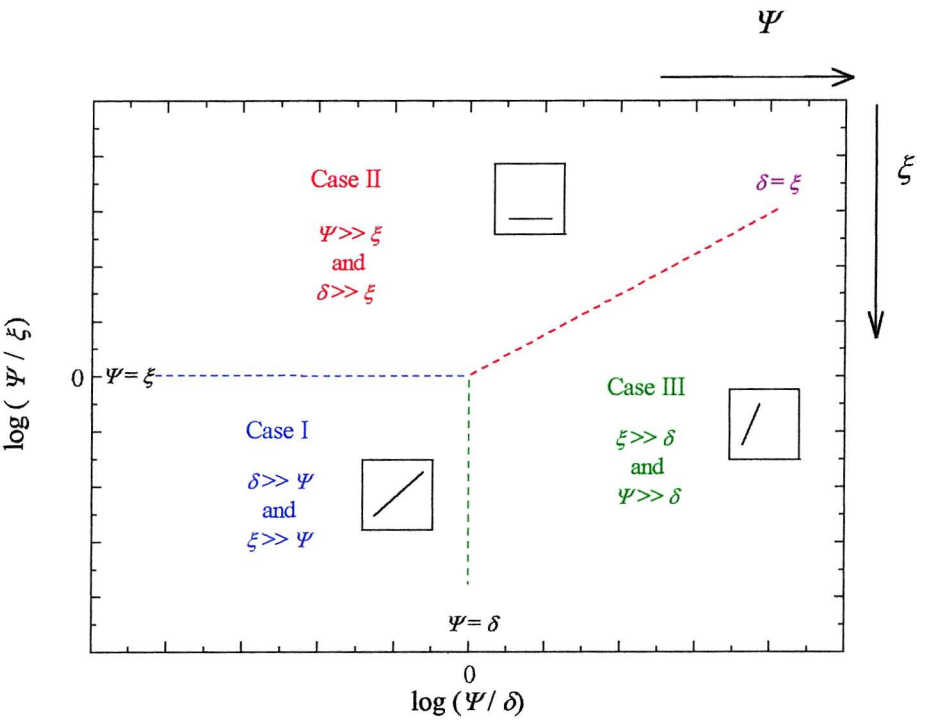

Figure 5.27: Case diagram of the QCM response for porous films showing the parameters simplified at relative sizes of Ψ, ξ and δ. The insets are the parametric plots for each case.

We now use the experimental data for the potentiostatic deposition of poly(aniline)-poly(vinylsulfonate) to see how it would fit to the model proposed by Urbakh. It is very difficult to find the proper value of the permeability, ξ^2, of the polymer film. AFM measurements of the surface topology of a poly(aniline)-poly(styrenesulfonate) film immersed in water showed a roughness of 400 ± 50 nm.[120] There is also an experimental problem to calculate the dry mass of polymer deposited. After the electrodeposition, the polymer film must be rinsed and dried in order to perform QCM measurements for find the dry mass of polymer. The solution of aniline with the poly(anions) are very viscous and during rinsing these thick solutions, part of the polymer film is also washed out introducing experimental errors in the calculation of the thickness of the porous film, ψ. For these reasons, only a qualitative analysis will be presented here. For a quantitative analysis, a porous rigid structure with well defined permeability, thickness and decay length of the acoustic wave should be used. The

system described by Bartlett using nanostructured cobalt films with regular pores of nanometer dimension is a good example to test quantitatively the Urbakh model for EQCM measurements of porous materials.[121] Metallic cobalt is a rigid material and the size of the pores can be adjusted by the concentration of the template mixture used during the electrochemical deposition of the cobalt film. Thus the permeability of the material could be changed and also the thickness could be controlled by the charge passed during deposition. The decay length of the acoustic wave can be modified by changing the viscosity and density of the solution in contact with the porous structure.

Figure 5.28 shows the parametric plot during the potentiostatic growth of the poly(aniline)-poly(vinylsulfonate) film. We confer different porosities to the polymer film 0%, 20%, 50% and 70%, where the rigid masses are 100%, 80%, 50% and 30% respectively of the total mass calculated by the QCM measurements (polymer and solution). The rigid mass of the porous polymer film deposited during time can calculated by correlating the mass the the charge passed during the deposition

$$X_{\mathrm{L},porous}(t) = \frac{X_{\mathrm{L},\mathrm{dry}}\, q(t)}{q_{\max}} \qquad \textbf{(5.35)}$$

where the $X_{\mathrm{L,dry}}$ is a percentage of the total X_{L} (0% porosity), $q_{\max}$ is the total charge passed during the deposition and $q(t)$ is the charge passed at time t.

By analysing Figure 5.28 it can be seen that with the increase in the permeability (porosity) of the polymer, the parametric plot changes. In this simulation, the values of ψ and δ are kept constant and ξ increased. The permeability (porosity) is mathematically increased by decreasing the percentage of polymer mass from the total mass measured by the QCM measurements. With the increase in permeability and thickness of the film, there is a change from Case I to Case III. But more studies on this topic are necessary for better conclusions.

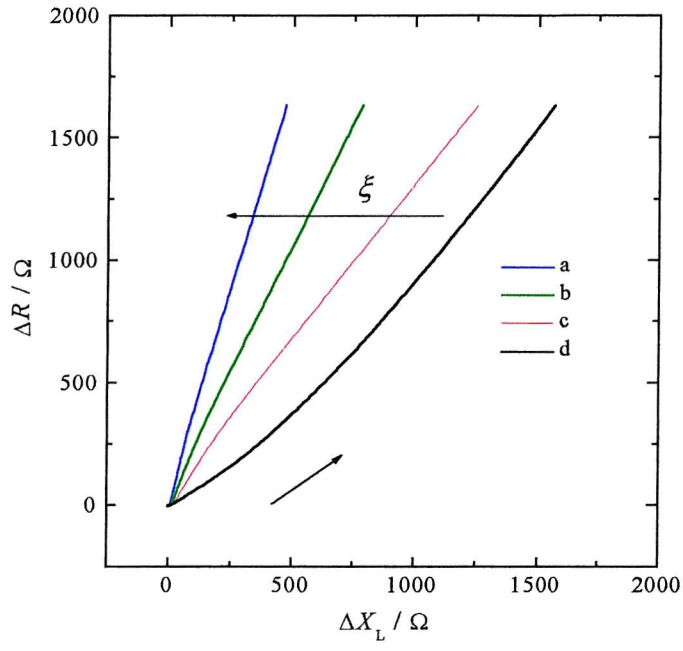

Figure 5.28: EQCM parametric plot for the potentiostatic deposition of poly(aniline)-poly(vinylsulfonate) film subtracting the Sauerbrey term. The rigid film is assumed to be a) 30 %, b) 50 %, c) 80 % and d) 100 % of the total mass.

5.2.4. Conclusion

There were no significant changes in the EQCM behaviour or SEM for poly(aniline) composite films deposited potentiostatically or potentiodynamically. Although the counterions used during electrodeposition do have a significant effect on the morphology of the films. The poly(aniline) film has a fibrous structure, the poly(aniline)-poly(vinylsulfonate) film has a globular structure and the poly(aniline)-poly(styrenesulfonate) film has a more compact structure.

During the QCM analysis of the electrochemical deposition of poly(aniline) composite films, a relationship between the QCM response and the porosity of the materials analysed was noted. We have applied the model proposed by Urbakh to analyse porous materials using QCM measurements.[97] This method considers only the non-laminar liquid flow caused on the irregular interface between the liquid and the porous material, without taking into account the Sauerbrey contribution of the rigid mass of the polymer film. We do not try to do quantitative analysis because the right

values of the permeability and the thickness of thin layers of porous polymers deposited on the quartz crystal are difficult to be obtained. The qualitative study of Urbakh model shows that for thin films with low permeability, there is liquid trapped on the pores of the material which vibrates as part of the film. This increases the parameter X_L without influencing R. (Case II). In the case of thin films with high permeability (porosity) the acoustic wave caused by the vibration of the quartz crystal is damped by the liquid placed inside the large pores of the material. The parameters of the QCM response, R and X_L, depends on the density and viscosity of the liquid in contact with the material and the growth of the films is sensed as an increase in the mass sensitive area of the quartz crystal (Case I). With the deposition of the porous material thicker than the decay length of the acoustic wave, the QCM analyses get compromised (Case III).

In the Urbakh method, the porous material is assumed to be rigid and the damping of the decay length of the acoustic wave occurs exclusively due to the non-laminar liquid flow on the irregular interface between the liquid and the porous material. Although in reality the liquid impregnates the material[12] modifying its rheology, increasing the response of the parameter R. From our knowledge, there is not yet a model combining the effect of porosity and viscoelasticity on QCM experiments.

We have chosen the poly(aniline)-poly(styrenesulfonate) film to analyse the changes in mass of the polymer during redox cycling in the following chapter. This film was chosen because it is the densest and the Sauerbrey equation can be applied to correlate changes in X_L to mass.

6. EQCM Analysis and Characterisation of poly(aniline)-poly(styrenesulfonate) films

Among the polymers analysed in the previous section, the Sauerbrey equation was only found to apply to the poly(aniline)-poly(styrenesulfonate) film, because only for this material is the condition that the parameter ΔR is maintained close to zero during the electrodeposition obeyed. As we are interested in measuring the changes in the mass of the polymer during redox switching by applying the Sauerbrey equation, the poly(aniline)-poly(styrenesulfonate) film was chosen for the next set of experiments. Many aspects need to be considered during the redox switching of conducting polymers because in addition to the electron transfer, there are also movement of ions, solvent, and other neutral molecules, and configurational changes on the polymer.[74] Our proposed mechanism for the reduction and oxidation of the protonated poly(aniline)-poly(styrenesulfonate) is shown in Figure 5.3. In the scheme we can see that the negatively charged poly(styrenesulfonate) keeps the poly(aniline) protonated, i.e. conductive, in the oxidised state.

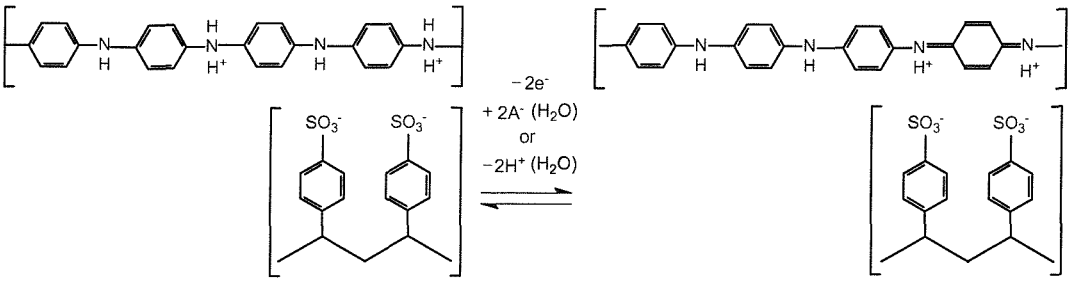

Figure 5.3: Protonated poly(aniline)-poly(styrenesulfonate) in the reduced and oxidised forms. The sketch shows the movement of anions or protons and solvent consequent on the electron movement in order to maintain electroneutrality of the polymer.

During an electrochemical reaction the EQCM detects simultaneously and *in situ* the transport of the electronic charge between the electrode and the polymer film and the subsequent movement of ions and solvent between the electrolyte and the polymer film. The combination of this information is a powerful tool for the comprehension of the mechanism of charge transport and redox switching in the polymer. A better understanding of the electronic and physical changes during doping and undoping of

conducting polymers is crucial for the success and improvement of their application in commercial devices.

The EQCM can detect the insertion of ions and solvent molecules into, and the release of ions and solvent molecules from, the polymer film since the transport of molecules causes changes in the mass of the polymer. However the EQCM cannot distinguish between the movement of charged (ions) and neutral species (water, in our case). Only charged species are used in the control of the electroneutrality of the polymer during redox switching. In order to identify anion movement different inorganic acids with anions of distinct molecular weights were used as electrolytes during voltammetric cycles of the poly(aniline)-poly(styrenesulfonate) film. Perchloric and hydrochloric acids were chosen for these experiments because they are strong monoprotonated acids and their anions have very different molecular weights. The molecular weight of the perchlorate anion is 99.5 g mol^{-1}, and that of the chloride anion is 35.5 g mol^{-1}. The calculation of the variation in mass of the polymer film during redox cycling using these two electrolytes indicates whether the anions are responsible for maintaining electroneutrality. The electrolytes are strong acids and the cations are exclusively protons. The concentration of protons in the electrolyte solution close to the surface of the polymer film is detected amperometrically in a combined measurement between the Electrochemical Quartz Crystal Microbalance and the Scanning Electrochemical Microscopy (SECM). A microelectrode, with a potential at which protons are reduced, is positioned very close to the surface of the polymer during the potential sweeping. The movement of protons into and out of the polymer film during potential cycling can be interpreted from the mass change in the polymer and the current registered at the microelectrode.

6.1. Literature Review

Several models have been proposed for the conversion of protonated leucoemeraldine to protonated emeraldine. Due to the large number of papers dedicated to this topic only a few of the most relevant to our experiments were selected to be mentioned here. Barbero et al.[13] have analysed the first oxidation peak of poly(aniline) in inorganic acids using the probe beam deflection technique. They have proposed that there is proton release followed by anion uptake during the oxidation scan and a consecutive anion release and proton insertion during the reduction scan. It was speculated that the expulsion of protons during the oxidation increases with the decrease of the electrolyte pH. The relative contribution of protons and anions depends on the degree of protonation of the leucoemeraldine, which is related to the electrolyte pH. Only protons are expelled from fully protonated leucoemeraldine, whereas anions are inserted in deprotonated leucoemeraldine. They have noticed that protons are expelled in higher proportion when HCl is used as the electrolyte instead of $HClO_4$. This could happen because the Cl^- is highly hydrated due to its high charge to radius ratio hindering the penetration of the solvated Cl^- into the film, thus favouring the release of protons instead.

Orata and Buttry [17] have studied poly(aniline) films as a function of redox state and pH using the Electrochemical Quartz Crystal Microbalance. They have used the Sauerbrey equation to analyse mass changes in the poly(aniline) during redox cycles. It has been verified that poly(aniline) films behave as elastic films by comparing the deposition charge to the change in the resonant frequency of the quartz. The film is considered rigid when there is linearity between these two variables. The charge shows the amount of electroactive polymer deposited, and the resonant frequency indicates the total mass deposited. They have noticed that poly(aniline) films behave as rigid films over a limited range of thickness. The linearity breaks down when the film is thicker than ca. 300 nm. However it was not proved that the polymer film remains rigid during the potential sweeps and the changes in the polymer mass might not be proportional to the variation in the resonant frequency. The resonant frequency decreased (mass increase) during oxidation and increased (mass decrease) during reduction of the poly(aniline) film in 1.0 M solutions of several inorganic acids. The increase in mass

was assumed to be caused by the insertion of anions, which neutralise the net charge on the polymer chains of the protonated poly(aniline) film in the emeraldine state.

Due to its complexity, a definitive mechanism for the redox switching of poly(aniline) has not been achieved yet.

Smyrl et al.[122] have observed from Electrochemical Quartz Crystal Microbalance measurements that conducting polymers show anion-insertion or cation-release during oxidation depending on the choice of the anion used during electropolymerisation. Small anions may move into or out of the polymer during redox cycles, but large polymeric anions do not, and as a result the cation movement is responsible for the maintenance of the net charge neutrality during voltammetric cycles.

6.2. Analysis of anion movement

The poly(aniline)-poly(styrenesulfonate) film deposited potentiodynamically (deposition is shown in Figure 5.20), was used in the experiments described throughout Chapter 6. The reproducibility of the experiments was observed using other thin poly(aniline)-poly(styrenesulfonate) films. It is important to state that only one film of poly(aniline)-poly(styrenesulfonate) was used for all the experiments in this chapter because the use of one single film is important for the comparison of the polymer mass when different electrolytes are used. Although data for only one film are shown replicate experiments showed that the behavior of the film was representative of that of poly(aniline)-poly(styrenesulfonate) films deposited in this way. The stability of the film was verified by cycling the film in 1 M $HClO_4$ at 20 mV s^{-1} before and after any replacement of a electrolyte and comparing the voltammograms. The thickness of the dry polymer film in vacuum can be measured from the SEM image shown in Figure 6.1. On the SEM measurement the sample is titled 70° relative to the *x* axis, so the thickness shown in the picture (0.96 μm) does not correspond to the actual value. In order to correct this value, the thickness of the film shown in the SEM image is divided by sin (70°). The thickness of the dry polymer in vacuum is 0.96 μm / 0.94 = 1.02 μm.

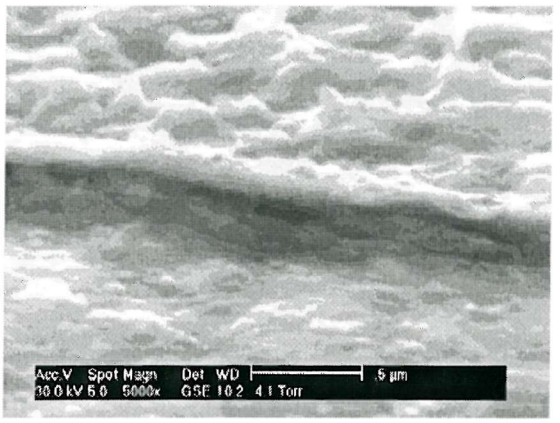

Figure 6.1: SEM image of the poly(aniline)-poly(styrenesulfonate) film used for the analysis of ionic movement during redox switching. According to the SEM picture, the thickness of the film is 0.96 / 0.94 = 1.02 µm.

The polymer film was cycled only between –0.2 V and 0.5 V *vs.* SCE. The cycling of the film to higher potentials could cause movement of different species to maintain the electroneutrality of the film, but due to the degradation of the film in the pernigraniline state only the reaction between the leucoemeraldine and the emeraldine was studied. The polymer film was kept at the initial potential, in the reduced state, for 3 min before the first cycle. This procedure ensures that the polymer always starts the redox cycles with the same solvation and configurational state.

Different scan rates were used in the voltammetric cycles to detect the occurrence of fast and slow mass transport into and out of the film. The scan rates used were 5 mV s^{-1}, 20 mV s^{-1} and 100 mV s^{-1}. At extremely fast scan rates, only fast processes occur. Over long time scales, or at slow scan rates, equilibrium predominates. The movement of neutral species is slower than the movement of charged species, and will occur depending on the experimental conditions.

6.2.1. Possible movement of perchlorate anion during redox cycles

Figure 6.2, Figure 6.3 and Figure 6.4 show the voltammograms and changes in the electroacoustic impedance of the poly(aniline)-poly(styrenesulfonate) film during redox switching in 1 M $HClO_4$ at different scan rates. The changes in the charge during the redox cycles are plotted on the same graphs as the voltammograms to allow better visualisation of the correlation between changes in the charge and changes in the imaginary part of the electroacoustic impedance, ΔX_L. The values of ΔR stay close to zero during the voltammetric cycles, therefore the Sauerbrey equation can be applied. The changes in ΔX_L, in the case of this thin layer of poly(aniline)-poly(styrenesulfonate), correspond to the mass change of the polymer. This variation in mass occurs due to ions moving into and out of the polymer film to keep the electroneutrality disturbed by the charge passed through the film. Accompanying the ion movement there are also solvent transport into and out of the polymer film. The total initial areal mass of this polymer film in the reduced state is 96 $\mu g\ cm^{-2}$ as seen in Figure 5.20. So the mass changes during potential cycling correspond to approximately 4 % in film mass.

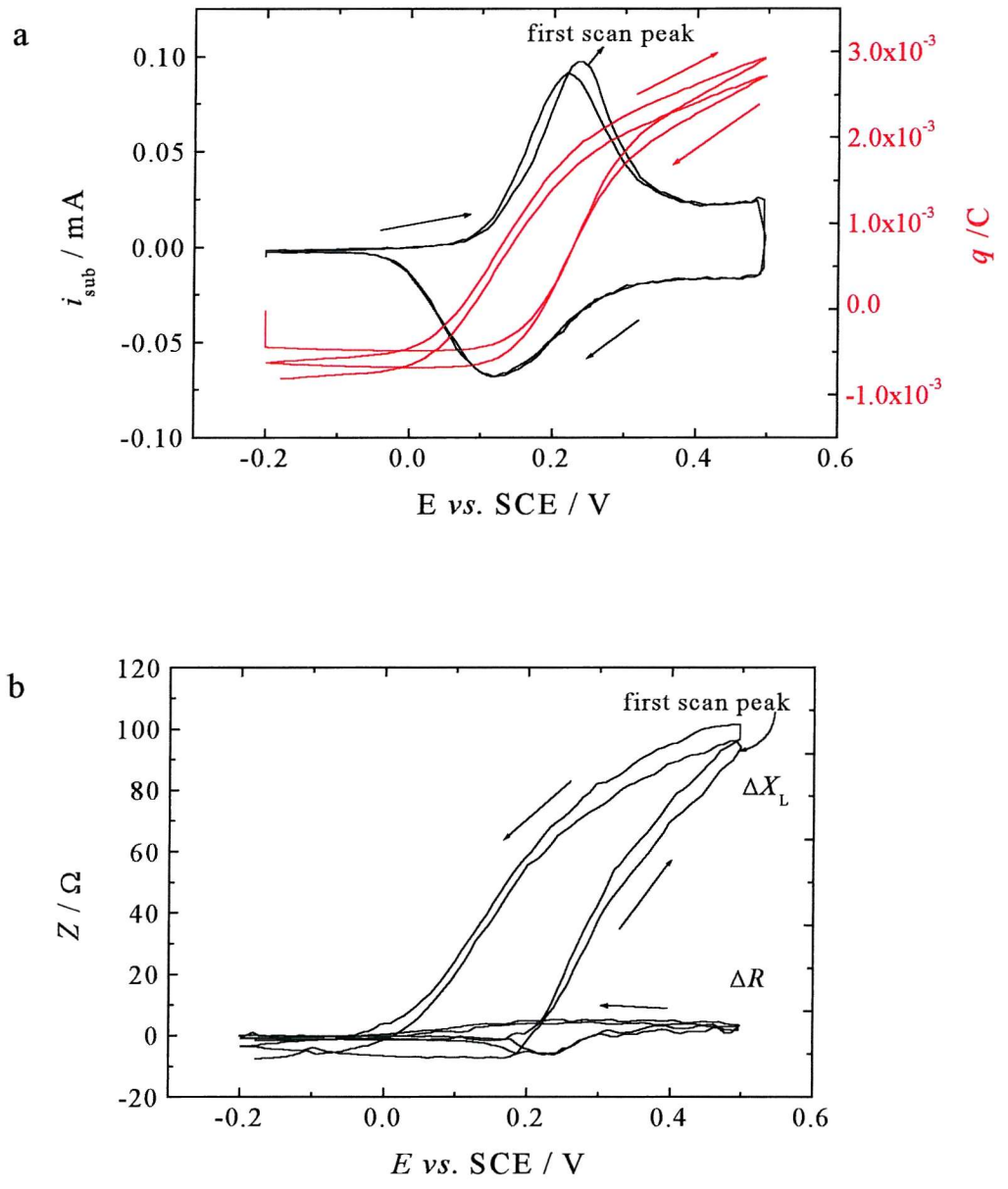

Figure 6.2: a) Voltammetric cycle and b) real and imaginary parts of the electroacoustic impedance during voltammetric cycling of 96 μg cm^{-2} of poly(aniline)-poly(styrenesulfonate) film in 1 M $HClO_4$ at 5 mV s^{-1}. The film was conditioned for 3 min at –0.2 V *vs.* SCE before cycling. The points are measured every 1.8 s at a difference of potential of 9 mV.

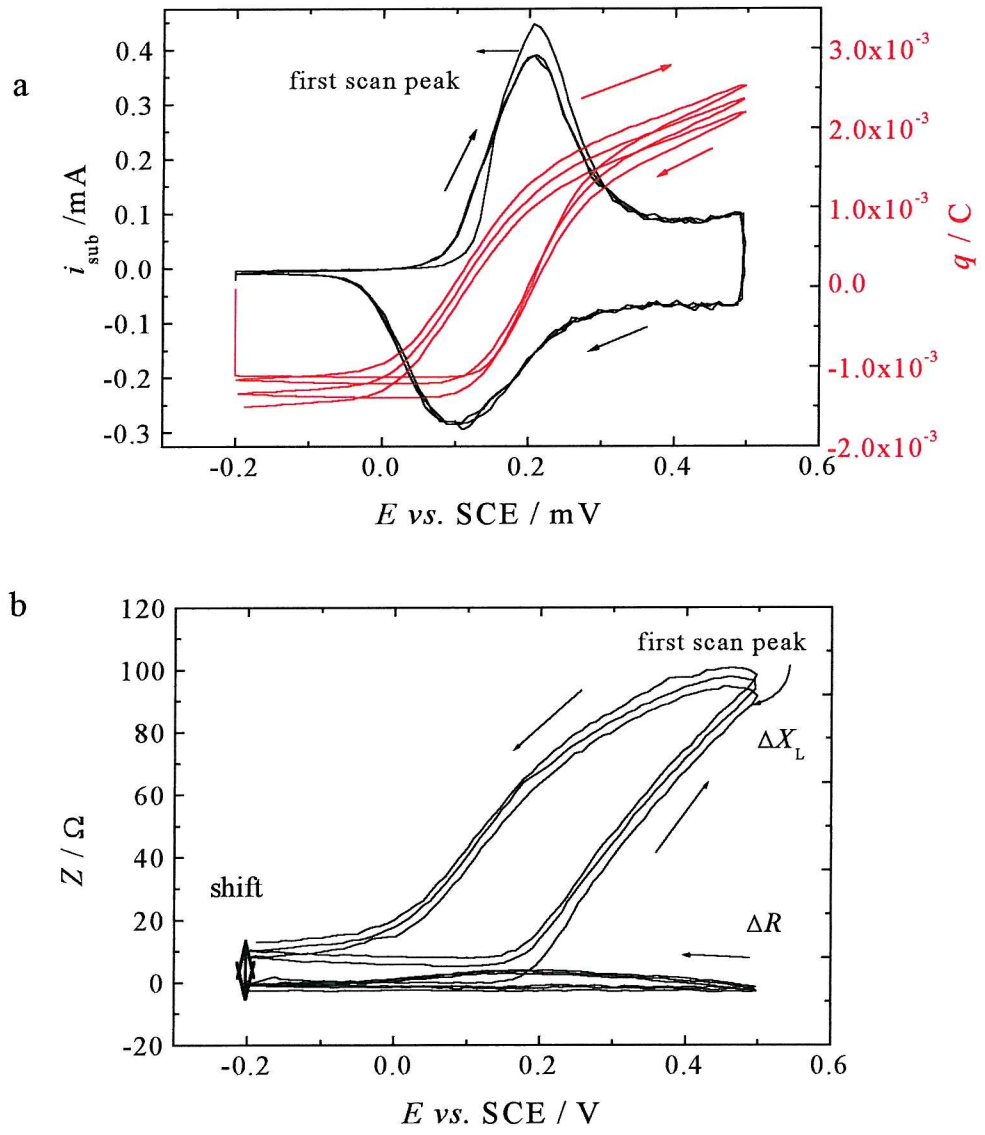

Figure 6.3: a) Voltammetric cycle and b) real and imaginary parts of the electroacoustic impedance during voltammetric cycling of 96 μg cm^{-2} of poly(aniline)-poly(styrenesulfonate) film in 1 M $HClO_4$ at 20 mV s^{-1}. The film was conditioned for 3 min at –0.2 V *vs.* SCE before cycling. The points are measured every 0.5 s at a difference of potential of 10 mV.

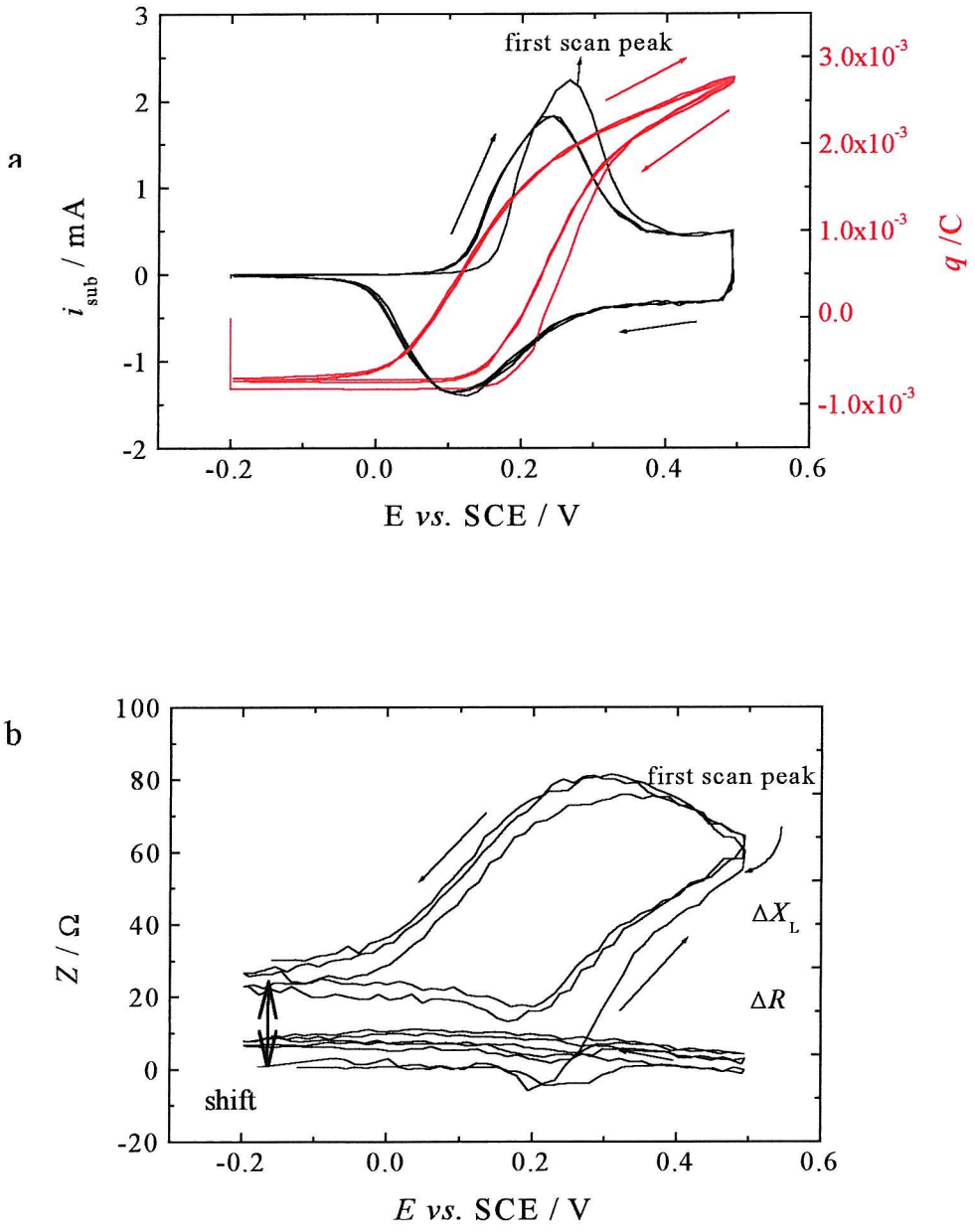

Figure 6.4: a) Voltammetric cycle and b) real and imaginary parts of the electroacoustic impedance during voltammetric cycling of 96 μg cm^{-2} of poly(aniline)-poly(styrenesulfonate) film in 1 M $HClO_4$ at 100 mV s^{-1}. The film was conditioned for 3 min at –0.2 V *vs.* SCE before cycling. The points are measured every 0.15 s at a difference of potential of 16 mV.

It can be seen in the voltammograms that the first scan oxidation peaks are shifted positively in potential and they have bigger peak currents than the subsequent scan oxidation peaks. This is commonly observed in voltammetric cycles of conducting polymers. This might happen because before the beginning of the voltammetric cycles the polymer film is maintained in the reduced state for 3 min and it is then fully converted to the reduced state. During the scans, the polymer film might not be in equilibrium and the initial reduction state would not be reached.[123] The idea of non equilibrium of the polymer during redox cycles is reinforced by the fact that the potential shift for the first oxidation peak is larger for faster scan rates.

The values of X_L do not return to the initial value after an electrochemical perturbation. The failure to return to the same physical state, which is characteristic of polymers, could be caused by mechanical deformation or swelling.[74] The shift is indicated in Figure 6.2, Figure 6.3 and Figure 6.4 and is again more noticeable at faster scans. Another cause of this shift could be the slow kinetic process involving motion of neutral species (solvent). The slower movement of water cannot keep up with the ionic charge of the polymer. This could be a reason of the continuous decrease in ΔX_L even when the direction of the scan is reversed at 100 mV s^{-1}.

By analysing Figure 6.2, Figure 6.3 and Figure 6.4 we see that the imaginary part of the electroacoustic impedance, ΔX_L, does not start to increase until about 0.2 V where the current is well into the oxidation peak, i.e. at first the mass of the film does not change much although charge passes. This is only possible if only very light species move (H^+) or the mass of ions moving one way is balanced by the mass of neutral species moving the other way. Then when we get to the peak in the cyclic voltammogram, ΔX_L starts to increase rapidly. When the direction of the scan is changed, ΔX_L decreases except for scan rates of 100 mV s^{-1} where ΔX_L continues to increase until the potential is about 0.25 V at which point the reduction peak starts and ΔX_L slowly decreases.

The poly(aniline)-poly(styrenesulfonate) film can be considered rigid and smooth in the reduced and oxidised states because R for the film during growth is close to zero and ΔR during the voltammetric cycles are negligible. The changes in mass of the polymer film were calculated from ΔX_L by applying the Sauerbrey equation. For every scan rate the mass of polymer increases during oxidation and decreases during reduction. The plots of the mass of the polymer film as a function of charge at different

scan rates are shown in Figure 6.5. The value of the charge is obtained from the integration of the current in the voltammograms, where the axis of the potential can be considered as a time axis.

The changes in mass of the poly(aniline)-poly(styrenesulfonate) film throughout the oxidation process in 1.0 M $HClO_4$ are not linearly proportional to the changes in the charge. This means that more than one species moves into the polymer film during the oxidation scan. Looking in Figure 6.5 at the voltammogram recorded at 5 mV s^{-1}, at the beginning of the oxidation scan the ratio between the changes in mass and charge is about 21 μg C^{-1} whereas at the end of the oxidation scan, the ratio is about 515 μg C^{-1}. The theoretical value of mass per unit charge for perchlorate is 1031 μg C^{-1}, for chloride it is 368 μg C^{-1}, for hydronium ion (H_3O^+) it is 196 μg C^{-1} and for the proton it is 10 μg C^{-1}. In the first region, it seems that there is a participation of protons in the compensation of the charge because of the small value of the ratio of mass to charge. In the second region, the relationship between the changes in mass and charge could mean that anions move into the film accompanied by a flux of solvent molecules contrary to the anions because the value of mass per charge found is smaller than that expected for perchlorate, or water molecules move into the film as protons continue to move out of the film. As the redox cycles are reproducible, the species, which were incorporated into the film or released from the film during the oxidation scan, should move in the opposite direction during the reduction scan. However for the reduction process, the mass decrease is linearly proportional to the decrease in charge with a ratio of 278 μg C^{-1}. This might mean that the ratio between the species moving into and out of the polymer is constant throughout the reduction scan. The change in mass as a function of charge during the oxidation scan is different from that during the reduction scan. The variation in potential is very likely to alter the relative contributions of the movement of ions and neutral molecules into and out of the film. This might occur due to the influence of the potential on the interactions inside the polymer and between the polymer and mobile species, changing the polymer structure.[74] Thus it is possible that the mechanism is modified during the course of a redox conversion in a given direction during the potential sweep. In addition the solvent population influences mobile species transference and polymer reconfiguration rates.[124]

At 20 mV s^{-1}, at the beginning of the oxidation scan, the ratio between the changes in mass and charge is 21 μg C^{-1} and at the end of the oxidation scan, the ratio is 243 μg C^{-1}. For the reduction process the ratio is constant at 144 μg C^{-1}.

At 100 mV s^{-1}, at the beginning of the oxidation scan, the mass changes with charge at a rate of 6 μg C^{-1} and then there is a large range of the oxidation over which the mass increases linearly with the charge with a ratio of about 120 μg C^{-1}. During this faster scan rate, the mass even continues to increase at the beginning of the reverse scan. For the reduction scan the mass decreases proportionally to the charge with a ratio of 116 μg C^{-1}. Clearly at higher sweep rate less neutral species (water) goes into the film during oxidation and therefore has to leave during reduction.

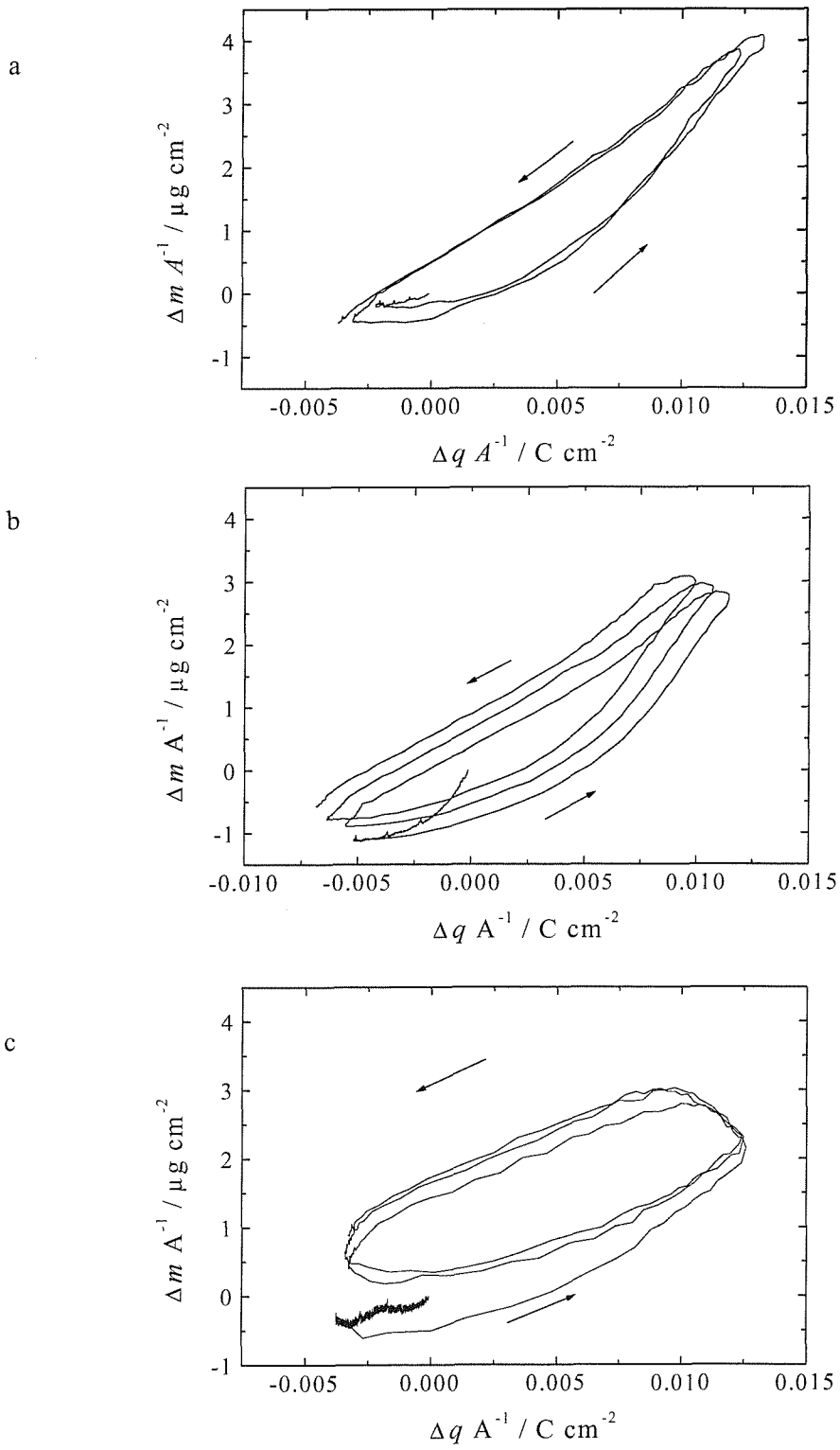

Figure 6.5: Changes in mass as a function of charge during voltammetric cycles of 96 μg cm^{-2} of poly(aniline)-poly(styrenesulfonate) film in 1 M $HClO_4$ at a) 5 mV s^{-1}, b) 20 mV s^{-1}, and c) 100 mV s^{-1}. The film was conditioned for 3 min at –0.2 V *vs.* SCE before cycling.

There is a drift on each cycle with mass increase which can be explained by a small permanent increase in mass observed in ΔX_L for all scan rates. This mass might be water that remains inside the film during the voltammetric cycles. For the protonated emeraldine, the water molecules are absorbed on the amine sites.[125] The absorbed water molecules can be reversibly or irreversibly bound where the mobile molecules are attached by one hydrogen bond and the fixed molecules create two hydrogen bonds.

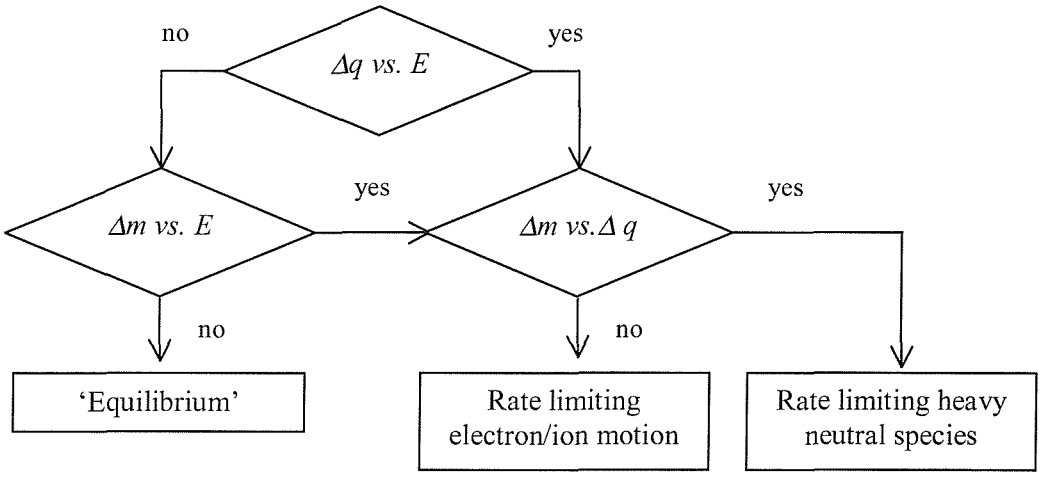

Figure 6.6: Logic diagram to determine the rate-limiting step during redox switching of polymer films.[74] The tracking *yes* is followed when there is hysteresis in the plot.

Hillman and Bruckenstein have proposed the flow chart shown in Figure 6.6 to identify the rate-limiting step involved in the redox switching of a polymer.[74] According to the flow chart the hysteresis of three plots has to be analysed during the redox switching of polymer films: the charge as a function of potential (Δq *vs.* E), the mass as a function of potential (Δm *vs.* E) and the mass as a function of charge (Δm *vs.* Δq). In our case the plot of mass as a function of potential is replaced by a plot of the imaginary part of the electroacoustic impedance as a function of charge (ΔX_L *vs.* E). This is exactly equivalent since the mass is obtained from the values of X_L by applying the Sauerbrey equation. The tracking *no* on the diagram corresponds to the absence of hysteresis in the specified plot. A conclusion about the rate-limiting step during redox cycles is reached after following the arrows of the diagram.

There is hysteresis in the three plots during redox cycles at the three scan rates, although for fast scan rates the hysteresis is bigger. Thus by applying the scheme

proposed by Hillman and Bruckenstein[74] the rate-limiting species is found to be the heavy neutral species, in this case water.

It is striking and significant that whilst the Δq *vs.* E plots in Figure 6.2, Figure 6.3 and Figure 6.4 overlay at all three sweep rates this is not the case for the ΔX_L plots. The mass change becomes less as the sweep rate increases. This is consistent with the protons moving in every case (fast on this time scale) but the water not being able to keep up. The movement of water is characterised by the fact that the mass per unit charge decreases as sweep rate increases because the rate at which the polymer can swell, or contract, is fixed by physico-chemical processes and does not increase as sweep rate increases.

6.2.1.1. Conclusion about perchlorate movement

Due to the small value of mass per charge at the beginning of the oxidation it seems that protons and not much else move out of the film.

The increase in mass after reversal of cycle at high sweep rate indicates movement of water lagging behind the charge.

Up to this point we can conclude only that initially protons move out of the film and water also moves during the cycles. No conclusion about anion transport can be made from this first set of experiments. In the next section these experiments are repeated in 1 M HCl as electrolyte and the question of anion movement during redox cycles is better clarified.

6.2.2. Possible movement of chloride anions during redox cycles

Figure 6.7, Figure 6.8 and Figure 6.9 show the cyclic voltammograms and the changes in the charge and the electroacoustic impedance as a function of potential for the poly(aniline)-poly(styrenesulfonate) film in 1 M HCl at three different scan rates. The poly(aniline)-poly(styrenesulfonate) film is the same as the one used in the previous experiments. After cycling the polymer in HCl, $HClO_4$ was once again used and the stability of the film checked by comparing the voltammograms. The result shown here are reproducible, the same results were also obtained when other thin layers of poly(aniline)-poly(styrenesulfonate) were used. The plots are very similar when 1 M $HClO_4$ or 1 M HCl are used at the three scan rates.

Figure 6.10 shows the plots of mass as a function of charge for the poly(aniline)-poly(styrenesulfonate) film in 1 M HCl at three different scan rates. The masses were obtained by applying the Sauerbrey equation since the polymer film behaves as a rigid and smooth film at the reduced and oxidised forms because R for the film when grown is close to zero and ΔR during the voltammetric cycles are negligible.

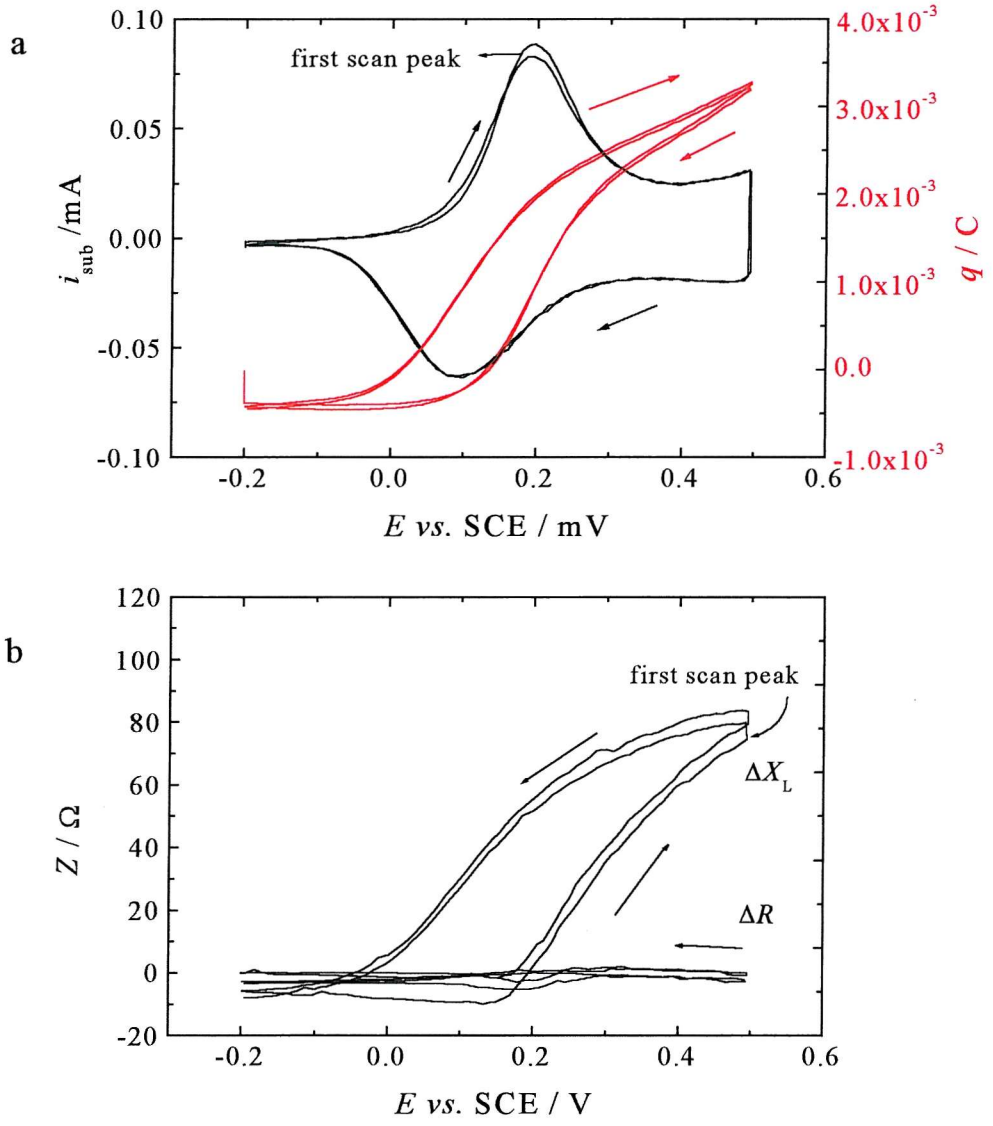

Figure 6.7: a) voltammetric cycle and b) real and imaginary parts of the impedance during voltammetric cycle of 96 μg cm^{-2} of poly(aniline)-poly(styrenesulfonate) film in 1 M HCl at 5 mV s^{-1}. The film was conditioned for 3 min at –0.2 V *vs.* SCE before cycling. The points are measured every 1.8 s at a difference of potential of 9 mV.

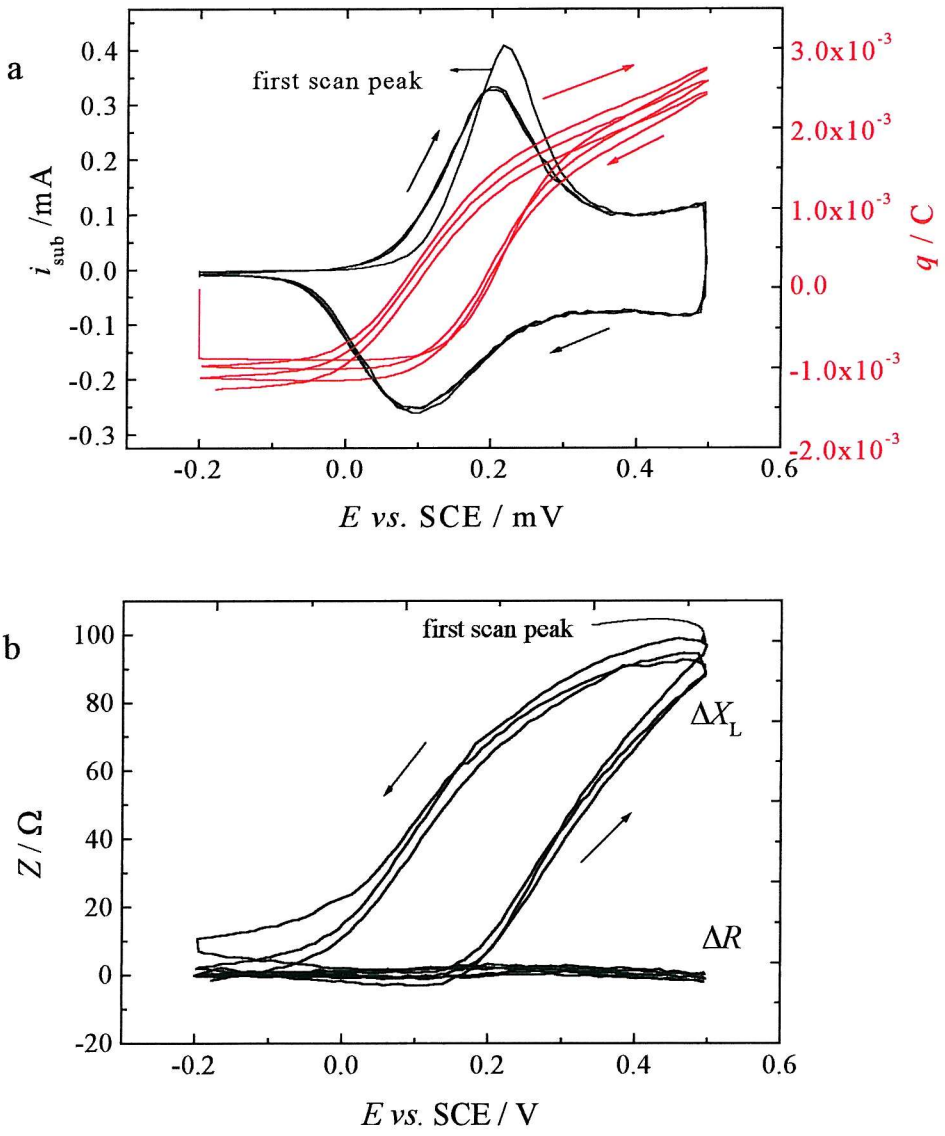

Figure 6.8: a) voltammetric cycle and b) real and imaginary parts of the impedance during voltammetric cycle of 96 μg cm^{-2} of poly(aniline)-poly(styrenesulfonate) film in 1 M HCl at 20 mV s^{-1}. The film was conditioned for 3 min at –0.2 V *vs.* SCE before cycling. The points are measured every 0.5 s at a difference of potential of 10 mV.

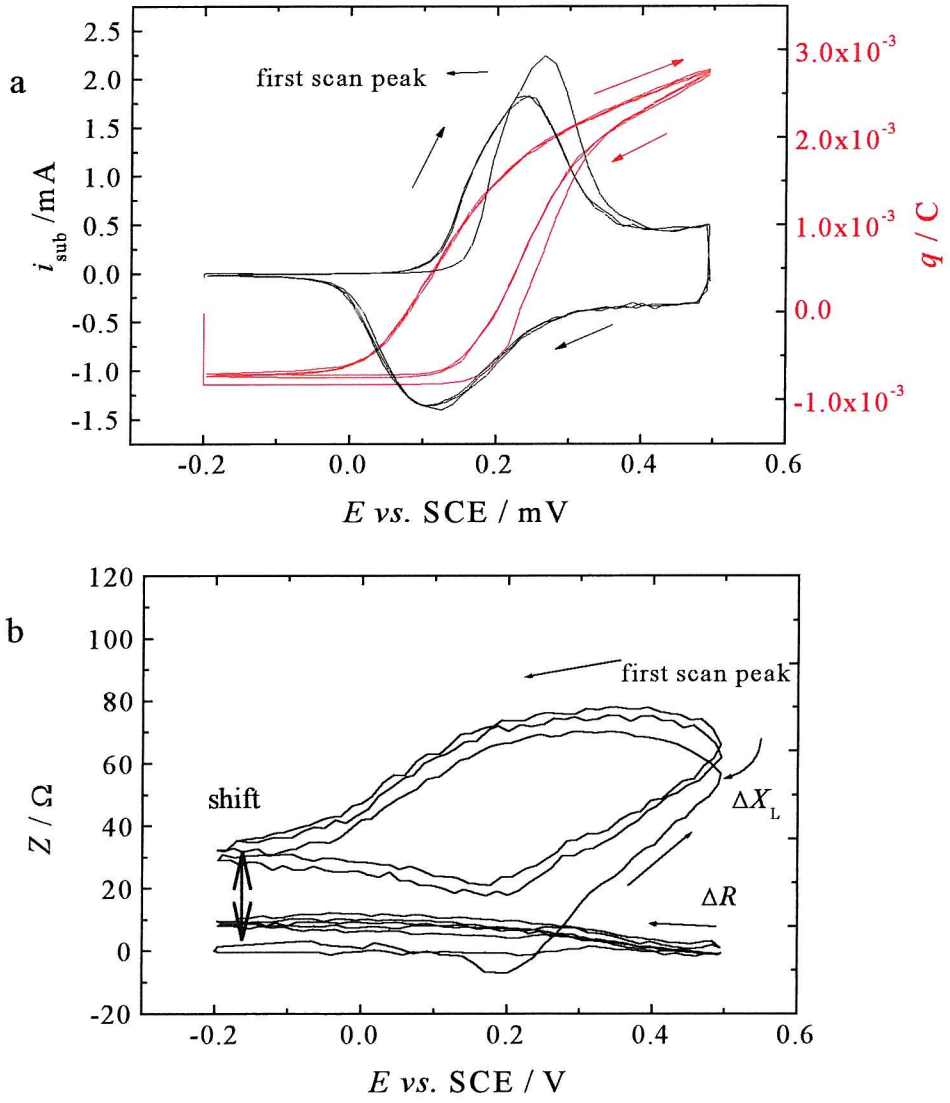

Figure 6.9: a) voltammetric cycle and b) real and imaginary parts of the impedance during voltammetric cycle of 96 μg cm^{-2} of poly(aniline)-poly(styrenesulfonate) film in 1 M HCl at 100 mV s^{-1}. The film was conditioned for 3 min at –0.2 V *vs.* SCE before cycling. The points are measured every 0.15 s at a difference of potential of 16 mV.

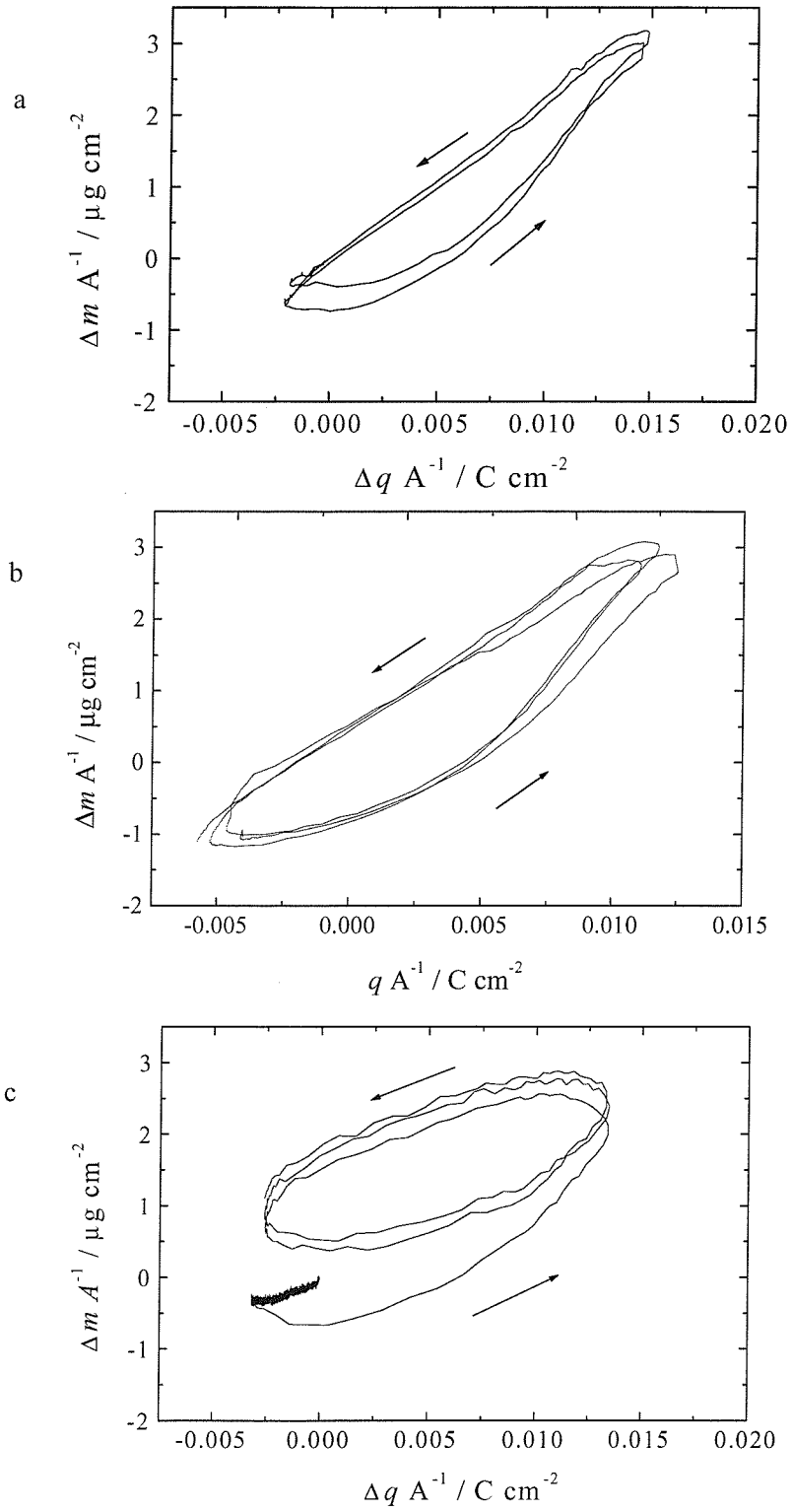

Figure 6.10: Changes in mass as a function of charge during voltammetric cycles of 96 μg cm^{-2} of poly(aniline)-poly(styrenesulfonate) film in 1 M HCl at a) 5 mV s^{-1}, b) 20 mV s^{-1}, and c) 100 mV s^{-1}. The film was conditioned for 3 min at –0.2 V *vs.* SCE before cycling.

The ratio of the species moving into and out of the poly(aniline)-poly(styrenesulfonate) film varies throughout the oxidation process in 1.0 M HCl. And the decrease in mass is linearly proportional to the charge during the reduction. As the polymer film behaves very similarly when 1 M $HClO_4$ or 1 M HCl are used, we conclude that the anions of the electrolytes do not participate in the maintenance of the electroneutrality of the film. This is consistent with the paper of Smyrl[122], cited in the page 112 of this thesis, where he noted that when there is a large poly(anion) incorporated in a poly(pyrrole) film anions do not move to keep the electroneutrality of the film during redox cycles. So the poly(aniline)-poly(styrenesulfonate) has permselectivity allowing only the exchange of protons and water with the electrolyte solution. It is most likely that protons leave the film and water moves into the film during the oxidation scan. During the reduction scan, the reverse occurs, but in a different ratio. For faster scan rates there is a delay in the water movement as it is the slowest species and not directly driven by the redox chemistry.

At 5 mV s^{-1}, at the beginning of the oxidation scan, the changes in mass of the film per unit charge is 1 μg C^{-1} which indicates that protons leave the film but water starts to move into the polymer. At the end of the oxidation scan the relationship between mass and charge gives 351 μg C^{-1}, indicating that more water molecules move into the film in the opposite direction to the flux of protons. In the reduction process the ratio obtained was constant at 219 μg C^{-1}.

At 20 mV s^{-1}, at the beginning of the oxidation scan, the ratio of mass per unit charge is about 10 μg C^{-1} and at the end of the scan, the ratio is 336 μg C^{-1}. For the reduction process the ratio obtained was 197 μg C^{-1}.

At 100 mV s^{-1}, at the beginning of the oxidation scan, the mass does not change as charge starts to increase and at the end of the scan the ratio is 262 μg C^{-1}. At this fast scan rate, the mass of the film increases during oxidation and even continues to increase at the beginning of the reduction cycle. For the reduction process the ratio of changes in mass per unit charge obtained was 112 μg C^{-1}.

By analysing the three plots and using Hillman and Bruckenstein model, the rate-limiting species are found to be the heavy neutral species, i.e. water, as for the case when $HClO_4$ was used.

6.2.3. Discussion

In this section we discuss the species that move into and out of the poly(aniline)-poly(styrenesulfonate) film during the redox switching.

The charge balance in the polymer film during redox switching can be obtained by the movement of protons (H^+) and/or anions (A^-) between the polymer and the electrolyte and it can be represented by the following equation:[114,58]

$$q(E) = F\vartheta_{A^-}(E) - F\vartheta_{H^+}(E) \tag{6.1}$$

where F is the Faraday constant (96484 C mol^{-1}), the charge for the proton and the anion are +1 and –1 respectively and ϑ corresponds to the number of moles exchanged.

The changes in the polymer mass during the redox cycles can be written as

$$\Delta m(E) = MW_{A^-}\vartheta_{A^-}(E) + MW_{H^+}\vartheta_{H^+}(E) + MW_{H_2O}\vartheta_{H_2O}(E) \tag{6.2}$$

where the MW are the molar masses of the different species, the anion (MW_{A^-}, A^- is perchlorate = 99.5 g mol^{-1} and chloride = 35.5 g mol^{-1}), proton (MW_{H^+} = 1 g mol^{-1}) or water (MW_{H2O} = 18 g mol^{-1}) and

$$MW_{HA} = MW_{A^-} + MW_{H^+} \tag{6.3}$$

By inserting equation (6.3) in the equation (6.1), and rearranging we have

$$\frac{q(E)}{F}\left(\frac{MW_{A^-} + MW_{H^+}}{MW_{HA}}\right) = \vartheta_{A^-}(E) - \vartheta_{H^+}(E) \tag{6.4}$$

then considering that $MW_{A^-} >> MW_{H^+}$

$$\frac{MW_{A^-}}{MW_{HA}}\frac{q(E)}{F} + \vartheta_{H^+}(E) = \vartheta_{A^-}(E) \tag{6.5}$$

Cancelling the term $MW_{H^+}\vartheta_{H^+}$ in equation (6.2) since $MW_{H^+} < MW_{H2O} << MW_{A^-}$ gives

$$\Delta m(E) = MW_{A^-}\vartheta_{A^-}(E) + MW_{H_2O}\vartheta_{H_2O}(E) \tag{6.6}$$

and then by rearranging equation (6.6) and dividing through by MW_{HA}, assuming that $MW_{HA} = MW_{A^-}$, gives

$$\vartheta_{A^-}(E)=\frac{\Delta m(E)}{MW_{HA}}-\frac{MW_{H_2O}}{MW_{HA}}\vartheta_{H_2O}(E) \tag{6.7}$$

By combining equations (6.5) and (6.7), the number of moles of H^+ exchanged together with the ratio of the number of moles of water can be calculated as a function of potential.

$$\boxed{\vartheta_{H^+}(E)+\frac{MW_{H_2O}}{MW_{HA}}\vartheta_{H_2O}(E)=\frac{\Delta m(E)}{MW_{HA}}-\frac{MW_{A^-}}{MW_{HA}}\frac{q(E)}{F}} \tag{6.8}$$

By reformulating equation (6.4) without considering MW_{H^+} which is close to zero

$$\vartheta_{H^+}(E)+\frac{MW_{A^-}}{MW_{HA}}\frac{q(E)}{F}=\vartheta_{A^-}(E)-\frac{MW_{H^+}}{MW_{HA}}\frac{q(E)}{F} \tag{6.9}$$

and by combining equations (6.9) and (6.8) we obtain the number of moles of A^- exchanged plus a ratio of the number of moles of water which can be calculated as a function of the potential.

$$\boxed{\vartheta_{A^-}(E)+\frac{MW_{H_2O}}{MW_{HA}}\vartheta_{H_2O}(E)=\frac{\Delta m(E)}{MW_{HA}}+\frac{MW_{H^+}}{MW_{HA}}\frac{q(E)}{F}} \tag{6.10}$$

Negative values of ϑ refer to release, and positive values to incorporation, of species from the film. For example, during oxidation protons must leave the polymer film, and so the number of moles of protons exchanged, ϑ_{H^+}, must be negative. These equations give the number of moles of the ionic species together with the number of moles of water molecules exchanged between the polymer and the electrolyte. Note that in both cases we cannot separate the ions from the water in these calculations.

The plots of equations (6.8) and (6.10) shown in Figure 6.11 and Figure 6.12 were obtained from the experimental values of the changes in mass and charge as a function of potential, and using the theoretical values for the molar masses and the Faraday constant. Figure 6.11 and Figure 6.12 show the movement of anion and proton with water in the poly(aniline)-poly(styrenesulfonate) film during redox switching in 1.0 M $HClO_4$ and HCl at different scan rates, respectively. As we have observed in the analysis of the previous experiments the fact that the same result is obtained by cycling the poly(aniline)-poly(styrenesulfonate) in either 1 M $HClO_4$ or HCl is a very significant piece of evidence that the anions are not involved in keeping the electroneutrality of the polymer film. Consequently as the anions do not move into and out of the polymer film during the redox switching, the number of moles of anions

transported is zero, $\vartheta_{ClO_4^-} = \vartheta_{Cl^-} = 0$, and the lines in the plots in Figure 6.11a and Figure 6.12a represent the movement of water molecules alone. The movement of 'salt' i.e. acidic solution (H^+ and anion together) could take part with the water movement. But the movement of the 'salt' would be seen in the EQCM experiments during the potential cycling of the polymer using different electrolytes because of the difference in mass between the chloride and the perchlorate. Since we see no difference we conclude that there is no movement of 'salt'. For Figure 6.11a the value of 0.18 x ϑ_{H_2O} at the end of the oxidation scan is 30 nmol cm^{-2} and for Figure 6.12a, 0.49 x ϑ_{H_2O} is about 80 nmol cm^{-2}, giving an estimate for the number of water molecules which move during the process of 170 nmol cm^{-2} for both electrolytes. Figure 6.11b and Figure 6.12b show the movement of protons and water during redox switching of the poly(aniline)-poly(styrenesulfonate) film. During oxidation scans the number of moles of protons is negative because they leave the film and the number of water molecules is positive because they move into the film. In order to obtain the number of protons exchanged between the polymer film and the electrolyte during redox switching shown in Figure 6.13 the values of the number of molecules of water obtained in plots of Figure 6.11a and Figure 6.12a are subtracted from the plots in Figure 6.11b and Figure 6.12b, which measures the flux of protons and water. The total number of protons exchanged is about 200 nmol cm^{-2} per redox cycle independent of the electrolyte used, as seen in Figure 6.13. It can be observed that the protons are expelled from the film at the beginning of the oxidation with more intensity and then the gradient decreases at the end of the oxidation, but it never reaches zero. The inverse happens at the reverse scan with the protons incorporating the film in a low amount and then it increases with the reduction of the polymer film. The number of protons exchanged during redox switching can also be obtained from the charge alone since only the protons move to reach the electroneutrality of the polymer film. Faraday's law can be applied using the charge passed through the polymer during the potential sweep to calculate the number of moles of proton exchanged to maintain the charge neutrality of the polymer. The charge can be seen in Figure 6.10 and it is about 17 mC cm^{-2} which gives 180 nmol cm^{-2} of protons. This number is in agreement with the one found by applying equation (6.8) (200 nmol cm^{-2}), which reinforce our argument that only protons move, and no anion, during the redox switching on the polymer.

By assuming 100 % Faraday efficiency for the polymer deposition, the number of water molecules per monomer in the polymer film can be calculated by applying Faraday's law

$$\frac{Q}{A_e} = \frac{nFN}{A_m} \qquad \textbf{(6.11)}$$

where Q/A_e is the charge consumed during the electrodeposition divided by the electroactive area of the quartz crystal (80.95 mC cm^{-2}), N/A_m is number of moles of monomer of aniline-styrenesulfonate deposited per mass sensitive area of the quartz crystal ($MW_{PANI-PSS}$ = 189 g mol^{-1}), n is the number of electrons involved in the deposition of the polymer at the reduced state (2), and F is the Faraday constant (96484 C mol^{-1}). The monomer is represented by one aniline and half a styrenesulfonate unit. The number of moles of monomer of the aniline-styrenesulfonate found is 420 nmol cm^{-2}, which represents a mass of 79.29 μg cm^{-2}. There is an additional 0.5 electron per monomer exchanged between the polymer and the electrode during redox reaction. The mass of polymer obtained by applying the Sauerbrey equation is 96.05 μg cm^{-2}. The difference between the electroactive and the total masses can be considered to be caused by water trapped in the structure of the polymer film in the reduced state. This mass is 16.76 μg cm^{-2}, corresponding to 931 nmol cm^{-2} of water. During the oxidation of the film, the mass increases by 4 μg cm^{-2} which corresponds to an increase of 220 nmol cm^{-2} of water in the oxidised polymer film. The ratio of number of moles of water to the moles of monomer is 2.2/1 for the reduced state and 2.75/1 for the oxidised film.

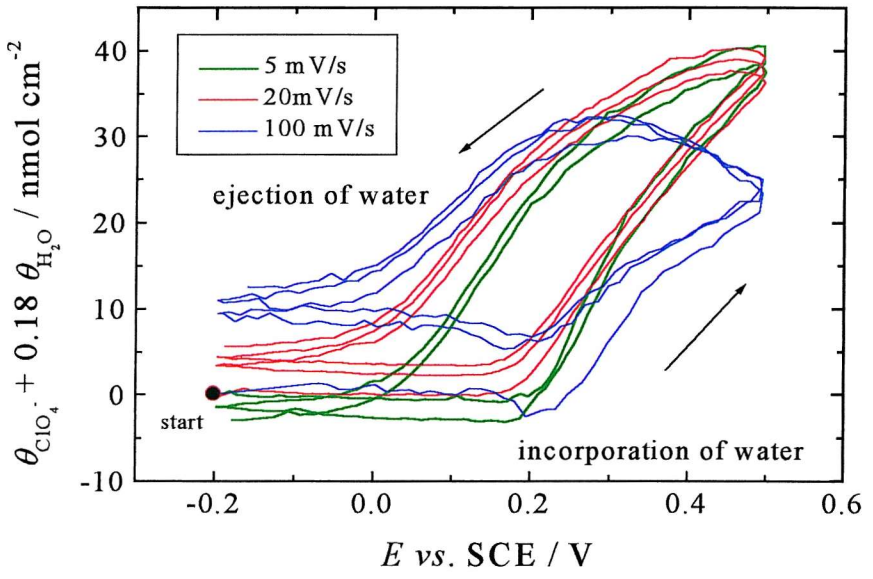

a

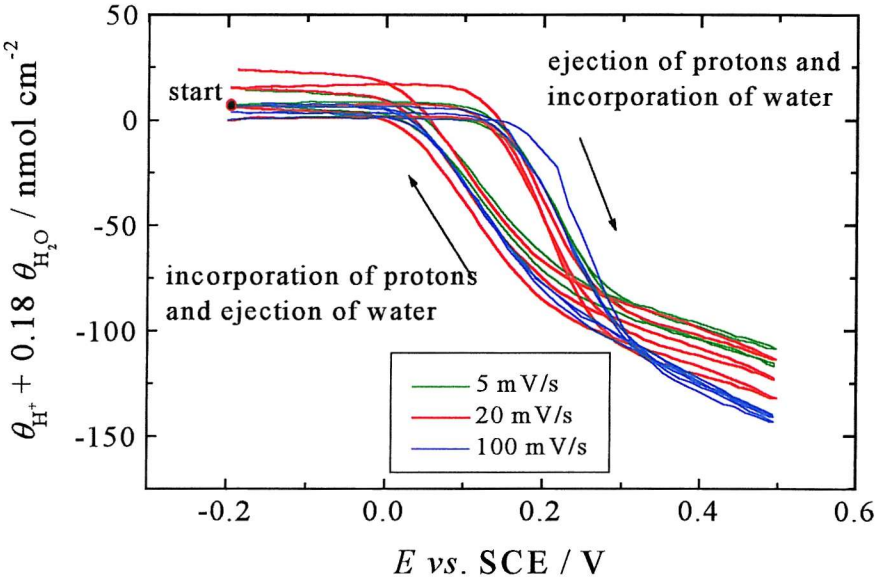

b

Figure 6.11: Number of moles exchanged during redox cycling of 96 μg cm^{-2} of poly(aniline)-poly(styrenesulfonate) film in 1.0 M $HClO_4$ at 5 mV s^{-1}, 20 mV s^{-1} and 100 mV s^{-1}. The film is kept at –0.2 V *vs* SCE for 3 min before the voltammetric cycles. a) number of moles of water and b) number of moles of proton and water exchanged.

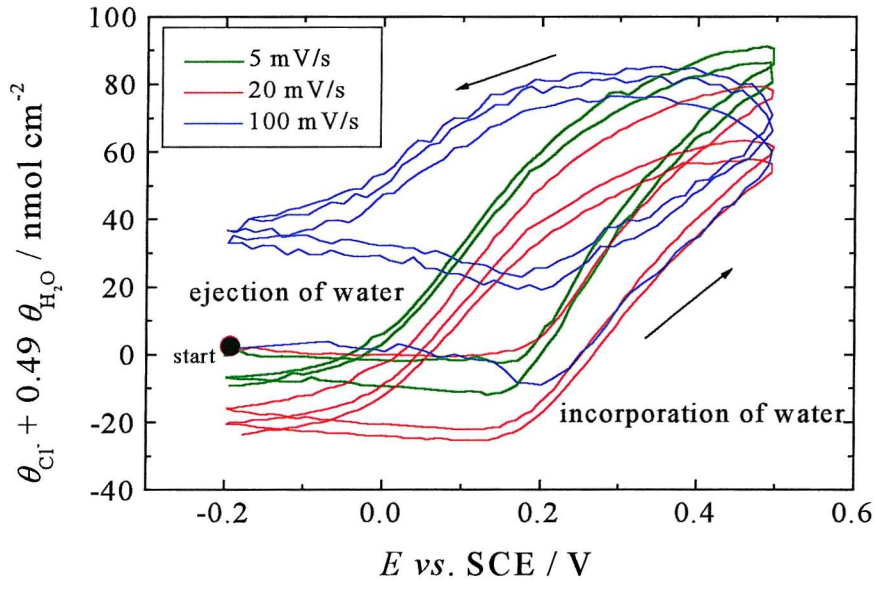

a

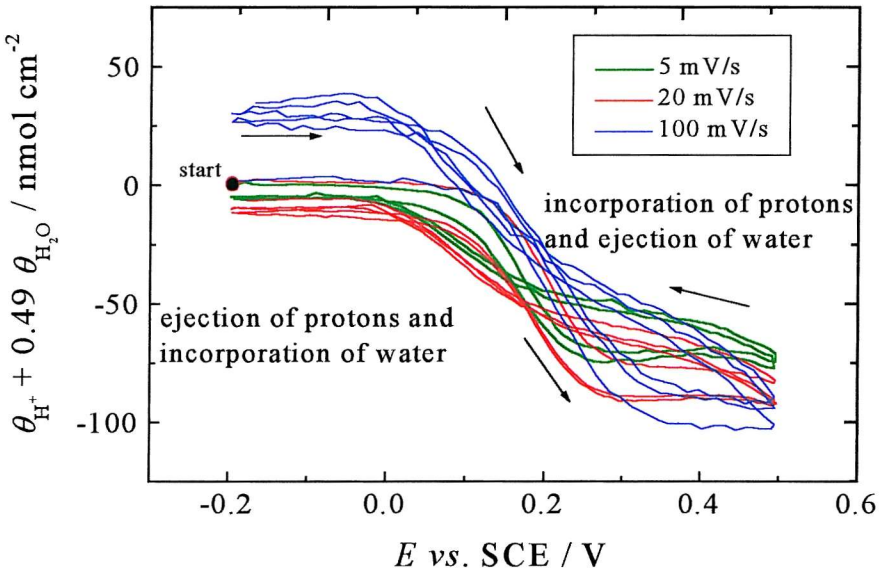

b

Figure 6.12: Number of moles exchanged during redox cycling of 96 μg cm^{-2} of poly(aniline)-poly(styrenesulfonate) film in 1.0 M HCl at 5 mV s^{-1}, 20 mV s^{-1} and 100 mV s^{-1}. The film is kept at –0.2 V *vs* SCE for 3 min before the voltammetric cycles. a) number of moles of water and b) number of moles of proton and water exchanged.

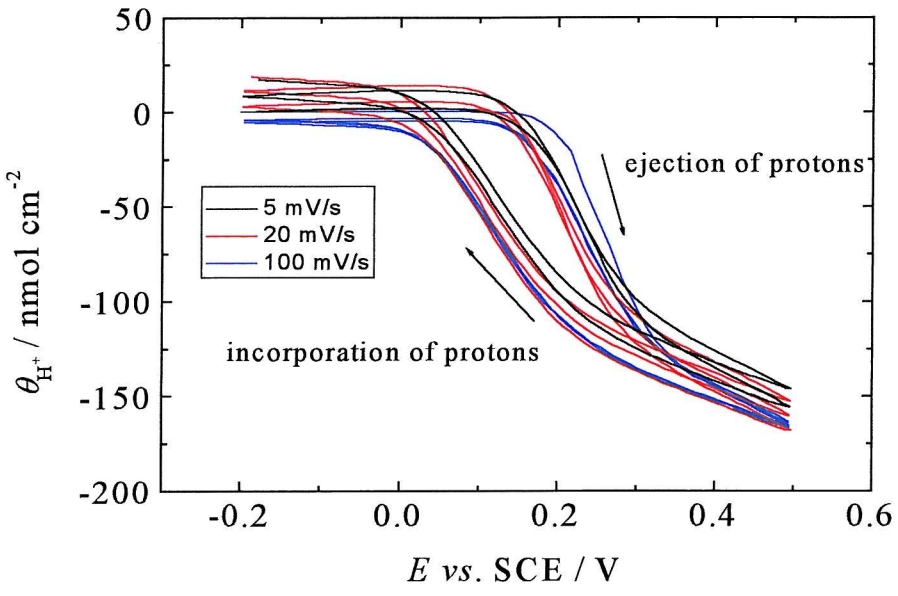

a

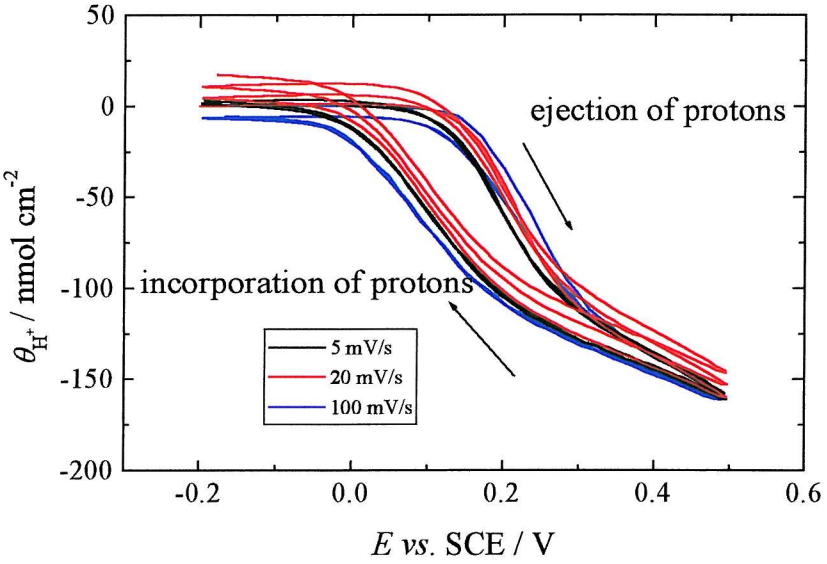

b

Figure 6.13: Number of moles of protons exchanged during redox cycling of 96 μg cm^{-2} of poly(aniline)-poly(styrenesulfonate) film in a) 1.0 M $HClO_4$ at 5 mV s^{-1}, 20 mV s^{-1} and 100 mV s^{-1} b) 1.0 M HCl at 5 mV s^{-1}, 20 mV s^{-1} and 100 mV s^{-1}. The film is kept at -0.2 V *vs* SCE for 3 min before the voltammetric cycles.

6.2.4. Conclusion about anion movement

As the redox cycling of poly(aniline)-poly(styrenesulfonate) films does not show significant differences when $HClO_4$ or HCl are used, we conclude that the anions do not contribute to maintain the charge neutrality of the polymer film. Rather proton movement is responsible for the electroneutrality of the polymer film and water molecules move in opposition to the flux of protons. During the oxidation scan the amount of water moving into the film increases gradually as indirectly the driving force increases. The water motion is driven indirectly by the redox change whereas protons are driven directly. In the next section the driving force for insertion of water into the polymer film during oxidation scan and expulsion of water during reduction is discussed.

6.2.5. Possible movement of water during redox cycles

As concluded in the last section, water moves into and out of the poly(aniline)-poly(styrenesulfonate) film during redox cycles. When the polymer is in the reduced state, the nitrogen is sp^3 hybridised (tetrahedral). During oxidation, electrons are removed from the conjugated polymer chains causing a change on the orbitals of the alternating nitrogens, which are then planar (sp^2 hybridised) as shown in Figure 6.14. With the change in hybridisation of nitrogen atoms from tetrahedral to planar, the polymer chain is straightened out when oxidised generating free volume, which is occupied by the counterions and water molecules from the solution causing a swelling of the film.[126] The variation in volume of conducting polymers during the potential sweep make these polymers useful on the application of artificial muscles, or electrochemical actuators.[2,127,128]

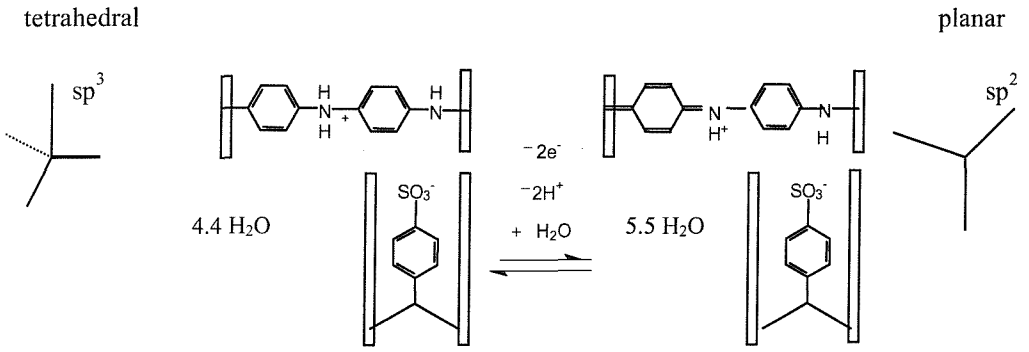

Figure 6.14: Sketch of the poly(aniline)-poly(styrenesulfonate). The nitrogen atoms are at tetrahedral form when the polymer is at the reduced state and at planar configuration on the polymer film at the oxidised state. The number of moles of water in the reduced film is calculated by the difference in mass of the electroactive film (Faraday's law) and the total polymer mass (Sauerbrey equation). The additional number of moles of water in the oxidised polymer is calculated by the mass of polymer gained during oxidation.

6.3. Analysis of cation movement

The cations in the electrolytes used in our EQCM studies of the electronic and ionic movement in poly(aniline)-poly(styrenesulfonate) films during redox switching are exclusively protons. The molecular weight of protons is very small relative to the molecular weight of solvent and anions, therefore it is difficult for the Quartz Crystal Microbalance to detect the small changes in mass caused by transport of protons. From the last section we know that protons and water move between the polymer and the electrolyte during potential sweep. In order to detect the concentration of proton close to the surface of the polymer film, and consequently try to explain the movement of proton into and out of the film, the Scanning Electrochemical Microscope was coupled with the Electrochemical Quartz Crystal Microbalance as shown in Figure 6.15. The microelectrode was placed very close to the surface of the polymer film using a *z* axis piezopositioner. The bipotentiostat fixes the potential of the microelectrode and simultaneously scans the potential of the substrate, in this case the polymer film on the QCM. At the same time the QCM measures the changes in the electroacoustic

impedance of the film. The bipotentiostat and the QCM measurements are triggered by a Schmitt trigger. All experiments were controlled and the data acquired using LabVIEW software.

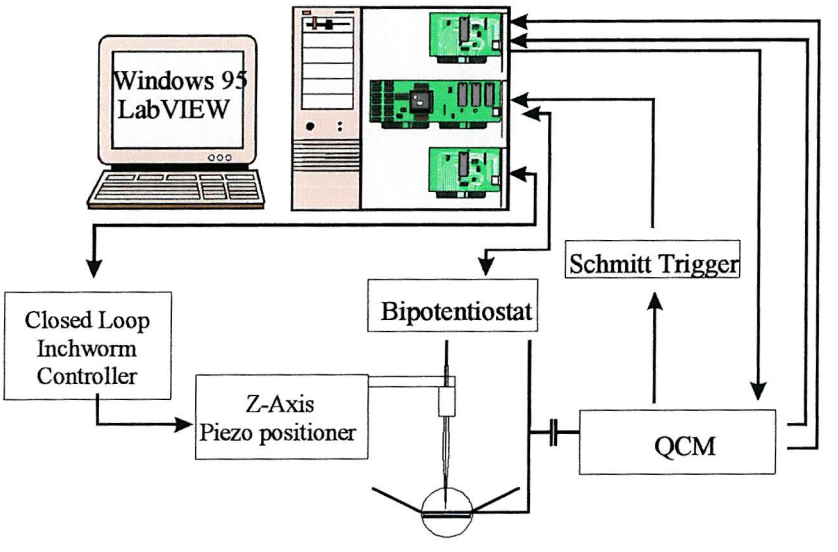

Figure 6.15: Sketch of the Electrochemical Quartz Crystal Microbalance coupled with the Scanning Electrochemical Microscope.[62]

The design of the combined EQCM and SECM was proposed by Gollas et al.[62] and the equipment was tested by plating and stripping copper film from copper solution. The interaction between the microelectrode and the oscillating quartz crystal has to be carefully considered during the arrangement of the EQCM/SECM instrumentation. The acoustic waves of the vibrating quartz crystal can be perturbed by the approach of the tip. The microelectrode tip is not positioned so close as to cause interaction with the transverse shear waves radiated into aqueous solution for 10 MHz resonators (140 nm),[44] although longitudinal and compressional waves originating from the oscillating crystal can propagate into the solution over distances of centimetres.[129] The proximity of a reflecting interface perpendicular to the shear motion of the quartz can lead to periodic variations of the QCM response due to the coupling of compressional waves reflected by the coplanar face plane of the electrode to the shear waves, both caused by the oscillating quartz crystal.[62] Although it has been demonstrated that for a cone-shaped tip with small coplanar face, expressed by the angle α in Figure 6.16,

bigger than 45°, the compressional waves are reflected upward at the cell wall and at the interface of the liquid with the air.[62]

The microelectrode measures proton concentrations in the solution above the surface of the polymer film as seen in Figure 6.16. The protons are reduced to hydrogen molecules on the surface of the microelectrode generating a reduction current, which quantifies the concentration of protons in solution. The release of protons from the film causes an increase in the reduction current. On the other hand, if the protons move into the polymer film the reduction current decreases. The water movement into and out of the film occured during the potential sweep also changes the concentration of protons in solution between the substrate and the microelectrode and might disturb the mass transport of protons. In addition the polymer film swells and contracts with water transport modifying the distance between the microelectrode and the substrate. The current of the proton reduction at the microelectrode tip is a function of the distance to the substrate as shown in the approach curve (Figure 6.17). The reduction current detected at the microelectrode is then determined by a combination of events mentioned above that modifies the concentration of protons between the microelectrode and the substrate and its separation distance.

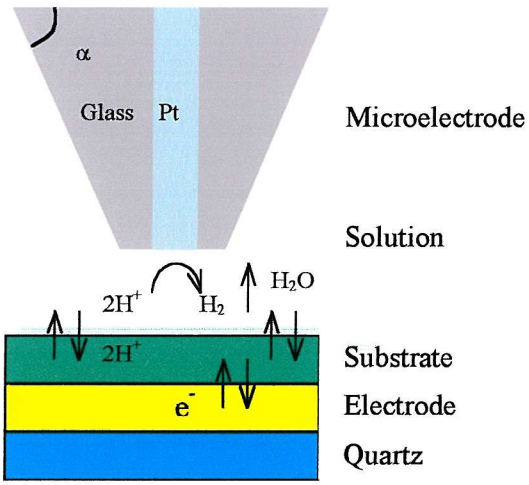

Figure 6.16: Sketch of the microelectrode detecting proton concentration in solution between the film and the electrolyte solution. The reduction current is proportional to the concentration of protons in solution and distance between the microelectrode and the substrate.

6.3.1. Scanning Electrochemical Microscopy

The Scanning Electrochemical Microscope (SECM) works by scanning a microelectrode very close to a conducting, or insulating, substrate. Controlled by a micropositioning device, the tip can move towards the substrate in the perpendicular direction, producing an approach curve; or the tip can also move parallel to the substrate mapping the conductivity of the surface or the flux of material from, or towards, the surface. The technique has been largely used due to its excellent spatial resolution.[130]

The microelectrode is produced from a very thin filament of conductive material such as Pt, Au, carbon fibre, etc. The conductive part is sealed with glass or epoxy leaving a microdisk with a well-defined area of the conductive material exposed at one end. The tip is polished in a cone shape as shown in Figure 6.16 to facilitate the diffusion of ions to the surface of the tip. The diffusion at the tip of the microelectrodes, < 50 μm diameter, is spherical rather than the planar diffusion obtained at conventional size electrodes. The diffusion field of a microelectrode enables the detection of material from a large area at the outer limits of the microelectrode and the decrease of the concentration of the reagent on the surface is not observed.[131] A steady state current, i_{ss}, is then registered at large times:[132]

$$i_{ss} = 4nFDcr \qquad \textbf{(6.12)}$$

where n is the number of electrons involved in the reaction, F is the Faraday, D and c are the diffusion coefficient and the concentration of the species analysed respectively and r is the radius of the electrode. The current is directly proportional to the concentration of the electroactive species analysed if all the other variables remain constant. The high value of the diffusion coefficient of protons (about 8.5 x 10^{-9} m^2 s^{-1} for acid solutions)[133] confers good current response even for small concentrations. The limiting current for the reduction of protons in 1 M acid measured by a 10 μm diameter microelectrode is 18 μA.

The disadvantages of microelectrodes over conventional sized electrodes are that the small area of the electrode is difficult to be quantified and cleaned, they are fragile to handle and they require a potentiostat with high current amplification.

The reduction of protons on a large electrode would create many bubbles of hydrogen at the surface of the electrode, which would disturb the electrochemical measurements. Large bubbles do not seem to be formed on microelectrodes.[132] A reason for this could be that the hydrogen molecules formed diffuse away fast due to the spherical diffusion geometry of the microelectrode.

There is a delay between the time protons are released or absorbed by the polymer and the current being detected by the tip. This time delay, t, is proportional to the distance, h, between the tip and the substrate[131]

$$t = \frac{h^2}{2D} \tag{6.13}$$

where t is the time needed for the proton to diffuse over the distance h. A proton released from the substrate reaches a microelectrode positioned 50 μm away 0.13 s later, which means a difference of 2.7 mV at a scan rate of 20 mV s^{-1}.

Frank and Denuault[134] have measured the amperometric response of protons by positioning a Pt microelectrode very close to a poly(aniline) film in acid solution during redox switching. A steady state current for the reduction of protons is recorded at the microelectrode while the potential of the polymer film is linearly scanned. The current obtained during the potential scan of the polymer registers the exchange of electrons between the polymer film and the electrode and the current at the microelectrode reflects the movement of ions between the film and the solution. We have used the same SECM technique but added the simultaneous EQCM measurements. The results presented in this thesis cannot be directly compared to Frank and Denuault's [134] because they have studied the poly(aniline) film during redox swithing while here the poly(aniline) film is electrodeposited with large poly(anion). This addition of the large poly(anion) in the structure of the poly(aniline) is believed to modify the anion movement during potential sweeping in order to keep the electroneutrality of the polymer. In addition, in our case, we consider the contribution of the water flow which is not the case in the work refered. To our knowledge, the present work is the first to couple EQCM and SECM to analyse ionic and electronic movement during redox switching of conducting polymers.

The combinations of EQCM and SECM have been previously reported although with other purposes. The radial sensitivity mapping of two different quartz crystals was studied by applying a single-potential control between a substrate and a microelectrode, which acts as a counter electrode.[135] The distance between the tip and the substrate was calibrated by frequency-distance response.[136] The SECM is used in combination with an EQCM to investigate the principle modes of tip-induced interactions. The focus is on the influence of acoustic waves and surface modifying processes on the resonant frequency of the quartz crystal.[137] Films of silver and C_{60} were studied by EQCM/SECM under bipotentiostatic control, although only the frequency was measured on the EQCM.[138]

6.3.2. Experimental

A ten micrometer diameter platinum microelectrode was used for the detection of the proton concentration close to the surface of the poly(aniline)-poly(styrenesulfonate) film. The electrolyte solutions must be pure[109] and ARISTAR grade chemicals were used in these experiments. Traces of contaminants would obstruct the small area of the microelectrode, interfering with the current, and leading to inaccurate amperometric measurement of the concentration of protons. As the area of the electrode disk is very small, any obstruction on the surface changes considerably the value of the original area producing errors on the application of equation (6.12). The polymer film must also be free of any residue of aniline monomer that might contaminate the solution and the tip. The polymer film was rinsed with ARISTAR grade acid solutions several times before the measurements with the microelectrode. A common way of verifying the cleanliness of the solution and the microelectrode surface is to perform a cyclic voltammogram for the Pt microelectrode in acid solutions.[134] If the voltammogram[139] does not correspond to that expectedfor a clean Pt surface, the microelectrode should be polished and the electrolyte replaced.

In order to carry out the experiments on microelectrodes, the acid concentration used for previous analyses had to be decreased from 1.00 M to 0.04 M. The reduction of protons in highly acidic solutions creates irreproducibility in the measurements

because the production of a great quantity of hydrogen gas disturbs the diffusion at the tip of the microelectrode. A concentration of 0.04 M for the acid was found to give a stable steady state current for the proton reduction. We have used 0.04 M $HClO_4$ and 0.04 M HCl as electrolytes for the experiments on proton movement on the poly(aniline)-poly(styrenesulfonate) film during redox switching. The poly(aniline)-poly(styrenesulfonate) film used for these experiments is the same as used for the studies on anions movement. This change in concentration of electrolyte does not seem to affect the ions which move during the potential sweep, since the voltammograms and electroacoustic impedance of the polymer film is very similar when any of the two concentration of acid solutions were used.

For the conditioning stage before the cyclic voltammetry, the microelectrode was maintained at +0.2 V and the substrate at -0.2 V *vs.* SCE while the solution was purged with argon for 3 min. Reproducible measurements were obtained with this conditioning stage and oxygen was not an interference. During the voltammetric cycles, the microelectrode was kept at –1.2 V *vs.* SCE while the polymer film was cycled between –0.2 V and 0.5 V *vs.* SCE at 20 mV s^{-1}.

The current registered at the microelectrode is a function of the distance between the microelectrode and the substrate. This distance was kept constant for all experiments described in this section. The tip has to be very close to the surface of the film to be able to detect changes in the concentration of protons that take place in that region. The tip has to be in the diffusion layer of the substrate. However the mass of film fluctuates during the redox switching due to ions and solvent exchange with the electrolyte, and so the tip must be far enough so as not to touch the polymer film during the redox cycles. Frank and Denuault [134] noticed on similar experiments that the poly(aniline) film swells during the oxidation and touches the microelectrode tip causing a perturbation in the current. In this case the measurement has to be stopped and the tip brought back to the bulk for reconditioning. However the poly(aniline)-poly(styrenesulfonate) is much more compact than the poly(aniline) film (as shown in the SEM images in Chapter 5) and should swell less during the redox switching. In order to find a good distance between the polymer film and the tip, an approach curve was performed using 0.04 M $HClO_4$ as shown in Figure 6.17. There is a limiting current for the reduction of protons at –1.0 V *vs* SCE as seen in the inset of Figure 6.17. During the approach curve the potential of the microelectrode was maintained at -1.0 V *vs* SCE. In this experiment the substrate is at open circuit and acts as an insulator

blocking the transport of protons from the electrolyte to the tip. The proton reduction current decreases as the tip gets closer to the substrate because there are fewer protons available to be reduced to hydrogen molecules. A decrease of about 40 % at the limiting current of the proton reduction over the bulk value is an indication that the tip is close enough to the polymer surface to detect changes in proton concentration at the surface of the polymer, and this position was adopted for the experiments of the analysis of proton movement. The absolute distance between the tip and the polymer film is not known. The bulk value is the limiting current obtained from the reduction of protons when the tip at an infinite distance from the substrate. In order to measure ion fluxes from poly(aniline) films, Frank and Denuault [134] used a distance at which the tip showed a 20 % decrease in the limiting current relative to the bulk value. In our experiments the tip is placed closer to the substrate.

The platinum microelectrode used in our experiments has a value of R_g of 10. The R_g represents the ratio between the radius of the glass surrounding the electroactive tip and the platinum radius. The value of R_g does not matter when the microelectrode measures a positive current feedback from a conductive substrate. On the other hand if the substrate is insulating, the current registered at the microelectrode decreases as the sheath radius increases. The insulating sheath blocks the diffusion to the disk electrode through the thin gap between the microelectrode and the insulating substrate.[140]

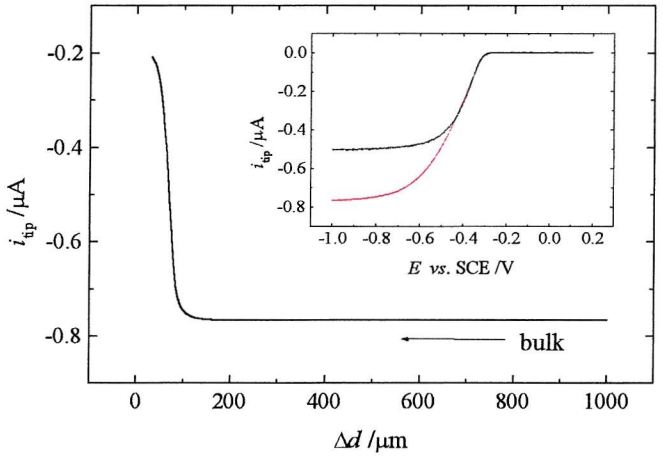

Figure 6.17: Approach curve of a 10 μm diameter Pt microelectrode with insulator/disk radius ratio, R_g, of 10 at –1.0 V *vs.* SCE on the surface of 96 μg cm^{-2} of poly(aniline)-poly(styrenesulfonate) film at open circuit in 0.04 M $HClO_4$. The inset shows the reduction of protons from 0.2 V to –1.0 V *vs.* SCE at 200 mV s^{-1} in 0.04 M $HClO_4$. The reduction was carried out with the microelectrode at different distances from the surface of the polymer film. In red, the tip is on the bulk and in black the tip is at the position where the reduction current registered 40 % of decrease relative to the bulk.

6.3.3. Results and Discussion

The experiments using the coupled EQCM and SECM simultaneously record the current at the polymer during the redox switching of the polymer, the current at the microelectrode which registers the proton concentration close to the surface of the polymer film and the QCM measurements. This combination is unique and has not been reported before on the analysis of conducting polymers during potential sweep.

Figure 6.18 and Figure 6.19 show the QCM measurements and the charge passed during the redox cycles of the poly(aniline)-poly(styrenesulfonate) film. Although the polymer film exchanges water with the electrolyte it is considered rigid as ΔR is close to zero at all potentials. The plots are similar to those previously analysed with the mass of the polymer increasing during the oxidation scan and decreasing during the reduction scan. The experiments are reproducible from one measurement to the next and also from one film to another (data not shown here). There is not a significant difference in the electroacoustic impedance response of the poly(aniline)-poly(styrenesulfonate) film on changing the electrolyte from $HClO_4$ to HCl. This reaffirms the conclusion made previously that the anions do not participate in the maintenance of charge neutrality of the poly(aniline)-poly(styrenesulfonate) film at our experimental conditions. After these experiments using 0.04 M acid solution, a voltammogram using 1 M of $HClO_4$ was performed and the polymer film presented the same response as registered previously confirming then the stability of the film throughout the experiments.

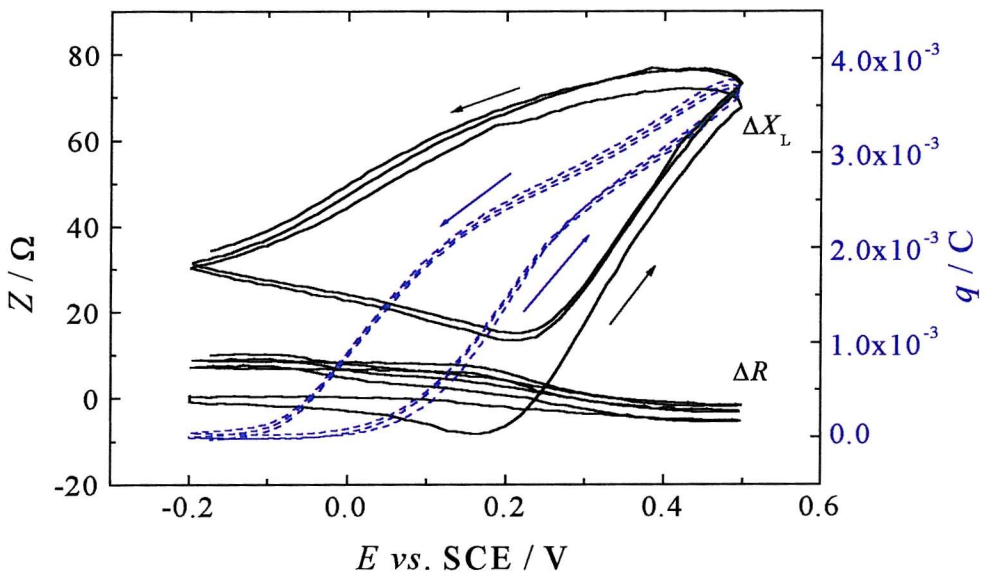

Figure 6.18: Electroacoustic impedance measurement and charge during redox cycles of 96 μg cm^{-2} of poly(aniline)-poly(styrenesulfonate) film in 40 mM $HClO_4$ at 20 mV s^{-1}. The system was conditioned purging argon for 3 min with the substrate at –0.2 V, the tip at 0.2 V *vs.* SCE. The substrate was cycled from –0.2 V to 0.5 V while the tip was kept at –1.2 V *vs.* SCE.

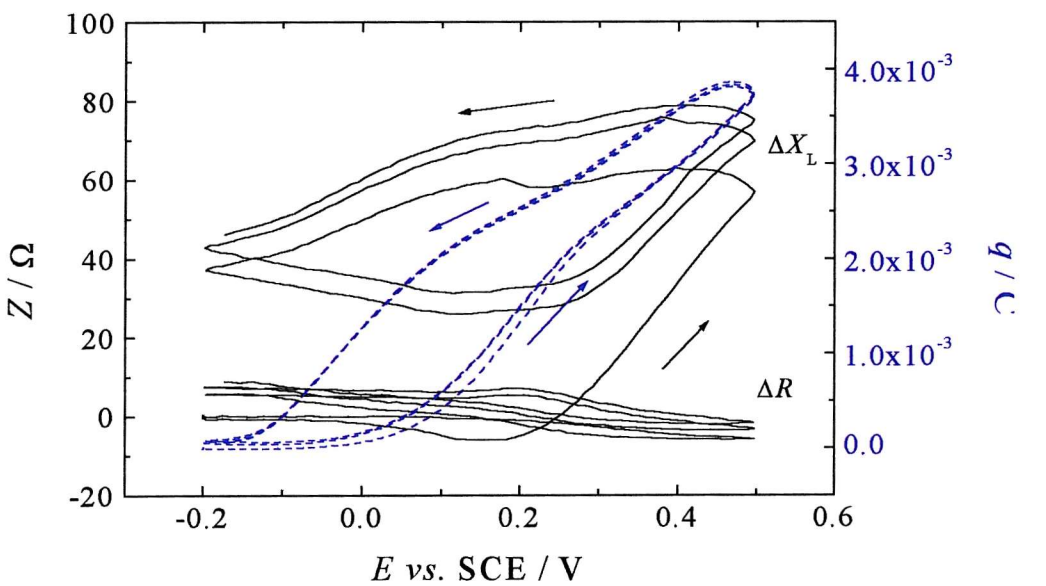

Figure 6.19: Electroacoustic impedance measurement and charge during redox cycles of 96 μg cm^{-2} of poly(aniline)-poly(styrenesulfonate) film in 40 mM HCl at 20 mV s^{-1}. The system was conditioned purging argon for 3 min with the substrate at –0.2 V, the tip at 0.2 V *vs.* SCE. The substrate was cycled from –0.2 V to 0.5 V while the tip was kept at -1.2 V *vs.* SCE.

Figure 6.20 shows the movement of water and movement of protons separately during the potential sweep of poly(aniline)-poly(styrenesulfonate) in 0.04 M $HClO_4$ by applying equations (6.8) and (6.10). The number of moles of anions is considered to be zero, $\vartheta_{ClO4^-} = 0$, and the fraction of the number of moles of water, 0.18 x ϑ_{H2O}, was transformed to the entire number of moles of water by dividing the values obtained from equation (6.10) by 0.18. The number of moles of protons is obtained by subtracting the equation (6.8) from the equation (6.10). The changes in mass in the polymer (calculated from the values of X_L shown in Figure 6.18) is related to the water movement alone as no anions take part in the maintenance of the electroneutrality of the polymer and the molecular mass of the protons is comparatively very small. The protons are expelled from the film during oxidation and inserted during reduction.

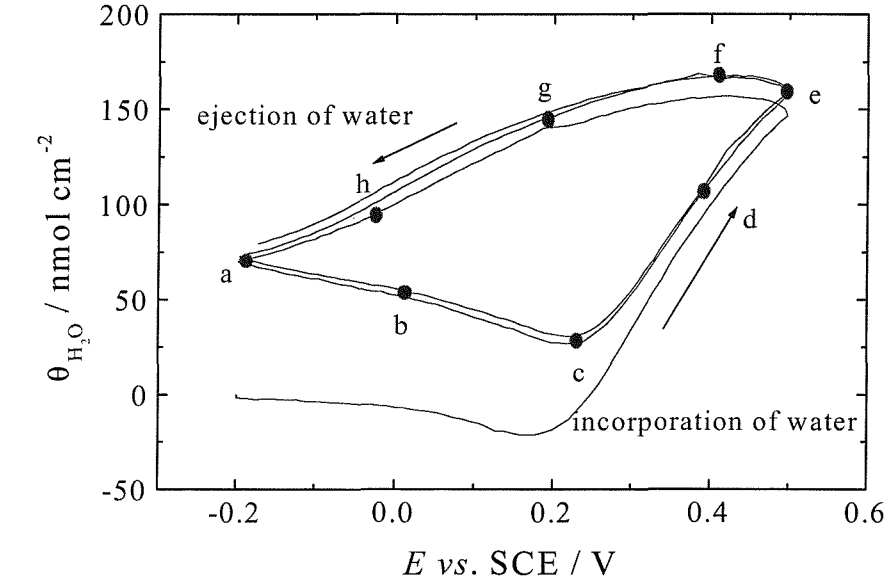

a

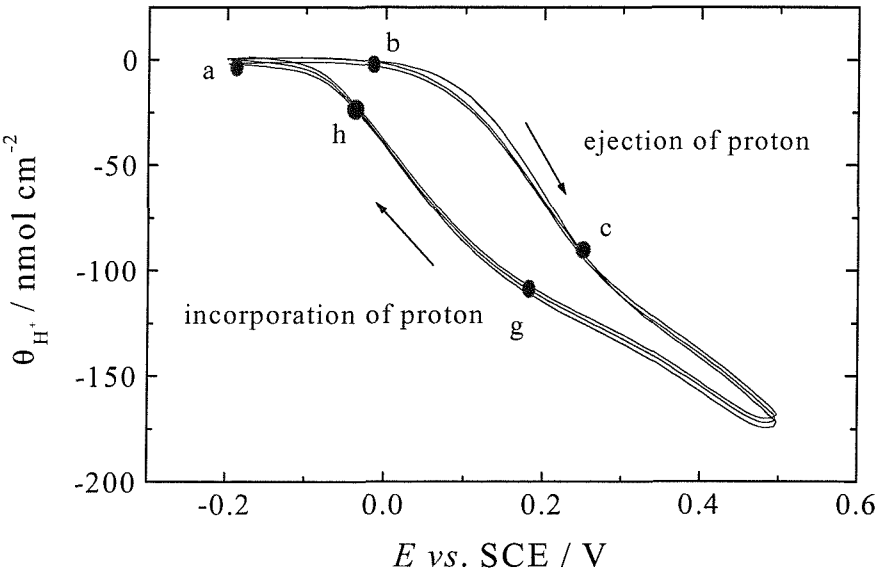

b

Figure 6.20: Number of moles exchanged during redox cycling of 96 μg cm^{-2} of poly(aniline)-poly(styrenesulfonate) film in 0.04 M $HClO_4$ at 20 mV s^{-1}. The film is kept at –0.2 V *vs* SCE for 3 min before the voltammetric cycles. a) number of moles of water and b) number of moles of protons exchanged. The points and the associated letters are used to explain the proton and the water movement on the polymer film during potential sweep in the text.

Figure 6.21 and Figure 6.22 show voltammograms of the poly(aniline)-poly(styrenesulfonate) films in different acid solutions. The normalised current registered at the microelectrode is plotted together with the current registered at the substrate during the potential scan of the polymer as a function of the polymer potential. Overlaying the two helps in the comparison between the electron and proton movement in the poly(aniline)-poly(styrenesulfonate) film. The current at the microelectrode was normalised against 40 % of the limiting current for the reduction of protons obtained when the tip is in the bulk. This is the current registered at the tip placed close to the substrate when the polymer film is at open circuit and the polymer has no influence on the concentration of protons. This normalisation is useful because the perturbation produced by the substrate upon the electrochemical reaction taking place at the tip can be detected.[134]

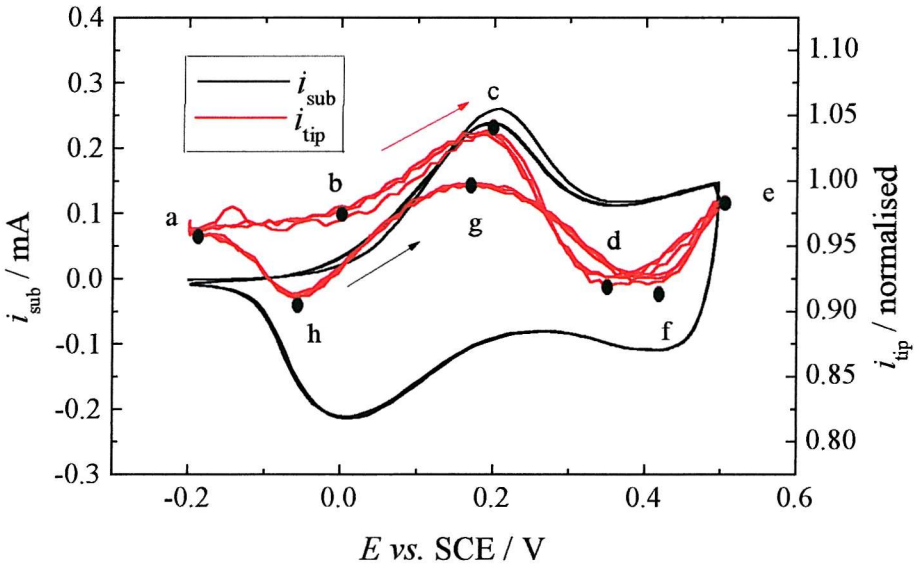

Figure 6.21: Voltammetric cycles of 96 μg cm^{-2} of poly(aniline)-poly(styrenesulfonate) film in 40 mM $HClO_4$ at 20 mV s^{-1}. The system was conditioned purging argon for 3 min with the substrate at –0.2 V, the tip at 0.2 V *vs.* SCE. The substrate was cycled from -0.2 V to 0.5 V while the tip was kept at –1.2 V close to the substrate. The points and the associated letters are used to explain proton and water movement on the polymer during potential sweep in the text.

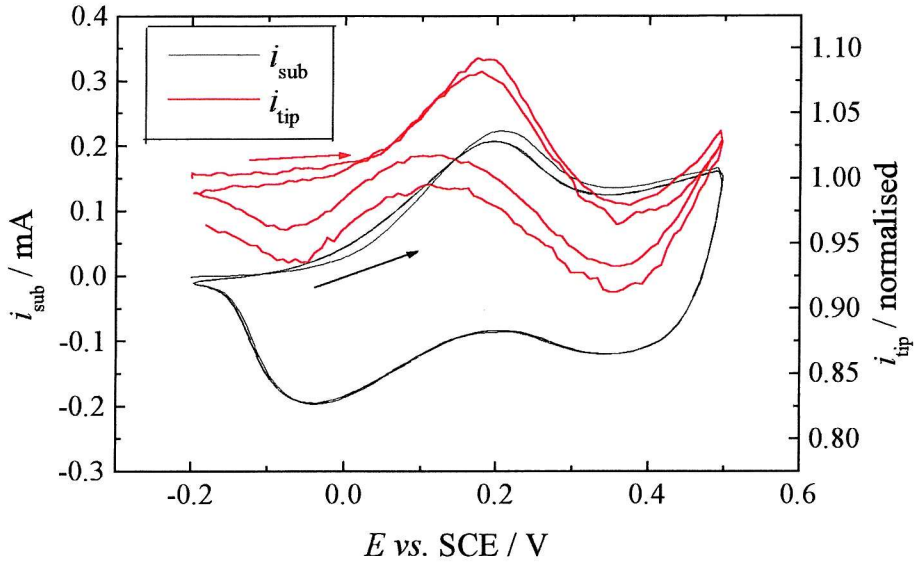

Figure 6.22: Voltammetric cycle of 96 μg cm^{-2} of poly(aniline)-poly(styrenesulfonate) film in 40 mM HCl at 20 mV s^{-1}. The system was conditioned purging argon for 3 min with the substrate at –0.2 V, the tip at 0.2 V *vs.* SCE. The substrate was cycled from -0.2 V to 0.5 V while the tip was kept at –1.2 V close to the substrate.

During the oxidation scan, the current at the microelectrode increases together with the oxidation current of the polymer film. The peaks in proton release and polymer current coincide. Then the normalised current at the microelectrode drops below 1, which could indicate that protons are taken up by the film, but it is not very probable since protons should leave the film during oxidation. The normalised current at the microelectrode reaches a minimum and then finishes the oxidation scan at the same current as it starts. At the beginning of the reduction scan there is a broad decrease at the microelectrode current which is the reverse of that happened on the oxidation scan. The normalised current at the microelectrode reaches the value of 1 just before the reduction peak starts and the normalised microelectrode current follows the reduction of polymer with a small time delay. The normalised microelectrode current ends the reduction scan from where the current starts the oxidation scan.

The increase in the normalised current at the microelectrode takes place with protons being released from the polymer film. The uptake of water into the polymer film, though increases the concentration of protons between the tip and the polymer film, however this is not significant relative to the sensitivity to proton movement because in 0.04 M acid there is 1 proton for every 1375 water molecules. As was seen

in the approach curve, the current at the microelectrode can also increase if the distance between the tip and the films grows with no simultaneous movement of protons between the film and the electrolyte.

By referring to the approach curve in Figure 6.17 we can calculate the thickness by which the polymer would need to increase in order to cause the effect seen in the current registered at the microelectrode in Figure 6.21 and Figure 6.22. The range of the normalised current shown in Figure 6.21 and Figure 6.22 is between 0.90 and 1.05 which corresponds to an absolute current at the microelectrode between 0.450 μA and 0.525 μA, since the normalisation is calculated against 0.5 μA. The correspondent expansion and shrinkage of the film would have to be about 4 μm according to the relation between the current registered at the tip and the distance between the tip and the substrate recorded during the apporach curve. The change in mass of the polymer during the potential sweep is 3 μg cm^{-2} by applying the Sauerbrey equation to the ΔX_L values of Figure 6.18. We can convert this mass change to a thickness change, $d = m / (A \times \rho)$, by considering that this mass is caused by water alone which has density of 1 g cm^{-3}. Thus we estimate that the thickness of the polymer film varies by only 0.03 μm during the potential sweep due to the movement of water. This is about one hundred times less than the charge required to explain the changes in the normalised current at the microelectrode. In addition we know that the dry polymer film is about 1 μm thick and it is not probable that the film absorbs water to four times its original thickness. Based on this analysis, we eliminate the possibility that the swelling, or contraction, of the polymer film is relevant on the current at the microelectrode.

By comparing the data obtained in the plots in Figure 6.20 and Figure 6.21 we can describe a possible model for the ionic and solvent transport during the redox switching of the poly(aniline)-poly(styrenesulfonate) film in 0.04 M $HClO_4$. At the beginning of the oxidation scan (between a and b) there is water moving out of the film and no movement of protons and the normalised current at the microelectrode can be considered constant. During the transition between the leucoemeraldine and emeraldine (between b and c) water is still leaving the film and in addition protons start to leave the film in order to maintain the electroneutrality causing the current at the microelectrode to increase considerably. After the oxidation peak (between c and d) water molecules change direction and move into the polymer film while some protons are still leaving the film. The current at the microelectrode decreases. The alteration in the direction of

the flux of water might disturb the mass transfer of protons in the solution between the polymer and the microelectrode decreasing the detection of the protons by the tip. Between d and e the current at the microelectrode increases slightly. The protons are still leaving the film and the amount of water being incorporated into the film decreases. With the stability of the flux of water into the film the microelectrode regains the measurement of the protons leaving the film. With the reversal of the scan (between e and f) the protons move into the film and the water movement slowly starts to change direction. The current at the microelectrode decreases detecting the proton incorporation into the film. When the film is temporarily in the emeraldine state (between f and g) there is water moving out of the film and protons are moving into the film and the current at the microelectrode increases. This increase in the microelectrode current when protons move into the film may again be caused by the change in the direction of the water. During the reduction peak (between g and h) protons move considerably into the film and water molecules leave the film leading to a decrease in the current at the microelectrode. When the polymer is at the reduced state (between h and a) the protons do not move much and water molecules leave the film. The microelectrode current increases.

The normalised current at the microelectrode is related to the concentration of protons in the electrolyte solution some micrometres away from the polymer film. The decrease in the normalised current between points c and d when an increase would be expected due to the ejection of protons from the polymer film; and the equally surprising increase in the normalised current between f and g and between h and a, could be explained by the change in the direction of the flux of water. This could disturb the mass transport of the protons in the solution between the tip and the polymer creating a misinterpretation about the flow of protons into and out of the polymer film during the redox switch. However this explanation seems unlikely because the gap between the polymer film and the microelectrode is large (about 20 to 50 μm) compared to the amount of water that moves (equivalent to a thickness of 0.03 μm).

Another hypothesis for the unexpected change in the direction of the microelectrode current between the points c and d, f and g and also h and a is based on the idea that the effects on the polymer beneath the tip where the microelectrode measurements are made are different from the rest of the polymer because of the blocking effects caused by the microelectrode. This localised alteration of the ionic flux

would not be sensed by the EQCM measurements and the current substrate because the total mass of polymer film is much greater than the amount of polymer which would suffer the effect of the microelectrode. Although it is not probable that the conically shaped microelectrode would alter the concentration of the electrolyte solution under the tip.

At this stage we do not have a plausible explanation for the unexpected current measured at the microelectrode between the points c and d, f and g and also h and a and more experiments are necessary to sort them out.

6.4. Conclusion about ion movement

The poly(aniline)-poly(styrenesulfonate) film is considered rigid during the redox cycles, so the Sauerbrey equation can be applied to the calculations of changes in polymer mass during redox cycling. This change in mass is caused by the movement of ions in order to maintain the polymer neutrally charged during the redox switching. Solvent also moves into and out of the film during the potential cycling.

The anions of the electrolyte do not take part in the process of charge neutrality of the film because large anions, poly(styrenesulfonate), are already incorporated into the polymeric structure. The protons are responsible for the electroneutrality of the poly(aniline)-poly(styrenesulfonate) film in acid solutions. During the oxidation of the poly(aniline)-poly(styrenesulfonate) film, protons move out of the film and water molecules move into the film. We speculate that the structure of the polymer film straightens out when in the oxidised stated creating free space for the inclusion of water molecules into the film. The reverse happens during the reduction. The proportion of the protons and water flux changes depend on the direction of the scan because the configurational conformation of the polymer film is related to the potential of the film. That is reason of the difference on the curves of mass per charge during reduction and oxidation.

The analysis of the amperometric response of protons at a microelectrode close to the surface of a polymer film, which is being reduced and oxidised, does not seem to be

converted exclusively to the flux of protons. Because of the difficulties in interpreting the results of the microelectrode current, the SECM is not the best technique to be coupled to the EQCM experiments in the analysis of ions and water flux during the redox switching of conducting polymers. Some reasons considered for the unlikeness of the results are that the change in the direction of the solvent in the polymer film during potential sweep could have an effect on the mass transport of the ion detected by the microelectrode. The change in the direction of the flux of water disturbs the mass transport of protons generating errors on the interpretation of the current at the microelectrode. Or even the physical impediment of the microelectrode might interfere locally the ion motion between the polymer and the microeletrode making it different than in the rest of the polymer film. So the response of the microelectrode current is not representative of the flux of ions and water that occurs in the great part of the polymer film.

7. Conclusion

There are two limiting cases for the EQCM measurements: when a thin, rigid and smooth layer is deposited on the quartz crystal its mass can be calculated by applying the Sauerbrey equation; when a Newtonian liquid is in contact with a quartz crystal, the product of its density and the viscosity can be calculated by using the Kanazawa equation. If the material analysed is neither a thin layer of a smooth and rigid material nor a perfectly viscous liquid, the Sauerbrey equation and the Kanazawa equation are both invalid and mathematical simulations are required. If the mass of the material analysed is the main quantity of interest in an EQCM measurement, it is essencial to prove that you have a thin, rigid and smooth layer to take advantage of the simplicity of the Sauerbrey equation. The validity of the Sauerbrey equation for a particular film can be readily checked by the observation of the parametric plot (ΔR vs. ΔX_L) since if Sauerbrey applies ΔR must stay close to zero while ΔX_L will represent the mass. The parameters R and X_L are obtained from EQCM experiments by representing the resonating quartz crystal in terms of a BVD equivalent electrical circuit. In our measurements we have used the transfer function method to operate the EQCM, this provides a fast and efficient way to perform and analyse the EQCM response. One of the major advantages of the transfer function method is the speed of the measurement - the technique is fast enough to follow rapid electrochemical reactions.

The aim in this thesis was to use the EQCM to study the electrodeposition, and the flux of ions and solvent during the redox switching, of poly(aniline) composite films. The poly(aniline) composite films show similar electrochemical and morphological properties when deposited either potentiostatically or potentiodynamically. On the other hand the choice of counterion used during electrodeposition influences the morphology of the film. Poly(aniline) films deposited with sulfate/bisulfate counterion have a fibrous structure, poly(aniline)-poly(vinylsulfonate) composite films have a globular structure, and poly(aniline)-poly(styrenesulfonate) composite films have a more compact structure. Starting from the model proposed by Urbakh for porous materials[97] we developed a relationship between the EQCM response, in terms of the parametric plot and the porosity of the material analysed. However we could not establish a quantitative fit between

experiment and theory because of the incertainties in the physical parameters for the polymer films (such as permeability and density).

We chose to study the flow of ions and solvent during redox cycles for the poly(aniline)-poly(styrenesulfonate) film because this was the only film which was smooth and behaved rigidly during the growth of a thin film. Consequently the Sauerbrey equation could be applied to calculate the change in mass of this polymer during redox cycling. This variation in mass is caused by the movement of ions, in order to maintain electroneutrality within the polymer during redox switching. The electrolytes used were strong inorganic acids composed exclusively of fully dissociated protons and anions. From the experimental results we conclude that the anions of the electrolyte do not take part in the process of oxidation or reduction of the poly(aniline)-poly(styrenesulfonate) film. Large anions, from the poly(styrenesulfonate), are already incorporated into the polymeric structure of the composite film. As the anions are not exchanged between the electrolyte and the polymer film, the movement of protons is believed to be responsible for maintaining electroneutrality of the poly(aniline)-poly(styrenesulfonate) film in acid solutions. The mass of protons is very small compared to the masses of polymer, anions and water, therefore it is not detected by the EQCM measurements. In order to observe the movement of protons between the polymer film and the electrolyte solution during the redox switching, SECM was coupled with the EQCM. A microelectrode was placed very close to the polymer film held at a potential at which protons were reduced to hydrogen molecules at a mass transport limited rate. The current at the microelectrode is proportional to the concentration of protons at the vicinity of the microelectrode, which is expected to increase if protons are expelled from the polymer film. We experienced unexpected difficulties in interpreting the current at the microelectrode during redox cycling of the polymer. More experiments such as potentiostatic measurements or potentiodynamic measurements using other scan rates and with the electrodes at different distances from the polymer film would help in the interpretation of the flux of protons between the polymer film and the electrolyte solution during potential cycling.

During the oxidation of the poly(aniline)-poly(styrenesulfonate) film there is an increase in mass in the polymer film caused by water molecules moving into the film. Due to orbital rearrangement, the backbone of the polymer film must straightened out when in the oxidised state and we suggest that this creates free space within the film which is taken up by the insertion of water molecules into the film so that it swells.

8. Appendices

8.1. Parameters of the BVD Equivalent Electrical Circuit

The components of the BVD equivalent circuit are converted to the physical properties of the resonant quartz and the materials attached on it by the following mathematical equations: [32,43]

$$C_o = \frac{D_q \varepsilon_o A_m}{l_q} \tag{8.1}$$

$$R_q = \frac{n^2 \pi^2 \eta_q l_q}{8 e_{26}^2 A_m} \tag{8.2}$$

$$L_q = \frac{\rho_q l_q^3}{8 e_{26}^2 A_m} \tag{8.3}$$

$$C_q = \frac{8 e_{26}^2 A_m}{l_q n^2 \pi^2 \mu_q} \tag{8.4}$$

$$L_1 = \frac{2 L_q \omega_o \rho_1}{n \pi \sqrt{\mu_q \rho_q}} \tag{8.5}$$

$$R_2 = \frac{L_q \omega_o}{n \pi} \sqrt{\frac{2 \omega_o \rho_2 \eta_2}{\mu_q \rho_q}} \tag{8.6}$$

$$L_2 = \frac{L_q \omega_o}{n \pi} \sqrt{\frac{2 \rho_2 \eta_2}{\omega_o \mu_q \rho_q}} \tag{8.7}$$

The mass sensitive area, A_m, and thickness of the quartz crystal, l_q, have an influence on the four parameters of the quartz crystal. The dielectric constant of the quartz, D_o, and the permittivity of free space, ε_0, appears only in C_o. The piezoelectric constant, e_{26}, is

present only on the motional branch. The acoustic viscosity of the quartz, η_q, is related to the dissipation of energy to the medium and hence to R_q. The density of the quartz, ρ_q, is associated to L_q and the elastic constant, μ_q, is associated with C_q. These last two physical properties of the quartz are present in the electric parameters of the non-piezoelectric materials deposited on the quartz.

8.2. Complex Numbers

Figure 8.1 shows a plot with input and output voltages with the same frequency but with a time delay between them that creates difference in phase.[141] The output voltage can be divided in two vectors: the in-phase (real) and the out-of-phase (imaginary) components with respect to the input voltage.

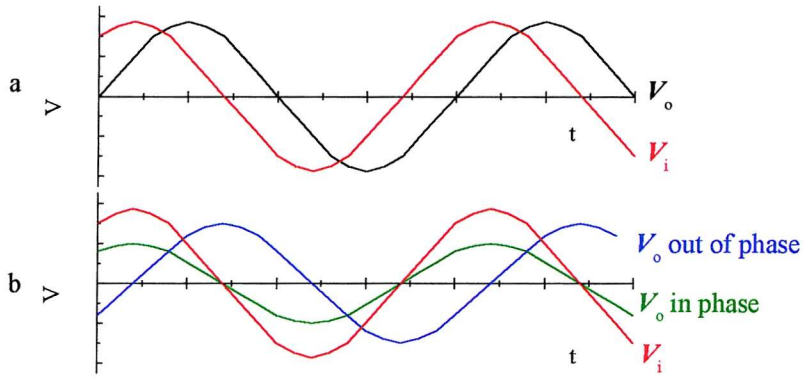

Figure 8.1: Sketch simplifying the differences in phases of a vector. a) Input and output voltages with the same frequency but different phases. b) Output voltage split in two: the in-phase and out-of-phase components with respect to the input voltage.

Numbers which are quantified by both a magnitude and a phase are called complex numbers. Complex numbers can be represented by a phasor and an angular rotation, θ, which indicates the phase difference.[141] Figure 8.2 shows the impedance $\boldsymbol{Z}$ represented in two forms: a magnitude and phase angle, $|\boldsymbol{Z}|\angle\theta$, or as the real and imaginary co-ordinates, R and X_L.

$$\begin{cases} R = |\boldsymbol{Z}| \cos\theta \\ X_{\mathrm{L}} = |\boldsymbol{Z}| \sin\theta \end{cases} \qquad \begin{cases} |\boldsymbol{Z}| = \sqrt{R^2 + X_L^2} \\ \tan^{-1}\theta = \dfrac{X_L}{R} \end{cases}$$

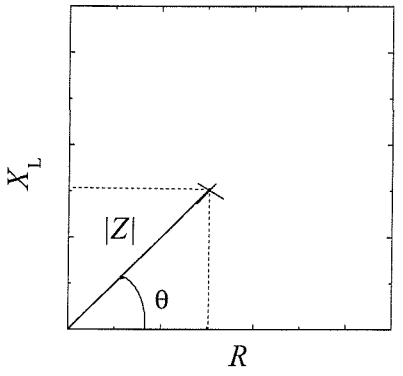

Figure 8.2: The impedance $\boldsymbol{Z}$ represented as a cartesian form $\boldsymbol{Z} = R + \mathrm{i}X_{\mathrm{L}}$, and in polar form $\boldsymbol{Z}=|Z|\mathrm{e}^{\mathrm{i}\theta}$.

In complex notation, $\boldsymbol{Z}$ can be represented as $R + \mathrm{i}X_{\mathrm{L}}$.[142] Numbers prefixed by i are known as imaginary numbers. The complex quantity $\boldsymbol{Z}$ is formed by the real part R and the imaginary part X_{L}. The real part R is the projection of $\boldsymbol{Z}$ on the horizontal axes (cosine) or the in-phase part and the imaginary part X_{L} is the projection of $\boldsymbol{Z}$ on the vertical axes (sine) or the out-of-phase part. The complex numbers are represented in bold type in this thesis.

8.3. Quick Basic Program

8.3.1. QCMFIT.BAS

The real and the imaginary components of the quartz crystal's electroacoustic impedance, R and X_L ($=\omega_o L$), are obtained from the non-linear least squares fitting program for equation (1.29) written in Quick Basic 4.5 by Etchenique[35]. This program calculates the values of R, L and C_o for each transfer function. The values of C_q is set at 3.36 x 10^{-14} F and C_m is equal 5.5 x10^{-11} F.

```
DECLARE SUB buscaframe ()
'     programa hecho en so'ton
'     fitberni

'     graba el primer set de datos en archivo NOMBRE.PRI


' ojo , 5 parametros , el 5to es admitancia de entrada del ampli !
' miq2 fitea la primera vez con 3 parametros , la segunda con 5 y
' despues vuelve a 3 clavando los otros 2


'     agarra muchos .DAT y los transforma en .FIT

      COMMON SHARED nomcru$, resmin%, resmax%, nummax%, kkk%

      COMMON SHARED res%(), vtg!, cserie



      'ON ERROR GOTO byerr

      OPTION BASE 1


      DIM res%(500)

      DEFDBL A-H, O-Z
      miny# = 1
      maxy# = 0

      ON KEY(10) GOSUB chao
```

```
        KEY(10) ON

        cm = 5.5E-11
        cserie = 3.36E-14       'valor impedancimetro = 3.192e-14
                        'este valor da correcta R=360 ohms !



conv:

        CLS

LOCATE 1, 1: PRINT "ESTE PROGRAMA OPERA SOBRE EL SUBDIRECTORIO
DONDE ESTE PARADO !"


        nvar% = 1: np% = 5: nobs% = 1000'(ES EL DEFAULT Y MAXIMO DE nobs%)


        DIM fobs(nobs%), fcalc(nobs%), ftemp(nobs%)
        DIM vobs(nobs%, nvar%), v(nobs%, nvar%), dfdv(nobs%, nvar%)
        DIM p(np%), pname$(np%), dfdp(nobs%, np%)
        DIM iflag%(nobs%), dlambda(nobs%)

        kkk% = 1

        iuserwt% = 0
        internalwt% = 0
        fract = 1


        LOCATE 5, 11: PRINT "Si quiere modificar valores de Cmedida y Cserie pulse
C"
        LOCATE 6, 11: PRINT "Si no , pulse ENTER"

modic:      l$ = INKEY$
            IF l$ = CHR$(13) THEN GOTO pidata
            IF UCASE$(l$) <> "C" THEN GOTO modic

        LOCATE 9, 11: PRINT USING "Valor de cserie en fentofarad (default = ##.# )";
cserie * 1E+15;

        INPUT cserie$
        IF cserie$ <> "" THEN cserie = VAL(cserie$) * 1E-15

        LOCATE 11, 11: PRINT USING "Valor de cmedida en picofarad (default = ###.#
)"; cm * 1E+12;
        INPUT cm$
        IF cm$ <> "" THEN cm = VAL(cm$) * 1E-12
```

```
pidata:

    CLS

LOCATE 1, 1: PRINT "ESTE PROGRAMA OPERA SOBRE EL SUBDIRECTORIO
DONDE ESTE PARADO !"

    LOCATE 5, 1: INPUT "Numero maximo de iteraciones (default = 30)        ",
numit%
    IF numit% = 0 THEN numit% = 30

    LOCATE 7, 1: INPUT "dERR/dFIT max p/ terminar regresion (Def = 1e-8) ",
erreg
    IF erreg = 0 THEN erreg = 1E-08


    LOCATE 9, 1: INPUT "One fit every ... how many points ?  (Def=1) ", kkk$
    IF kkk$ <> "" THEN kkk% = VAL(kkk$)

    autofram$ = "N"

    IF autofram$ = "N" THEN
        LOCATE 11, 1: INPUT "Numero de puntos iniciales que deja afuera       ",
xnpun%
        LOCATE 13, 1: INPUT "Numero de puntos FINALES  que deja afuera
", xnpunf%
    END IF



    LOCATE 15, 1: INPUT "Resistencia , valor inicial en ohms (default = 100)  ",
p(1)
    IF p(1) = 0 THEN p(1) = 100
    LOCATE 17, 1: INPUT "Capacidad Co , valor inicial en F   (default = 2e-11) ",
p(3)
    IF p(3) = 0 THEN p(3) = 2E-11
    LOCATE 19, 1: INPUT "Inductancia , valor inicial en Hy   (default = reson) ",
p(2)

    LOCATE 21, 1: INPUT "Fitea 3-5-4-3 o solo 3 FIJOS ?      (default = 3543)    ",
fittype%
    IF fittype% <> 3 THEN fittype% = 3543
    np% = 3

    LOCATE 23, 1: INPUT "Factor #D (inicial o fijo)       (default = 2)  ", factor
    IF factor = 0 THEN factor = 2
    p(4) = factor
    admitin = .0001
    p(5) = .0001
```

```
CLS

LOCATE 3, 1: PRINT "Nombres de los archivo a convertir SIN EL PATH y SIN
.DAT ! "
LOCATE 5, 1: PRINT "Ponga solo ENTER para el terminar ..."


DIM nom$(50)

      numfile% = 1
loopfile:
          INPUT nom$(numfile%)


          IF nom$(numfile%) <> "" THEN numfile% = numfile% + 1: GOTO loopfile

      num% = 0



      FOR numero% = 1 TO numfile% - 1

      IF nom$(numero%) = "nuevo" THEN num% = 0: p(2) = 0: GOTO nesnumero

      p(2) = 0


      num% = num% + 1


      nom$ = nom$(numero%)




      SCREEN 12
      CLS



nomcru$ = nom$ + ".DAT"
nomfit$ = nom$ + ".FIT"
numfit% = 1
```

```
    IF autofram$ = "Y" THEN CALL buscaframe


OPEN nomcru$ FOR INPUT AS #1
OPEN nomfit$ FOR OUTPUT AS #2

INPUT #1, titulo$           'dummy

INPUT #1, datfreq$

minfreq = 1000000! * VAL(MID$(datfreq$, 7, 10))
maxfreq = 1000000! * VAL(MID$(datfreq$, 27, 10))



INPUT #1, dummy1$
INPUT #1, dummy2$
INPUT #1, dummy3$


maxda% = 0
minda% = 0
stepda% = 20

cuentada:                   'aca cuenta cuantos puntos hay

    INPUT #1, transf$

    maxda% = maxda% + stepda%

    IF VAL(transf$) <> 0 THEN GOTO cuentada
    maxda% = maxda% - stepda%



da% = maxda%

punto% = 0
prim% = -2
minmodulo# = 1E+20
i% = 1

otroset:

    l$ = INKEY$
    IF UCASE$(l$) = "P" THEN np% = 5


  ' IF numfit% > 5 THEN
```

```
'       IF solouna% = 1 THEN
'       factor = p(4)
'       admitin = p(5)
'       np% = 3
'       GOTO juira
'       END IF

        'IF devsq > .001 THEN np% = 5: solouna% = 1
    'END IF
juira:

    IF autofram$ = "Y" THEN

        npun% = res%(numfit%) - resmin%
        npunf% = resmax% - res%(numfit%)

    ELSE
        npun% = xnpun%
        npunf% = xnpunf%

    END IF


otro:

IF EOF(1) THEN GOTO byebye


LINE INPUT #1, dat$

IF dat$ = "" THEN GOTO otro


IF (LEFT$(dat$, 1) = "E" OR LEFT$(dat$, 1) = "t" OR LEFT$(dat$, 1) = "q") AND
punto% = 0 THEN punto% = 1: prim% = -2: viejdat$ = dat$: GOTO otro
IF (LEFT$(dat$, 1) = "E" OR LEFT$(dat$, 1) = "t" OR LEFT$(dat$, 1) = "q") AND
punto% = 1 THEN prim% = -2: viejdat$ = dat$: da% = maxda%: GOTO otrocacho



IF prim% = -1 THEN prim% = 0:  GOTO otro    'para comerse el 1er dato
```

```
IF prim% = -2 THEN prim% = -1:  GOTO otro    'para comerse el 2do dato tambien

'F UCASE$(INKEY$) = "Q" THEN END


antdat$ = viejdat$

   x = maxda% - da%

      fr = minfreq + x * (maxfreq - minfreq) / (maxda% - minda%)
      w# = 2 * 3.1415927# * fr

       modulober = VAL(MID$(dat$, 1, 5))

'      modulo# = .003871 * modulober ^ 2 - 23.2205 * modulober + 42555.25
       modulo# = modulober

       modulo# = modulo# / 10000


'     esta es la ecuacion para pasar de los datos de bernhard a los
'     mios, debido a la distinta forma de agarrarlos



    '  LOCATE 9, 1: PRINT da%, ch1!, ch2!, vo#, vi#
    '  LOCATE 11, 1: PRINT w#, modulo#


      da% = da% - stepda%



IF modulo# = 0 THEN GOTO otro


     IF modulo# < minmodulo# THEN minmodulo# = modulo#: wres# = w#

  IF j% < npun% THEN GOTO dummypunt
  IF modulo# > 2 THEN GOTO dummypunt
```

```
            vobs(i%, 1) = w#
            fobs(i%) = modulo#


            IF fobs(i%) > maxy# THEN maxy# = fobs(i%)
            IF fobs(i%) < miny# THEN miny# = fobs(i%)


            i% = i% + 1
dummypunt:
            j% = j% + 1



GOTO otro


byebye:

CLOSE 1
CLOSE 2

nesnumero:      NEXT numero%


   END


otrocacho:

'si no tiene valor inicial para p(2) lo busca del minimo de modulo
'hallado

      IF numfit% > 5 THEN


      jjj% = jjj% + 1
      IF jjj% < kkk% THEN GOTO otroarch

      jjj% = 0
      END IF


      LOCATE 27, 1: PRINT "F10 to quit";


      IF p(2) = 0 THEN
            p(2) = 1 / (wres# ^ 2 * cserie)
```

```
    END IF

    'GOTO casifin

' aca esta el nolin6

'   programa fiteador , es el nonlin sin comments

10050

    nobs% = i% - 1 - npunf%


    miny# = miny#
    maxy# = maxy#
    wmax = vobs(nobs%, 1)
    wmin = vobs(1, 1)

    'iF vezz% = 0 THEN vezz% = 1:
    WINDOW (wmin, miny#)-(wmax, maxy#)


    pname$(1) = "R"
    pname$(2) = "Co"
    pname$(3) = "L"


    devsq1 = 1D+20: devsq2 = 1D+20



    'IF UCASE$(INKEY$) = "Q" THEN END


    FOR it% = 1 TO numit%


        GOSUB 12000
        GOSUB 13000
        IF nonconvergence% = 1 THEN PRINT "nonconvergence !!": END

        GOSUB 13500
```

```
            IF internalwt% = 1 THEN GOSUB 14500

            GOSUB 15000
            GOSUB 16000
            GOSUB 17000

        NEXT it%

        GOSUB 19000
        GOSUB 20000

casifin:
        IF LEFT$(antdat$, 1) = "t" THEN


          eot! = VAL(MID$(antdat$, 3, 5))


          'ioq! = VAL(MID$(antdat$, 25, 14))
          'vtg! = VAL(MID$(antdat$, 45, 14))


        ELSE

          'eot! = VAL(MID$(antdat$, 5, 11))
          'ioq! = VAL(MID$(antdat$, 25, 24))

        END IF

'si son los 3 primeros datos chotos , no escribe !


    IF num% > 1 OR numfit% >= 5 THEN

        IF np% = 2 THEN

        PRINT #2, USING "#####.### , #.####^^^^,#.####^^^^, #####.##, ##.######,
##.##"; eot!; ioq!; vtg!; p(1); p(2) * 1000!; capa * 1E+12

        ELSE

        PRINT #2, USING "#####.### , #.####^^^^,#.####^^^^, #####.##, ##.######,
##.##"; eot!; ioq!; vtg!; p(1); p(2) * 1000!; p(3) * 1E+12

        END IF

    END IF


        GOTO otroarch
```

```
11000
      FOR i% = 1 TO nobs%


      x = vobs(i%, 1)



      IF np% = 2 THEN
      fcalc(i%) = factor * SQR(p(1) ^ 2 + (x * p(2) - 1 / (x * (cserie))) ^ 2) / SQR((x *
p(2) - 1 / (x * cserie) + x * p(2) * capa / cm - capa / (x * cserie * cm) - 1 / (x * cm) -
p(1) * admitin / (x * cm)) ^ 2 + (p(1) + p(1) * capa / cm + _
admitin * p(2) / cm - admitin / (x * x * cserie * cm)) ^ 2)
      END IF

      IF np% = 3 THEN
      fcalc(i%) = factor * SQR(p(1) ^ 2 + (x * p(2) - 1 / (x * (cserie))) ^ 2) / SQR((x *
p(2) - 1 / (x * cserie) + x * p(2) * p(3) / cm - p(3) / (x * cserie * cm) - 1 / (x * cm) - p(1)
* admitin / (x * cm)) ^ 2 + (p(1) + p(1) * p(3) / cm + _
admitin * p(2) / cm - admitin / (x * x * cserie * cm)) ^ 2)
      END IF

      IF np% = 4 THEN
      fcalc(i%) = p(4) * SQR(p(1) ^ 2 + (x * p(2) - 1 / (x * (cserie))) ^ 2) / SQR((x *
p(2) - 1 / (x * cserie) + x * p(2) * p(3) / cm - p(3) / (x * cserie * cm) - 1 / (x * cm) - p(1)
* admitin / (x * cm)) ^ 2 + (p(1) + p(1) * p(3) / cm + admitin _
* p(2) / cm - admitin / (x * x * cserie * cm)) ^ 2)
      END IF

      IF np% = 5 THEN
      fcalc(i%) = p(4) * SQR(p(1) ^ 2 + (x * p(2) - 1 / (x * (cserie))) ^ 2) / SQR((x *
p(2) - 1 / (x * cserie) + x * p(2) * p(3) / cm - p(3) / (x * cserie * cm) - 1 / (x * cm) - p(1)
* p(5) / (x * cm)) ^ 2 + (p(1) + p(1) * p(3) / cm + p(5) * p(2) _
/ cm - p(5) / (x * x * cserie * cm)) ^ 2)
     END IF


      NEXT i%
      RETURN


12000
      GOSUB 12200
      GOSUB 11000
      GOSUB 12500
      RETURN

12200
```

```
    CLS
    LOCATE 2, 4: PRINT nomcru$; "  >>>   "; nomfit$

    LOCATE 4, 4
    PRINT "Parameters , iteration "; it%: PRINT ; " time = "; TIME$
    LOCATE 7, 2
    PRINT "Name       Value       Change"; : PRINT

    IF ABS(p(1)) > 100000 OR ABS(p(2)) > 1 OR ABS(p(3)) > .000001 OR
ABS(p(4)) > 10 OR ABS(p(5)) > 1E+12 THEN
    CLS
    PRINT "overflow"

    END
    END IF



LOCATE 9, 2: PRINT USING " R    ####.##       ####.##"; p(1); -1 * rhs(1)

IF np% > 2 THEN
LOCATE 10, 2: PRINT USING "  Co   ####.##       ####.##"; p(3) * 1E+12; -1E+12 *
rhs(3)
ELSE
LOCATE 10, 2: PRINT USING "  Co   ####.##     no change"; capa * 1E+12;
END IF


LOCATE 11, 2: PRINT USING "  L     ##.######      #.######"; p(2) * 1000; -1000 *
rhs(2)

IF np% > 3 THEN
  LOCATE 13, 2: PRINT USING "  D      #.###        #.###"; p(4); rhs(4)
  LOCATE 14, 2: PRINT USING " Rin    ###.###     Kohm     "; .001 / p(5)


ELSE
  LOCATE 13, 2: PRINT USING "  D      #.###"; factor
  IF admitin > .00001 THEN LOCATE 14, 2: PRINT USING " Rin      ###.###
Kohm     "; .001 / admitin

END IF



    PRINT
    RETURN
```

```
12500
    irow% = 1: icol% = 40: ioffset% = 20: iroom% = 40: numrows% = 20
    devsq = 0

    VIEW (350, 1)-(610, 400), , 14
    CLS


    IF numfit% = 5 THEN

    nompri$ = nom$ + ".PRI"
    OPEN nompri$ FOR OUTPUT AS #3
    END IF



    FOR i% = 1 TO nobs%

    IF numfit% = 5 THEN PRINT #3, USING "######## , #.####"; vobs(i%, 1);
fobs(i%) / factor

    PSET (vobs(i%, 1), fobs(i%)), 14
    PSET (vobs(i%, 1), fcalc(i%)), 7

12630       dev = fobs(i%) - fcalc(i%)
        devsq = devsq + dev * dev
    NEXT i%

    CLOSE #3


    LOCATE 20, 5: PRINT USING "Error = #.##^^^^"; devsq
    IF it% = 1 THEN GOTO 12690
    LOCATE 21, 5: PRINT USING "Cambio= #.##^^^^"; devsq - devsq1;
    IF ABS(devsq - devsq1) < erreg THEN it% = numit%
    'IF (devsq - devsq1) > 1000 * erreg THEN nonconvergence% = 1


12690  RETURN

13000
    'IF (devsq > devsq1 AND devsq1 > devsq2) THEN nonconvergence% = 1
    devsq2 = devsq1
    devsq1 = devsq
    RETURN

13500
    FOR i% = 1 TO nobs%
```

```
        dlambda(i%) = (fcalc(i%) - fobs(i%))

    NEXT i%
    RETURN

14000
    GOSUB 11000

    FOR iw% = 1 TO nobs%

        ftemp(iw%) = fcalc(iw%)
    NEXT iw%

    FOR iw% = 1 TO nvar%

        FOR jw% = 1 TO nobs%

            iflag%(jw%) = 0

            IF ABS(vobs(jw%, iw%)) < 9.999999999999999D-21 THEN
                vobs(jw%, iw%) = .0005#: iflag%(jw%) = 1
            ELSE
                vobs(jw%, iw%) = vobs(jw%, iw%) * 1.0005#
            END IF


            PRINT "modified var:"; vobs(jw%, iw%)

        NEXT jw%

        GOSUB 11000

        FOR jw% = 1 TO nobs%

            IF iflag%(jw%) = 1 THEN
                dfdv(jw%, iw%) = (fcalc(jw%) - ftemp(jw%)) / .0005#
                vobs(jw%, iw%) = vobs(jw%, iw%) - .0005#
            END IF

            IF iflag%(jw%) <> 1 THEN
                dfdv(jw%, iw%) = (fcalc(jw%) - ftemp(jw%)) / (.0005# *
vobs(jw%, iw%))
                vobs(jw%, iw%) = vobs(jw%, iw%) / 1.0005#
            END IF

            PRINT "dfdv("; jw%; iw%; ");dfdv(jw%,iw%)"
        NEXT jw%

    NEXT iw%
    RETURN
```

```
14500
    IF it% = 1 THEN RETURN
    GOSUB 14000

    FOR iw% = 1 TO nobs%
        sum = 0#

        FOR jw% = 1 TO nvar%

            sum = sum + dfdv(iw%, jw%) * dfdv(iw%, jw%)
        NEXT jw%


    NEXT iw%

    PRINT "new function weights:"

    FOR iw% = 1 TO nobs%
        PRINT
    NEXT iw%

    RETURN


15000
    GOSUB 17500

    FOR i% = 1 TO np%

        rhs(i%) = 0#

        FOR j% = 1 TO nobs%

            rhs(i%) = rhs(i%) + dfdp(j%, i%) * dlambda(j%)
        NEXT j%

        FOR j% = 1 TO np%
            b(i%, j%) = 0#
            FOR k% = 1 TO nobs%
                b(i%, j%) = b(i%, j%) + dfdp(k%, i%) * dfdp(k%, j%)
            NEXT k%
        NEXT j%
    NEXT i%
    RETURN

16000
    DETERM = 1#
    FOR i% = 1 TO np%
        INDEX(i%, 3) = 0
```

```
    NEXT i%

    FOR i% = 1 TO np%
        MAX# = 0#

        FOR j% = 1 TO np%
            IF INDEX(j%, 3) = 1 THEN GOTO 16260
            FOR k% = 1 TO np%
                IF INDEX(k%, 3) > 1 THEN GOTO 16700
                IF INDEX(k%, 3) = 1 THEN GOTO 16250
                IF MAX# > ABS(b(j%, k%)) THEN GOTO 16250
                irow% = j%
                icol% = k%
                MAX# = ABS(b(j%, k%))
16250           NEXT k%
16260       NEXT j%

        INDEX(icol%, 3) = INDEX(icol%, 3) + 1
        INDEX(i%, 1) = irow%
        INDEX(i%, 2) = icol%

        IF irow% = icol% THEN GOTO 16380
        DETERM = -1# * DETERM

        FOR j% = 1 TO np%
            SWAP b(irow%, j%), b(icol%, j%)
        NEXT j%

        SWAP rhs(irow%), rhs(icol%)
16380   PIVOT = b(icol%, icol%)
        DETERM = DETERM * PIVOT
        b(icol%, icol%) = 1#

        FOR j% = 1 TO np%
            b(icol%, j%) = b(icol%, j%) / PIVOT
        NEXT j%

        rhs(icol%) = rhs(icol%) / PIVOT

        FOR j% = 1 TO np%

            IF j% = icol% THEN GOTO 16540
            T = b(j%, icol%)
            b(j%, icol%) = 0#

            FOR k% = 1 TO np%
                b(j%, k%) = b(j%, k%) - b(icol%, k%) * T
            NEXT k%

            rhs(j%) = rhs(j%) - rhs(icol%) * T
```

```
16540         NEXT j%
      NEXT i%


      FOR i% = np% TO 1 STEP -1
            IF INDEX(i%, 1) = INDEX(i%, 2) THEN GOTO 16640
            irow% = INDEX(i%, 1)
            icol% = INDEX(i%, 2)

            FOR j% = 1 TO np%
                  SWAP b(j%, irow%), b(j%, icol%)
            NEXT j%
16640   NEXT i%


      FOR i% = 1 TO np%
            IF INDEX(i%, 3) <> 1 THEN GOTO 16700
      NEXT i%
      RETURN


16700   PRINT "singular matrix error"



17000

      FOR i% = 1 TO np%
            p(i%) = p(i%) - rhs(i%) * fract
      NEXT i%
      RETURN

17500
      GOSUB 11000

      FOR iss% = 1 TO nobs%
            ftemp(iss%) = fcalc(iss%)
      NEXT iss%

      FOR iss% = 1 TO np%
            tp = p(iss%)
            IF tp < 9.999999999999999D-21 THEN
                  p(iss%) = tp + .0005#
            ELSE
                  p(iss%) = tp * 1.0005#
            END IF

            GOSUB 11000

            FOR js% = 1 TO nobs%
```

```
            IF tp < 9.999999999999999D-21 THEN
                dfdp(js%, iss%) = (fcalc(js%) - ftemp(js%)) / .0005#
            ELSE
                dfdp(js%, iss%) = (fcalc(js%) - ftemp(js%)) / (.0005# * tp)
            END IF
        NEXT js%

        p(iss%) = tp
    NEXT iss%
    RETURN



19000
    GOSUB 11000

    RETURN


19500
    IF nobs% <= np% THEN var = 0# ELSE var = devsq / (nobs% - np%)

    FOR i% = 1 TO np%
        FOR j% = 1 TO np%
            b(i%, j%) = b(i%, j%) * var
        NEXT j%
    NEXT i%

    RETURN

20000
20080   RETURN



65000
    PRINT "nopt in ascci"
    END



' aca termina el nolin 6

otroarch:

    i% = 1
    j% = 1
    LOCATE 23, 70: PRINT numfit%
```

```
        numfit% = numfit% + 1

 IF num% = 1 THEN

  IF fittype% = 3543 THEN

        IF numfit% = 2 THEN np% = 5

        IF numfit% = 3 THEN admitin = p(5): np% = 4

        IF numfit% = 4 THEN
              np% = 3
              factor = p(4)

              IF p(1) > 0 THEN
                    admitin = p(5)
              ELSE
                    admitin = -p(5)
                    p(1) = -p(1)


              END IF
        END IF


  END IF


 END IF


       GOTO otroset



chao:   END




byerr:  CLS
PRINT "error"
END

SUB buscaframe


OPEN nomcru$ FOR INPUT AS #1
```

```
punto% = 0
prim% = -2
i% = 1
dataset% = 1

resmax% = 0
resmin% = 10000

otro2:
minmodulo# = 1E+20

otro3:

IF EOF(1) THEN GOTO byebye3

INPUT #1, dat$

IF dat$ = "" THEN GOTO otro3


IF (LEFT$(dat$, 1) = "E" OR LEFT$(dat$, 1) = "t" OR LEFT$(dat$, 1) = "q") AND
punto% = 0 THEN punto% = 1: prim% = -2: viejdat$ = dat$: GOTO otro3
IF (LEFT$(dat$, 1) = "E" OR LEFT$(dat$, 1) = "t" OR LEFT$(dat$, 1) = "q") AND
punto% = 1 THEN prim% = -2: viejdat$ = dat$: GOTO otrocacho3


IF prim% = -1 THEN prim% = 0:  GOTO otro3    'para comerse el 1er dato
IF prim% = -2 THEN prim% = -1:  GOTO otro3    'para comerse el 2do dato tambien


antdat$ = viejdat$
numdat% = numdat% + 1




freq# = VAL(MID$(dat$, 1, 8))

vocru# = VAL(MID$(dat$, 10, 7))

vicru# = VAL(MID$(dat$, 17, 8))

IF vocru# = 0 AND vicru# = 0 THEN GOTO otro3


'  convierte en modulo verdadelo de Vo/Vi con la ecuacion corresp
'  y en fase verdadera el intervalo leido con el frecuencimetro
```

```
    vo# = -.79298457# + .0014679212# * vocru#
    vi# = -.32209714# + .0014204474# * vicru#


  modulo# = vo# / vi#


  w# = freq# * 3.1415927# * 2

     IF modulo# < minmodulo# THEN minmodulo# = modulo#: numres% = numdat%


GOTO otro3

otrocacho3:
     IF nummax% = 0 THEN nummax% = numdat%
     numdat% = 1

     IF numres% > resmax% THEN resmax% = numres%
     IF numres% < resmin% THEN resmin% = numres%
     res%(dataset%) = numres%
     dataset% = dataset% + 1


     GOTO otro2


byebye3:

CLOSE 1


CLS

PRINT "Auto frame decition is:"
PRINT
PRINT "from  wres -"; resmin% + 1
PRINT "to    wres +"; nummax% - resmax%


END SUB
```

8.3.2. BASEQCM.BAS

This program corrects any shift in frequency occured on the VCO during the measurements of the transfer functions. It combines the data fitted by the previous program (.fit) with the data obtained by the baseline measurements (.bsl).

```
DIM basedl(5000)
DIM basetime(5000)

CLS

tiempovie = 0
ivie = 0
q = 0



INPUT "Raw data file to be linebased ", raw$
      rawdata$ = raw$ + ".FIT"
      finaldata$ = raw$ + ".FIN"


      baseline$ = raw$ + ".BSL"



OPEN baseline$ FOR INPUT AS #1
      n% = 1

      WHILE NOT EOF(1)

        INPUT #1, basetime(n%), basefr
        IF n% = 1 THEN basebase = basefr
        basedl(n%) = .0000015835# * (basefr - basebase) 'conversion between henry
and hertz

        n% = n% + 1
      WEND
      CLOSE 1
        basetime(n%) = 1E+10        'tiempo gigante para terminar



      indibas% = n% - 1       'maximum of baseline array
```

```
        OPEN rawdata$ FOR INPUT AS #1
        OPEN finaldata$ FOR OUTPUT AS #2

        CLS

        LINE INPUT #1, dummy$

        WHILE NOT EOF(1)


        INPUT #1, tiempo, i, e, r, l, co

                n% = 1
more:
                IF basetime(n%) > 1E+09 THEN GOTO final


                IF basetime(n%) < tiempo THEN
                    n% = n% + 1
                    GOTO more
                END IF

' here basetime(n%-1) < tiempo but basetime(n%) >= tiempo


                IF tiempo = basetime(n%) THEN deltal = basedl(n%): GOTO ex

'here tiempo is between the two (n%-1) and n% base points

                grad = (basedl(n%) - basedl(n% - 1)) / (basetime(n%) - basetime(n% - 1))
                c = basedl(n%) - grad * basetime(n%)

                deltal = grad * tiempo + c



                GOTO ex

ex:


                LOCATE 8, 1: PRINT USING "##.######"; deltal

                LOCATE 10, 1


                dq = .5 * (i + ivie) * (tiempo - tiempovie)
```

```
        q = q + dq


        IF ABS(e) > 9.9999 THEN e = 0

        LOCATE 18, 1

        PRINT "time/sec     i/A        q/C        E/V     R/ohm     L/mH     Co/pF "
        PRINT
        PRINT USING "######.### , #.####^^^^ , #.####^^^^ , ##.#### , ####.## ,
##.######## , ###.## "; tiempo; i; q; e; r; 1 - deltal; co
        PRINT #2, USING "######.### , #.####^^^^ , #.####^^^^ , ##.#### ,
####.## , ##.######## , ###.## "; tiempo; i; q; e; r; 1 - deltal; co



        tiempovie = tiempo
        ivie = i



        WEND


final:
        CLOSE 2
        CLOSE 1

        END
```

8.4. Mathematica Program

This program was used on the analysis of the viscoelastic polymer. Initial and final values should be set up for the thickness and shear viscosity of the polymer. The file with the values of the fitted R and X_L is named 'file1.txt' and the output file with the values of d and G is callled file1out.txt

dini = 1.9 x10^{-7};
dfin = 3 x 10^{-7};
di = 1.7 x 10^{6};
df = 2.56 x 10^{6};
w = 6.28 x 10^{7};
r1 = 10^{3};
r2 = 10^{3};
G2 = 6.4 x 10^{4};
equ = 0.0339 x (r1 G alpha Tanh w alpha (rf / Galpha) + r2 G2 alpha)/((r2 G2/r1G) Tanh w alpha d (r1/G) +1);
Re[equ];
Im[equ];
m = ComplexExpandRe[equ], TargetFunctions [Re,Im];
n = ComplexExpandIm[equ], TargetFunctions [Re,Im];
z = ReadList"filetext1.txt", NumberRecordList True;
l = TableFindRoot m = =zi 1, n= =zi 2 , d,dini,dfin,G,gi,gf,MaxIterations 50, AccuracyGoal 3, I, Length z;
MatrixForml;
s = [d,G] .1;
TableForm;
Matoutd=OpenWrite"file1out.txt";
DoWriteStringmatoutd,ToStringFortranFormsi, 1,",",ToStringFortranForms,2 ,"\n" , i,1,Lengthz
Closematout;
!!file1out.txt

8.5. Permeability

Permeability is more correlated to the size of flow channels inside a porous material than by its quantity. The permeability of a porous material formed by a network of straight cylindrical capillaries with radius $\Re$ and porosity ϕ is:[118]

$$\xi^2 = \frac{\Re^2}{8}\varphi \tag{8.8}$$

The model proposed by Daikhin and Urbakh for acoustic measurements of porous materials is based on Brinkman's equation, which describes the flow of a liquid through an interfacial layer. [59,143]

$$i\omega\rho v_x(z,\omega) = \eta\frac{\partial^2}{\partial z^2}v_x(z,\omega) + V_o\frac{\eta}{\xi^2}\sqrt{1+\frac{i\omega\rho\xi^2}{\eta}} - v_x(z,\omega)\frac{\eta}{\xi^2} \tag{8.9}$$

where η is the liquid viscosity, ρ is the liquid density, ω is the quartz oscillating frequency, $v_x(z,\omega)$ is the liquid flow through the interfacial layer, x is the axis parallel to the quartz and z is the distance on the normal direction from the quartz, ξ^2 is the permeability, V_o is the amplitude of the velocity oscillation of the constrained quartz surface.

The first term on the right-hand side represents the viscous coupling of the liquid. The second and third terms describe the resistive force and it has Darcy-like form, which quantifies the energy dissipation caused by the non-laminar liquid motion due to effect of the solid phase on the liquid flow.

The concept of permeability was first studied by Darcy, who derived Darcy's law for a fluid at non-turbulent flow with non-slip boundary condition at the interface between the solid and the liquid. The description of the flow of an incompressible, viscous fluid through porous media is described as[144]

$$\xi^2 = \frac{\eta}{\Delta p}U = \frac{\eta\Theta\Delta l}{\Delta p\, A} \tag{8.10}$$

where U is the average velocity, Θ is the volumetric flow rate in a direction through a slab of the medium of thickness Δl and area A with a pressure difference Δp at the ends of the slab and η is the viscosity of the fluid. The SI unit of permeability is m^2, but for practicality the most used unit is millidarcy mD, which is 9.869×10^{-16} m^2.

8.6. Resonant Frequency - Fundamental and Overtones

Any solid material can vibrate at different frequencies. The thickness of the quartz crystal is adjusted so that the structure resonates at the required frequency. As a consequence of the vibration on the quartz crystal, an acoustic wave propagates from the quartz crystal. The disk of quartz crystal is considered as one-dimensional system regarding the vibration propagated in the thickness direction because its height and length are much longer than its thickness.[32] The equation which describes the vibration is:[32]

$$\frac{\partial^2 \Lambda}{\partial t^2} = v^2 \frac{\partial^2 \Lambda}{\partial z^2} \tag{8.11}$$

where Λ is the displacement of a point of a body during vibration at time t in the z direction, v is the propagation velocity of flexural waves along the body in the z (thickness) direction. The parameter Λ can be written as:

$$\Lambda(z,t) = a(t)b(z) \tag{8.12}$$

Substituting equation (8.12) in (8.11):

$$\frac{1}{a}\frac{\mathrm{d}^2 a}{\mathrm{d}t^2} = \frac{v^2}{b}\frac{\mathrm{d}^2 b}{\mathrm{d}z^2} \tag{8.13}$$

The terms in equation (8.13) depend on different variables a and b. In order to find the value of the variables, the two terms are set equal to a constant, which is called $-\omega^2$.

$$\frac{1}{a}\frac{\mathrm{d}^2 a}{\mathrm{d}t^2} = -\omega^2 \qquad \frac{v}{b}\frac{\mathrm{d}^2 b}{\mathrm{d}z^2} = -\omega^2 \tag{8.14}$$

For harmonic motion:

$$\begin{aligned} a(t) &= A\sin(\omega t) + B\cos(\omega t) \\ b(z) &= C\sin\left(\frac{\omega z}{v}\right) + D\cos\left(\frac{\omega z}{v}\right) \end{aligned} \tag{8.15}$$

For the calculation of the parameters A, B, C and D, it is necessary to satisfy the boundary conditions:

1) The oscillating disk with thickness l_q is free on the edges and the largest displacement takes place on the extremities of the disk.

$$\frac{\partial A(z,t)}{\partial z}=0, \qquad z=0 \tag{8.16}$$

2) The half thickness of the disk is a nodal plane, see Figure 8.3.

$$A(z,t)=0, \qquad z=\frac{l_q}{2} \tag{8.17}$$

3) At $t = 0$ the disk has no movement.

$$A(z,t)=0, \qquad t=0 \tag{8.18}$$

The first condition requires that C = 0;

The second condition requires that:

$$\frac{\omega\, l_q}{v}=n\pi, \qquad n=1,3,5,... \tag{8.19}$$

The third condition requires that B=0.

And as consequence, the displacement of the disk is represented as:

$$A(z,t)=E\sin\left(\frac{n\pi v}{l_q}t\right)\cos\left(\frac{n\pi}{l_q}z\right) \tag{8.20}$$

It is important to emphasise that the frequencies characteristic of this system are :

$$\omega=\frac{n\pi v}{l_q}, \qquad n=1,3,5,...$$

where n has to be an odd number because it needs to fulfil with the second condition, equation (8.19). The fundamental resonance occurs when n = 1. Figure 8.3 shows the harmonic frequencies on a solid material with thickness l_q. Note that the only if n is an odd number is the half thickness of the disk a node.

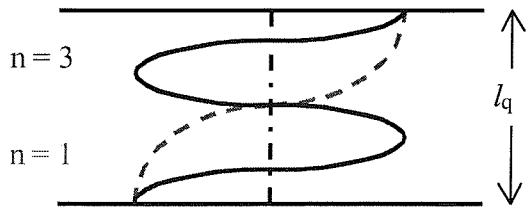

Figure 8.3: Modes of natural oscillation. Observe that the oscillation occurs across the thickness of the disk, l_q.

8.7. Manual of the LabVIEW program used for the Quartz Crystal Microbalance

This manual consists of an overview description of how to use the LabVIEW program QCM25lu2.vi to control and acquire data from the Quartz Crystal Microbalance. The words in bold type are part of the "Panel" of the LabVIEW program, and the words in italic type are found on the case of the Quartz Crystal Microbalance.

Panel:

The *Control Voltage* input on the back of the Quartz Crystal Microbalance connects to the output voltage ramp from the computer D/A card. The range of the voltage ramp is determined by **x axis: from** and **to** set on the panel of the LabVIEW program QCM25lu2. This digital voltage ramp is transformed into a frequency ramp on the Voltage Control Oscillator, VCO. The VCO is part of the Quartz Crystal Microbalance. The input signal going to the Quartz Crystal Microbalance is an ac voltage with constant amplitude and increasing frequency. The quartz crystal is connected to the *Xtal*. The central frequency is manually adjustable at the *VCO adjust* accessible through the lid of the Quartz Crystal Microbalance. See the Quartz Crystal Block Diagram in Figure 2.2.

The *RF* V_i and *RF* V_o terminals are amplified signals from the *VCO* and the crystal respectively. The amplitude of the amplified and rectified sinusoidal wave that excites the quartz crystal, *ADC* V_i, and the correspondent to the response of the quartz crystal, *ADC* V_o, are measured. The *ADC* V_i and *ADC* V_o outputs are the dc levels representing the peak values of the RF outputs. The ratio ADC V_o / ADC V_i plotted against the applied frequency is the transfer function graphed in the panel of the LabVIEW program. The number of transfer functions registered during a measurement is registered on the **transfer function**. The transfer function is the output of the Quartz Crystal Microbalance and it is recorded in a file with termination .dat.

The transfer function is formed by a number of points determined by the **no of steps** and the **no of points/step**. As an example is shown in Figure 8.4 where **x axis: from** = 0.0, **to** = 5.0, **no. steps** = 11, **no of points / step** = 3.

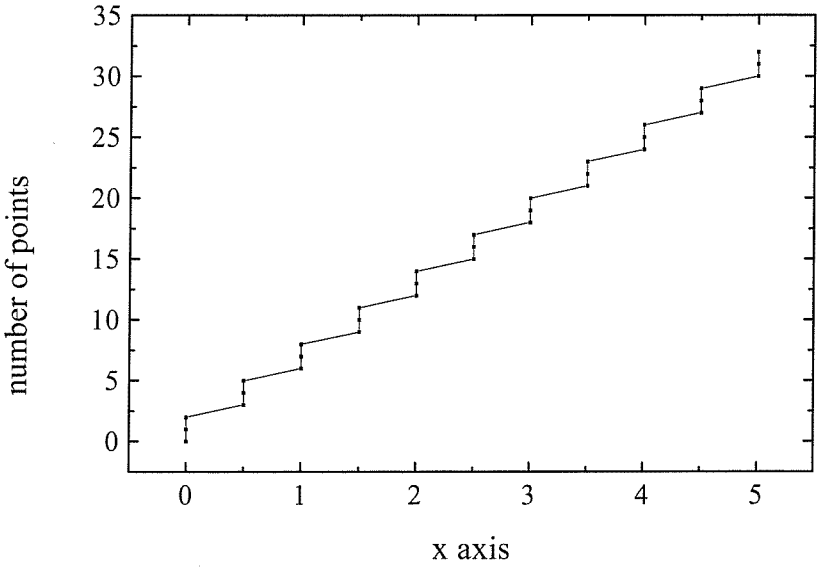

Figure 8.4: The output voltage ramp with **x axis:** from = 0.0, **to** = 5.0, **no. steps** = 11, **no of points / step** = 3.

In the example in Figure 8.4, between the range of 0 V and 5 V there will be 11 separate values of frequency. At each frequency, 3 measurements of $ADC\ V_o$ / $ADC\ V_i$ will be taken and averaged. The higher the no of steps, the better resolution the data will have. In the experiments described in this theses, 100 steps were used, between –5 V and + 5 V. And the **no of points/step** used is between 20 and 100 depending on the speed of measurements required.

The time interval for the points measured is determined by **point rate /s^{-1}**. Complete transfer functions are measured according to the value set on **integration** and averaged.

The record of data is started, when **SAVE** is pressed. At the initial time the minimum (**min freq**) and maximum frequency (**max freq**) are calculated for the extreme voltages defined by **x axis: from** and **to** respectively. This conversion of voltage to frequency is done by a subVI part of the program QCM25lu2.vi. When a

multiple of the time determined by the value of the **baseline /s** coincides with the **elapsed time /s**, the maximum frequency is measured and recorded on a file with termination .bsl. The maximum frequency will then be used for correcting the relation voltage to frequency that can be altered during the measurements. This correction is important for the determination of the parameter L ($L = (\omega_0 C)^{-1/2}$) for the quartz crystal equivalent electrical circuit. The measurements are taken for the duration defined on **final time/ s** or until **STOP** is pressed.

Scan Backlog is the amount of data that cannot be processed by the LabVIEW program because it cannot run fast enough. If the value registered in scan backlog is larger than zero, fewer points should be taken. The parameters that might be adjusted for decreasing the amount of data are **integration** and **point rate /s^{-1}**.

8.8. Calibration of the voltage amplitude of the Quartz Crystal Microbalance

The amplitude of the voltage input, V_i, and voltage output, V_o, need to be calibrated and corrected on the diagram of the LabVIEW program that controls the QCM. For this calibration, it is necessary an oscilloscope that measures frequencies close to 10 MHz. The calibration is performed following the steps:

1. Connect a quartz crystal on the *Xtal*.
2. Applying the usual voltage ramp (-5 V to +5 V) on the Panel of the LabVIEW program, centre the transfer function within the graph of the panel of the LabVIEW program, using the trimming tool.
3. Connect the *RF* V_i and *RF* V_o to an oscilloscope. Set up the oscilloscope for a frequency close to 10 MHz (25 ns).
4. Go to the options tools palette on the diagram of the LabVIEW program and activate the probe on the arrays that follow the AI Buffer Read.vi. There are three arrays: one provides the value of the axis x of the transfer function, the other two arrays indicate the values of V_i and V_o.
5. On the Panel of the LabVIEW program, apply the same value in the boxes **x axis from: and to:**
6. Write a table with the values of x axis applied, V_o and V_i obtained from the probe on the LabVIEW program and the amplitude of V_o and V_i measured at the oscilloscope. Make at least ten different measurements varying from the minimum to the maximum values usually used on the x axis range.
7. Plot V_o obtained from the probe of LabVIEW versus the amplitude of the voltage output registered at the oscilloscope. V_i should be constant for different values applied on x axis.
8. Use the linear equation obtained from the best fit of the plot of V_o as the calibration curve. The calibration equation is written on the Diagram of the LabVIEW program after the array correspondent to V_o.
9. The calibration equation is divided by the value of the amplitude of V_i obtained on the oscilloscope and wired to the y axis of the transfer function.

8.9. DAQ Boards

The DAQ boards from National Instrument make the connection between the LabVIEW software and the QCM and the potentiostat.

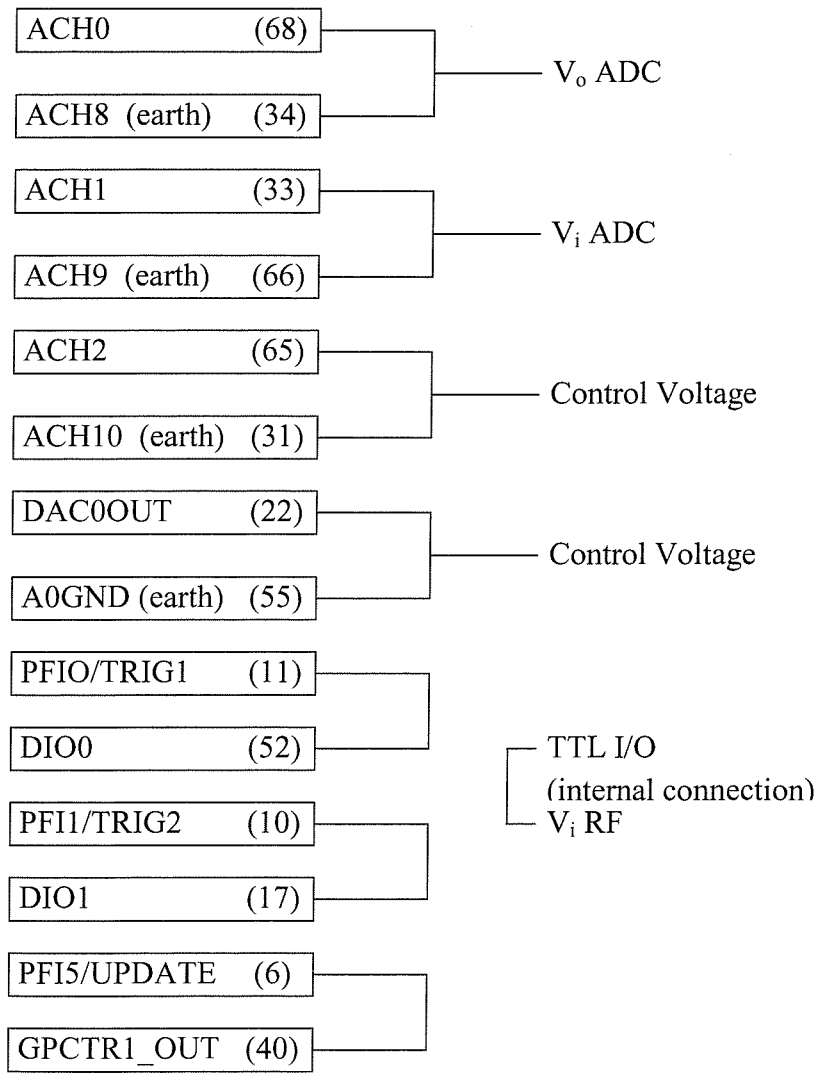

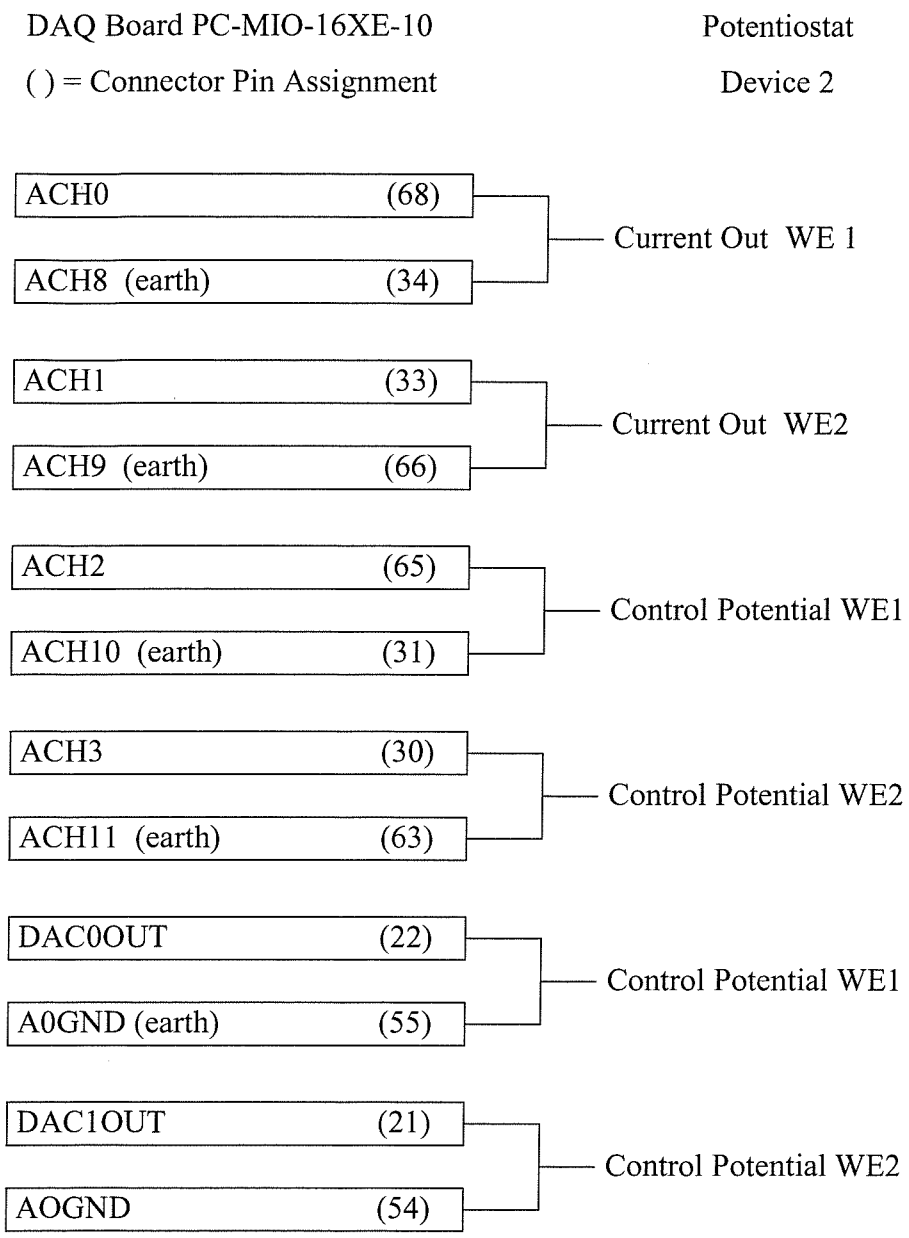
DAQ Board PC-MIO-16XE-10
( ) = Connector Pin Assignment
Potentiostat
Device 2
QCM
Device 1
ACH0 (68)
ACH8 (earth) (34)
Current Out WE 1
ACH1 (33)
ACH9 (earth) (66)
Current Out WE2
ACH2 (65)
ACH10 (earth) (31)
Control Potential WE1
ACH3 (30)
ACH11 (earth) (63)
Control Potential WE2
DAC0OUT (22)
A0GND (earth) (55)
Control Potential WE1
DAC1OUT (21)
AOGND (54)
Control Potential WE2

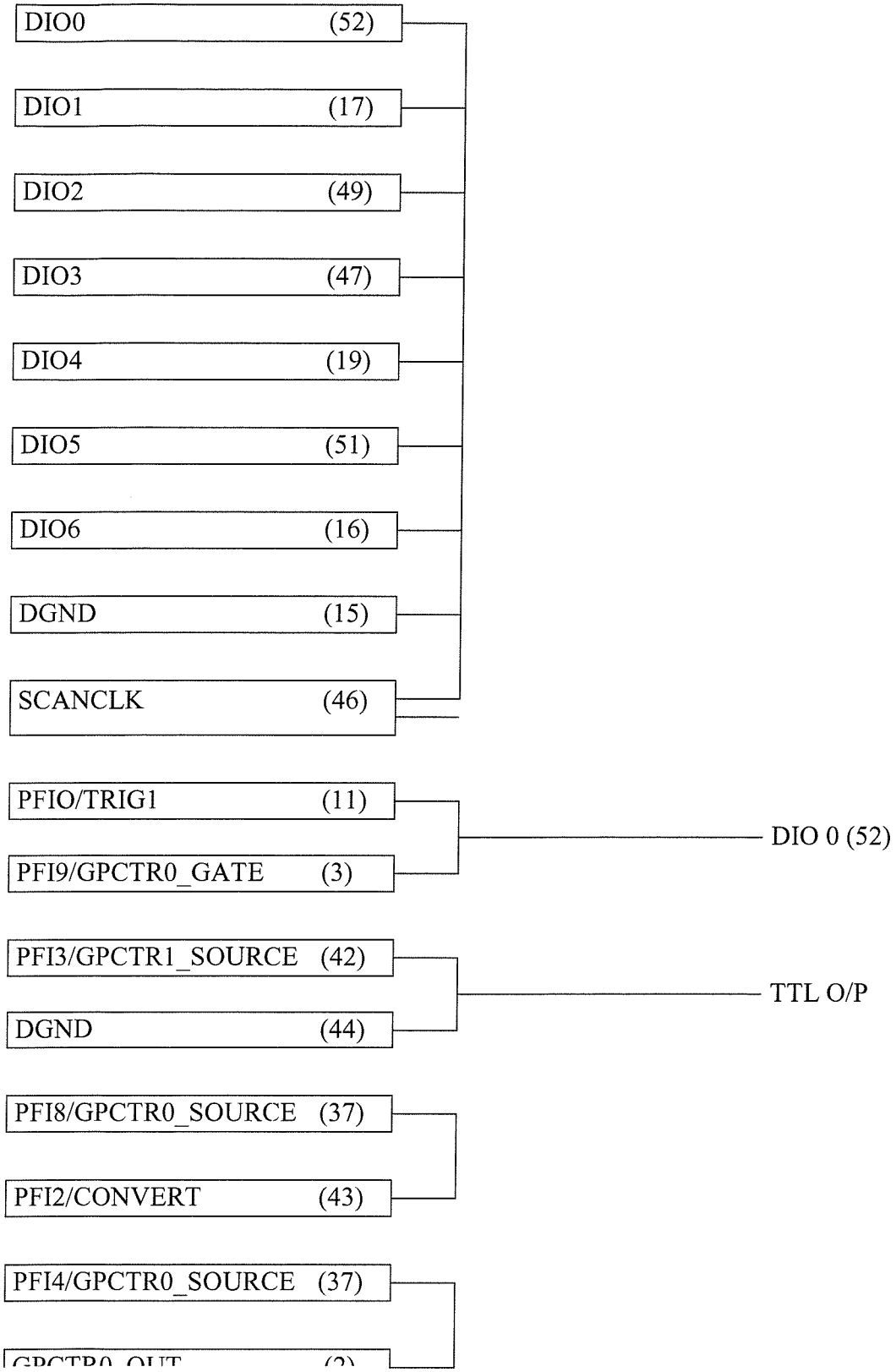
DIO0 (52)
DIO1 (17)
DIO2 (49)
DIO3 (47)
DIO4 (19)
DIO5 (51)
DIO6 (16)
DGND (15)
SCANCLK (46)
PFIO/TRIG1 (11)
PFI9/GPCTR0_GATE (3)
DIO 0 (52)
PFI3/GPCTR1_SOURCE (42)
DGND (44)
TTL O/P
PFI8/GPCTR0_SOURCE (37)
PFI2/CONVERT (43)
PFI4/GPCTR0_SOURCE (37)

8.10. Design and construction of the Quartz Crystal Microbalance

The QCM consists of three main circuits. They are the 10 MHz tuneable oscillator, the amplifier stage and the peak level detector.

Tuneable Oscillator

The oscillator frequency is controlled using a voltage of 0-10 V from an independent voltage source. This voltage alters the capacitance of a varicap diode to alter the tuned frequency of the oscillator. The circuit components were chosen to ensure that the oscillator has good stability, so that the user can set the control voltage to correspond to a particular frequency, with minimum fluctuation. The resistors were all surface mounted devices that are accurate to 1%, and being surface mounted, they are ideally suited to high frequency applications as they reduce stray inductance usually associated with conventional resistors. Silver mica capacitors were used in the circuit for stability as they are very accurate (± 1%) and have low leakage compared to others such as ceramic and polystyrene capacitors, which have a typical accuracy of ± 10%.

Amplifier stage

The amplifiers chosen were MAX436 transconductance amplifiers that have wide bandwidth capabilities to achieve substantial gain values at high frequency. The gain of the amplifier is defined as $A_v=K(Z_L/Z_t)$. Z_L is 180 R for both amplifiers, but Z_t is 44 R for amplifier 1 and 22 R for amplifier 2. K is internally trimmed to be ± 2.5%. This makes the theoretical gains for the amplifiers:

Amplifier 1 (V_i) = 7.8 x (180/44) = 31.9 (min)
8.2 x (180/44) = 33.55 (max)

Amplifier 2 (V_o) = 7.8 x (180/22) = 63.8 (min)
8.2 x (180/22) = 67.1 (max)

The measured gains for the amplifiers at 10 MHz are:

Amplifier 1 (V_i) = 32

Amplifier 2 (V_o) = 64

Power supply bypass capacitors were used to reduce interference on the power supply lines, and also to limit inductive effects caused by the amplifier.

Peak Detector

The peak detector circuit is used to measure the peak voltage values of both the oscillator and the crystal amplifiers. It is constructed using two RF diodes, which operate at speeds greater than that of normal diodes for a faster and more accurate response.

9. References

1 A. J. Heeger, *J. Phys. Chem. B*, **2001**, *105*, (36), 8475-8491.

2 T. F. Otero and J. M. Sansinena, *Adv. Mater.*, **1988**, *10*, (6), 491-494.

3 K. Kaneto and M. Kaneko, *Appl. Biochem. Biotech.*, **2001**, *96*, (1-3), 13-23.

4 L. B. Wingard, C. H. Shaw, and J. F. Castner, *Enzyme Microb. Technol.*, **1982**, *4*, 137-142.

5 C. v. Dijk, C. Laane, and C. Veeger, *Recl. Trav. Chim. Pays-Bas*, **1985**, *104*, 245-252.

6 G. Tayhas, R. Palmore, H. Bertschy, S. H. Bergens, and G. M. Whitesides, *J. Electroanal. Chem.*, **1998**, *443*, 151-161.

7 I. Willner and E. Katz, *Angew. Chem. Int. Ed.*, **2000**, *39*, 1180-1218.

8 P. N. Bartlett and E. Simon, *Phys. Chem. Chem. Phys.*, **2000**, *2*, 2599-2606.

9 P. G. Bruce, *Solid State Electrochemistry*, Cambridge University Press, Cambridge, 1997.

10 D. A. Buttry and M. D. Ward, *Chem. Rev.*, **1992**, *92*, 1355-1379.

11 E. J. Calvo, R. Etchenique, P. N. Bartlett, K. Singhal, and C. Santamaria, *Faraday Discuss.*, **1997**, *107*, 141-157.

12 A. R. Hillman, A. Jackson, and S. J. Martin, *Anal. Chem.*, **2001**, *73*, 540-549.

13 C. Barbero, M. C. Miras, O. Haas, and R. Koetz, *J. Electroanal. Chem.*, **1991**, *138*, (3), 669-672.

14 R. Greef, M. Kalaji, and L. M. Peter, *Faraday Discuss. Chem. Soc.*, **1989**, *88*, 277-289.

15 E. M. Genies and M. Lapkowski, *J. Electroanal. Chem.*, **1987**, *236*, 199--204.

16 T. Kobayashi, H. Yoneyama, and H. Tamura, *J. Electroanal. Chem.*, **1984**, *177*, 281-291.

17 D. Orata and D. A. Buttry, *J. Am. Chem. Soc.*, **1987**, *109*, 3574-3581.

18 D. H. Dawson, PhD Thesis, University of Bath, 1992.

19 P. N. Bartlett, P. R. Birkin, and E. N. K. Wallace, *J. Chem. Soc., Faraday Trans.*, **1997**, *93*, (10), 1951-1960.

20 P. N. Bartlett and E. N. K. Wallace, *J. Electroanal. Chem.*, **2000**, *486*, 23-31.

21 P. N. Bartlett, *Biosensors. Fundamentals and Applications*, Oxford University Press, Oxford, 1987.

22 P. N. Bartlett, J. H. Wang, and E. N. K. Wallace, *Chem. Commun.*, **1996**, 359-360.

23 E. F. Murphy, J. R. Lu, J. Brewer, J. Russell, and J. Penfold, *Langmuir*, **1999**, *15*, (4), 1313-1322.

24 F. Soavi, C. Arbizzani, and M. Mastragostino, *Phys. Chem. Chem. Phys.*, **2000**, *2*, 2993-2998.

25 G. Inzelt, V. Kertesz, and A. Nyback, *J. Solid State Electrochem.*, **1999**, *3*, (5), 251-257.

26 K. Johannsen, D. Page, and S. Roy, *Electrochim. Acta*, **2000**, *45*, (22-23), 3691-3702.

27 A. Bund and G. Schwitzgebel, *Electrochim. Acta*, **2000**, *45*, (22-23), 3703-3710.

28 C. Eickes, J. Rosenmud, S. Wasle, K. Doblhofer, K. Wang, and K. G. Weil, *Electrochim. Acta*, **2000**, *45*, (22-23), 3623-3628.

29 J. Teledgi, A. Shaban, and E. Kalman, *Electrochim. Acta*, **2000**, *45*, (22-23), 3639-3648.

30 A. Glidle, C. S. Hadyoon, A. E. G. Cass, and J. M. Cooper, *Electrochim. Acta*, **2000**, *45*, (22-23), 3823-3831.

31 P. Curie and J. Curie, *C. R. Acad. Sci.*, **1880**, *91*, 383.

32 A. A. Vives, *El Sensor de Cuarzo*, Moliner 40, Valencia, 2000.

33 A. W. Warner and C. D. Stockbridge, *Mass measurement with resonating crystalline quartz, Vacuum microbalance techniques*, Plenum Press, 1963.

34 K. S. V. Dyke, *Proceedings of the Institute of Radio Engineers*, **1945**, *33*, (1), 15-20.

35 R. Etchenique, PhD Thesis, Universidade de Buenos Aires, 1998.

36 C. Barbero, E. J. Calvo, R. Etchenique, G. M. Morales, and M. Otero, *Electrochim. Acta*, **2000**, *45*, 3895-3906.

37 A. L. Briseno, A. J. Baca, Q. Zhou, R. Lai, and F. Zhou, *Anal. Chim. Acta*, **2001**, *441*, 123-134.

38 M. D. Ward, *Physical Electrochemistry*, Marcel Dekker, New York, 1995.

39 E. J. Calvo, C. Danilowicz, and R. Etchenique, *J. Chem. Soc. Faraday Trans.*, **1995**, *91*, (22), 4083-4091.

40 G. Sauerbrey, *Z. Phys.*, **1959**, *155*, 206.

41 H. L. Bandey, A. R. Hillman, M. J. Brown, and S. J. Martin, *Faraday Discuss.*, **1997**, *107*, 105-121.

42 V. E. Granstaff and S. J. Martin, *J. Appl. Phys.*, **1994**, *75*, (3), 1319-1329.

43 S. J. Martin, V. E. Granstaff, and G. C. Frye, *Anal. Chem.*, **1991**, *63*, 2272-2281.

44 K. K. Kanazawa and J. G. Gordon, *Anal. Chem.*, **1985**, *57*, 1770-1771.

45 S. Bruckenstein and M. Shay, *Electrochim. Acta*, **1985**, *30*, 1295-1300.

46 E. Gileadi and V. Tsionsky, *J. Electrochem. Soc.*, **2000**, *147*, (2), 567-574.

47 H. L. Bandey, S. J. Martin, and R. W. Cernosek, *Anal. Chem.*, **1999**, *71*, 2205-2214.

48 K. S. V. Dyke, *Phys. Rev.*, **1925**, *25*, 895.

49 J. Merhaut, *Theory of Electroacoustics*, McGraw-Hill, New York, 1981.

50 G. Sauerbrey, *Z. Phys.*, **1964**, *178*, 457-471.

51 K. H. Behrndt and R. W. Love, *Vacuum*, **1962**, *12*, (1), 1-8.

52 W. H. King, *Anal. Chem.*, **1964**, *36*, 1735-1739.

53 J. G. Miller and D. I. Bolef, *J. Appl. Phys.*, **1968**, *39*, (10), 4589-4593.

54 V. Mecea and R. V. Bucur, *Thin Solid Films*, **1979**, *60*, (1), 73-84.

55 K. K. Kanazawa, *J. Appl. Phys.*, **1990**, *68*, (5), 1993-2001.

56 G. Inzelt, *Electrochim. Acta*, **2000**, *45*, (22-23), 3865-3876.

57 M. T. Colberg, K. Carnes, A. E. Saez, C. S. Grant, K. Hutchinson, and D. Hesterberg, *Thin Solid Films*, **1998**, *327-329*, 247-251.

58 S. L. A. Maranhao and R. M. Torresi, *Electrochim. Acta*, **1999**, *44*, 1879-1885.

59 L. Daikhin and M. Urbakh, *Langmuir*, **1996**, *12*, 6354-6360.

60 C. Filiatre, G. Bardeche, and M. Valentin, *Sens. Actuat. A*, **1994**, *44*, 137-144.

61 M. Yang and M. Thompson, *Anal. Chim. Acta*, **1993**, *282*, 505-515.

62 B. Gollas, P. N. Bartlett, and G. Denuault, *Anal. Chem.*, **2000**, *72*, (2), 349-356.

63 D. M. Soares, W. Kautek, C. Fruboese, and K. Doblhofer, *Ber. Bunsenges. Phys. Chem.*, **1994**, *98*, (2), 219-228.

64 R. Lucklum and P. Hauptmann, *Electrochim. Acta*, **2000**, *45*, (22-23), 3907-3916.

65 H. Muramatsu, X. Ye, T. Sakuhura, and T. Ataka, *J. Electroanal. Chem. Interfacial Electrochem.*, **1992**, *322*, 311-323.

66 B. Gollas, J. M. Elliot, and P. N. Bartlett, *Electrochim. Acta*, **2000**, *45*, (22-23), 3711-3724.

67 C. K. O'Sullivan and G. G. Guilbault, *Biosens. Bioelectron.*, **1999**, *14*, 663-670.

68 M. J. Brown, A. R. Hillman, S. J. Martin, R. W. Cernosek, and H. L. Bandey, *J. Mater. Chem.*, **1999**, *9*, (1), 115-126.

69 M. A. Malik, K. Miecznikowski, and P. J. Kulesza, *Electrochim. Acta*, **2000**, *45*, (22-23), 3777-3784.

70 S. Bruckenstein, K. Brzezinska, and A. R. Hillman, *Electrochim. Acta*, **2000**, *45*, (22-23), 3801-3812.

71 W. Paik, I.-H. Yeo, H. Suh, Y. Kim, and E. Song, *Electrochim. Acta*, **2000**, *45*, (22-23), 3833-3840.

72 C. Visy, J. Kankare, and E. Krivan, *Electrochim. Acta*, **2000**, *45*, (22-23), 3851-3864.

73 M. J. Henderson, A. R. Hillman, and E. Vieil, *Electrochim. Acta*, **2000**, *45*, (22-23), 3885-3894.

74 A. R. Hillman and S. Bruckenstein, *J. Chem. Soc., Faraday Trans.*, **1993**, *89*, (2), 339-348.

75 J. Rishpon, A. Redondo, C. Derouin, and S. Gotttesfeld, *J. Electroanal. Chem.*, **1990**, *294*, 73-85.

76 K. Shimazu, M. Yanagida, and K. Uosaki, *J. Electroanal. Chem.*, **1993**, *350*, 321-327.

77 F. Huguenin, R. M. Torresi, D. A. Buttry, J. E. P. Silva, and S. I. C. Torresi, *Electrochim. Acta*, **2001**, *46*, 3555-3562.

78 K. Ogura, K. Nakaoka, and M. Nakayama, *J. Electroanal. Chem.*, **2000**, *486*, (2), 119-125.

79 Z. Jusys, H. Massong, and H. Baltruschat, *J. Electrochem. Soc.*, **1999**, *146*, (3), 1093-1098.

80 H. D. Abruna, in 215th ACS National Meeting, Dallas, 1998 (American Chemical Society).

81 M. J. Henderson, H. French, A. R. Hillman, and E. Vieil, *Electrochem. Solid-State Lett.*, **1999**, *2*, (12), 631-633.

82 E. Szocs, G. Vastag, A. Shaban, G. Konczos, and E. Kalman, *J. Appl. Electrochem.*, **1999**, *29*, (11), 1339-1345.

83 P. N. Bartlett, K. Brace, E. J. Calvo, and R. Etchenique, *J. Mater. Chem.*, **1999**, *10*, (1), 149-156.

84 M. H. T. Frank and G. Denuault, *J. Electroanal. Chem.*, **1993**, *354*, 331-339.

85 H. Muramatsu, X. Ye, M. Suda, T. Sakuhara, and T. Ataka, *J. Electroanal. Chem.*, **1992**, *322*, 311-323.

86 *LabVIEW User Manual*, Ed. National Instruments Corporate Headquarters, 1996.

87 J. D. Ferry, *Viscoelastic properties of polymers.*, 3 ed., John Wiley & Sons, New York, 1980.

88 H. A. Barnes, J. F. Hutton, and K. Walters, *An Introduction to Rheology*, Elsevier Science Publisher, Amsterdam, 1989.

89 *Handbook of Chemistry and Physics*, 45th ed., Chemical Rubber Publishing Co, Cleveland, OH, 1959.

90 A. Domack and D. Johannsmann, *J. Appl. Phys.*, **1996**, *80*, (5), 2599-2604.

91 J. M. G. Cowe, *Polymers: Chemistry & Physics of Modern Materials*, 2 ed., Blackie Academic & Professional, Suffolk, 1997.

92 S. J. Martin and G. C. Frye, *Appl. Phys. Lett.*, **1990**, *57*, (18), 1867-1869.

93 http://www.Biocompatibles.co.uk

94 J. Hayward, *Biomaterials*, **1984**, *5*, 135-138.

95 E. F. Murphy, J. R. Lu, A. L. Lewis, J. Brewer, J. Russell, and P. Stratford, *Macromolecules*, **2000**, *33*, 4545-4554.

96 L. R. G. Treloar, *Introduction to Polymer Science*, Wykeham Publications Ltd, London, 1970.

97 R. Etchenique and V. L. Brudny, *Langmuir*, **2000**, *16*, 5064-5071.

98 D. Orata and D. A. Buttry, *J. Electroanal. Chem.*, **1988**, *257*, 71-82.

99 P. A. Topart and M. A. M. Noel, *Anal. Chem.*, **1994**, *66*, 2926-2934.

100 S. Basak, C. S. C. Bose, and K. Rajeshwar, *Anal. Chem.*, **1992**, *64*, 1813-1818.

101 P. J. Nigrey, A. G. MacDiarmid, and A. J. Heeger, *Chem. Commun.*, **1979**, *96*, 594-596.

102 R. G. Lindford and G. Roger, *Electrochemical Science and Technology of Polymers*, Elsevier Applied Science, London, 1987.

103 S. Pruneanu, E. Csahok, V. Kertesz, and G. Inzelt, *Electrochim. Acta*, **1998**, *43*, (16-17), 2305-2323.

104 J. Silvestro and W. Scheifele, *J. Mater. Chem.*, **1993**, *3*, (3), 263-272.

105 J. Silvestro, W. Scheifele, and O. Haas, *J. Electrochem. Soc.*, **1992**, *139*, (10), 2727-2736.

106 G. Horanyi and G. Inzelt, *Electrochim. Acta*, **1988**, *33*, (7), 947-952.

107 G. Denuault, M. H. T. Frank, and L. M. Peter, *Faraday Discuss.*, **1992**, *94*, 23-35.

108 N. Oyama and F. C. Anson, *J. Electrochem. Soc.*, **1980**, *127*, 640-647.

109 M. H. T. Frank, PhD Thesis, Universidade Pontificia Catolica do Rio de Janeiro, 1994.

110 E. N. Wallace, PhD Thesis, University of Southampton, 1997.

111 G. E. Asturias, G. W. Jang, A. G. MacDiamird, K. Doblhofer, and C. Zhong, *Ber. Bunsenges. Phys. Chem.*, **1991**, *95*, (11), 1381-1384.

112 Y. Kang, M.-H. Lee, and S. B. Rhee, *Synth. Metal.*, **1992**, *52*, 319.

113 T. Hirai, S. Kuwabata, and H. Yoneyama, *J. Chem. Soc., Faraday Trans. 1*, **1989**, *85*, (4), 969-976.

114 S. L. A. Maranhao and R. M. Torresi, *J. Electrochem. Soc.*, **1999**, *146*, (11), 4179-4182.

115 J. Heinze, *Topics in Current Chemistry*, Springer Verlag, Berlim, 1990.

116 M. R. Anderson, B. R. Mattes, H. Reis, and R. B. Kaner, *Science*, **1991**, *252*, (5011), 1412-1415.

117 R. Beck, U. Pittermann, and K. G. Weil, *J. Electrochem. Soc.*, **1992**, *139*, (2), 453-461.

118 T. Bourbie, O. Coussy, and B. Zinszner, *Acoustic of Porous Media*, Gulf Publishing Company, Paris, 1987.

119 S. Bruckenstein, A. Fensore, Z. Li, and A. R. Hillman, *J. Electroanal. Chem.*, **1994**, *370*, 189-195.

120 R. Etchenique and V. L. Brudny, *Electrochem. Commun.*, **1999**, *1*, 441-445.

121 P. N. Bartlett, P. R. Birkin, M. A. Ghanen, P. d. Groot, and M. Sawicki, *J. Electrochem. Soc.*, **2001**, *148*, (2), C119-123.

122 K. Naoi, M. Lien, and W. H. Smyrl, *J. Electrochem. Soc.*, **1991**, *138*, (2), 440-445.

123 M. Kalaji, L. M. Peter, L. M. Abrantes, and J. C. Mesquita, *J. Electroanal. Chem.*, **1989**, *274*, 289-295.

124 I. Jureviciute, S. Bruckenstein, and A. R. Hillman, *J. Electroanal. Chem.*, **2000**, *488*, 73-81.

125 W. Luzny, M. Sniechowski, and J. Laska, *Synth. Met.*, **2000**, *126*, 27-35.

126 W. Tashima, T. Uesugi, M. Fukui, M. Kaneto, and K. Kaneto, in Int. Conf. on Science and Technology of Synthetic Metals, Snowbith, 1996, p. P1-217.

127 R. H. Baughman, *Synth. Met.*, **1996**, *78*, 339-353.

128 M. Kaneto and K. Kaneko, *Synth. Met.*, **1999**, *102*, 1350-1353.

129 B. A. Martin and H. E. Hager, *J. Appl. Phys.*, **1989**, *65*, 2627-2629.

130 R. C. Engstrom, M. Weber, D. J. Wunder, R. Burgess, and S. Winquist, *Anal. Chem.*, **1986**, *58*, 844-848.

131 A. J. Bard and L. R. Faulkner, *Electrochemical Methods*, John Wiley & Sons, New York, 1980.

132 M. Ciszkowska, Z. Stojek, S. E. Morris, and J. G. Osteryoung, *Anal. Chem.*, **1992**, *64*, 2372-2377.

133 P. R. Unwin and A. J. Bard, *J. Phys. Chem.*, **1992**, *96*, 5035-5045.

134 M. H. T. Frank and G. Denuault, *J. Electroanal. Chem.*, **1994**, *379*, 399-406.

135 A. C. Hillier and M. D. Ward, *Anal. Chem.*, **1992**, *64*, 2539-2554.

136 M. Shin and I. C. Jeon, *Bull. Korean Chem. Soc.*, **1998**, *19*, 1227-1232.

137 C. Hess, K. Borgwarth, and J. Heinze, *Electrochim. Acta*, **2000**, *45*, (22-23), 3723-3736.

138 D. E. Cliffel and A. J. Bard, *Anal. Chem.*, **1998**, *70*, 1993-1998.

139 H. Angerstein-Kozlowska, B. E. Conway, and B. A. Sharp, *J. Electroanal. Chem. Interfacial Electrochem.*, **1973**, *43*, 9-36.

140 J. Kwak and A. J. Bard, *Anal. Chem.*, **1989**, *61*, 1221-1227.

141 F. F. Kuo, *Network Analysis and Synthesis*, 2nd ed., John Wiley &Sons, New York, 1966.

142 R. G. Meadows, *Electric Network Analysis*, Penguin Education, Harmondworth, 1972.

143 H. C. Brinkman, *Appl. Sci. Res.*, **1947**, *A1*, 27-34.

144 M. Sahimi, *M. Rev. Modern Phys.*, **1993**, *65*, 1393.